

Novel Antibody-Targeted Liposomes for the Treatment of Solid Tumors

Michiel Bolkestein



Novel Antibody-Targeted Liposomes for the Treatment of Solid Tumors

Michiel Bolkestein

© Michiel Bolkestein, 2016

No part of this thesis may be reproduced, stored or transmitted in any form by any means without prior written permission from the author.

ISBN: 978-94-6169-966-4

The research described in this thesis was performed at the departments of Surgery and Cell Biology, Erasmus Medical Center, Rotterdam, the Netherlands

Cover and printing: Optima Grafische Communicatie, Rotterdam, the Netherlands

Novel Antibody-Targeted Liposomes for the Treatment of Solid Tumors

Nieuwe Antilichaam-Gerichte Liposomen
voor de Behandeling van Solide Tumoren

Thesis

to obtain the degree of Doctor from the Erasmus University Rotterdam
by command of the rector magnificus Prof. dr. H.A.P. Pols
and in accordance with the decision of the Doctorate Board

The public defense shall be held on
Wednesday 23 November 2016 at 11:30 h

by

Michiel Bolkestein
born in Tiel, the Netherlands

Erasmus University Rotterdam



DOCTORAL COMMITTEE

Promoters: Prof. dr. A.M.M. Eggermont
Prof. dr. F.G. Grosveld

Other members: Prof. dr. M. de Jong
Prof. dr. H. Grill
Prof. dr. T. Lammers

Copromoter: Dr. G.A. Koning

“And once the storm is over, you won’t remember how you made it through, how you managed to survive. You won’t even be sure, whether the storm is really over. But one thing is certain. When you come out of the storm, you won’t be the same person who walked in. That’s what this storm’s all about.”

Haruki Murakami

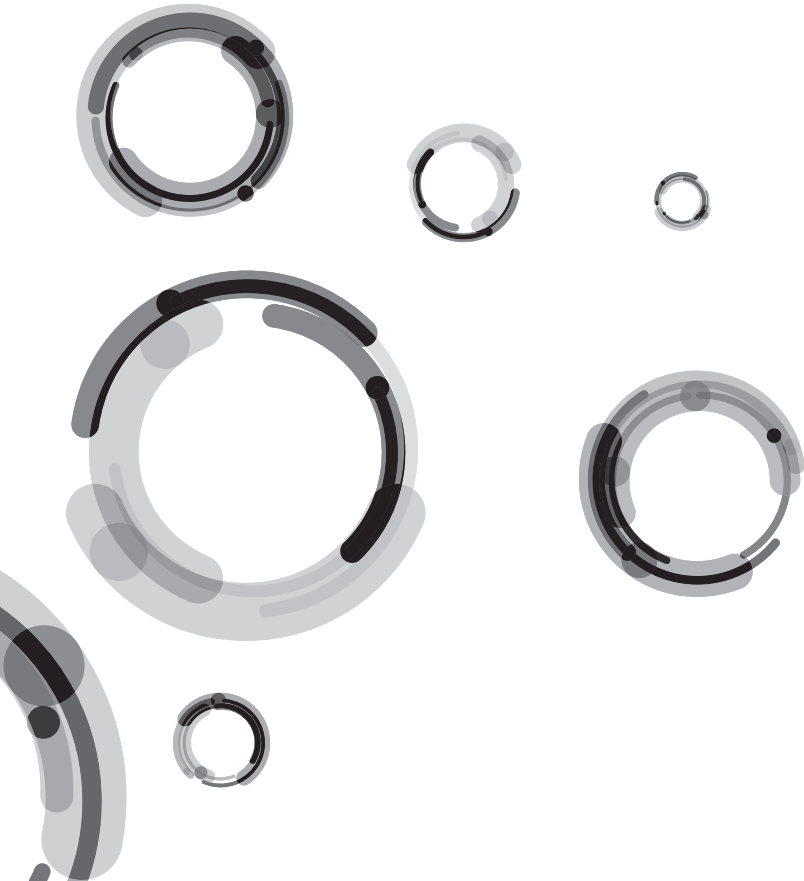
TABLE OF CONTENTS

Chapter 1	General introduction	9
Chapter 2	Generation of novel heavy-chain antibodies against MUC1	25
Chapter 3	A novel indium-111 labeled anti-prostate-specific membrane antigen nanobody for targeted SPECT/CT imaging of prostate cancer	37
Chapter 4	Nanobody-targeted prostate cancer therapy with anti-PSMA doxorubicin-loaded liposomes	55
Chapter 5	Investigation of factors determining the enhanced permeability and retention effect in subcutaneous xenografts	73
Chapter 6	Investigation of particle accumulation, chemosensitivity and thermosensitivity for effective solid tumor therapy using thermosensitive liposomes and hyperthermia	97
Chapter 7	General discussion	121
	References	133
	Summary, future perspectives / Samenvatting, toekomstvisie	165
	List of publications	175
	PhD portfolio	179
	Acknowledgements	181
	Curriculum vitae	185



CHAPTER 1

General Introduction



CANCER AND CHEMOTHERAPY

Cancer is a disease where genetic instability leads to a pathological condition which gives normal cells an unlimited growth potential and the ability to disseminate and invade other parts of the body. Cancer afflicts millions of people worldwide each year and is one of the leading causes of morbidity and mortality. Almost every tissue in the human body can give rise to cancer, leading to a range of cancers, each possessing unique features¹. The therapeutic corner stones to treat solid tumors are surgery, radiotherapy and chemotherapy²⁻⁴. Surgery and radiotherapy can provide local control, but disseminated disease usually requires systemic therapy. A lack of selectivity and specificity of such systemic treatments have led to numerous side effects, decreased efficacy due to resistance and suboptimal dosing regimens, which eventually results in disease recurrence and metastatic spread. To overcome these limitations, many conventional chemotherapeutics have been adapted to cope with drug resistance and minimize adverse drug-related effects by creating increasingly specific therapies targeted against cancer.

One of these chemotherapeutics is doxorubicin, a clinically important and often-used anticancer drug. Clinically, doxorubicin is used in the treatment of several cancers including; acute leukemia, breast cancer, gastric cancer, (non-)Hodgkin lymphoma, neuroblastoma, ovarian cancer, small cell lung cancer, soft tissue and bone sarcomas, thyroid cancer, transitional cell bladder cancer and Wilms tumors⁵. Doxorubicin was first isolated in 1969 from *Streptomyces peucetius*, and is formed by C-14 hydroxylation of its precursor, daunorubicin⁶. The main mechanism of action is the inhibition of proliferation by intercalating base pairs of DNA/RNA, which is selective for cells with a higher proliferation rate. As a result, the drug is cytotoxic to fast growing cancer cells, although the nonspecific activity of the drug also affects normal tissues with high proliferation rates such as blood cells, the gastrointestinal tract and hair follicles⁷. A major adverse effect of doxorubicin is its cardiotoxicity, which may lead to congestive heart failure⁸. Doxorubicin-induced cardiotoxicity is probably caused by one or more of the following; increased oxidative stress⁹, decreased antioxidants and sulfhydryl groups^{10,11}, inhibition of nucleic acid and protein synthesis¹², and decreased cardiomyocyte-specific gene expression¹³. Serious adverse effects of doxorubicin and other anticancer drugs lead to suboptimal dosing, and in combination with drug resistance, often results in discontinuation of the treatment. To solve these problems, anticancer drugs need to be delivered more selectively to cancer tissue with minimal exposure to healthy tissues.

This can in principal be achieved by using antibody- or ligand-mediated targeting in combination with drug carriers, which have the added benefit of lengthening the short circulation times of free drugs. The antibodies or ligands would be designed to bind

antigens or receptors uniquely present and/or overexpressed on cancer cells. This will reduce systemic exposure and increase biodistribution of the encapsulated drug.

LIPOSOMES

Early phospholipid research led to the description of swollen phospholipids which, within years, enabled the production of enclosed phospholipid bilayer structures called liposomes¹⁴⁻¹⁸. Liposomes are composed of natural phospholipids, which makes them biologically inert, less immunogenic, non-toxic and ideal for drug entrapment^{19,20}. The combination of a hydrophobic bilayer and an aqueous center makes them ideal for encapsulating both lipophilic and hydrophilic drugs, and even compounds with an intermediate partition coefficient²¹. These characteristics facilitate their use as effective delivery systems, preventing free drug from interacting with the body and thereby reducing side effects and immune reactions.

Early liposomal formulations were cleared rapidly from circulation via opsonization²², and captured by the mononuclear phagocyte system (MPS)²³. To prevent this, long-circulating liposomes were created by the addition of hydrophilic polymers, such as polyethylene glycol (PEG), to the liposome surface²⁴. These polymers can be anchored to the liposomal membrane via cross-linked lipids such as pegylated 1,2-distearoyl-sn-glycero-3-phosphoethanolamine (DSPE-PEG)²⁵. The flexible chain of the polymer causes steric hindrance for macromolecules, reduces clearance by macrophages and enables long circulation times. In addition, liposomes are not stable in plasma due to interactions with high and low density lipoproteins²⁶. Incorporation of cholesterol in the lipid bilayer facilitates a bidirectional transfer of phospholipids, which otherwise would lead to phospholipid depletion and liposome degradation²⁷⁻²⁹. Although the use of saturated phospholipids also increases the stability of liposomes³⁰, this might lead to a decrease in the rate of drug release from the liposomes.

Drug loading of liposomes is highly dependent on the nature of the drug. Like most lipid membranes, liposomes have a high permeability to hydrophobic drugs which makes drug entrapment difficult^{31,32}. Drug loading progressed significantly with the development of pH gradient-dependent or remote drug loading methods^{33,34}. In addition, some drugs like doxorubicin have the added bonus of precipitation after loading, which creates a very stable liposomal drug formulation³⁵. Liposomes can encapsulate several thousand drug molecules, ensuring a high drug load delivery, although drug loading, retention and release have to be optimized for every nanoparticle formulation. This resulted in liposomal doxorubicin (Doxil) being the first liposomal formulation to reach clinical trials^{36,37}. Although Doxil has been approved for use against ovarian cancer, Kaposi sarcoma and multiple myeloma³⁸; overall the slow release³⁷, lack of specificity, and the reliance on passive accumulation via the enhanced permeability and

retention (EPR) effect have left room for improvement. Targeting with antibodies or other ligands could improve site-specific accumulation and efficacy, whereas triggered release tactics can be implemented to avoid the insufficient drug release.

TARGETED LIPOSOMES

Cancer cells have structural and functional differences which can be exploited for targeted therapies. To enhance specificity of liposomal chemotherapy, liposomes can be functionalized with a targeting moiety to generate targeted or immunoliposomes. The target should have a high density on tumor cells or tumor vasculature, and should preferably not be expressed on other tissues. To this end, liposomes have been formulated with ligands to target the tumor itself or its surrounding microenvironment, such as the extracellular matrix or the tumor-associated vasculature³⁹⁻⁴². The general principle of extravasation and binding of targeted liposomes is shown in Figure 1. When using sterically stabilized liposomes, antibodies or antibody fragments can be linked to the end of PEG chains with conventional chemical conjugation techniques^{43,44}, while retaining an enhanced circulation and decreased uptake in the liver and spleen^{45,46}. Initial studies investigating antibody-conjugated liposomes suggested that this approach could increase the efficacy of liposomal chemotherapy^{47,48}.

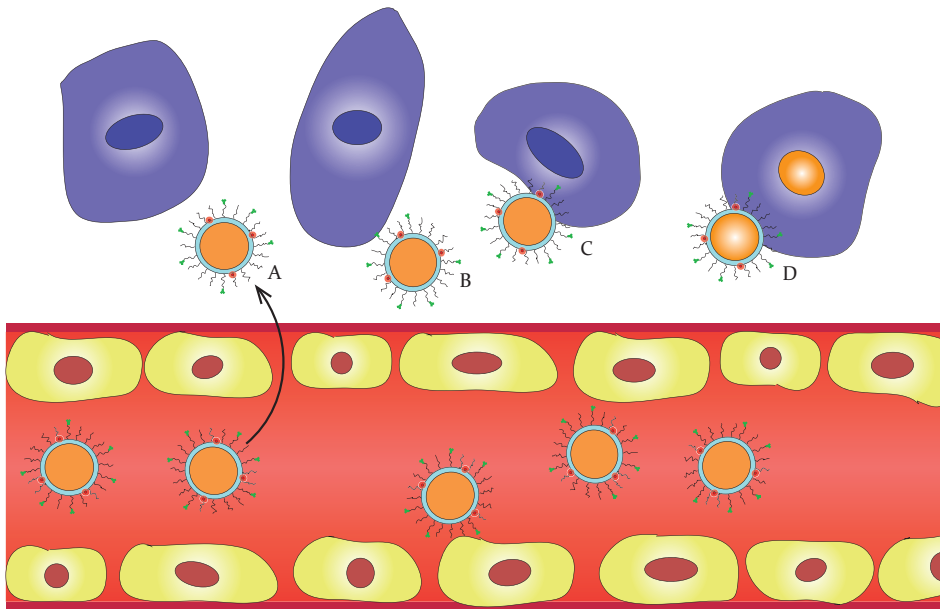


Figure 1. Liposomes extravasate due to enhanced permeability in tumor vasculature (A), upon which tumor cell specific binding of targeted liposomes can take place (B). After binding, liposomes may be internalized (C) resulting in intracellular drug release (D).

The therapeutic efficacy of targeted liposomes is dependent on the number of antigens available for binding on the cell surface⁴⁹. Heterogeneity in antigen expression within a tumor may lead to reduced efficacy; moreover, some antigen-negative cells might be affected simply due to their location close to antigen-positive cells. This so-called bystander effect might occur when the drug is released from the carriers into the tumor interstitial space and can be taken up by other cells, resulting in sometimes unwanted cytotoxicity⁵⁰. Additionally, shedding or downregulation of antigens is counterproductive, as this might lead to binding competition or loss of specificity, which in the end causes loss of efficacy or adverse effects. If non-internalizing ligands are used, the liposomes will attach to the cell surface where over time the drug is released and taken up as free drug. In contrast, liposomes can be coated with internalizing ligands which initiate receptor-mediated endocytosis and help internalize the drug and/or carrier^{51,52}. A higher dose of drug will be released into the cell with internalizing ligands, resulting in a higher efficacy compared to non-internalizing liposomes⁵³. Some studies have even suggested that internalization is a prerequisite for efficient cytotoxicity⁵⁴⁻⁵⁶. Additionally, upon cellular uptake, the drug has to be capable of surviving the endosomes and lysosomes it may end up in. Free drugs such as doxorubicin are readily taken up by cells via passive diffusion, whereas other drugs can use cell membrane transporters.

Aside from liposomal doxorubicin, various other formulations have made it to the clinic or are in preclinical development⁵⁷. Liposomal vincristine⁵⁸ and liposomal irinotecan⁵⁹ were approved by the US Food and Drug Administration (FDA) for lymphoblastic leukemia in 2012 and metastatic pancreatic cancer in 2015, respectively. Others remain in clinical trials, and include liposomal formulations containing cytarabine/daunorubicin⁶⁰, mitoxantrone, cisplatin, or paclitaxel. Usually after initial FDA approval of the nanoparticle, extended approval is sought for additional cancer types or combination therapies and further optimization of the nanoparticle is performed. Currently, HER2-targeted liposomal doxorubicin has reached a phase II clinical trial⁶¹. Cationic liposomes functionalized with an anti-transferrin receptor antibody are used to deliver a wildtype p53 sequence to restore p53 tumor suppressor gene function in humans⁶². PSMA-targeted polymeric nanoparticles containing docetaxel are being used in phase I clinical trials for prostate cancer^{63,64}. In addition, other ligands such as RGD, folate and transferrin have been used to target cellular adhesion molecules or growth-factor receptors, respectively. Despite their lack of specificity due to their ubiquitous expression, these ligands are currently used in various imaging and treatment regimens^{65,66}.

The use of targeted liposomes has been controversial with studies advocating improved efficacy^{67,68}, and studies showing no improvements in survival due to instability of drug loaded liposomes or a lack of liposome internalization^{69,70}. Nonetheless, current research remains focused on improving specificity, bioavailability and efficacy with the help of targeting ligands. Where targeting ubiquitous ligands, like folate and

transferrin, has lacked specificity, monoclonal antibodies have been more specific towards tumor antigens yet have increased immune related adverse effects. To combine the specificity of antibodies with a lesser involvement of the body's immune system, smaller antibody fragments have been generated.

HEAVY CHAIN ANTIBODIES

Monoclonal antibodies have been around for quite some time and are used in the clinic as therapy against various diseases, including cancer. Normally immunoglobulin-gamma (IgG) antibodies have two identical heavy chains and two identical light chains and it is highly conserved in mammals⁷¹. The heavy and light chains which make up a full antibody can be divided into domains, four for the heavy chains and two for the light chains. The N-terminal domain of both chains is highly variable and is called the variable domain. Both variable domains of the heavy and light chain compose the antigen-binding site or paratope, with the heavy chain variable region being primarily responsible for the binding specificity. The other, more conserved regions are called constant domains, where the two last regions of the heavy chain (Fc region) are necessary for the recruitment of immune cells. This happens through binding Fc receptors on for example macrophages, which unfortunately leads to high liver and spleen uptake of antibody functionalized drugs.

Antibodies targeted against tumor-associated antigens can be useful in a number of ways. First of all, diagnosis through imaging and real time imaging of tumors can be used to aid surgery or to ascertain efficacy of given anticancer treatment. Secondly, antibodies can have an effect via receptor binding and inhibit tumor cell growth and proliferation, or induce apoptosis by suppression of signal transduction. Thirdly, antibodies can deliver therapeutic loads via nanoparticles, drug-conjugates or radionuclide antibody-conjugates. Currently, 62 monoclonal antibodies have been approved for therapy by the FDA and numerous more are in development⁷². Despite their tremendous contribution to medicine, monoclonal antibodies have some disadvantages. They are large molecules (150 kDa, 14.2 x 8.5 nm)⁷³ which have a typical half-life of several days⁷⁴. Although the long exposure is an advantage in some applications, it also leads to immune reactions that are counteractive. The majority of monoclonal antibodies are produced by generating hybridomas, which involves fusing a tumor myeloma cell with an antibody-producing cell from an immunized mouse⁷⁵. These murine antibodies can give rise to human anti-mouse antibodies and immune responses in the patient leading to increased clearance, decreased accumulation and adverse effects⁷⁶. Their large size inhibits tumor penetration and biodistribution, impairing successful application as an anticancer therapy. To improve pharmacological properties, antibodies have been developed with a reduction in size⁷⁷. One particular type of antibody was discovered in

camels as described by Hamers-Casterman et al. in 1993. Camels and other members of the biological family Camelidae were found to express antibodies devoid of a light chain and lacking the first constant domain (CH1). It has been suggested that an extended spacer replaces the CH1 region⁷⁸. Normally, all mammals contain antibodies with two heavy chains and two light chains, but in humans with heavy chain diseases⁷⁹, heavy chain antibodies can be produced as a result of a genetic deletion, although these antibodies are nonfunctional^{80,81}. In addition, the production of antibodies lacking a light chain and CH1 has been observed in nurse sharks, wobbegong, and other species⁸². The expression of heavy-chain antibodies is variable, since conventional IgGs are also expressed in camelids. In camels, heavy-chain antibodies can account for up to 80% of circulating antibodies, whereas in South American camelids (llamas, alpacas) it only accounts for 10-25%⁸³. Conventional antibodies are generated by recombination and selection of V, D, and J elements, each of which are sequentially organized as multiples in the gene locus. The variability increases exponentially by selection of differently recombined copies and, through further hypermutation of the variable regions, a repertoire of antibodies is created, which can be expanded when needed to repel invaders. Somatic hypermutations and selection during maturation of the antibodies can increase the diversification⁸⁴. Nucleotide mutations were found upstream of the first antigen-binding loop, which create additional somatic hypermutation hotspots. These hotspots enable easy mutation of amino acids during the affinity maturation process^{85,86}.

The camelid genome contains constant region elements to produce both conventional heavy chain and heavy-chain(-only) antibody in the same locus⁸⁷. To eliminate the CH1 region, the constant region sequence carries a point mutation that leads to a change in RNA splicing and “skipping” of the CH1 region from the mRNA⁸⁸. Mimicking this mutation in mice does not lead to heavy-chain antibodies, but the deletion of the entire CH1 exon does lead to the successful generation of heavy-chain antibodies⁸⁹. Whereas conventional antibodies have two domains contributing to the antigen-binding site, the heavy-chain antibodies have only one domain and thus a less diverse paratope. The two constant domains (CH2 and CH3) of the heavy-chain antibodies are linked by a hinge region connecting it to a variable domain (VHH)⁷⁸. The variable domain of the heavy-chain antibody can be isolated relatively easily after immunization of a camelid, after which VHHs can be cloned and used for selection through, for example, phage display^{90,91}. Phage display and other selection techniques, such as yeast and ribosome display, enable selection of high affinity antibodies⁹². These VHHs are also called single domain antibodies or nanobodies, due to their size in the nanometer range.

NANOBODIES

VHs contain four conserved framework regions interspersed with three hypervariable complementary-determining regions (CDR), which are complementary to the epitope surface and play a major role in antigen recognition and binding⁹³. The hypervariable regions form loops, which in conventional antibodies can be structured to recognize small molecules, linear peptides or large proteins by formation of a cavity, groove or flat surface⁹⁴. In the absence of a light chain, highly conserved hydrophilic amino acids (usually) replace four hydrophobic amino acids that are normally used for binding to the light chain and promote solubility of the heavy-chain antibody^{95,96}. To compensate for the loss of the variable light chain domain, the loops in the variable domain of heavy-chain antibodies can be longer than conventional antibodies⁸⁵. It can be expected that a longer loop is more flexible, yet has a lower binding capacity. Therefore the loops in VHs are constrained with disulfide bonds⁹⁷. Especially, the first and third antigen-binding loops have more cysteine residues to facilitate inter- and intraloop disulfide bonds than its conventional antibody counterparts^{98,99}. The loop increases the potential antigen-binding surface by protruding from the rest of the binding site¹⁰⁰. When heavy-chain antibodies are generated in mice the variable domains are very similar in length compared to regular antibodies. Nanobodies (only the variable domain; 15 kDa, 4.2 x 2.5 nm)⁹³ are much smaller than monoclonal antibodies and have protruding CDR loops to interact with antigens with CDR3 being responsible for 60-80% of antigen binding^{101,102}. The three-dimensional shape of a nanobody is prolate (rugby ball-like) and thus exposes a convex paratope, which enables easier access to difficult to reach epitopes¹⁰².

Although nanobodies are derived from the Camelidae family, it has been reported that for application in humans, the immunogenicity is low and anti-drug antibodies are absent¹⁰³⁻¹⁰⁷. This is probably a result of the large sequence homology with the human VH III gene family^{108,109}. Nevertheless, a discourse continues, with groups reporting significant immune adverse events and the presence of autoantibodies¹¹⁰⁻¹¹². This has led to humanization strategies of amino acids differing between human and camelid variable domains¹¹³. After *in vivo* administration of nanobodies, these small molecules distribute throughout the body, penetrating most tissues¹¹⁴. Although, with a size below the renal molecular weight cut-off, nanobodies will be rapidly cleared¹¹⁵. When labeled with a radionuclide or fluorophore, these characteristics make nanobodies ideal as *in vivo* imaging tools^{106,116}. Additionally, the use of an alpha or beta emitting radionuclide conjugated to the nanobodies can be used for targeted radionuclide therapy or so-called radioimmunotherapy (RIT)¹¹⁷. The high specificity of nanobodies is combined with a high dose of radiation which damages the cancer cells and causes minimal damage to healthy tissue. One major disadvantage is kidney retention of nanobodies, although

this can be reduced by removing the His-tag from nanobodies, by co-injection of the positively charged plasma-expander GeloFusin¹¹⁸, or by generation of His-tag free nanobodies.

In the treatment of cancer, nanobodies can be used in a similar manner as monoclonal antibodies; for the imaging of tumors, direct antagonistic effects via receptor binding or as targeting modality for drug delivery systems. Nanobodies are very efficient for the imaging of tumor cells, due to a homogeneous distribution in most tumors¹¹⁹. As antagonists, nanobodies are less efficacious, since they lack an Fc domain and cannot initiate the complement immune system¹²⁰. Despite this, nanobodies have been developed which inhibit tumor growth by targeting EGFR¹²¹, HGF¹²², CXCR7¹²³, and VEGF-A¹²⁴ and VEGFR2¹²⁵. Finally, nanobodies can be used to functionalize nanoparticles or drug-conjugates to specifically target tumor cells¹²⁶. In this case, the small size and low immunotoxicity of the nanobodies works together with the nanoparticles' capability to deliver large drug doses, while protecting the body against systemic toxicity. Although the large size of the nanoparticles impairs tumor penetration compared to nanobodies alone, the prolonged circulation time enables sufficient accumulation via the EPR effect, which includes poor lymphatic drainage^{127,128}. A number of drug delivery systems have been described using nanobodies for targeting. For example, IGF-1R kinase inhibitor-loaded liposomes were targeted against EGFR to facilitate simultaneous blocking of both receptors¹²⁹. EGFR-targeted micelles loaded with doxorubicin were effective inhibitors of tumor growth¹³⁰. Polymersomes have been developed containing nanobodies targeted against HER2 and PlexinD1^{131,132}. Besides the use in anticancer therapy, nanobodies can be used in the treatment of infections, inflammations, and in neurodegenerative diseases, as has been reviewed elsewhere¹³³.

There are some downsides to the use of nanobodies instead of conventional antibodies. Partially due to their monovalent nature, most nanobodies have a lower affinity/avidity than bivalent antibodies. In some instances this is a benefit, for example if the binding site barrier effect is taken into account, but in general, higher affinities are preferable. Luckily, affinity maturation processes have been developed to improve antibody affinities¹³⁴. For instance an error-prone PCR can be applied on the desired nanobody to generate a highly diversified nanobody library¹³⁵. In addition, the reduced affinity of nanobodies can be compensated with the use of nanoparticles. Depending on the size of the antibody fragment, up to hundreds of antibodies can be attached to the surface of a nanoparticle. This in turn will lead to a high affinity of targeted nanoparticles. Although, studies have also shown that a higher affinity does not always lead to a higher accumulation¹³⁶. In addition, tumor penetration will be impaired due to the binding-site barrier effect where the first target encountered will bind the antibody permanently¹³⁷⁻¹³⁹. A second downside, is the relatively expensive immunization of camelids, although transgenic mice have been developed expressing hybrid human

or llama antibody loci where conventional antibody development is blocked by using endogenous heavy (and light) chain knockout mice^{89,140,141}.

Recent developments show major improvements on the use of conventional antibodies and novel antibody formats have enabled the production of highly specific and low immunogenic anticancer therapies, in addition to several other applications.

THE ENHANCED PERMEABILITY AND RETENTION EFFECT

First described in 1986, the enhanced permeability and retention (EPR) effect is based on observations that most solid tumors have a defective blood vessel architecture and usually produce various vascular permeability factors¹⁴². Newly formed tumor blood vessels have an abnormal architecture, defective endothelial cells, lack of a smooth muscle layer and an irregular vascular alignment^{143,144}. Tumor vessels show an enhanced vascular permeability, which ensures the tumor of sufficient nutrients and oxygen needed for rapid growth. In addition, an impaired lymphatic system was observed that increased retention of macromolecules in the tumor^{142,145}. Increased permeability of tumor blood vessels facilitates increased extravasation of macromolecules compared to normal blood vessels. The tumor vessels lack tight junctions between their endothelial cells^{146,147}. The gaps in tumor vessels range from 100-600 nm¹⁴⁸, enabling extravasation of almost all nanoparticles into the interstitial space. However, the impaired lymphatic system in tumors may increase osmotic pressures within large tumors, resulting in an impaired accumulation or even an outflow of nanoparticles¹⁴⁹. The EPR effect is highly dependent on the molecular size, which needs to be larger than the renal clearance threshold (> 40 kDa) to enable longer circulation times and slow body clearance. The size of the drug or nanoparticle has a large effect on tumor penetration, which is highly heterogeneous¹⁵⁰⁻¹⁵³. Clearance from circulation by macrophages, Kupffer cells or scavenger receptors is just as important as size, where more biocompatible molecules have a longer plasma half-life and eventually a bigger chance of extravasation.

Tumors show a high degree of morphological heterogeneity, which means that the EPR effect is not always present in the entire tumor or in every stage of tumor progression. Larger tumors often have a hypovascular or necrotic core which reduces the chance of nanoparticle extravasation¹⁵⁴, whereas small early stage tumors often show a high vascular density (hypervascularity)¹⁵⁵. Tumor tissue is surrounded by the extracellular matrix (ECM), which in addition to facilitating tumor-associated angiogenesis, promotes metastasis and the generation of a tumorigenic microenvironment. It is also a major bottleneck for macromolecular drugs, since the ECM in tumors is abnormally structured and more dense than in normal tissues^{156,157}.

Extravasation of nanomedicine is the rate-limiting step of liposomal accumulation and is dependent on the EPR effect. The presence or degree of the EPR effect relies

on many parameters within the tumor and tumor microenvironment, and predictors remain to be elucidated. Therefore the promise of liposomal accumulation in the tumor via the EPR effect has been discussed controversially^{150,158}, yet it is clear that targeting modalities are ineffective without access to the tumor tissue. Luckily, vascular permeability can be increased by the use of chemicals, hyperthermia and other methods, which allow enhanced liposomal accumulation in tumors^{159,160}.

MILD HYPERTHERMIA

The goal of increasing the *in vivo* stability of liposomes has led to an undesirable side effect; the drug remains encapsulated and is released slowly from the liposomes which results in decreased bioavailability. To circumvent this issue, modes of triggered drug release have been extensively investigated and includes the use of heat, ultrasound and pH, among others¹⁶¹⁻¹⁶⁶. Here we will focus on triggered drug release upon application of heat, which has the added benefit of increasing liposomal accumulation in the tumor by enhancing vascular permeability (Figure 2)^{160,167}. Release of the drug from liposomes based on mild hyperthermia (40-43°C) was first described by Yatvin and Weinstein^{168,169}, and liposomes capable of hyperthermia triggered release are termed thermosensitive liposomes. The goal of thermosensitive liposomes is to minimize

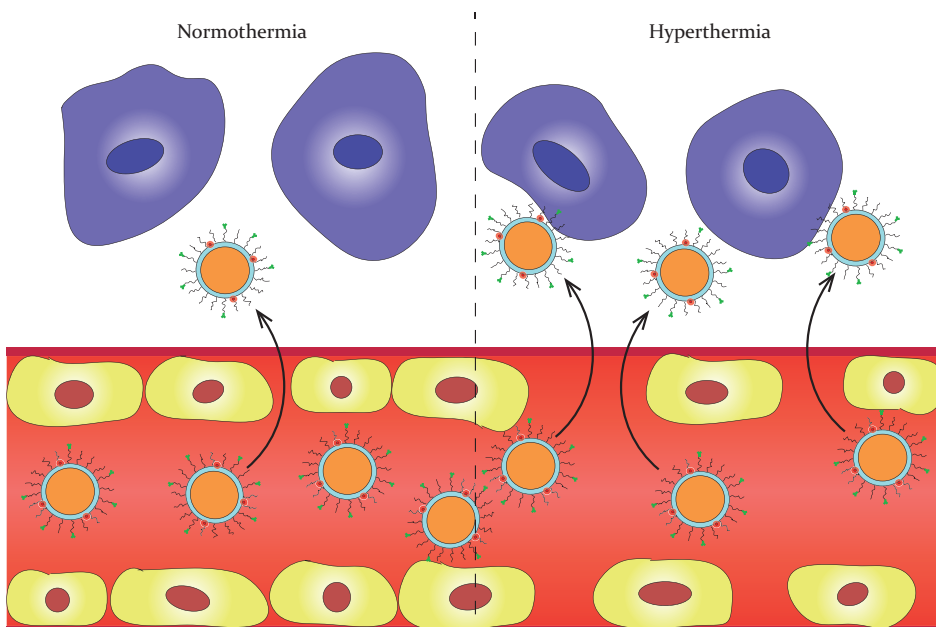


Figure 2. Increased liposomal extravasation after pretreatment of the tumor with mild hyperthermia.

unwanted drug leakage during circulation at physiological temperatures and a quick drug release upon application of mild hyperthermia.

Thermosensitive formulations are based on the melting phase transition temperature (T_m) of the lipids, which indicates the temperature at which the lipids transfer from a solid gel phase to a liquid-crystalline phase. The original formulation used by Yatvin et al. was made with 1,2-dipalmitoyl-*sn*-glycero-3-phosphocholine (DPPC, $T_m = 41.4^\circ\text{C}$) and 1,2-distearoyl-*sn*-glycero-3-phosphocholine (DSPC, $T_m = 54.9^\circ\text{C}$) in a molar ratio of 3:1¹⁶⁸. The composition of lipids determines the permeability to water and hydrophilic drugs, where the liposomes are more permeable in the liquid-crystalline phase¹⁷⁰⁻¹⁷². In addition, it has been suggested that permeability is highest around the transition temperature, due to the formation of grain boundaries between solid and liquid phase areas¹⁷³⁻¹⁷⁵. Continued heating past the transition temperature leads to a reduction in the interfacial areas and eventually into a pure liquid phase which is accompanied by a reduction in permeability¹⁷¹. Thermosensitive liposomes can also be formulated using lysolipids, a product of phospholipid hydrolysis which can act as detergents in the presence of lipid membranes and have been reported to create hydrophilic pores along liquid-solid boundaries^{171,176}. A further development has been the incorporation of cholesterol and PEG lipids to generate stealth thermosensitive liposomes, which circumvents the low circulation times of conventional liposomes^{177,178}.

ThermoDox is a lysolipid thermosensitive liposomal formulation encapsulating doxorubicin that releases the drug upon a mild hyperthermia treatment of 42°C ¹⁷⁹. Clinical studies in ovarian cancer (phase I) and breast cancer (phase I/II) are underway. In a clinical phase III trial (HEAT study) it was shown that a combination of image-guided radiofrequency ablation (RFA) with ThermoDox did not produce a therapeutic doxorubicin concentration in primary liver cancer, although it was suggested that a standardized dwell time of more than 45 min might increase clinical efficacy of ThermoDox (ongoing OPTIMA study)¹⁸⁰. For this drug the mechanism of intravascular release is used, where prior to administration the tumor site is heated so that the release of doxorubicin occurs within the tumor blood vessels damaging perivascular tumor cells and tumor associated endothelial cells¹⁸¹. It was shown that thermosensitive liposomes release their drug intravascularly upon application of localized hyperthermia¹⁸¹. As a result a high dose of free drug was able to penetrate the tumor tissue deeper than controls with free drug or Doxil. It is important to note that the higher dose of drug delivered to the tumor might also be attributed to an increase in vascular permeability as a consequence of the hyperthermia treatment¹⁸².

Thermosensitive liposomes have been developed further and are currently equipped with targeting moieties to enhance specificity^{183,184}. In recent years, thermosensitive liposomes targeted against HER2¹⁸⁵, CD13¹⁸⁶, and the folate receptor¹⁸⁷ have been reported. Although the use of hyperthermia and other triggered release systems is clearly

beneficial in that it enables the localized delivery of a high drug dose to the tumor, its application remains limited to superficial or otherwise accessible tumors. Disseminated metastatic disease remains the major cause of cancer related mortality and thus there is an urgent need to improve on current drug delivery systems to enhance targeted drug delivery. Current research is therefore focused on enhancing specificity and bioavailability of liposomal chemotherapy.

AIMS AND SCOPE OF THIS THESIS

There still is an urgent need for the development of effective treatments against various unresectable and metastatic cancers. This thesis explores the development of targeted nanoparticles that could overcome current challenges in anticancer therapies, such as drug resistance, adverse drug-related effects and limited drug accumulation in the tumor. In addition, we have tried to elucidate the factors influencing the aforementioned issues.

Chapter 2 describes the production and characterization of novel heavy-chain antibodies against the cell surface antigen MUC1.

In **Chapter 3**, we applied novel anti-PSMA nanobodies as a tool to image prostate cancer by site-specific labeling with indium-111.

In **Chapter 4**, the anti-PSMA nanobodies were used as a targeting moiety by conjugation with doxorubicin-loaded liposomes. The efficacy of targeted and non-targeted liposomes was determined with and without hyperthermia to increase vessel permeability.

Chapter 5 investigates the impact of the enhanced permeability and retention (EPR) effect on the accumulation of liposomes in various tumor types and attempts to elucidate the factors regulating this effect.

In **Chapter 6**, the efficacy of thermosensitive liposomes after 1- and 2-step hyperthermia protocols was investigated before further studies into the effect of tumor morphology on liposomal accumulation.

Chapter 7 discusses the results of these studies in light of current developments in nanomedicine, antibody research and imaging.

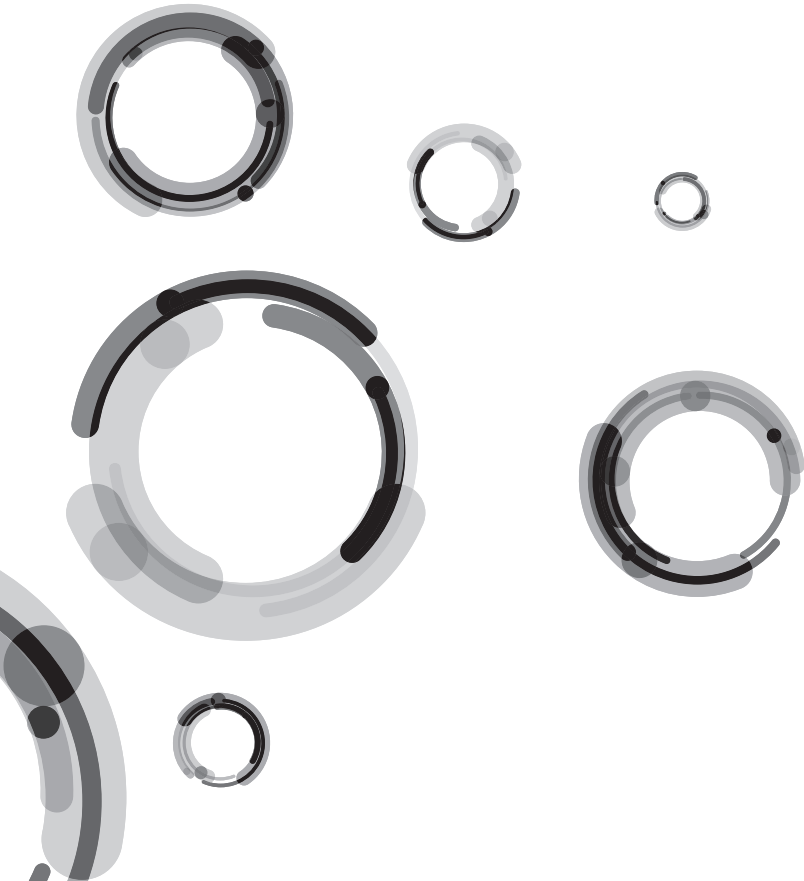


CHAPTER 2

Generation of Novel Heavy-Chain Antibodies against MUC1

Michiel Bolkestein, Dubravka Drabek, Rien van Haperen,
Alexander M.M. Eggermont, Frank Grosveld, Gerben A. Koning

In preparation



INTRODUCTION

Heavy-chain antibodies are produced naturally in the Camelidae species, where in the absence of a light chain, the antigen binding site is completely formed by the single heavy chain variable domain^{78,188}. Camelid variable domains may display surface loops longer than conventional human antibodies⁸⁵. To avoid cumbersome immunization of Camelids, transgenic mice have been generated, which are able to generate antigen specific humanized heavy-chain antibodies (HCAs) upon immunization⁸⁹. The first generated transgenic mice contained two llama variable regions (VHH), while later generation transgenic mouse lines utilizes human variable regions (VH). All transgenic mouse lines are made in a mouse heavy-chain knockout background to prevent rearrangement and expression of endogenous mouse immunoglobulins¹⁸⁹. Antibody production is maintained by long-lived antibody producing cells migrating to survival niches within the bone marrow and spleen¹⁹⁰⁻¹⁹².

MUC1 is a large transmembrane mucin protein which, when glycosylated, extends 200-500 nm above the cell membrane¹⁹³. The extracellular region of MUC1 is composed of a variable number of 20 amino acid repeats that are enriched in serine, threonine and proline residues. It is overexpressed in epithelial cancer cells where it is abnormally glycosylated with short oligosaccharides¹⁹⁴⁻¹⁹⁶. MUC1 is usually expressed on the apical surface of epithelial cells, yet in tumor cells it is expressed over the entire cell surface¹⁹⁷. Increased MUC1 levels have been reported in the blood of patients with breast cancer^{198,199} and ovarian cancer²⁰⁰, and is associated with metastatic competence and poor prognosis^{201,202}. MUC1 mediated signaling influences metabolic pathways, which support tumor cell growth and invasiveness²⁰³.

The aim of this study was to generate high affinity MUC1-specific antibodies and conjugate them to liposomes as a drug delivery system to MUC1-overexpressing cancer cells. To this end, transgenic mice were immunized with a peptide representing the 20-amino acid tandem repeat present in the extracellular region of MUC1. Using direct cloning of plasma cell repertoires into eukaryotic HCAs vectors yielded a HEK cell antibody library. Screening of the library resulted in a number of antigen specific HCAs that recognize the peptide used for immunization, but also the MUC1 expressed on the surface of MUC1 positive cancer cells. These will be used for conjugation to liposomes and further cell binding experiments. In future studies, this antibody-liposome platform can be used for targeted delivery of chemotherapeutics to MUC1-positive tumors.

MATERIALS AND METHODS

Immunization

All animal experiments were approved by the Committee on Animal Research of the Erasmus MC (Rotterdam, the Netherlands). Transgenic mice were immunized with MUC1 tandem repeat peptide, PDTRPAPGSTAPPAHGVTSA, conjugated to keyhole limpet hemocyanin (KLH) (Bio-Synthesis Inc. Lewisville, TX) dissolved in PBS using Stimune adjuvant (Thermo Fisher Scientific Inc., Waltham, MA). Mice were injected s.c. with 20 µg of peptide conjugate, 6 times with two weeks intervals. 4 d after the last i.p. injection, mice were sacrificed and plasma cells were isolated from the spleen and bone marrow.

Plasma cell isolation and library construction

A single cell suspension was made in 0.5% BSA, 2 mM EDTA in PBS, from the spleen, femurs and tibias of the transgenic mice. Magnetic cell sorting of CD138-positive cells was performed using a mouse CD138+ plasma isolation kit (Miltenyi Biotec GmbH, Germany), which first depletes non-plasma cells (by indirect labeling of CD49b and CD45R) and then enables selection of plasma cells (by direct labeling of CD138). Plasma cells eluted from the column were centrifuged and resuspended in 400 µL Ultraspec™ RNA reagent (Biotecx Laboratories Inc, Houston, TX). Total RNA was prepared according to manufacturer's instructions and dissolved in dH₂O before first strand cDNA synthesis using SuperScript™ II RT (Invitrogen, Carlsbad, CA) using oligo dT priming. RT-PCR was performed using specific primers, forward from leader sequences and reverse from G2/G3 hinge region, and high fidelity DNA polymerase Phusion (Finnzymes, Finland) with an annealing temperature of 68°C and 35 cycles in total. PCR products were cut with PvuII/BstEII and cloned into pCAGhygroG2 vector containing an Ampicillin resistance gene for bacterial selection and a Hygromycin B (Thermo Fisher Scientific Inc.) resistance gene for eukaryotic selection. Ligations were performed o/n at 16°C.

Preparation and transfection into HEK293 cells

1 µL of 5x diluted ligation product was used to transform electrocompetent MegaX DH10B T1R cells (Invitrogen) according to manufacturer's instructions. The resulting product was plated on 2xTY/Amp agar plates and 1920 individual colonies were picked and incubated o/n in 1.5 mL of 2xTY/Amp medium in 96-well format. DNA plasmid preparations were made using NucleoSpin 96 Plasmid (Macherey-Nagel GmbH, Germany). An estimated 200 ng of DNA was used for transfection into HEK293 cells. HEK cells were plated in 96-well plates and transfected using Lipofectamine 2000 Transfection Reagent (Thermo Fisher Scientific Inc.) according to the manufacturer's

instructions. The next day, hygromycin B (final concentration of 200 µg/mL) medium was added to the medium (DMEM medium supplemented with non-essential amino acids (NEAA, Lonza, Belgium), 10% fetal bovine serum (FBS) and penicillin and streptomycin (P/S; Lonza). After 4 d, 50 out of 200 µL of medium was taken per well to perform an antigen specific ELISA.

Antigen specific screening ELISA and sequencing

ELISA plates were coated o/n at 4°C with 10 µg/mL MUC1-peptide conjugated to BSA. Plates incubated with BSA alone were used as a negative control. After washing with PBS/Tween 0.5% and PBS, the plates were blocked for 1 h with 2% milk in PBS (w/v). Plates were further washed three times with PBS/Tween 0.5% and PBS. 50 µL of the HEK cells supernatant were added to the plates with 50 µL of 4% milk in PBS (w/v) and incubated for 2 h at room temperature. After another washing step, 50 µL of goat anti-human IgG peroxidase (1:5000) in 2% milk in PBS was added to the wells and incubated for 1 h. A final washing step was performed before addition of 50 µL BM Blue POD substrate (Roche). The reaction was stopped with H₂SO₄ and the plate was analyzed on an ELISA plate reader. Sequencing of positive DNA clones was done using the primer VH3-23 leader 5'-TACACCGGTCCACCATGGAGT-3'.

Purification, cell binding and affinity measurements

Positive clones were stably transfected into HEK293 cells and these were used for production of specific heavy-chain antibodies against MUC1. In short, 4 x 10⁶ cells were seeded in 145 mm culture dishes and grown in DMEM + 10% FBS till semi-confluent. The medium was changed to serum free production medium, OptiMEM Glutamax (Thermo Fisher Scientific Inc.). The production medium was harvested and cell free medium was used to purify HCAs on Protein A agarose (Sigma Aldrich). HCAs were eluted with 3 M KCN and dialyzed 3 times against PBS, before use in other experiments.

The pancreatic cell line, CFPAC-1, was used to test the specificity of the generated MUC1 HCAs and was obtained from the American Type Culture Collection (ATCC, Manassas, VA). Cell culture reagents, unless otherwise specified, were obtained from Sigma-Aldrich, St. Louis, MO. CFPAC-1 was grown in Dulbecco's Modified Eagle Medium (DMEM) supplemented with 10% FBS and P/S, and was routinely cultured in a well humidified incubator at 37°C and 5% CO₂.

Cell binding was established with flow cytometry analysis, for which cells were harvested by trypsinization and resuspended in cold PBS (Sigma-Aldrich) containing 1% BSA (Sigma-Aldrich). Cell suspensions were incubated with HCAs at a concentration of 50 µg/mL for 30 min at 4°C. Post incubation, the cells were washed twice with cold PBS/1% BSA and incubated with a secondary antibody against human IgG conjugated to FITC (goat-anti-human IgG FITC, Anogen Biotech Laboratories Ltd., Toronto,

Canada) After a second wash, the cells were subjected to flow cytometry analysis using the LSRFortessa cell analyzer (BD Biosciences, Franklin Lakes, NJ). Data analysis was performed using the FlowJo software (TreeStar Inc, Ashland, OR).

Affinity measurements were performed using the Octet QK (Forte Bio, Menlo Park, CA). Briefly, after pre-hydration anti-human IgG Fc coated tips (FortéBio) were dipped in PBS for 300 s to obtain a stable baseline signal. The tips were loaded with anti-MUC1 HCAs for 180 s in a concentration range from 0 to 20 $\mu\text{g}/\text{mL}$ in PBS, before another baseline step of 600 s in PBS. Then association with MUC1 peptide (10 $\mu\text{g}/\text{mL}$) was ascertained over 600 s before dissociation over 900 s in PBS. The association and dissociation curves were fitted to a 1:1 binding model and the dissociation constant (Kd) was calculated using Octet software.

RESULTS AND DISCUSSION

Generation of heavy-chain antibodies

The immunized transgenic mice successfully produced HCAs, which are lacking a CH1 region (Figure 1A). The entire procedure from immunization up to screening of antigen-specific HCAs is depicted in Figure 1B. From the MUC1 specific ELISA screen, 150 clones were found positive based on comparison with a negative control (BSA coated plates). The corresponding cDNA was sequenced, which showed a certain degree of homology between various antibodies. Out of 150 clones 73 were unique (data not shown), and based on the CDR3 regions, the HCAs were classified into distinct groups of which 18 clones were selected for further testing (Figure 2). These antibodies were generated and produced in a relatively short period of time (*circa* 2-3 months), in comparison to other techniques, such as hybridoma production or phage display selection followed by bacterial or yeast expression. Further expansion and production of antibodies can be done in mammalian cells in a limited time span.

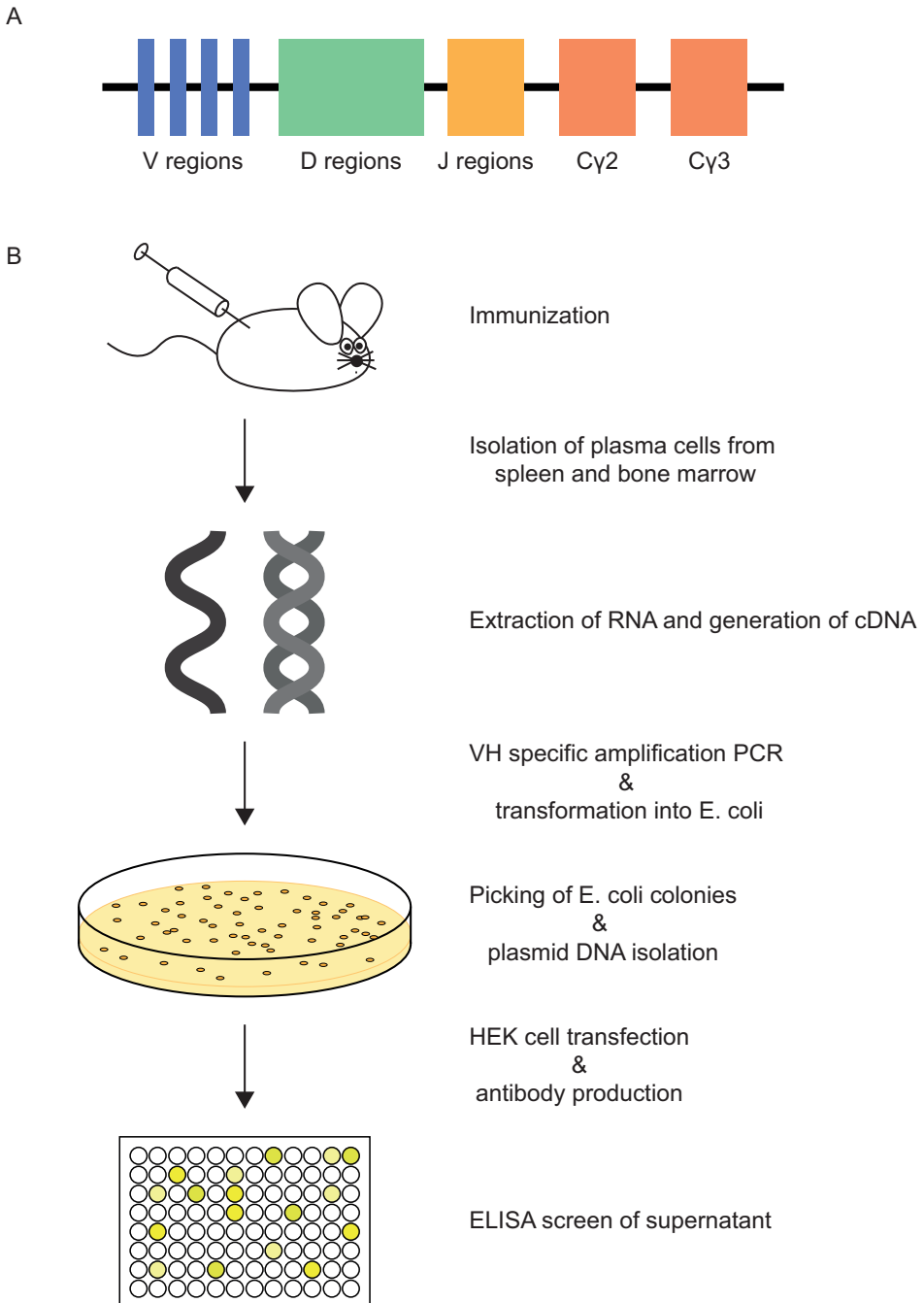


Figure 1. Human HCAb locus construct used for transgenesis, containing human V, D and J regions and constant regions lacking the CH1 domain (A). Schematic overview of the experimental procedure followed to obtain heavy-chain antibodies from transgenic mice (B).

```

          CDR1                CDR2                CDR3
6C2:  EVQLVESGG...SVYV...MHVVRQAPGKGLEWAV IYVD...GSKN YYADSVK...GRFTISRDNKNTLYLQMSLRAEDTAVYVC AREGTMYRGAL-----DY WQ0GTLTVSS
5C6:  EVQLVESGG...SVYV...MHVVRQAPGKGLEWAV IYVD...GSKN YYADSVK...GRFTISRDNKNTLYLQMSLRAEDTAVYVC ARESYCGGACVF-----DY WQ0GTLTVSS
4D11: EVQLVESGG...SVYV...MHVVRQAPGKGLEWAV IYVD...GSKN YYADSVK...GRFTISRDNKNTLYLQMSLRAEDTAVYVC ARGVERRYVYVGM-----DY WQ0GTLTVSS
5F7:  EVQLVASSG...GVVQGRSLRLSCAAS GFTF...SSYV MRVGRQAPGKGLEWAV IYVD...GSKN YYADSVK...GRFTISRDNKNTLYLQMSLRAEDTAVYVC ARDISTDPF-----DY WQ0GTLTVSS
5B5:  EVQLQESGP...GLVNPSETLSLTCVAVS GHSIS...SGYV MWIROPKPKGLEWIGS IYHS...GST YNPSLKL...SRVTISVDTSKNQPSLKLSSVTAADTAVYVC ARVRLRFYVGM-----DY WQ0GTLTVSS
5F6:  EVQLQESGP...GLVNPSETLSLTCVAVS GHSIS...SGYV MWIROPKPKGLEWIGS IYHS...GST YNPSLKL...SRVTISVDTSKNQPSLKLSSVTAADTAVYVC ARVRLRFYVGM-----DY WQ0GTLTVSS
3G9:  EVQLQESGP...GLVNPSETLSLTCVAVS GGSII...SSYV MSWIRSPKPKGLEWIGR IYSS...GFT YNPSLKL...SRVTISVDTSKNQPSLKLSSVTAADTAVYVC ARGVCRTRSCGV-----DY WQ0GTLTVSS
3F6:  EVQLQESGP...GLVNPSETLSLTCVAVS GGSII...SSYV MSWIRSPKPKGLEWIGY IYYS...GST RYNPSLKL...SRVTISVDTSKNQPSLKLSSVTAADTAVYVC ARGVCRTRSCGV-----DY WQ0GTLTVSS
8G2:  EVQLQESGP...RLVKPSETLSLTCVAVS GGSII...SSYV MSWIRSPKPKGLEWIGY IYYS...GST RYNPSLKL...SRVTISVDTSKNQPSLKLSSVTAADTAVYVC ARGVCRTRSCGV-----DY WQ0GTLTVSS
4D8:  EVQLQESGP...GLVNPSETLSLTCVAVS GGSII...SSYV MSWIRSPKPKGLEWIGR IYYS...GST YNPSLKL...SRVTISVDTSKNQPSLKLSSVTAADTAVYVC ARGVCRTRSCGV-----DY WQ0GTLTVSS
5G12: EVQLQESGP...GLVNPSETLSLTCVAVS GGSII...SSYV MSWIRSPKPKGLEWIGR IYSS...GFT YNPSLKL...SRVTISVDTSKNQPSLKLSSVTAADTAVYVC ARGVCRTRSCGV-----DY WQ0GTLTVSS
3G8:  EVQLQESGP...GLVNPSETLSLTCVAVS GGSII...SSYV MSWIRSPKPKGLEWIGR IYYS...GST YNPSLKL...SRVTISVDTSKNQPSLKLSSVTAADTAVYVC ARGVCRTRSCGV-----DY WQ0GTLTVSS
8F6:  EVQLQESGP...GLVNPSETLSLTCVAVS GGSII...SSYV MSWIRSPKPKGLEWIGY IYDT...GST YNPSLKL...SRVTISVDTSKNQPSLKLSSVTAADTAVYVC ARGVCRTRSCGV-----DY WQ0GTLTVSS
7A8:  EVQLQESGP...GLVNPSETLSLTCVAVS GGSII...SSYV MSWIRSPKPKGLEWIGR IYYS...GNT YNPSLKL...SRVTISVDTSKNQPSLKLSSVTAADTAVYVC ARGVCRTRSCGV-----DY WQ0GTLTVSS
3F5:  EVQLQESGP...GLVNPSETLSLTCVAVS GGTII...SGYV MSWIRSPKPKGLEWIGR IYMS...GST YNPSLKL...SRVTISVDTSKNQPSLKLSSVTAADTAVYVC ARGVCRTRSCGV-----DY WQ0GTLTVSS
5C2:  EVQLQESGP...GLVNPSETLSLTCVAVS GGTII...SGYV MSWIRSPKPKGLEWIGR IYSS...GST YNPSLKL...SRVTISVDTSKNQPSLKLSSVTAADTAVYVC ARGVCRTRSCGV-----DY WQ0GTLTVSS
5F2:  EVQLQESGP...GLVNPSETLSLTCVAVS GGTII...SGYV MSWIRSPKPKGLEWIGR IYSS...GNT YNPSLKL...SRVTISVDTSKNQPSLKLSSVTAADTAVYVC ARGVCRTRSCGV-----DY WQ0GTLTVSS
6B2:  EVQLQESGP...GLVNPSETLSLTCVAVS GGTII...SGYV MSWIRSPKPKGLEWIGR IYSS...GST YNPSLKL...SRVTISVDTSKNQPSLKLSSVTAADTAVYVC ARGVCRTRSCGV-----DY WQ0GTLTVSS
    
```

Figure 2. Sequence alignment of 18 selected antibodies, which tested positive on the ELISA screen against the MUC1 peptide. Conserved regions in the CDR3 (blue) are shown with somatic hypermutations (red, yellow).

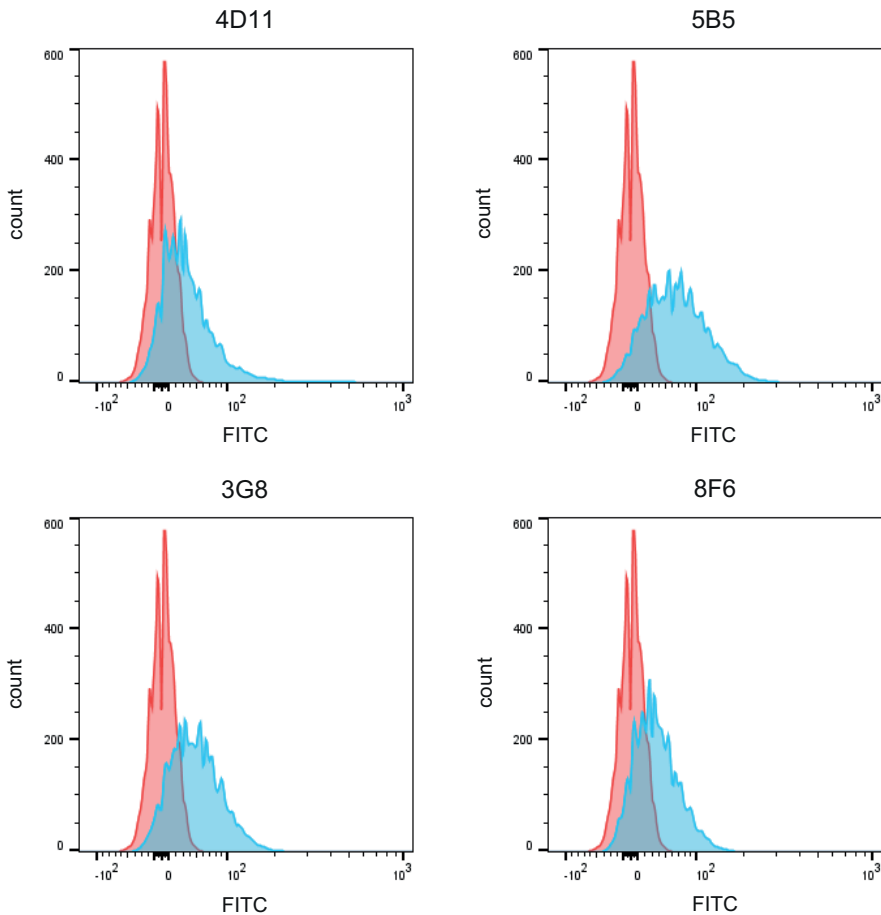


Figure 3. Cell binding of heavy-chain antibodies (HCAs, blue) compared to background (red) in MUC1 positive cell line CFPAC-1 depicted for four HCAs. Cells were incubated with 50 µg/mL of HCAs for 30 min followed by incubation with goat anti-human IgG-FITC secondary antibody (1:40). Y-axis, cell count; X-axis, FITC fluorescence.

Affinity and cell binding

Flow cytometry experiments were performed to assess binding of the HCABs to the MUC1-positive cell line CFPAC-1 (Figure 3, Table 1). Based on the mean fluorescence intensity we conclude that at least 4 antibodies show a moderate to good binding to CFPAC-1 cells. The moderate binding to CFPAC cells may be a result of the internalization of MUC-1, before recycling to the surface of the cells with 0.9% of receptors being recycled per minute²⁰⁴.

Table 1. Cell binding of heavy-chain antibodies to CFPAC-1

Heavy-chain antibody	MFI
6C2	4.7 (2.5 - 6.0)
5C6	4.0 (3.5 - 4.5)
4D11	34.7 (26.5 - 45.0)
5F7	12.3 (9.5 - 14.0)
5B5	68.3 (57.0 - 81.5)
5F6	2.0 (2.0 - 2.0)
3G9	2.7 (2.5 - 3.0)
3F6	2.5 (2.2 - 2.7)
8G2	4.7 (4.0 - 5.0)
4D8	2.0 (2.0 - 2.0)
5G12	2.3 (2.0 - 2.5)
3G8	30.3 (20.5 - 36.5)
8F6	24.7 (18.0 - 29.0)
7A8	17.0 (14.5 - 20.0)
3F5	7.3 (6.5 - 8.0)
5C2	7.7 (7.0 - 8.5)
2F2	4.3 (2.0 - 5.5)
6B2	3.3 (3.0 - 3.5)

Median fluorescence intensity is shown with 25th and 75th percentiles. All experiments have been performed 3 times.

These antibodies were tested for further binding on the Octet system, to determine avidity between HCABs and the MUC1 peptide (Figure 4). Nanomolar dissociation constants (Kd) were reached; 4D11 = $2.25 \pm 0.49 \times 10^{-9}$ M, 5B5 = $3.54 \pm 0.21 \times 10^{-9}$ M, which indicates moderate strength binding antibodies. This might be a benefit, since it has been shown that diabodies with low affinity scFv are more effective in accumulating in the tumor than higher affinity antibodies²⁰⁵. This might be explained by inhibition of tumor penetration due to irreversible association with peripheral antigen presenting cells^{206,207}.

By generating HCABs with human variable domains, we offer clinically interesting therapeutics with the benefits of antibody fragments. These are the more economical

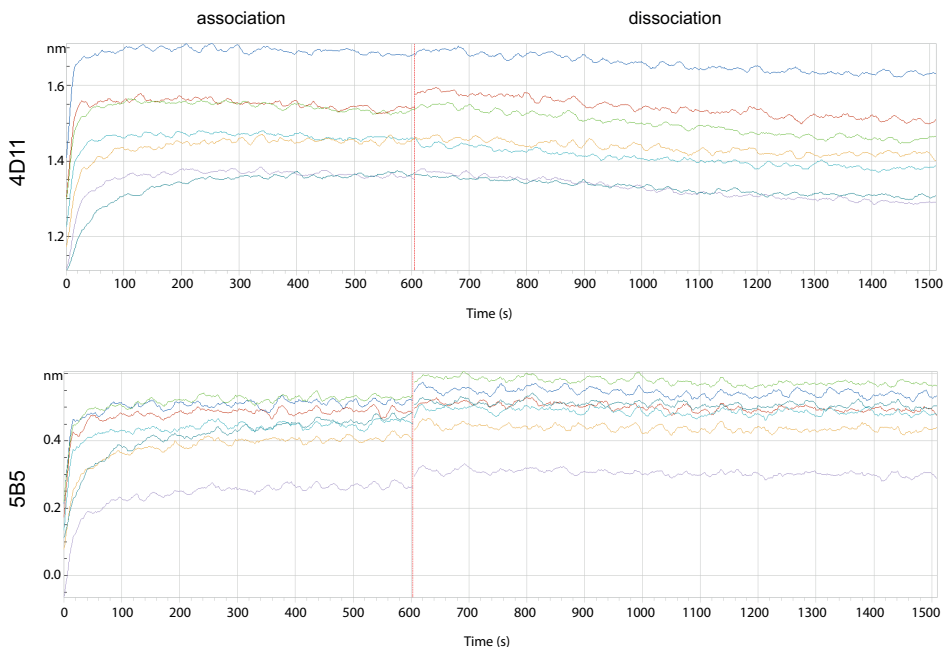


Figure 4. Octet binding analysis of HCABs showing association (left) and dissociation (right) curves. 10 $\mu\text{g}/\text{mL}$ HCABs were loaded onto anti-human IgG-Fc tips and assessed for binding using a dilution range of MUC1 peptide.

production, easy conjugation techniques to develop therapeutics, and reduced immunogenicity¹⁰³. Human single variable heavy chain domains obtained from classical antibodies showed affinities comparable to the parent antibody, but had poor solubility and aggregation problems²⁰⁸. The heavy-chain antibodies generated in this study retain their structure and remain highly soluble and functional, because they are generated in mice and isolated by expression cloning which selects against insoluble antibodies. It has been suggested that nanomedicine in a size range of 10 to 50 nm is ideal for an efficient biodistribution^{209,210}. The size of HCABs might facilitate rapid tissue penetration and rapid blood clearance^{211,212}, while remaining high target retention due to affinities comparable to conventional antibodies⁹⁹.

Further research is aimed at combining these MUC1-specific antibodies with nanomedicine to deliver large quantities of drugs to antigen-presenting cells. The generated heavy-chain antibodies can be used to produce human single variable domain only proteins, or nanobodies, targeted against MUC1. Provided that affinity and stability remain, these could be used for diagnostic purposes in combination with radionuclides or for image-guided drug delivery in combination with drugs or drug carriers.

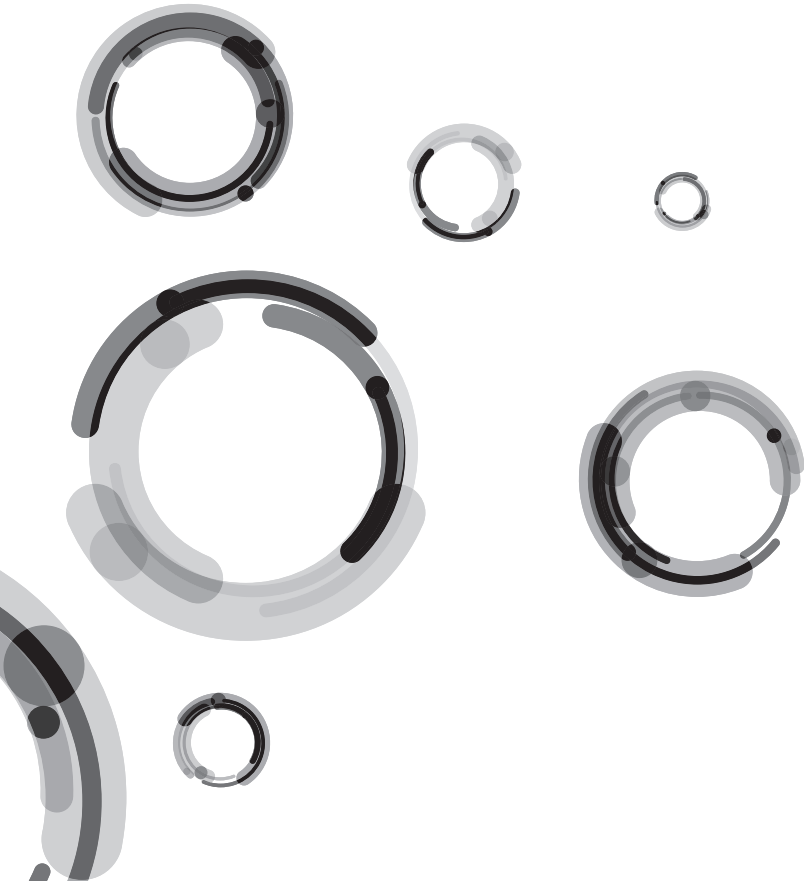


CHAPTER 3

A Novel Indium-111 Labeled Anti-Prostate-Specific Membrane Antigen Nanobody for Targeted SPECT/CT Imaging of Prostate Cancer

Kristell L.S. Chatalic, Joke Veldhoven-Zweistra, Michiel Bolkestein,
Sander Hoeben, Gerben A. Koning, Otto C. Boerman, Marion de Jong,
Wyske M. van Weerden

Adapted from Journal of Nuclear Medicine, 2015



ABSTRACT

Prostate-specific membrane antigen (PSMA) is overexpressed in prostate cancer and a promising target for molecular imaging and therapy. Nanobodies are the smallest antibody-based fragments possessing ideal molecular imaging properties, such as high target specificity and rapid background clearance. We developed a novel anti-PSMA nanobody (JVZ-007) for targeted imaging and therapy of prostate cancer. Here, we report on the application of the indium-111 (^{111}In) radiolabeled nanobody for SPECT/CT imaging of prostate cancer. A nanobody library was generated by immunization of a llama with four human prostate cancer cell lines. Anti-PSMA nanobodies were captured by biopanning on PSMA-overexpressing cells. JVZ-007 was selected for evaluation as an imaging probe. JVZ-007 was initially produced with a c-myc-hexahistidine (His-)tag allowing purification and detection, which was subsequently replaced by a single cysteine at the C-terminus, allowing site-specific conjugation of chelates for radiolabeling. JVZ-007-c-myc-His was conjugated to 2-(4-isothiocyanatobenzyl)-diethylenetriaminepentaacetic acid (p-SCN-DTPA) via lysines, whereas JVZ-007-cys was conjugated to maleimide-DTPA via the C-terminal cysteine. PSMA targeting was analyzed *in vitro* by cell binding experiments using flow cytometry, autoradiography, and internalization assays with various prostate cancer cell lines and patient-derived xenografts (PDXs). The targeting properties of radiolabeled nanobodies were evaluated *in vivo* with SPECT/CT imaging experiments, using nude mice bearing PSMA-positive PC-310 and PSMA-negative PC-3 tumors. JVZ-007 was successfully conjugated to DTPA for radiolabeling with indium-111 at room temperature. ^{111}In -JVZ007-c-myc-His and ^{111}In -JVZ007-cys internalized in LNCaP cells and bound to PSMA-expressing PDXs and, importantly, not to PSMA-negative PDXs and human kidneys. Good tumor targeting and fast blood clearance were observed for ^{111}In -JVZ-007-c-myc-His and ^{111}In -JVZ-007-cys. Renal uptake of ^{111}In -JVZ-007-c-myc-His was initially high, but was efficiently reduced by coinjection of gelofusine and lysine. The replacement of the c-myc-His-tag by the cysteine contributed to a further reduction of renal uptake without loss of targeting. PC-310 tumors were clearly visualized by SPECT/CT with both tracers, with low renal uptake (< 4% injected dose per gram) for ^{111}In -JVZ-007-cys already at 3 h after injection. We developed an indium-111 radiolabeled anti-PSMA nanobody, showing good tumor targeting, low uptake in nontarget tissues, and low renal retention, allowing excellent SPECT/CT imaging of prostate cancer within a few hours after injection.

INTRODUCTION

Prostate cancer is the second leading cause of cancer-related death among men in the western world. Early detection and accurate staging of prostate cancer is crucial because the survival rate decreases dramatically when the cancer has spread beyond the prostate²¹³. Because of the heterogeneity of prostate cancer, and the lack of specificity of conventional imaging techniques, there is currently no universal imaging method approved for detection of early prostate cancer lesions. PSMA is an interesting target for molecular imaging of prostate cancer, as it is overexpressed in 90-100% of local prostate cancer lesions, as well as on cancerous lymph nodes, and bone metastases^{214,215}, with some reports suggesting PSMA expression levels are further enhanced in high-grade, metastatic, and castration-resistant prostate cancer^{216,217}. PSMA is also expressed in other tissues including normal prostate epithelium, small intestine, renal tubular cells, and salivary glands, but the expression in these organs is 100–1,000 fold less than in prostate cancer²¹⁸.

PSMA, also referred to as glutamate carboxypeptidase II (GPCII), *N*-acetyl- α -linked acidic dipeptidase I (Naaladase I), or folate hydrolase, is a type II transmembrane glycoprotein exhibiting glutamate carboxypeptidase and folate hydrolase enzymatic activity. The first clinical tracer for imaging PSMA was based on the murine anti-PSMA antibody 7E11, binding to an epitope on the intracellular domain of PSMA. The indium-111 labeled version of 7E11, ¹¹¹In-capromab, commonly known as ProstaScint (Cytogen Corp.), was approved by the Food and Drug Administration in 1997 for detection of soft-tissue metastases and recurrence of prostate cancer²¹⁹. Its use for staging primary prostate cancer is suboptimal, with an average sensitivity and specificity of 60% and 70%, respectively²²⁰. ¹¹¹In-capromab was also not reliable for the detection of bone metastases, which are often the initial site of metastasis in advanced prostate cancer²²¹. After the discovery of 7E11, next-generation monoclonal antibodies (mAbs) binding to the extracellular domain of PSMA were developed, including mAb J591. Initially developed for therapeutic purposes, J591 was also evaluated for SPECT imaging in clinical trials, showing characteristics superior to ¹¹¹In-capromab, revealing most soft-tissue and bony metastases^{222,223}. Despite improved targeting of J591 and next-generation PSMA mAbs, the major disadvantage of the use of antibodies for imaging is the slow clearance from nontarget tissues, often requiring several days between tracer administration and imaging.

An interesting alternative for molecular imaging of PSMA is the development of small-molecule PSMA inhibitors. Because PSMA possesses an enzymatic site in its extracellular domain that cleaves endogenous substrates such as *N*-acetylaspartylglutamate and poly- γ -glutamyl folic acid, a series of substrates has been designed. These small-molecule PSMA inhibitors consist of zinc-binding compounds attached to a glutamate

moiety. Several radiolabeled PSMA small-molecule inhibitors have been synthesized, starting with phosphonate and phosphate inhibitors, followed by phosphoramidate-, thiol-, and urea-based inhibitors, which are discussed in an extensive review by Mease and colleagues²²⁴. Some have shown promising results in early clinical studies, such as ¹²³I-MIP-1072, ¹²³I-MIP-1095²²⁵, N-[N-[(S)-1,3-dicarboxypropyl]carbonyl]-4-¹⁸F-fluorobenzyl-L-cysteine²²⁶, ⁶⁸Ga-HBED-CC²²⁷, and BAY1075553²²⁸. These compounds localize rapidly to tumor lesions, including soft-tissue and bone metastases, but also show high uptake in kidneys and salivary glands, attributed to PSMA expression in these organs.

Another approach aiming at circumventing the long circulation time of mAbs is the use of antibody fragments, such as single-domain antibodies (VHH). Nanobodies display attractive features for molecular imaging, including fast nontarget tissue clearance, good tumor penetration capability, and recognition of unique epitopes that are less accessible for mAbs²²⁹. In this study, we describe the development of a nanobody targeting PSMA and showing good tumor targeting and fast blood clearance, resulting in impressive tumor-to-background ratios within a few hours after injection. The nanobody was conjugated to a diethylenetriaminepentaacetic acid (DTPA) chelator, allowing facile and stable radiolabeling with indium-111 at room temperature in a 1-step procedure. The structure of the nanobody was optimized to minimize renal retention using a novel method for production and labeling of cys-tagged nanobodies. We report on the production and radiolabeling of anti-PSMA nanobodies as well as *in vitro* and *in vivo* evaluation in patient-derived prostate cancer xenograft models.

MATERIALS AND METHODS

Immunization and VHH-library construction

A llama (*Lama glama*) was immunized subcutaneously at 1, 30, 60 and 90 d with a mixture of four androgen-responsive human-derived prostate cancer cell lines (LNCaP, PC346C, VCaP, and MDA PCa 2b) (33×10^6 cells per cell line) to generate a VHH library targeting prostate cancer. Blood was collected after the third immunization and peripheral blood lymphocytes were isolated. Library construction was performed as previously described²³⁰. Briefly, RNA was isolated and cDNA was synthesized with reverse transcriptase. VHH (variable domains of camelid heavy-chain antibodies) genes were amplified by PCR introducing NotI and SfiI restriction enzyme sites (forward and backward primers). VHH fragments were isolated from a 1% agarose gel, digested with SfiI and NotI, ligated into the pHEN1-6HISGS phagemid and transformed into TG1 *Escherichia coli* cells to generate a library of 3.3×10^9 transformants (LIP4 library). The VHH library was kindly provided by Dr. Patrick Chames (IBISA).

Selection and screening by phage display

A phage display library was produced by infecting the nanobody library with M13 K07ΔpIII hyperphages (Progen Biotechnik). PSMA-specific nanobodies were captured by three rounds of biopanning. Each round consisted of a negative selection using wild-type B16 cells followed by a positive selection on B16-PSMA transfected cells. Briefly, 1×10^7 B16 cells were scraped in PBS with 10% FCS. B16 cells and phages were incubated in PBS with addition of 10%FCS and 2% protivar milk (Nutrica) for 30 min at RT. B16 cells were incubated with 2×10^{11} phages in PBS/10% FCS/2% protivar milk for 45 min at RT. Meanwhile, B16-PSMA cells were scraped in PBS/10% FCS and incubated in PBS/10% FCS/2% protivar milk (Nutrica) for 30 min at RT. B16 cells were then spun down, and the supernatant containing unbound phages was incubated with 10^7 B16-PSMA transfected cells in PBS/1% BSA/2% protivar milk for 45 min at RT. Cells were washed ten times with PBS/1% BSA/2% protivar milk and two times with PBS. Phages bound to PSMA-transfected B16 cells were eluted with 200 mM triethylamine (Sigma) and reamplified in TG1 cells. Colonies were grown on 2xTY (16 g/L tryptone, 10 g/L yeast extract and 5 g/L NaCl)/ampicillin (100 μg/mL)/glucose (2%) agar plates. Colonies were scraped from the 2xTY plates, and stored at -80°C in the presence of 20% glycerol. Selected single clones were plated in 100 μl 2xTY/ampicillin (100 μg/mL)/glucose (2%) broth in 96-well plates and shaken overnight at 30°C . From each well, 5 μl was replated in 150 μl 2xTY/ampicillin (100 μg/mL)/glucose (2%) broth and shaken for 2.5 h at 37°C . Phages presenting a VHH were produced by adding 0.5×10^9 M13 K07ΔpIII helper phage to each well and incubating for 30 min at 37°C . Plates were centrifuged (1700 rpm, 10 min). Bacterial pellet was resuspended in 2xTY/ampicillin (100 μg/mL)/kanamycin (25 μg/mL) and grown under vigorous shaking overnight at 30°C . Phage-containing supernatants were tested for binding to PSMA by ELISA using B16 and B16-PSMA cells. Briefly, B16 and B16-PSMA cells were collected by scraping in PBS containing 1% bovine serum albumin (BSA). Cells were incubated with phage supernatant for 1.5 h at room temperature, shaking. Binding of phages to PSMA was detected with a horseradish peroxidase (HRP)-conjugated anti-M13 mouse antibody (27-9421-01, GE Healthcare). Cells were then incubated with OPD substrate (Sigma) and measurement was done at OD 490 nm. Clones found positive in cell ELISA were further analyzed by FACS analysis. Binding of phages was detected with an anti-M13 mouse antibody (GE Healthcare), followed by a phycoerythrin (PE)-conjugated anti-mouse goat antibody (550589, BD Biosciences). Fluorescence was measured on a FACScan (BD).

Nanobody sequencing, production and purification

Selected clones were sequenced, and distinct nanobody clones were identified. The sequence of JVZ-007 clone is shown in Figure 1. Clones were produced as c-myc-His-

```

1           10           20           30           40           50
|           |           |           |           |           |
EVQLVESGGGLVQPGGSLTLSCAASRFMISEYSMHWRQAPGKGLEWVSTINPAGTTDY

60          70          80          90          100         110
|          |          |          |          |          |
AESVKGRFTISRDNAKNTLYLQMNSLKPEDTAVVYCDGYGYRGQGTQVTVSS

```

Figure 1. Amino acid sequence of JVZ-007 nanobody.

tagged proteins to facilitate purification by affinity chromatography and detection by flow cytometry. The plasmid containing JVZ-007 sequence was isolated from the TG1 cells (JetStar™ 2.0 plasmid purification MIDI kit, Genomed) and transformed into HB2151 cells. Production in HB2151 cells was performed overnight at 37°C in 2xTY (16 g/L tryptone, 10 g/L yeast extract and 5 g/L NaCl) medium supplemented with 100 µg/mL ampicillin and 0.1% glucose. Cells were collected by centrifugation for 30 min at 4000 rpm, washed with PBS and lysed by freeze-thaw cycles in lysis buffer (50 mM KPO₄ pH 7.8, 400 mM NaCl, 100 mM KCl, 10% glycerol, 0.5% Triton X-100). The lysate was centrifuged and filtered (40 µm filter), and c-myc-His-tagged nanobodies were trapped on a HisTrap FF column (GE Healthcare) on a ÄKTA preparative protein purification system (GE Healthcare) and eluted with 500 mM imidazole. Buffer was changed for phosphate-buffered saline (PBS) using a Vivaspin sample concentrator (5-kDa cut-off, GE Healthcare). C-myc-His-tagged nanobody purity was assessed with reducing SDS-PAGE and western blot analysis with anti-c-myc mouse antibody (M4439, Sigma), followed by HRP-anti-mouse goat antibody (p0447, Dako) and visualized with a Chemiluminescence kit (Thermo Fisher Scientific Inc). The protein concentration was determined using a BCA protein assay kit (Thermo Fisher Scientific Inc).

Additionally, JVZ-007 nanobody was cloned from the pHEN vector, introducing a cysteine at the C-terminus, and expressed as a fusion protein to SUMO3 (Smt3 ubiquitin-like protein) using the pETM11-SUMO3GFP vector (kindly provided by EMBL). The nanobody sequence was cloned from the pHEN vector using two primers. The forward primer contains a restriction enzyme site AgeI and two glycine molecules, necessary for SenP2 digestion (5' ACT ATG ACC GGT GGA GAG GTG CAG CTG GTG 3'). The backward primer contains a cysteine sequence, a stop sequence and a HindIII restriction enzyme site (3' TCA GTA AAG CTT TCA ACA TGA GGA GAC GGT GAC 5'). The nanobody was ligated into the pETM11-SUMO3GFP vector after digestion with AgeI and HindIII. After expression of the recombinant plasmid in BL21 bacteria and protein extraction, JVZ-007-cys-SUMO3 was isolated with a HisTrap column. The SUMO3 protein was cleaved off by a SUMO-specific protease, Sentrin-specific protease 2 (SenP2, provided by Guy Salvesen, Addgene)²³¹. Digestion was performed overnight

at 4°C with a ratio of 1:10 (w/w) of SenP2 to JVZ-007-cys-SUMO3. His-tagged SenP2 and SUMO3 were removed with a HisTrap FF column (GE Healthcare). JVZ-007-cys nanobody purity was assessed with reducing SDS-PAGE.

Flow cytometry

PSMA-specific binding was assessed by flow cytometry on PC-346C, LNCaP, and PC-3 cells. Briefly, cells were collected by scraping in polypropylene tubes and incubated with the c-myc-His-tagged nanobody for 60 min at 4°C, followed by incubation with an anti-c-myc mouse antibody (M4439, Sigma) for 30 min, and finally PE-conjugated anti-mouse goat antibody (550589, BD Biosciences) for 30 min. As negative control, cells were incubated using the same procedure, without the nanobody. As positive control, cells were incubated with anti-PSMA mouse antibody (SAB4200257, Sigma), and PE-conjugated goat anti-mouse antibody (550589, BD Biosciences). Flow cytometry was performed using a BD FACScan system (Becton Dickinson).

Conjugation to DTPA and radiolabeling

JVZ-007-c-myc-His was incubated with a 5-fold molar excess of p-SCN-Bn-DTPA (Macrocyclics) in 0.1 M sodium carbonate buffer (pH 9.5) for 2.5 h at room temperature. JVZ-007-cys was reduced with 1 mM 2-mercaptoethylamine-HCl in phosphate-buffered saline (PBS), 5 mM ethylenediaminetetraacetic acid for 90 min at 37°C. Reduced JVZ-007-cys was then incubated with 5 mM maleimide-DTPA for 2 h at 37°C. Conjugated nanobodies were then dialyzed for 3 d in a Slide-A-Lyzer (3.5-kDa cutoff; Life Technologies) against 0.25 M ammonium acetate (NH₄Ac), pH 5.5.

Nanobody-DTPA conjugates were labeled with ¹¹¹InCl₃ (Covidien) in 20 mM sodium acetate, pH 5.0, for 30 min at room temperature. Radioprotectants (3.5 mM ascorbic acid, gentisic acid, and methionine) were used to prevent radiolysis. Labeling efficiency was assessed by instant thin-layer chromatography using silica gel-coated paper (Varian Inc.) and 0.1 M citrate buffer, pH 5.0, as the mobile phase. After incubation, an excess of DTPA (final concentration, 0.15 mM) was added to complex free ¹¹¹InCl₃.

Cell culture, autoradiography and internalization

Cell lines were purchased from the American Type Culture Collection. B16-PSMA was kindly provided by Marco Colombatti (University of Verona). Cell cultures media and reagents were obtained from Lonza unless stated otherwise. LNCaP, VCaP and PC-3 cells were cultured in RPMI 1640 medium containing 10% (5% for PC-3) fetal calf serum (FCS). PC-346C cells were cultured in Dulbecco's modified Eagle's F12 medium supplemented with 2% FCS, 0.01% BSA (Boehringer-Mannheim), 1% insulin-transferin-selenium (Life Technologies), 0.1 µg/mL fibronectin (Alfa Aesar), 0.1 nM R1881 androgen, 10 ng/mL epidermal growth factor, 0.5 µg/mL dexametason, 1 nM triio-

dothyronine, 0.1 mM phosphoethanolamine, 50 ng/mL cholera toxin and 20 µg/mL fetuin (all from Sigma). B16 cells were cultured in Dulbecco's modified Eagle's medium containing 10% FCS, 10 mM HEPES (Sigma), 20 µM 2-mercaptoethanol (Sigma) and 2 mM glutamine. For B16-PSMA, 1200 µg/mL geneticin (G418, Gibco) was added to this medium. MDA PCa 2b cells were grown in Ham's F12 medium containing 15% FCS, 25 ng/mL cholera toxin, 10 ng/mL epidermal growth factor, 5 µM phosphoethanolamine, 120 pg/mL hydrocortisone and 1% insulin-transferrin-selenium. Penicillin (100 units/mL), and streptomycin (100 µg/mL) were added to cell culture media. Cells were grown in tissue culture flasks at 37°C in a humidified atmosphere containing 5% CO₂.

Binding of ¹¹¹In-JVZ-007-c-myc-His and ¹¹¹In-JVZ-007-cys to frozen cryostat section of PDXs and kidneys (mouse/human) was evaluated using autoradiography, as described previously²³². Tissue sections were incubated for 1 h with ¹¹¹In-JVZ-007-c-myc-His or ¹¹¹In-JVZ-007-cys (10⁻⁹ M). In saturation binding experiments, concentrations ranging from 10⁻⁶ to 10⁻¹² M of ¹¹¹In-JVZ-007-c-myc-His were used.

The internalization of ¹¹¹In-JVZ-007-c-myc-His and ¹¹¹In-JVZ-007-cys was assessed using LNCaP and PC-3 cells. Cells were trypsinized and incubated with ¹¹¹In-JVZ-007-c-myc-His or ¹¹¹In-JVZ-007-cys (10⁻¹⁰ M) in RPMI 1640/GlutaMAX (Life Technologies)/20 mM *N*-(2-hydroxyethyl)piperazine-*N'*-(2-ethanesulfonic acid)/1% bovine serum albumin (pH 7.4) for 90 min at 37°C or 4°C. JVZ-007-c-myc-His was used for blocking (10⁻⁶ M). After incubation, the cells were centrifuged and washed 2x with PBS. Cell surface-bound nanobodies were eluted using a solution of 50 mM glycine/100 mM NaCl (pH 2.8), and cells were washed with PBS. Cells were then lysed in 1 M sodium hydroxide to collect internalized nanobody. Membrane-bound and internalized fractions were counted in a γ counter. Binding was expressed as percentage of added amount of radioactivity per number of cells.

Biodistribution and SPECT/CT imaging

Male NMRI *nu/nu* mice (8-week-old) were transplanted with PC-310 tumor fragments near the left shoulder and injected subcutaneously near the right shoulder with PC-3 cells (3 × 10⁶ cells, 200 µL, 66% RPMI, 33% Matrigel [BD Bioscience]). Three to four weeks after inoculation, when tumor size averaged 200 mm³, mice were injected intravenously with radiolabeled nanobody (200 µL). Radiolabeled nanobody was diluted in PBS containing 0.1% v/w bovine serum albumin. When coinjection of lysine (20 mg) and gelofusine (4 mg) was performed, radiolabeled nanobody was mixed 1:1 with a solution of lysine (400 mg/mL), and 100 µL of this solution were coinjected with 100 µL of gelofusine (40 mg/mL).

Mice were injected with 0.7 MBq of radiolabeled nanobody (amount ranging from 1 to 100 µg) and euthanized 4 or 24 h after injection for biodistribution studies. Blood, tumor, and relevant organs and tissues were collected, weighed, and counted in a γ

counter (Perkin-Elmer) with a counting time of 60 s per sample with an isotope-specific energy window and a counting error not exceeding 5%. The percentage injected dose per gram (%ID/g) was determined for each tissue sample.

For SPECT/CT imaging experiments, mice were injected with 30 MBq of ^{111}In -JVZ007-c-myc-His (10 μg) or 15 MBq of ^{111}In -JVZ007-cys (10 μg). Mice were scanned under isoflurane/ O_2 anesthesia at 3 and 24 h after injection on a small-animal nanoSPECT scanner (Mediso) with heated bed. SPECT emission scans were acquired for 30–42 min, with a matrix of 256 x 256 and 20 projections (120 s per projection). Multi-pinhole mouse collimators with 9 pinholes (1.4 mm diameter) per head were used. SPECT scans reconstruction and processing were performed with InVivoScope/VivoQuant software 2.0 (inviCRO). All animal experiments were approved by the Animal Experiments Committee under the Dutch Experiments on Animal Act and adhered to the European Convention for Protection of Vertebrate Animals used for Experimental Purposes (Directive 86/609/EEC).

Statistical Analysis

Statistical analysis was performed using GraphPad Prism version 5.01 (San Diego, CA, USA). Biodistribution data are represented as the mean %ID/g \pm SD, with group sizes of 4 mice. Statistical analysis of biodistribution data was performed using a 1-way ANOVA with Bonferroni post-hoc test, and the level of significance was set at $p < 0.05$.

RESULTS

Generation of anti-PSMA nanobodies

A prostate cancer specific nanobody library was generated by immunization of a llama with four prostate cancer cell lines (LNCaP, PC346C, VCaP, and MDA PCa 2b). PSMA-specific nanobodies were retrieved by biopanning using phage display for three positive and negative selection rounds with B16-PSMA and B16 cell lines, respectively. Selection on PSMA-expressing cells was preferred rather than using the recombinant PSMA protein, to increase the chance of capturing nanobodies binding to an accessible epitope on the extracellular domain of PSMA. Several distinct PSMA-specific nanobodies were isolated and sequenced (data not shown). Selected clones were produced as c-myc-His-tagged proteins to facilitate purification by affinity chromatography and detection by flow cytometry. PSMA-specific binding was assessed by flow cytometry on PC-346C, LNCaP, and PC-3 cells. Results of flow cytometry analysis of a few selected nanobodies are displayed in Figure 2. JVZ-005, JVZ-007, and JVZ-012 all bound to PSMA-expressing LNCaP and PC346C, as shown by the increase in the geometric mean of the fluorescence intensity. No binding was observed on the PSMA-negative PC-3 cells, showing the specificity of the nanobodies for PSMA. JVZ-007, showing the high-

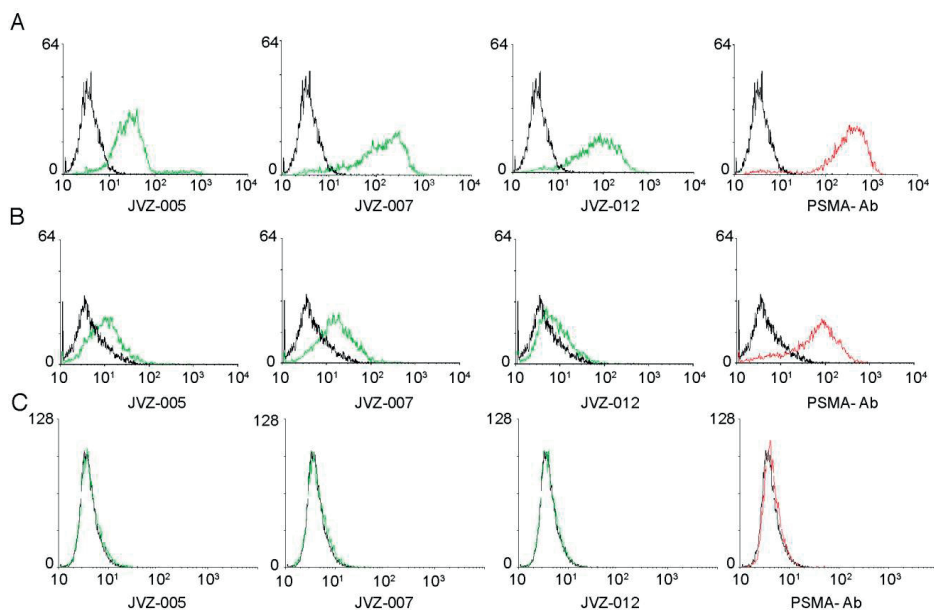


Figure 2. Flow cytometry analysis of JVZ-005, JVZ-007 and JVZ-012 on LNCaP (A), PC346C (B) and PC-3 cells (C). Green, in the presence of nanobody; red, in the presence of PSMA-antibody (PSMA-Ab); black, control, in the absence of nanobody; x-axis, fluorescence intensity; y-axis, number of events. Binding was observed with the PSMA-positive LNCaP and PC346C cells, while no binding was observed with the PSMA-negative PC-3 cells.

est binding, was selected for further evaluation as the imaging probe. Its sequence is indicated in Figure 1. JVZ-007-c-myc-His and JVZ-007-cys were successfully produced in bacteria using the pHEN and pETM11-SUMO3GFP expression vectors, respectively.

Labeling and *in vitro* binding studies

JVZ-007-c-myc-His was conjugated to p-SCN-Bn-DTPA via lysine residues, to allow radiolabeling with indium-111 for SPECT imaging of prostate cancer. JVZ-007-cys was site-specifically conjugated with DTPA by reacting it with maleimide-DTPA. JVZ-007-cys formed dimers via cysteine bridging, and mild reduction was necessary to free the thiol in the cysteine. Indium-111 radiolabeling was performed, with specific activities up to 60 MBq/nmol, whereas the labeling efficiency always exceeded 90%. No release of indium-111 was observed at 4°C up to 72 h after radiolabeling. Binding to frozen sections of PDXs and kidney using autoradiography is shown in Figure 3. Binding affinity of ¹¹¹In-JVZ-007-c-myc-His was estimated by saturation binding on the PSMA-positive PC-310 tumor, resulting in an equilibrium dissociation constant value of 27.4 nM (14.1–40.7, 95% confidence interval). ¹¹¹In-JVZ-007-c-myc-His and ¹¹¹In-JVZ-007-cys showed high binding to all PSMA-expressing tumor sections (PC310, LNCaP, PC82,

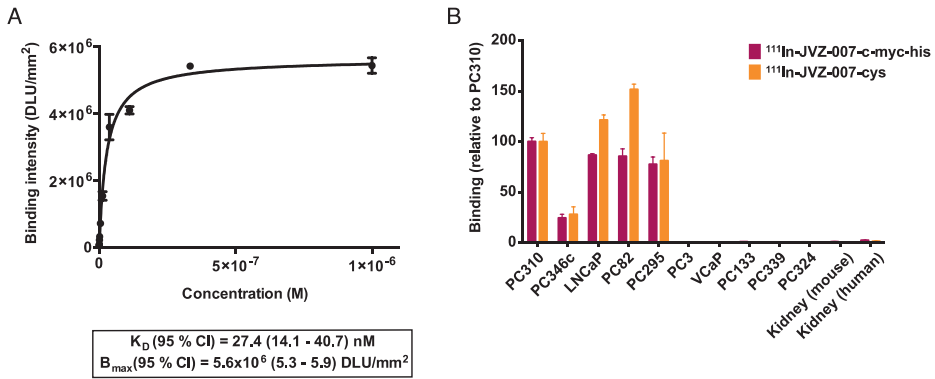


Figure 3. Saturation binding of ¹¹¹In-JVZ-007-c-myc-His on PC-310 frozen sections using autoradiography (A). Binding of ¹¹¹In-JVZ-007-c-myc-His and ¹¹¹In-JVZ-007-cys to tumor and kidney frozen sections using autoradiography (B). High binding is observed with PSMA-expressing tumor sections (PC310, PC346c, LNCaP, PC82 and PC295) while no binding is observed with the PSMA-negative tumors PC-3 VCaP, PC133, PC339, PC324) and kidneys (mouse or human).

and PC295), with lower binding to the weakly PSMA-positive PC346c. The absence of binding was observed on the PSMA-negative tumors (PC-3 VCaP, PC133, PC339, and PC324). These results are in line with previous PSMA RNA expression data of these PDXs (Affymetrix data not shown). Binding to mouse and human kidneys was low (< 1%) in comparison with PSMA-positive tumors.

Cell binding assays on PSMA-positive LNCaP cells (Figure 4) showed 30% and 37% internalization after 90 min at 37°C, for ¹¹¹In-JVZ-007-c-myc-His and ¹¹¹In-JVZ-007-cys,

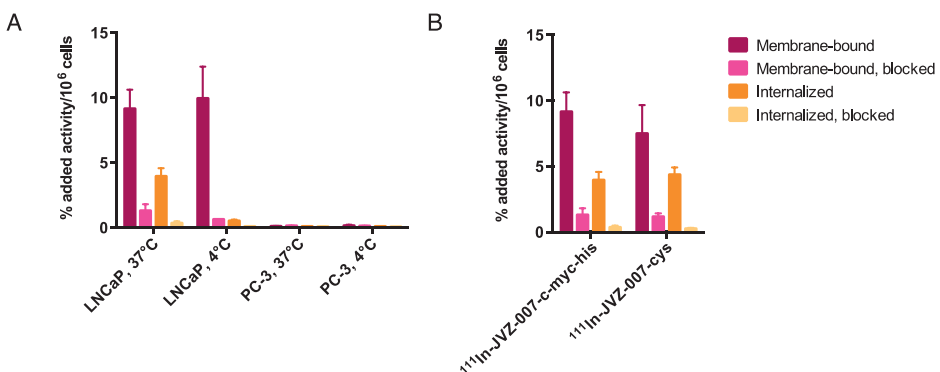


Figure 4. Internalization of ¹¹¹In-JVZ-007-c-myc-His in LNCaP and PC-3 cells, after incubation for 90 min at 37°C and 4°C (A). Comparison of internalization of ¹¹¹In-JVZ-007-c-myc-His and ¹¹¹In-JVZ-007-cys in LNCaP cells after incubation for 90 min at 37°C (B). ¹¹¹In-JVZ-007-c-myc-His and ¹¹¹In-JVZ-007-cys internalized in PSMA-expressing LNCaP cells at 37°C, while no internalization was observed at 4°C, or in PSMA-negative PC-3 cells.

respectively. Cell binding of both tracers was blocked in the presence of an excess of unlabeled JVZ-007-c-myc-His, confirming target specificity. Internalization of ^{111}In -JVZ-007-c-myc-His was confirmed by the strongly reduced amount of radioactivity in the internalized fraction (0.05% of total binding) observed at 4°C. Low binding (< 1% relative to LNCaP cells) and absence of internalization of ^{111}In -JVZ-007-c-myc-His was observed for the PSMA-negative cell line PC-3, confirming nanobody specificity for PSMA.

Biodistribution and SPECT/CT imaging

The PSMA-targeting properties of ^{111}In -JVZ-007-c-myc-His and ^{111}In -JVZ-007-cys were evaluated further in mice bearing PC-310 and PC-3 tumors. Biodistribution studies are displayed in Figure 5, showing good tumor targeting, with low background intensity except for the kidneys. Four hours after injection, the uptake of ^{111}In -JVZ-007-c-myc-His in the PC-310 tumor was $3.91 \pm 1.13\%$ injected dose per gram. Uptake in the

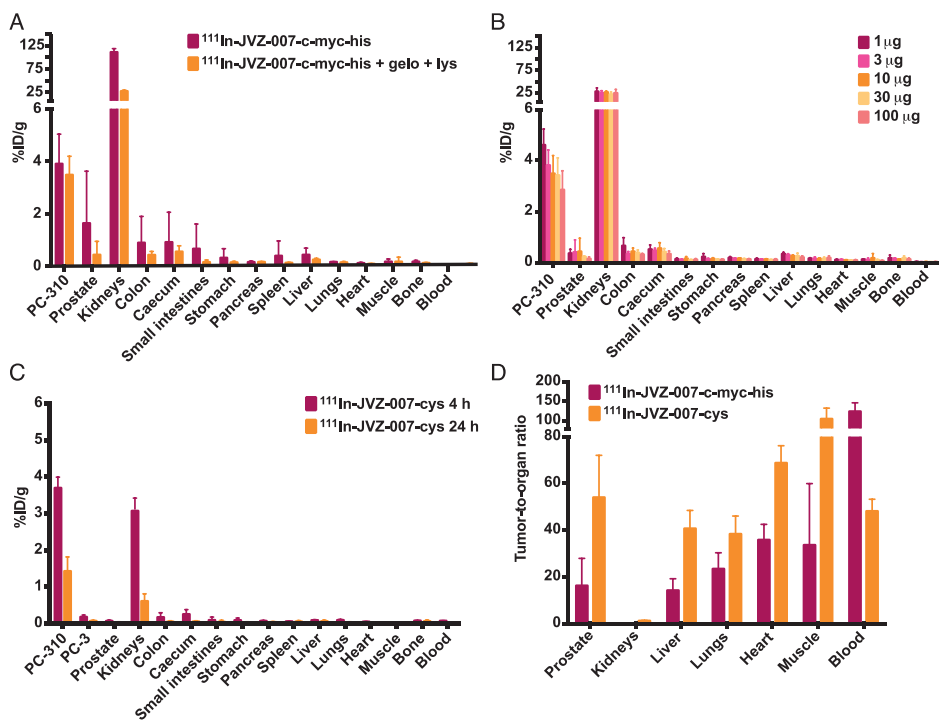


Figure 5. Biodistribution studies in mice bearing PC-310 and PC-3 tumors. Effect of co-injection of gelofusine and lysine (A) and dose (B) on biodistribution of ^{111}In -JVZ-007-c-myc-His (10 µg) at 4 h after injection (A). Biodistribution at 4 h and 24 h after injection of ^{111}In -JVZ-007-cys (10 µg) with co-injection of gelofusine and lysine (C). Tumor-to-organ ratios at 4 h after injection of ^{111}In -JVZ-007-c-myc-His (10 µg) or ^{111}In -JVZ-007-cys (10 µg) with co-injection of gelofusine and lysine (D).

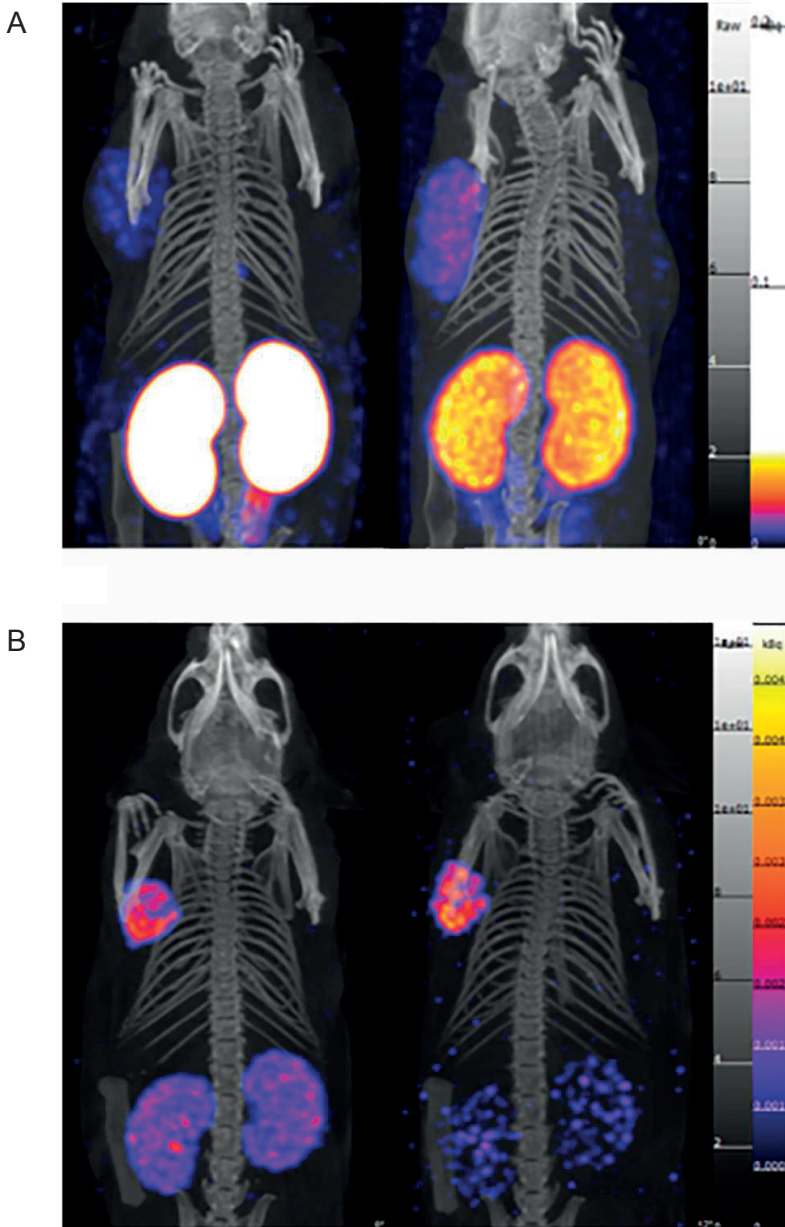


Figure 6. SPECT/CT images of mice bearing PC-310 (left shoulder) and PC-3 (right shoulder) tumors. Images acquired 3 h after injection of ^{111}In -JVZ-007-c-myc-His (A) with co-injection of PBS (left) or gelofusine and lysine (right). Images acquired 3 h (left) and 24 h (right) after injection of ^{111}In -JVZ-007-cys (B). Scale from 0 to 0.2 kBq (A); 0 to 0.015 kBq (B, left); 0 to 0.005 (B, right). PSMA-expressing PC-310 tumor could be clearly visualized with high contrast on the left shoulder, while no uptake was observed in PC-3 tumor on the right shoulder.

kidneys was $110.89 \pm 7.35\%$ injected dose per gram, but could be reduced to $27.77 \pm 2.02\%$ injected dose per gram by coinjection of gelofusine and lysine. Increasing doses of JVZ-007-c-myc-His showed a slight decrease in tumor uptake. Similarly, ^{111}In -JVZ-007-cys in combination with gelofusine and lysine showed uptake in PC-310 and PC-3 tumors of 3.70 ± 0.29 and $0.18 \pm 0.05\%$ injected dose per gram at 4 h after injection, respectively. Importantly, kidney uptake was approximately 10-fold lower than that of JVZ-007-c-myc-His, with values of only 3.13 ± 0.30 and $0.61 \pm 0.20\%$ injected dose per gram, at 4 and 24 h after injection, respectively. Moreover, ^{111}In -JVZ-007-cys showed higher tumor-to-background ratios at 4 h after injection than ^{111}In -JVZ-007-c-myc-His, with a tumor-to-muscle ratio of 104.8 ± 27.4 and tumor-to-kidney ratio of 1.2 ± 0.1 . The tumor-to-blood ratio was significantly lower for ^{111}In -JVZ-007-cys (48.1 ± 5.1) than for ^{111}In -JVZ-007-c-myc-His.

SPECT/CT images of mice bearing PC-310 and PC-3 tumors 3 h after injection of ^{111}In -JVZ-007-c-myc-His and ^{111}In -JVZ-007-cys are shown in Figure 6. PSMA-expressing PC-310 tumor could be clearly visualized with high contrast on the right shoulder, whereas no uptake was observed in PC-3 tumor on the left shoulder. Signal intensity in kidneys after injection of ^{111}In -JVZ-007-c-myc-His was very high but could be efficiently reduced by a coadministration of gelofusine and lysine. Importantly, kidney signal intensity of ^{111}In -JVZ-007-cys was markedly lower.

DISCUSSION

Development of PSMA-based imaging tracers for prostate cancer has increased tremendously in the past few years. After the approval of the PSMA mAb ^{111}In -capromab as an imaging agent in 1997, a panel of novel PSMA-targeted imaging agents was developed, including next-generation antibodies, antibody fragments, aptamers, and PSMA inhibitors²²⁴. PSMA small-molecule inhibitors localize rapidly to tumor lesions, including soft-tissue and bone metastases, but also show a high uptake in the kidneys and salivary glands. The high uptake of PSMA inhibitors in these organs was attributed to PSMA expression, although the expression of PSMA in these organs was shown to be 100- to 1,000-fold lower than in prostate cancer²¹⁸. This lower PSMA expression in normal organs may suggest that other (receptor-mediated) processes may be involved in tracer uptake in normal organs as well.

In parallel to these developments, alternative strategies have been pursued using smaller variants of mAb, such as antigen-binding fragments (Fab) and F(ab')_2 ²³³, and minibodies or diabodies^{234,235}, aiming to circumvent the long circulation time of mAb. These antibody fragments have shown fast target recognition and rapid blood clearance, but also show unspecific accumulation in the liver and kidneys. A more recent approach is the use of nanobodies (V_{HH}), the smallest antibody-based fragments (12–15 kDa),

offering ideal characteristics for molecular imaging. Because of their small size below the renal threshold for glomerular filtration (60 kDa), they are mainly cleared via the renal pathway. Moreover, it is possible to humanize nanobodies for clinical translation using the recently described universal humanized nanobody scaffold technique¹¹³. Nanobodies targeting PSMA were developed, showing moderate tumor targeting, low liver uptake, and high kidney uptake²³⁶. Retention of tracers in the kidneys might be the result of a combination of different factors, including glomerular filtration by the kidneys, PSMA-specific binding, and trapping of metabolites in the lysosomes of renal tubular cells. Tracer retention in the kidneys is not desirable, because it may interfere with visualization of small tumor lesions in the vicinity of the kidneys and especially with staging of prostate cancer. Renal tracer retention also limits the application of the PSMA tracer for radionuclide therapy by inflicting a high dose to the kidneys. We have developed a nanobody (JVZ-007) that shows good tumor targeting in PSMA-expressing PC-310 PDX tumors. JVZ-007 was initially produced with a c-myc-His-tag and conjugated to p-SCN-Bn-DTPA via the lysine residues, to allow radiolabeling with indium-111 for SPECT imaging of prostate cancer. ¹¹¹In-JVZ-007-c-myc-His was internalized in LNCaP cells and showed high binding on all PSMA-expressing PDX sections *in vitro*, whereas low binding to the PSMA-negative PDX sections was observed and 50-fold lower binding to the human kidney than the PC-310 tumor, indicating the markedly lower expression levels of PSMA in the kidney. ¹¹¹In-JVZ-007-c-myc-His was evaluated further in mice bearing PC-310 tumors, showing good tumor targeting as early as 4 h after injection, with low background intensity, except for the kidneys. It was recently described that renal retention of an anti-epidermal growth factor receptor nanobody could be reduced by coinjection of gelofusine and lysine²³⁷. Indeed, efficient reduction of renal uptake of our anti-PSMA nanobody was obtained when gelofusine and lysine were coadministered. These results support that high renal uptake may be due to reabsorption in the renal proximal tubule after glomerular filtration. Moreover, studies from D'Huyvetter et al. have also shown that the His-tag plays a major role in the high retention of radiolabeled nanobodies in the kidneys¹¹⁷. Therefore, we have engineered a new nanobody construct, based on JVZ-007, in which the c-myc-His-tag was removed. In addition, we introduced a cysteine at the C-terminus for site-specific coupling to maleimide-DTPA. For this purpose we used the pETM11-SUMO3GFP expression vector, allowing production of a protein with a C-terminal cysteine and retrieval of the protein by cleavage of SUMO3 by a specific protease. ¹¹¹In-JVZ-007-cys showed similar binding on PSMA-expressing cells and PDXs. More importantly, a further drop in renal uptake to 3% injected dose per gram was observed at 4 h after injection, without loss of tumor targeting. In comparison, these renal uptake values in mice were superior to those found with other PSMA tracers: 100% injected dose per gram for ⁶⁸Ga-HBED-CC-PSMA (1 h)²³⁸ and ¹¹¹In-D₂B-Fab fragments (4 h)²³³. Kidney uptake of 78 and 36%

injected dose per gram was reported for ^{123}I -MIP-1095 and ^{123}I -MIP-1072 (4 h), respectively²³⁹. Tumor-to-blood and tumor-to-muscle ratios obtained with ^{111}In -JVZ-007-cys at 4 h after injection were superior to those obtained with ^{111}In -D₂B-Fab fragments²³³ and comparable to those obtained with ^{123}I -MIP-1095²³⁹, in LNCaP xenograft mice (4 h). The novel method described here for production and site-specific labeling of cyst-tagged nanobodies could have a significant impact for the clinical implementation of a wide range of nanobodies. The site-specific coupling offers a well-defined labeling procedure, while the absence of the c-myc-His-tag limits reabsorption in renal tubular cells. This minimal renal retention also broadens the applicability of this nanobody to radionuclide therapy.

CONCLUSION

We developed a specific anti-PSMA nanobody containing a cysteine for site-specific conjugation to radioactive labels. The indium-111 radiolabeled anti-PSMA nanobody shows good tumor targeting and fast blood clearance, allowing SPECT/CT imaging within a few hours after injection. Unlike most radiolabeled small-molecule PSMA inhibitors, anti-PSMA nanobody JVZ-007 displays a low kidney uptake. These results warrant further evaluation of anti-PSMA nanobody JVZ-007 for detection and radionuclide therapy of metastatic lesions in PSMA-expressing prostate cancer, for which few treatment options are currently available.

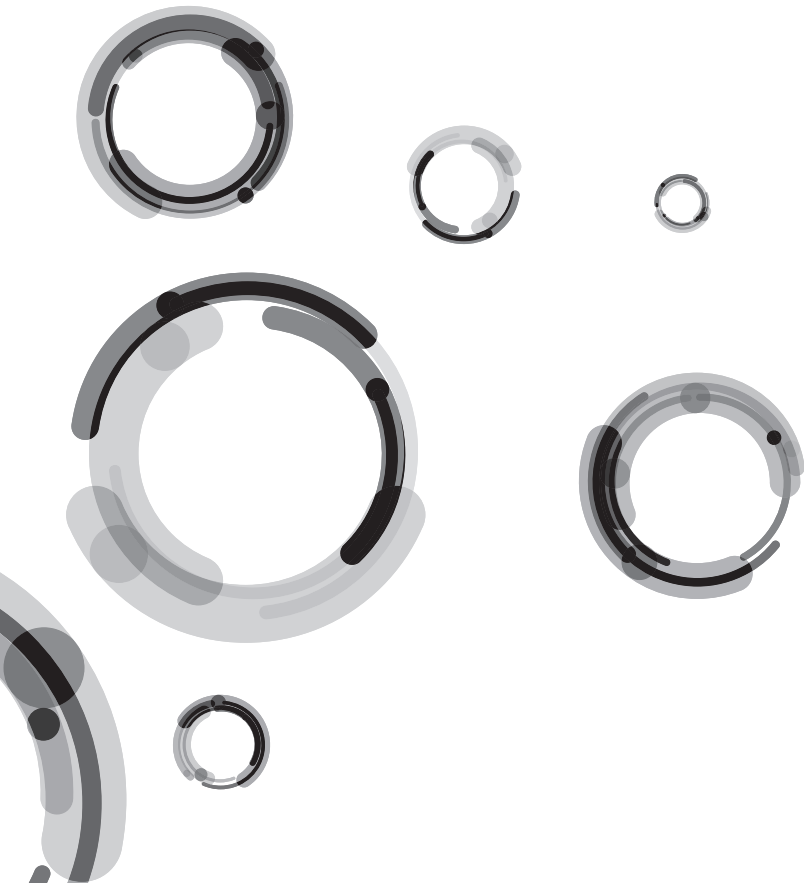


CHAPTER 4

Nanobody-Targeted Prostate Cancer Therapy with Anti-PSMA Doxorubicin-Loaded Liposomes

Michiel Bolkestein, Gabriela N. Doeswijk, Erik de Blois, Joost A.P. Rens, Wiggert A. van Cappellen, Marion de Jong, Frank Grosveld, Alexander M.M. Eggermont, Gerben A. Koning, Wytske M. van Weerden

Submitted



ABSTRACT

Advanced prostate cancer remains difficult to treat, yet combining hormonal therapy with chemotherapy has resulted in improved overall survival. Chemotherapy with docetaxel has been used as first-line treatment of advanced castration-resistant prostate cancer since 2004, however intrinsic and acquired resistance to docetaxel, and serious adverse effects limit the use of the drug. To circumvent these problems and increase specific drug uptake in the tumor, nanobody-targeted liposomes against prostate specific membrane antigen (PSMA) were prepared and investigated. The PSMA-specific targeting of these liposomes was analyzed *in vitro* and *in vivo* using flow cytometry and SPECT/CT imaging, respectively. Efficacy of drug-loaded liposomes was tested on cell lines, and in cell line and patient-derived xenografts. The distribution of liposomes in the tumor was investigated with whole tumor microscopy. Pretreatment with hyperthermia was used to alleviate restrictive vascular permeability in these slow-growing xenografts. Targeted liposomes had an increased cytotoxic effect on PSMA-positive cell lines. A twofold increase in liposomal accumulation was observed in LNCaP xenografts after injection of targeted liposomes. Efficacy experiments with targeted and non-targeted doxorubicin-loaded liposomes showed no difference, and whole tumor microscopy revealed limited extravasation and retention in the perivascular space. Pre-treatment of tumors with hyperthermia enhanced liposomal accumulation, with a maximum of $11.58\% \pm 3.75\%$ injected dose per cm^3 of PSMA-targeted liposomes at 24 h after injection. This study shows that tumor-targeting modalities can increase accumulation of nanoparticles, although limited extravasation and retention may prevent maximal efficacy. The use of hyperthermia in conjunction with targeted liposomes appears to be a promising combination.

INTRODUCTION

Prostate cancer is one of the most prevalent cancers among men with an annual incidence of more than 180,000 new cases and with over 26,000 deaths in the United States alone²⁴⁰. First-line therapy of advanced disseminated prostate cancer starts with androgen deprivation therapy, although within a few years the disease progresses to castration-resistant prostate cancer (CRPC)^{241,242}. Since 2004, docetaxel is the first-line chemotherapy of CRPC²⁴³⁻²⁴⁵, and currently novel androgen receptor-targeting agents such as enzalutamide and abiraterone are being evaluated in pre- and post-docetaxel settings^{246,247}. Clinical trials have evaluated the use of docetaxel before or in combination with hormone therapy and these trials showed remarkable benefit of docetaxel²⁴⁸, although the drug also provoked severe adverse effects such as alopecia, nausea and neutropenia²⁴⁹. In order to use docetaxel in early stage disease, such issues need to be addressed. Moreover, intrinsic resistance to docetaxel is another major problem, since more than half of the patients do not show a biochemical response²⁴⁴. This may be caused by cross-resistance between microtubule-regulated androgen receptor trafficking²⁵⁰, reduced drug influx²⁵¹, increased cellular metabolism²⁵², and/or an unfavorable tumor microenvironment (aberrant vasculature, high interstitial fluid pressure, hypoxia) leading to reduced intratumoral drug levels²⁵³ and resulting in patient withdrawal. Therefore, strategies that address docetaxel resistance and reduce severe drug-induced toxicities are needed, and to this end several nanomedicines have been developed²⁵⁴.

Targeted nanoparticles have been developed with the aim of reducing adverse effects by shielding the drug from interactions during circulation, decreasing exposure to non-target tissues and increasing accumulation at the target site. The rationale for using nanoparticles as anti-cancer treatment is based on the discovery that macromolecules accumulate in solid tumors due to the enhanced permeability and retention (EPR) effect¹⁴². This phenomenon is based on observations that solid tumors have a leaky and dysfunctional vasculature; macromolecules leak into the tumor where they remain present due to poor drainage by an impaired lymphatic system. One of the most well-known nanoparticles developed is Doxil, a doxorubicin-loaded liposome approved by the FDA in 1995, which has been proven effective in the clinic²⁵⁵. Doxil reduces side effects that are seen after administration of free doxorubicin^{256,257}, and facilitates an increased accumulation of drug in solid tumors²⁵⁸. Delivery of docetaxel with liposomes has shown high specific release and decreased resistance compared to free docetaxel administration²⁵⁹. To improve drug delivery to prostate tumors and reduce adverse effects, targeted antibody conjugated liposomal docetaxel formulations are being developed²⁶⁰.

Prostate cancer cells express high levels of prostate-specific membrane antigen (PSMA), allowing targeted nanoparticles to show improved specific targeting and receptor mediated endocytosis, internalization and intracellular release^{261,262}, yet pre-

venting multi-drug resistance²⁶³. PSMA is a membrane-bound glycoprotein expressed by almost all prostate cancers and is upregulated in advanced stages of the disease²⁶⁴. Its expression is independent from androgen²⁶⁵ and therefore remains a valid target in hormone-refractory cells after androgen ablation treatment. Moreover, it has been suggested to be upregulated after surgical or hormonal ablation²¹⁷. PSMA is currently one of the most promising targets for prostate cancer with clinical implementation of PSMA-targeted imaging and developments in radionuclide therapy²⁶⁶. Targeting agents against PSMA have been reviewed extensively²⁶⁷⁻²⁶⁹, and include the recently developed nanobodies¹¹⁸, which combine the avidity of monoclonal antibodies with the ease of production and efficient biodistribution of peptides. Nanobodies, or single domain antibodies, were isolated after the discovery of functional heavy-chain antibodies in camelidae^{78,270} and are considered the smallest naturally derived antibodies retaining sufficient antigen binding⁹⁸.

In this study we report on the delivery, tumor accumulation and efficacy of chemotherapeutics via anti-PSMA nanobody targeted liposomes using doxorubicin as a reference drug. The resulting PSMA-targeted liposomes were evaluated for targeting and therapeutic benefit both *in vitro* and *in vivo*, using different PSMA positive and negative prostate cancer cell lines, and cell-based and patient-derived xenograft (PDX) models. The use of nanobody-targeted liposomes created a highly specific platform for prostate cancer treatment which, in combination with hyperthermia, could further enhance tumor-specific accumulation.

MATERIALS AND METHODS

Anti-PSMA nanobody

The production and characterization of the anti-PSMA nanobody targeting the extracellular domain of PSMA has been described elsewhere¹¹⁸.

Liposome preparation, drug loading and radiolabeling with indium-111

Liposomes were composed of hydrogenated soy phosphatidylcholine (HSPC; Lipoid GmbH, Ludwigshaven, Germany), cholesterol (Sigma-Aldrich, St. Louis, MO), 1,2-distearoyl-*sn*-glycerol-3-phosphoethanolamine-N-[methoxy(polyethylene glycol)-2000] (ammonium salt) (18:0 PEG2000 PE; Lipoid GmbH), 1,2-distearoyl-*sn*-glycerol-3-phosphoethanolamine-N-[maleimide(polyethylene glycol)-2000] (ammonium salt) (DSPE-PEG(2000)-Maleimide; Avanti Polar Lipids Inc., Alabaster, AL), and 1,2-distearoyl-*sn*-glycerol-3-phosphoethanolamine-N-diethylenetriaminepentaacetic acid (ammonium salt) (18:0 PE-DTPA; Avanti Polar Lipids Inc.) in a molar ratio of 57:38:4:1:0.1 and were dissolved in chloroform/methanol 9:1 (vol/vol) before lipid film hydration and extrusion²⁷¹.

Doxorubicin-loaded liposomes were prepared with ammonium sulfate to enable active loading of doxorubicin at 60°C with a 1:0.15 lipid to drug molar ratio. After drug loading, the functional PEG-maleimide groups in the liposomes were used to couple the anti-PSMA nanobody in a molar ratio of 1:100 of total lipid to nanobody. The size distribution of the liposomes was measured with a Zetasizer NanoSeries (Malvern Instruments Ltd., Worcestershire, United Kingdom). The total amount of phospholipid was determined by phosphate assay, as described before²⁷².

Radiolabeling of the liposomes with ¹¹¹In was performed for the *in vivo* localization studies and has been described before¹²⁷. Briefly, approximately 30 MBq of ¹¹¹In was coupled to 1 μmol of liposomes before *i.v.* injection.

Cell lines and culture conditions

Cell culture reagents, unless otherwise specified, were obtained from Sigma-Aldrich. Human prostate cancer cell lines LNCaP, PC-3, MDA PCa 2b and DU145 were obtained from the American Type Culture Collection (ATCC, Manassas, VA). The transfected murine melanoma cell line B16-PSMA was kindly provided by Marco Colombatti (University of Verona, Italy). LNCaP, PC-3 and DU145 were propagated using Roswell Park Memorial Institute (RPMI) 1640 medium supplemented with penicillin and streptomycin (P/S; Lonza, Basel, Switzerland), and 5% fetal bovine serum (FBS). MDA PCa 2b was cultured in Ham's F12 medium (Lonza) supplemented with 15% FBS, 25 ng/mL cholera toxin, 10 ng/mL epidermal growth factor (EGF), 5 μM phosphoethanolamine, 120 pg/mL hydrocortisone and 1% insulin-transferrin-selenium (Thermo Fisher Scientific, Waltham, MA). B16-PSMA was cultured in Dulbecco's Modified Eagle Medium (DMEM) supplemented with 10% FBS under selection of 1.2 mg/mL geneticin (G418; Thermo Fisher Scientific). All cell lines were routinely cultured in a humidified incubator at 37°C and 5% CO₂. LNCaP, MDA PCa 2b²⁷³ and B16-PSMA are positive for PSMA, whereas PC-3 and DU145 are PSMA negative²⁷⁴.

FACS analysis

Cells were harvested after trypsinization and resuspended in cold PBS (Sigma-Aldrich) containing 1% BSA (Sigma-Aldrich). The cell suspensions were incubated with targeted and non-targeted liposomes containing rhodamine B (1,2-dipalmitoyl-*sn*-glycero-3-phosphoethanolamine-N-(lissamine rhodamine B sulfonyl; Avanti Polar Lipids Inc.) for 30 min at 4°C. After incubation, cells were washed twice with cold PBS/1% BSA and subjected to flow cytometric analysis using the LSRFortessa cell analyzer (BD Biosciences, Franklin Lakes, NJ). Data analysis was performed using the FlowJo software (TreeStar Inc, Ashland, OR).

Cytotoxicity assay

Cells were plated in 96-well cluster plates at 5,000 cells (PC-3 and DU145) or 10,000 cells (LNCaP and MDA PCa 2b) per well in 100 μ L of their respective medium. To determine sensitivity to doxorubicin and doxorubicin liposomes, cells were exposed to concentrations ranging from 10^{-5} to 10^2 μ M doxorubicin or empty liposomes as control with comparable lipid concentration for 24, 48 and 72 h. At each time point, cells were fixed with 10% trichloroacetic acid (TCA, Sigma-Aldrich) after which cell viability was assessed using the Sulphorhodamine B (Sigma-Aldrich) colorimetric assay.

***In vivo* imaging**

All animal experimentation procedures were approved by the Animal Welfare Committee of the Erasmus Medical Center in Rotterdam, the Netherlands. Immune competent C56Bl/6 mice (for B16-PSMA) and NMRI *nu/nu* (for LNCaP, PC-3, MDA PCa 2b) were purchased from Envigo (Cambridgeshire, UK). Athymic NMRI *nu/nu* mice were obtained from Taconic (Ry, Denmark) for experiments with patient-derived xenografts. LNCaP, PC-3, MDA PCa 2b cells were resuspended in High Concentration Matrigel (BD Biosciences, San Jose, CA) at a concentration of 5×10^6 cells/100 μ L. B16-PSMA was reconstituted at a concentration of 1×10^6 cells/100 μ L PBS. Cell suspensions (100 μ L) were injected subcutaneously in the right flank of 9-week old mice. Patient-derived xenografts, PC-295 and PC-310, were propagated subcutaneously in NMRI *nu/nu* mice which were supplemented with testosterone (Sigma-Aldrich)²⁷⁵ through silastic implants. When tumors reached approximately 200 mm³ in size, mice were injected with radiolabeled liposomes (1 μ mol of liposomes in 200 μ L) for SPECT/CT (nanoSPECT/CT; Mediso Medical Imaging Systems) imaging. Imaging was performed using the following settings: SPECT static scan with 20 projections, 60 s/projection, and a quality factor of 0.8. APT1 apertures were in place with 1.4 mm diameter pinholes (FOV 24 + 16 mm). For CT, 240 projections were made using 24 kVp tube voltage and 500 ms exposure. T = 0 scans were followed by scans at 4, 8, 24, 48, 72 and 96 h after liposomal injection. Analysis of SPECT/CT scans was performed using InVivoScope/VivoQuant software (inviCRO), where three-dimensional regions of interest were drawn over the tumor to calculate the amount of radiolabeled liposomes (%ID/cm³) taken up by the tumor.

***In vivo* efficacy**

To assess antitumor efficacy, LNCaP and PC-3 xenografts were established as described above. When tumors were established (*circa* 200 mm³), mice were randomized into 3 groups of at least 5 animals and treated with unloaded liposomes, doxorubicin-loaded non-targeted liposomes, or doxorubicin-loaded PSMA-targeted liposomes by intravenous injection of 5 mg/kg doxorubicin (or comparable lipid concentration for the unloaded liposomes) once every 3 d for 4 consecutive times. Body weight and

tumor size were measured every 2 d. Tumor volumes were calculated with the following formula: $Volume = height \times width \times depth \times 0.4$, where the day before the first injection ($t = 0$) was set at 100%.

Hyperthermia to enhance EPR and improve liposomal uptake

MDA PCa 2b tumor grafts (circa 10 mm³ fragments), harvested from donor mice, were xenografted subcutaneously on the right hind leg of NMRI *nu/nu* mice. Tumors were allowed to grow till 100 mm³, after which the tumor was subjected to mild hyperthermia for 1 h at 41°C, followed by an intravenous injection of unloaded PSMA-targeted and non-targeted ¹¹¹In-labeled liposomes. Liposomal uptake was followed with SPECT/CT imaging using the same settings as described above.

Microscopic evaluation of intratumoral liposomal localization

Mice were inoculated with LNCaP cells. When the tumors had reached approximately 200 mm³, mice were injected i.v. with 1 μmol of drug-loaded PSMA-targeted liposomes 4 h before sacrifice. Xenograft tumors were excised and imaged with an Leica SP5 AOBS upright confocal microscope with multiphoton laser (Leica, Wetzlar, Germany) using a water immersion objective (HCX APO L 20x/1.0 W, Leica) with a ceramic front. Immediately after excision, tumors were submerged in PBS and imaged using the following settings: pixel size 1.4 μm for 512 x 512 pixel images and 0.7 μm for 1024 x 1024 pixel images, 300 μm stacks with a 10 μm step size. Rhodamine liposomes were imaged with pinhole at 2 Airy units, excitation 561 nm and emission BP 570-620 nm, and the tumor was imaged using reflectance microscopy with pinhole at 2 Airy units, excitation 633 nm and emission BP 630-636 nm.

Statistical analysis

Statistical analyses were performed using GraphPad Prism (version 5.01; GraphPad Software). All statistical tests were two-tailed, and a *p* value lower than 0.05 was considered statistically significant.

RESULTS

Characterization of Liposomes

Empty liposomes were generated using lipids and cholesterol in the ratio as described. These empty liposomes were subsequently coupled with anti-PSMA nanobody and loaded with doxorubicin or labeled with ¹¹¹In. Empty liposomes were obtained with an average size of 82.69 ± 1.47 nm and polydispersity index (PDI) of 0.026 ± 0.013. PSMA-targeted liposomes had an average size of 87.71 ± 4.02 nm and PDI of 0.038 ± 0.018. Loading with doxorubicin did not result in an increase in the size of liposomes,

since doxorubicin-loaded liposomes were 82.45 ± 1.63 nm, PDI of 0.030 ± 0.018 , and PSMA-targeted doxorubicin liposomes were 87.88 ± 3.27 nm, PDI of 0.052 ± 0.021 . The radiolabeling efficiency of liposomes with ^{111}In was $> 99\%$. On average the liposomes were labeled with 32.52 ± 4.41 MBq ^{111}In per μmol liposomes.

***In vitro* specificity of anti-PSMA nanobody targeted liposomes**

Flow cytometry analysis was performed to confirm targeting specificity of the PSMA-targeted liposomes using several PSMA positive and negative prostate cancer cell lines.

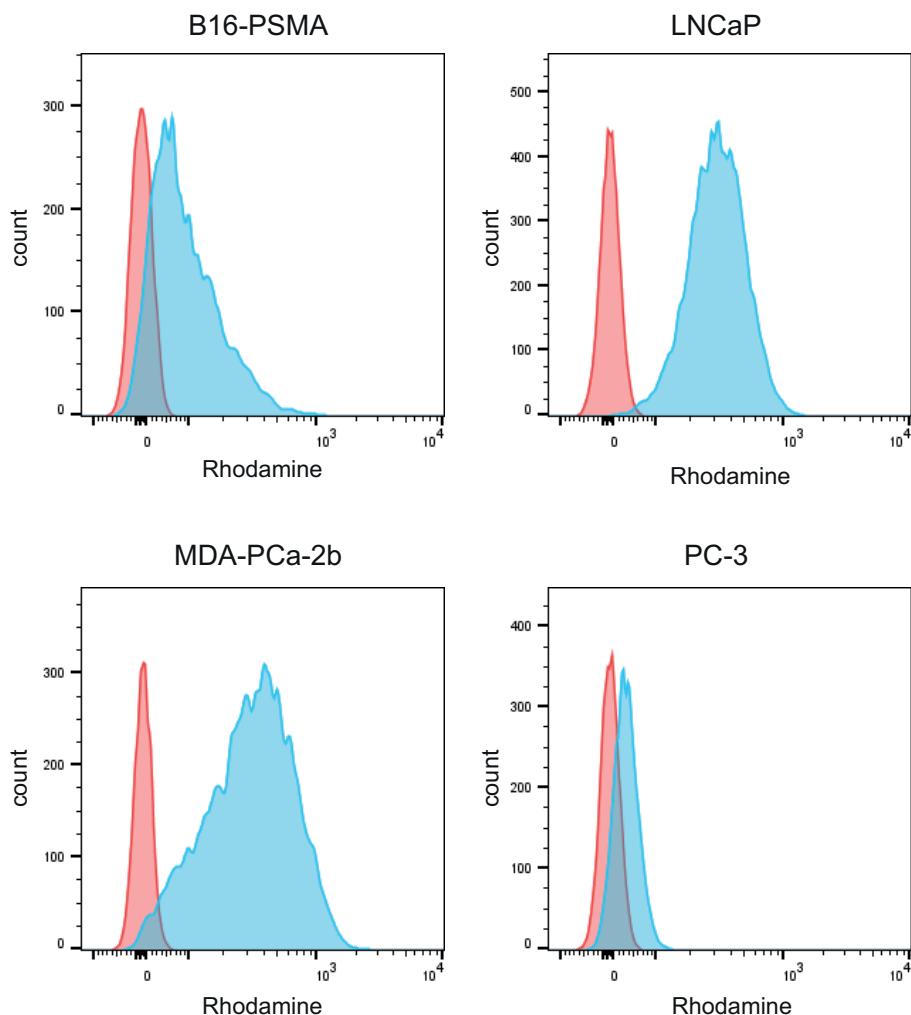


Figure 1. Representative graphs depicting binding of non-targeted (red) versus targeted empty liposomes (blue) in PSMA positive cell lines B16-PSMA, LNCaP, MDA PCa 2b and PSMA negative cell line PC-3.

Table 1. Cell binding of PSMA-specific liposomes

Cell line	MFI (non targeted)	MFI (anti-PSMA)
B16-PSMA	3.21 (0.64 - 3.85)	59.1 (27.4 - 112.7)
DU-145	1.28 (1.28 - 1.28)	1.28 (1.28 - 1.28)
LNCaP	3.85 (2.57 - 4.17)	195.0 (165.3 - 269.3)
MDA-PCa-2b	3.85 (2.57 - 3.85)	310.0 (310.0 - 339.0)
PC-3	3.85 (2.57 - 3.85)	2.57 (1.28 - 5.13)
VCaP	3.85 (3.85 - 3.85)	2.57 (1.60 - 2.57)

Median fluorescence intensity is shown with 25th and 75th percentiles. All experiments have been performed for a minimum of 3 times.

Table 1 shows the comparison of the median fluorescence intensity for unloaded non-targeted and targeted liposomes. Non-targeted liposomes showed aspecific binding to all cell lines irrespective of the presence of PSMA, which was similar for all cell lines (comparable to a background mean fluorescent intensity of 1.13 ± 0.94). The targeted liposomes showed increased binding to the PSMA positive cell lines, B16-PSMA, LNCaP and MDA PCa 2b as compared to the non-targeted liposomes, confirming the specific binding of these liposomes (Figure 1). Based on these results PSMA expressing LNCaP cells and PSMA negative PC-3 cells, as negative control cell line, were selected for further efficacy experiments.

Cytotoxicity of targeted and non-targeted doxorubicin liposomes

To determine the sensitivity of prostate cancer cells to free and liposomal doxorubicin, cells were exposed to the various treatments and cell viability was calculated using the SRB assay. EC₅₀ values for the prostate cancer cell lines LNCaP, MDA PCa 2b (PSMA-positive) and PC-3, DU145 (PSMA-negative) after treatment with free doxorubicin, drug-loaded targeted and non-targeted liposomes are shown in Table 2. For all cell lines tested, free doxorubicin was more effective than both targeted and non-targeted liposomal doxorubicin. Encapsulated doxorubicin showed a lesser efficacy and higher

Table 2. Cytotoxicity of free and liposomal doxorubicin

Cell line	EC ₅₀ free dox (in μM)	EC ₅₀ DL (in μM dox)	EC ₅₀ TDL (in μM dox)
DU-145	0.011 ^{a,b}	3.834 ^a	3.030 ^b
LNCaP	0.092 ^{a,b}	4.021 ^{a,c}	0.361 ^{b,c}
MDA-PCa-2b	0.012 ^{a,b}	1.026 ^a	0.282 ^b
PC-3	0.122 ^{a,b}	40.02 ^a	22.26 ^b

Statistical test used: two-tailed one-way ANOVA with Bonferroni multiple comparison test. ^a Free doxorubicin versus Doxil is significant at $p < 0.05$ level; ^b Free doxorubicin versus Doxil-A7 is significant at $p < 0.05$ level; ^c Doxil versus Doxil-A7 is significant at $p < 0.05$ level.

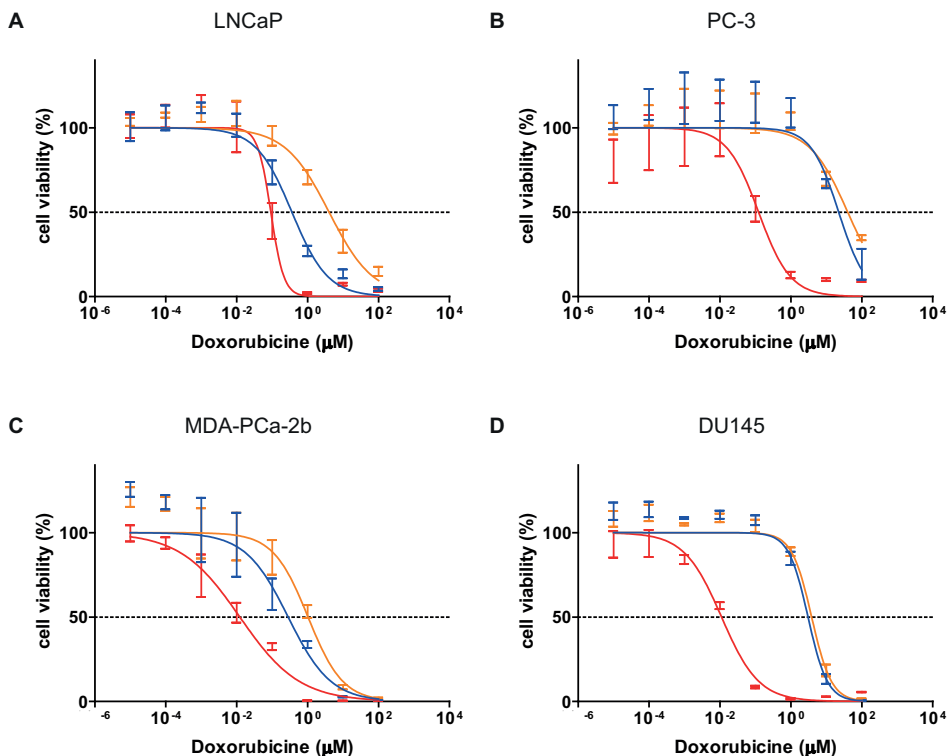


Figure 2. Cell viability after treatment with free doxorubicin (red), doxorubicin liposomes (orange) or targeted doxorubicin liposomes (blue). The left panels show the PSMA positive cell lines LNCaP and MDA PCa 2b (A, C), the right panels show the PSMA negative cell lines PC-3 and DU145 (B, D). Data represents mean \pm SEM of 3 independent experiments performed in duplicate.

EC50 values compared to free doxorubicin, which can be explained by the slow release of doxorubicin from liposomes. Figure 2 shows cytotoxicity of LNCaP and PC-3 cells after treatment with free doxorubicin, non-targeted doxorubicin liposomes and targeted doxorubicin liposomes. The increased cytotoxicity of targeted liposomes was most significant for LNCaP, with an EC50 for targeted and non-targeted liposomes of 0.361 μM and 4.021 μM doxorubicin, respectively. MDA PCa 2b cells showed an EC50 of 0.282 μM and 1.026 μM , for targeted and non-targeted liposomes. As expected, no additional benefit of the targeted liposomes was observed for the PSMA negative PC-3 cells.

Accumulation of indium-111 labeled liposomes in prostate tumor xenografts

While *in vitro* experiments showed that targeted liposomes can be cytotoxic to cells, *in vivo* uptake and accumulation of (targeted) liposomes in the tumor is very much determined by the EPR effect, which is influenced by a number of different factors¹²⁷.

Different xenografts, both patient-derived (PDX) and cell line-based were selected representing PSMA-negative and PSMA-positive tumors, to assess the uptake of ^{111}In -labeled liposomes. Surprisingly, the high PSMA-expressing PDXs, PC-295 and PC-310, did not show an enhanced uptake of the targeted liposomes as compared to non-targeted liposomes (Figure 3A). In contrast, the PSMA-positive cell line-based

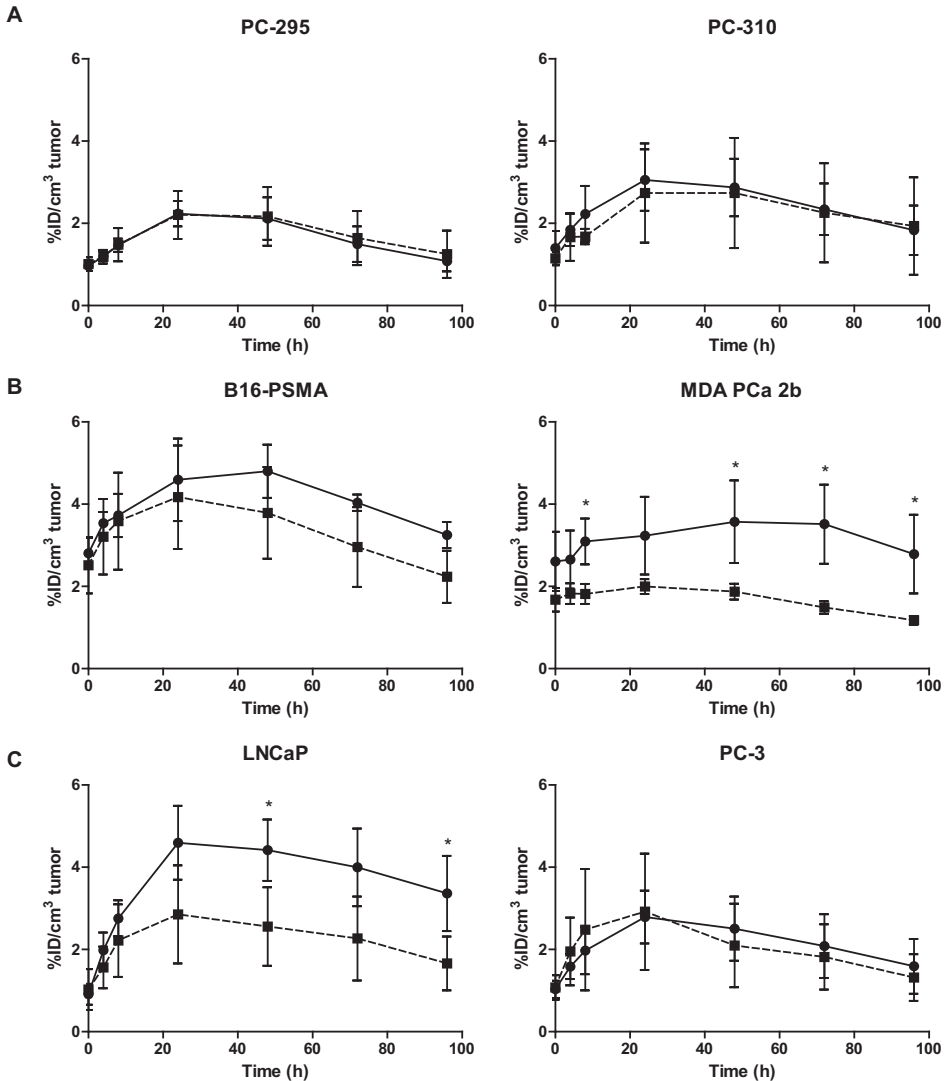


Figure 3. Graphs depicting tumor uptake after injection with indium-111 labeled empty liposomes, both non-targeted (square) and targeted (circle) with anti-PSMA nanobodies. PDXs derived from prostatic carcinomas PC-295 and PC-310 (A); Transfected B16-PSMA and MDA PCa 2b xenografts (B); LNCaP and PC-3 xenografts (C). * statistical significance $p < 0.05$ with unpaired two-tailed t-test. Data represents mean \pm SD of 3 or more animals.

xenografts showed higher accumulation of the PSMA-targeted liposomes: B16-PSMA tumors showed a relatively high uptake both with targeted (max. at 48 h with 4.80% injected dose per cm³) and non-targeted liposomes (max. at 24 h at 4.17% injected dose per cm³) compared to the PDXs (Figure 3B, left panel) and MDA PCa 2b showed a 2-fold increase in tumor uptake of targeted liposomes over non-targeted liposomes with a maximum uptake of 3.57% injected dose per cm³ at 48 h (Figure 3B, right panel). LNCaP tumors showed the largest increase in tumor uptake with targeted liposomes (max. 4.59% injected dose per cm³ at 24 h) when compared to non-targeted liposomes (Figure 3C, left panel). No difference between targeted and non-targeted liposomal accumulation was observed for the PSMA-negative PC-3 tumors, confirming the absence of significant amounts of PSMA in this model (Figure 3C, right panel). Based on these results, we decided to continue with efficacy experiments on the LNCaP xenografts, using PC-3 xenografts as non-target controls.

***In vivo* efficacy of non-targeted and PSMA-targeted doxorubicin liposomes**

PSMA-expressing LNCaP and PSMA-negative PC-3 tumor bearing mice were injected with doxorubicin-loaded liposomes to ascertain inhibitory effects of the liposomal formulations on tumor growth. A treatment schedule was chosen with 4 subsequent injections of 5 mg/kg doxorubicin encapsulated in PSMA-targeted or non-targeted liposomes. Tumor growth arrest was immediately induced after the first injection with both PSMA-targeted and non-targeted liposomal doxorubicin and continued for at least 30 d after the last injection for both cell lines (Figure 4). Empty PSMA-targeted liposomes served as control and showed no inhibitory effect. The already high efficacy of liposomal doxorubicin did not allow a discrimination between a potential effect of targeted liposomes over the non-targeted liposomes.

***Ex vivo* localization of doxorubicin-loaded liposomes**

To gain insight into the lack of effect of the PSMA-targeted doxorubicin liposomes, LNCaP tumors were harvested intact and imaged immediately. Liposomes were observed in and around blood vessels and accumulating to a certain degree in the cytoplasm of tumor cells. In general, the penetration of PSMA-targeted liposomes in the tumor was limited and large areas of the LNCaP tumor remained void of liposomes (Figure 5).

Localization and uptake of empty liposomes after mild hyperthermia

To enhance liposomal accumulation in the tumor, PSMA-expressing subcutaneously xenografted MDA PCa 2b tumors were preheated locally. Hyperthermia pretreatment did not diminish the ratio between accumulation of targeted and non-targeted liposomes originally seen in non-heated xenografts, which leads to a high accumulation of targeted liposomes after hyperthermia. Whereas tumors showed significantly improved

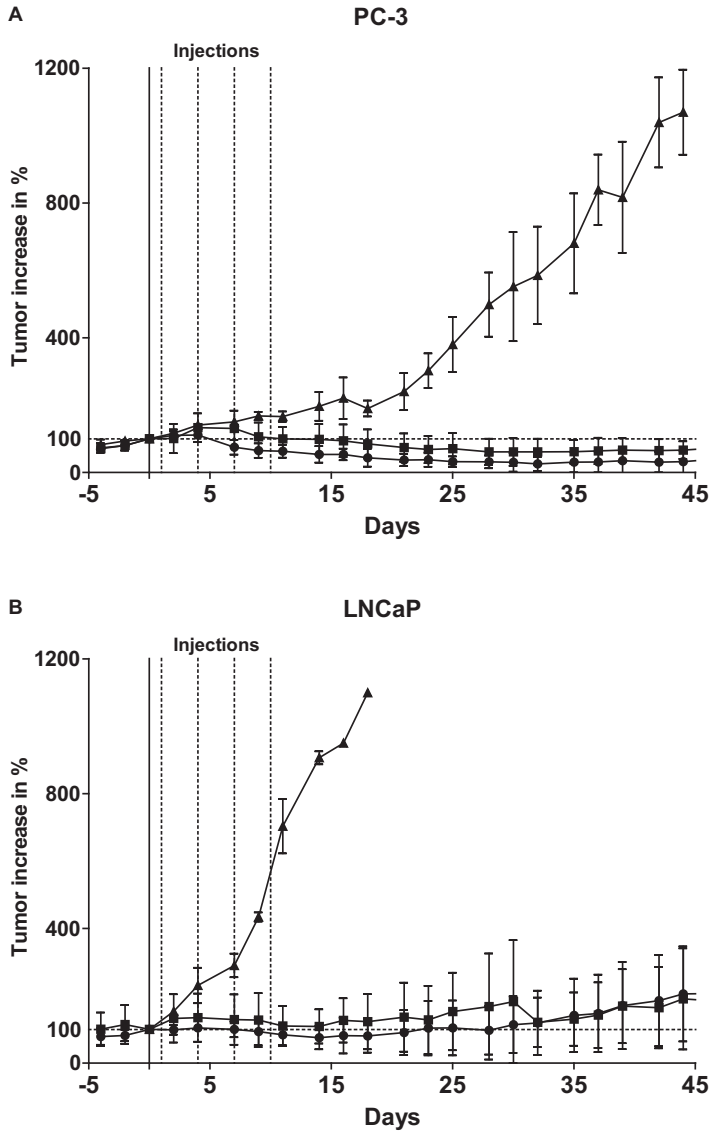


Figure 4. Tumor growth of PC-3 (A) and LNCaP (B) xenografts after 4 subsequent injections with empty liposomes (triangle), doxorubicin liposomes (square) and targeted doxorubicin liposomes (circle). Data represents mean \pm SD of 5 or more animals.

accumulation for targeted versus non-targeted liposomes (3.23 ± 0.94 and $2.00 \pm 0.18\%$ injected dose per cm^3 at 24 h) (Figure 3), after pretreatment with hyperthermia, accumulation increased to 11.24 ± 3.34 and $7.10 \pm 1.55\%$ injected dose per cm^3 at 24 h for targeted and non-targeted liposomes, respectively (Figure 6).

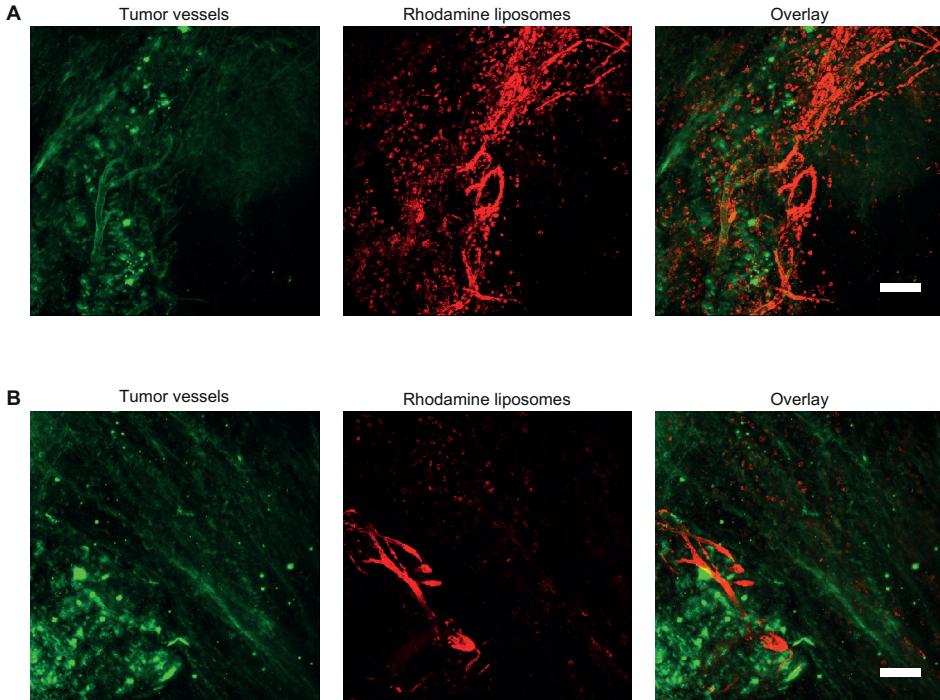


Figure 5. Whole tumor microscopy showing liposomal distribution in tumors. Representative maximum projections of an LNCaP xenograft injected with targeted doxorubicin liposomes. Area showing targeted liposomes within the tumor vasculature and those that have extravasated and accumulated in the tumor cells (A), indicating internalization. Poorly vascularized area within the same tumor with lower permeability where the liposomes are confined to the vessels (B). Scale bars = 100 μm .

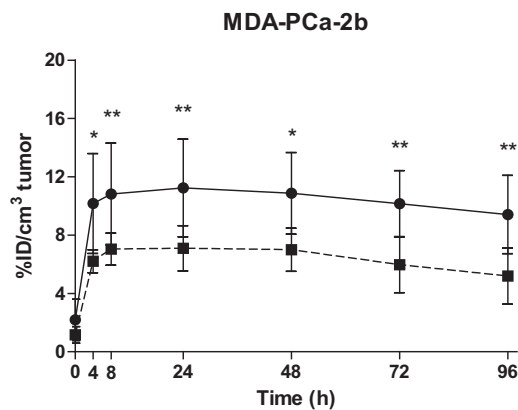


Figure 6. Tumor accumulation of injected indium-111 labeled empty liposomes in MDA-PCa-2b xenografts after 1 h of hyperthermia (41°C applied locally to the tumor), both non-targeted (square) and targeted (circle) with anti-PSMA nanobody. Statistical significance * = $p < 0.05$ and ** = $p < 0.01$ with Mann Whitney test. Data represents mean \pm SD of > 5 animals.

DISCUSSION

The principle of highly specific targeted drugs has always been appealing, since these personalized targeted drugs would theoretically only accumulate in the target region resulting in decreased side effects and an increased therapeutic effect. Targeting would be especially interesting in combination with nanomedicines, which shield the drugs during long circulation and have the capability to deliver large quantities of drugs into the cell. While the targeting of nanoparticles is primarily aimed to improve localization to the target tissue, added advantages are an increased internalization and target tissue retention²⁶⁰. Studies with targeted liposomes have provided mixed results²⁷⁶, but it seems that internalizing targeting moieties, like the one used in this study, are more effective as therapy⁵⁶.

We have previously reported the generation of a highly specific PSMA nanobody which is capable of accumulating in PSMA-expressing xenografts. Here we conjugated the nanobody to liposomes and we showed that PSMA-targeted liposomes can specifically bind to PSMA-positive cells and tumors, yet we could not show an added therapeutic benefit of these targeted liposomes *in vivo*. The chosen dosing regimens may have been too frequent for long circulating liposomes, as it has recently been shown that dosing every other day can diminish the added benefit of targeting moieties, whereas a once-weekly dosing schedule showed targeted nanoparticles to be more efficacious than non-targeted nanoparticles²⁷⁷. It has been suggested that frequent administration causes a continuous supply to the tumor, rendering targeting irrelevant or even a factor reducing efficacy. Therefore, it seems that the higher dose intensity in this study resulted in an efficacy too high to elucidate an added effect of targeted liposomes. Furthermore, there may be additional reasons for the absence of a difference between PSMA-targeted and non-targeted liposomes. The difference in accumulation between targeted and non-targeted liposomes was limited (average $\Delta = 1.37 \pm 0.43\%$ injected dose per cm^3), which might not be enough to elucidate a difference in efficacy.

Despite these findings, benefits of encapsulated drugs as alternative treatment options have led to the generation of several new nanoparticles against prostate cancer in (pre)clinical trials. For example, Cellax, is a self-assembled nanoparticle composed of docetaxel conjugated to PEG-acetylated carboxymethylcellulose²⁷⁸, and BIND-014, is a nanoparticle where docetaxel is encapsulated in biodegradable polymer based particles targeted against PSMA with S,S-2[3[5-amino-1-carboxypentyl]-ureido]-pentanedioic acid^{63,279,280}. The results of these nanomedicines are hopeful, and continued investigation of barriers in tumor morphology and physiology may further enhance the efficacy of nanomedicine.

Targeted liposomes tend to bind to the first barrier of target-positive cells which strongly reduces the penetration of liposomes throughout the tumor and hence may

reduce efficacy. This so-called binding site barrier effect may act as a bottleneck, where high avidity antibodies bind the first possible antigen and effectively are stopped at the periphery of the target site^{207,281,282}. Another issue is the limited extravasation or accumulation in the perivascular space as has been investigated before as an important aspect of the EPR effect¹²⁷ and indeed extravasation from the tumor vasculature has been recognized as the rate-limiting step for tumor accumulation⁵². It is known that the penetration depth for liposomes is limited to a few dozen μm ²⁸³. To counteract this, we have shown in this study that liposomal accumulation can be enhanced with the use of mild hyperthermia, which possibly widens the restrictive gaps in the endothelial layer to enhance extravasation¹⁸², supporting the notion that limited extravasation of liposomes is a major restrictive factor in nanoparticle delivery. In this study, the difference between tumor accumulation of targeted and non-targeted liposomes remained significant, which may warrant a follow-up study where efficacy of targeted liposomes in combination with hyperthermia is investigated.

CONCLUSION

We used a highly specific anti-PSMA nanobody to functionalize doxorubicin loaded liposomes. The anti-PSMA targeted liposomes showed high specificity for PSMA-positive cell lines and xenografts, although we were unable to show enhanced therapeutic efficacy. Additional studies revealed that limited extravasation and/or a restrictive penetration of the tumor tissue is a major limiting factor, resulting in the accumulation of liposomes in the (peri)vascular space rather than the tumor. Nonetheless, extravasation from the tumor blood vessels could be enhanced with the application of mild hyperthermia resulting in a more than 3-fold increase in liposomal accumulation, proving to be an interesting option to enhance drug delivery to the tumor site and improve drug efficacy.

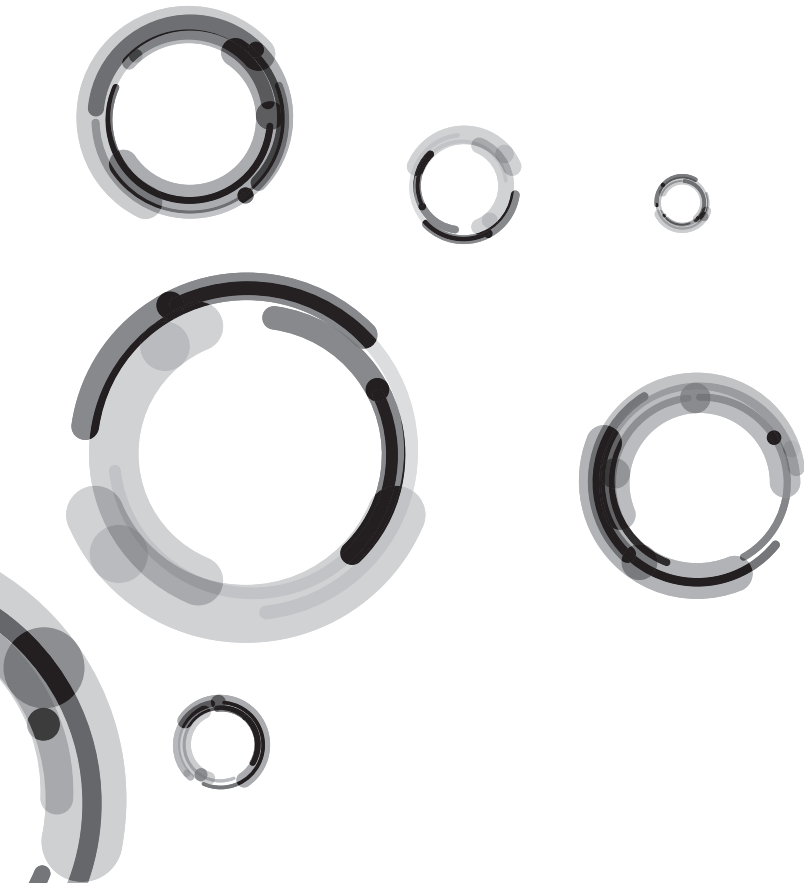


CHAPTER 5

Investigation of Factors Determining the Enhanced Permeability and Retention Effect in Subcutaneous Xenografts

Michiel Bolkestein, Erik de Blois, Stuart J. Koelewijn, Alexander M.M.
Eggermont, Frank Grosveld, Marion de Jong, Gerben A. Koning

Adapted from Journal of Nuclear Medicine, 2016



ABSTRACT

Liposomal chemotherapy offers several advantages over conventional therapies, including high intratumoral drug delivery, reduced side effects, prolonged circulation time, and the possibility to dose higher. The efficient delivery of liposomal chemotherapeutics relies, however, on the enhanced permeability and retention (EPR) effect, which refers to the ability of macromolecules to extravasate leaky tumor vessels and accumulate in the tumor tissue. Using a panel of human xenograft tumors, we evaluated the influence of the EPR effect on liposomal distribution *in vivo* by injection of pegylated liposomes radiolabeled with indium-111. Liposomal accumulation in tumors and organs was followed over time by SPECT/CT imaging. We observed that fast-growing xenografts, which may be less representative of tumor development in patients, showed higher liposomal accumulation than slow-growing xenografts. Additionally, several other parameters known to influence the EPR effect were evaluated, such as blood and lymphatic vessel density, intratumoral hypoxia, and the presence of infiltrating macrophages. The investigation of various parameters showed a few correlations. Although hypoxia, proliferation, and macrophage presence were associated with tumor growth, no hard conclusions or predictions could be made regarding the EPR effect or liposomal uptake. However, liposomal uptake was significantly correlated with tumor growth, with fast-growing tumors showing a higher uptake, although no biological determinants could be elucidated to explain this correlation.

INTRODUCTION

Almost all nanocarriers, including liposomes¹⁵, and many other anticancer drugs rely on the enhanced permeability and retention (EPR) effect for accumulation in tumor tissue. The EPR effect is defined as the process of extravasation of large molecules from leaky tumor vasculature, leading to accumulation in tumor tissue¹⁴². The EPR effect is dependent on many biological parameters, with the development of the abnormal tumor vasculature playing a major role, although other parameters such as the composition of the surrounding stroma, absence of functional lymphatics, and presence of tumor infiltrating macrophages also play an important role²⁸⁴. Abnormally upregulated growth factors affect the vasculature of the tumor¹⁵¹ and lead to large endothelial junctions at the luminal surface, resulting in a leaky vasculature²⁸⁵. In addition, vessels lack smooth muscle cell layers and supporting cells²⁸⁶, and the fast recruitment of blood vessels results in tumor neovasculature that is not hierarchically organized, causing a heterogeneous spatial distribution^{151,287,288}. Finally, tumors overexpress many permeability-enhancing factors, which contribute to an enhanced EPR effect²⁸⁹. These observations suggest that most tumors may be susceptible to nanoparticle treatment, but thus far such particles show only a limited effect *in vivo* due to various barriers such as the mononuclear phagocyte system, extracellular matrix, low pH, low oxygenation, and high interstitial fluid pressure²⁹⁰⁻²⁹². The intra- and intertumoral heterogeneity are major factors influencing the EPR effect, especially in patients, where tumor growth and vessel development are slower¹⁵⁰. The Food and Drug Administration–approved liposomal doxorubicin (Doxil or Caelyx; Janssen Products, LP) is one of the most successful nanoparticle drugs for several cancer types²⁹³⁻²⁹⁶. Unfortunately, Doxil has a limited effect on overall survival when compared with conventional chemotherapy²⁸⁴, as has been shown in various clinical trials^{294,297,298}. This and previous results suggest that tumor physiology influences the efficacy of nanoparticle drugs, possibly due to variations in the EPR effect²⁹⁹. Because the EPR effect is essential for the efficacy and mode of action of liposomes *in vivo*, the aim of this study was to investigate major parameters influencing EPR and their effects on liposomal uptake in tumor xenografts. To this end, we injected unloaded, long-circulating, pegylated Doxil-like liposomes to determine liposomal tumor accumulation. Various human xenograft tumor models, including squamous cell carcinoma, breast cancer, and pancreatic cancer, were selected on the basis of tumor growth rate, taking into consideration that slow-growing tumors are more representative of tumor growth in patients. Our results show that it is difficult to elucidate single determinants of the EPR effect and we therefore suggest that liposomal uptake and distribution in tumors is a multifactorial process involving physiological and morphological parameters.

MATERIALS AND METHODS

Preparation of unloaded Doxil liposomes

Doxil liposomes were prepared by the lipid film hydration and extrusion method³⁰⁰. A mixture containing hydrogenated soy phosphatidylcholine (HSPC; Lipoid GmbH, Ludwigshaven, Germany), cholesterol (Sigma-Aldrich, Zwijndrecht, the Netherlands), 1,2-distearoyl-*sn*-glycerol-3-phosphoethanolamine-N-[methoxy(polyethylene glycol)-2000] (ammonium salt) (18:0 PEG₂₀₀₀ PE; Lipoid GmbH), 1,2-distearoyl-*sn*-glycerol-3-phosphoethanolamine-N-diethylenetriaminepentaacetic acid (ammonium salt) (18:0 PE-DTPA; Avanti Polar lipids, Alabaster, AL) in a molar ratio 57:38:5:0.1 was dissolved in chloroform/methanol 9:1 (vol/vol). After the addition of 0.1 mol% 1,2-dipalmitoyl-*sn*-glycero-3-phosphoethanolamine-N-(lissamine rhodamine B sulfonyl) (ammonium salt) (Rhodamine-PE; Avanti Polar lipids), the solvent was evaporated in vacuo using a rotary evaporator (Büchi Rotavapor R-210, Büchi Labortechnik, Flawil, Switzerland) until a homogeneous lipid film was formed. The lipid film was hydrated in 4-(2-hydroxyethyl)-1-piperazineethanesulfonic acid (HEPES) buffered saline (10 mM HEPES, 135 mM NaCl, pH 7.4). The newly formed vesicles were extruded at 60°C through a high-pressure Lipex thermoline extruder (Northern Lipids Inc, Vancouver, Canada) by passing through Nucleopore polycarbonate membrane filters (Whatman, Newton, MA) with pore diameters of 200, 100, 80, and 50 nm (5 extrusions per filter). The average diameter and size distribution (polydispersity index) of the liposomes were determined by dynamic light scattering using a Zetasizer Nano (Malvern Instruments, Worcestershire, United Kingdom). Total phospholipid content was determined by phosphate assay, as described elsewhere²⁷².

Cell lines

Established human cell lines were obtained from the American Type Culture Collection, among which: one squamous cell carcinoma cell line (A431), four pancreatic adenocarcinoma (AsPC-1, BxPC-3, CFPAC-1, HPAF-II), one epithelioid carcinoma (PANC-1), two breast adenocarcinoma (MDA-MB-231, MDA-MB-468), and one primary ductal breast carcinoma (UACC-893). Cell culture reagents were purchased from Lonza (Breda, the Netherlands). A431, CFPAC-1, and PANC-1 were grown in Dulbecco's Modified Eagle Medium with glutamine supplemented with 10% fetal bovine serum; AsPC-1, BxPC-3, MDA-MB-231, MDA-MB-468, and UACC-893 were grown in Roswell Park Memorial Institute 1640 medium supplemented with 10% fetal bovine serum; HPAF-II was grown in Roswell Park Memorial Institute 1640 medium with glutamine supplemented with 5% fetal bovine serum.

Indium-111 labeling of liposomes

Liposomes contained 0.1 mol% 1,2-distearoyl-*sn*-glycero-3-phosphoethanolamine-*N*-diethylenetriaminepentaacetic acid (DTPA-PE) lipid (Avanti Polar Lipids, Inc.), which enabled conjugation with $^{111}\text{InCl}$ (Mallinckrodt Medical B.V.). Approximately 30 MBq indium-111 was incubated per μmol of liposomes for 15 min at room temperature; 2.5 M sodium acetate was used to set the pH at 5.0. Instant thin-layer chromatography silica gel (silica gel-coated paper [Varian Inc.]; 0.1 M sodium citrate, mobile phase) was performed to ascertain complete labeling³⁰¹. Because of the molar excess of DTPA lipid over indium-111, lipid labeling efficiencies of greater than 99% were achieved. Before injections, the volume was adjusted to 200 μL per μmol of liposomes with *N*-(2-hydroxyethyl)piperazine-*N*-(2-ethanesulfonic acid) (HEPES)-buffered saline (10 mM HEPES, 135 mM NaCl, pH 7.4).

In vivo biodistribution studies

NMRI *nu/nu* mice were obtained from Harlan (Horst, the Netherlands). All experiments were performed according to the guidelines for research animals and approved by the Animal Welfare Committee of the Erasmus Medical Center. 9-week-old male NMRI *nu/nu* mice were injected subcutaneously in the right flank with $3\text{--}5 \times 10^6$ cells in 100 μL phosphate buffered saline. Mice were anesthetized with the inhalation anesthetic isoflurane during injection of cells and SPECT/CT imaging. Tumors were measured by caliper every other day till grown to an average size of 200 mm^3 . Tumor volumes were calculated using the formula: $V = 0.4 * (a * b * c)$, where *a*, *b* and *c* represent the length, width and depth of the tumor, respectively. Mice were injected intravenously (tail) with 1 μmol of liposomes labeled with indium-111. Immediately after injection, the animal was scanned ($t = 0$), using the following settings: SPECT (nanoSPECT/CT; Mediso Medical Imaging Systems) static scan with 20 projections, 60 s per projection, and a quality factor of 0.8. APT1 apertures were used with 1.4 mm diameter pinholes (FOV 24 + 16 mm). The following were the CT scan settings: 240 projections, 45 kVp tube voltage, and 500 ms exposure. The $t = 0$ scan was followed by scans at 4, 8, 12, and 24 h after injection. SPECT/CT analysis was performed using InVivoScope/VivoQuant software (inviCRO). Three-dimensional regions of interest were drawn over the heart (blood pool) and tumor to calculate uptake of indium-111 liposomes at the selected time points, after which they were corrected for volume ($\%ID/\text{cm}^3$). Representative figures were made with the same software after correction for indium-111 decay.

Ex vivo biodistribution

Tumors and tissue samples (blood [cardiac puncture], heart, lung, liver, spleen, pancreas, kidney, stomach, duodenum, caecum, colon, tail, and muscle) were harvested and weighed. Radioactivity was determined with a γ counter (Perkin Elmer), and liposomal

accumulation was calculated as percentage injected dose per gram of tissue (%ID/g) and corrected for radioactive decay of indium-111 (half-life, 2.81 d). The injected dose was calculated by measuring the syringe before and after injection.

Immunohistochemical staining

After the final scan, pimonidazole (60 mg/kg of body weight) was injected intraperitoneally and allowed to circulate for 4 h before dissection of tumor and organs. Harvested tumors were snap-frozen in liquid nitrogen, and frozen tumor sections (10 μm thick) were mounted on Superfrost++ slides (VWR, Radnor, PA). The slides were fixed with acetone at 4°C for 10 min and stained for the following morphological parameters: blood vessels (Rat-anti-mouse CD31, 1:100; Becton Dickinson, Franklin Lakes, NJ), PEGylated liposomes (Rabbit-anti-PEG, 1:100; Abcam, Cambridge, United Kingdom), macrophages (Rat-anti-mouse CD11b, 1:100; eBioscience, San Diego, CA), lymphatic vessels (rabbit-anti-LYVE1, 1:100; Abcam) and vessel integrity (Rabbit-anti-Collagen IV, 1:100; Millipore, Billerica, MA). Hypoxia was detected with a rabbit-anti-pimonidazole antibody (1:200, Hypoxiprobe, Burlington, MA). Secondary antibodies were species-specific donkey-antibodies conjugated with AF488 or AF647 (1:500) (Molecular Probes, Waltham, MA) in appropriate combinations. Tile scans of fluorescently stained tumor sections were acquired using an LSM 510 Meta confocal microscope (Carl Zeiss B.V.) with a Plan-Neofluar 10x objective. Quantifications were performed with ImageJ (National Institutes of Health), using manual thresholding (range, 0–255) for density analysis and a colocalization threshold tool to ascertain the ratio between PEG and CD31, and collagen IV and CD31. To avoid regional bias, all quantifications were performed on whole tile scans of tumor sections.

***In vitro* stability assay**

Liposomes were made and radiolabeled with indium-111 as described before. These liposomes were incubated in 100% fetal bovine serum at 37°C for 24, 48, 72, 96 h. The solution was eluted over a size exclusion chromatography column (PD-10, GE Healthcare, Buckinghamshire, United Kingdom) and fractions of 1 mL were collected. After elution the column was washed with 25 mL phosphate buffered saline to check for free ^{111}In -DTPA.

***In vivo* stability assay**

Mice were injected with 1 μmol ^{111}In -labeled liposomes and were followed over time. After 24 and 96 h the mice were used for biodistribution experiments as described before.

Statistical analysis

Statistical analyses were performed using GraphPad Prism (version 5.01; GraphPad Software). The differences between fast-, intermediate-, and slow-growing xenografts were evaluated using 1-way ANOVA with nonparametric Kruskal–Wallis H test and Dunn’s multiple comparison post-test. Comparisons between the high- and low-uptake groups were performed using the 2-tailed Mann–Whitney U test. Correlation analysis between the various parameters evaluated in this study was performed using the Spearman rho test. All statistical tests were 2-sided, and a p value of lower than 0.05 was considered statistically significant.

RESULTS

Characterization of liposomes

Lipids and cholesterol were used in the ratio as described for preparing liposomes comparable to Doxil. The addition of cholesterol increases liposome stability in plasma and pegylation provides a long circulation half-life by creating a steric barrier against opsonization³⁰². Doxil is one of the few liposomal drugs approved for clinical use in breast cancer²⁹⁵, ovarian cancer²⁹³, multiple myeloma, and HIV-related Kaposi’s sarcoma^{294,296}. The formulation used here was not loaded with doxorubicin, as the principal objective was to assess the distribution behavior of the liposomes *in vivo*. All other characteristics are similar to Doxil, such as an average size of 83.13 ± 2.69 nm and polydispersity index of 0.036 ± 0.016 . To perform image-guided delivery, the liposomes were labeled with indium-111 for SPECT imaging. The radiolabeling efficiency with indium-111 after 15 min labeling at room temperature was greater than 99%. The indium-111 conjugated

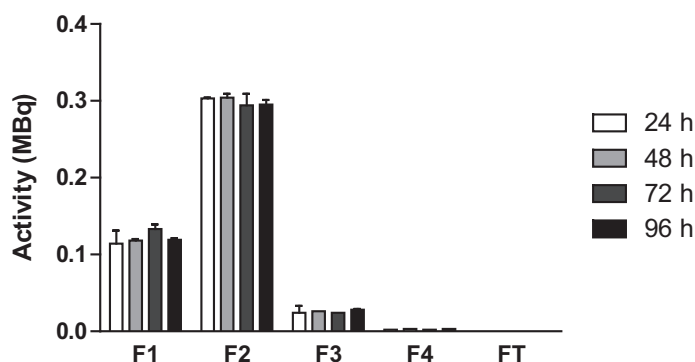


Figure 1. Indium-111 liposomes were incubated in 100% fetal bovine serum at 37°C for $t = 24, 48, 72, 96$ h, after which the sample was used for size exclusion chromatography (PD-10 column). Retention activity in MBq is depicted of fractions (F1–F4 = 1 mL) collected during size exclusion chromatography and after washing the column (FT = 25 mL).

liposomes were tested for stability for up to 96 h as shown in Figure 1. On average the liposomes were labeled with 34.54 ± 1.04 MBq of indium-111 per μmol of liposomes.

Tumor characterization

After inoculation tumor volume was measured every other day until a size of 200-300 mm^3 was reached. Figure 2 shows the growth rate of individual s.c. xenografts subdivided in groups of fast (Figure 2A), intermediate (Figure 2B), and slow growing xenografts (Figure 2C). The squamous cell carcinoma A431, and pancreatic adenocarcinoma's CFPAC-1 and HPAF-II are fast growing tumors, which grew to the target size within 1 month. Pancreatic adenocarcinomas AsPC-1, BxPC-3, and breast adenocarcinoma MDAMB-231 needed 1.5-2.5 months, whereas slow growing tumors, such as primary ductal carcinoma UACC-893, epithelioid carcinoma PANC-1, and breast adenocarcinoma MDA-MB-468 needed 3-6 months. With few exceptions (e.g. MDA-MB-231),

Table 1. Correlation between morphological parameters and tumor growth

Characteristics (median, IQR)	Fast growing xenografts (n = 9)	Intermediate growing xenografts (n = 9)	Slow growing xenografts (n = 8)	p^a	p^b	p^c
Time in days	21 (18 - 25)	60 (44 - 67)	79 (72 - 145)	< 0.05	< 0.001	ns
Morphological parameters						
PEG percentage	4.98 (2.51 - 7.24)	3.55 (2.35 - 8.53)	2.26 (0.88 - 3.84)	ns	ns	ns
CD31 percentage	3.63 (2.56 - 4.36)	2.30 (2.06 - 4.42)	2.69 (1.85 - 5.60)	ns	ns	ns
Pimonidazole percentage	26.18 (16.32 - 37.21)	41.19 (32.28 - 47.58)	37.74 (30.09 - 44.70)	< 0.05	ns	ns
Ki67 percentage	6.10 (5.24 - 9.21)	5.55 (5.09 - 7.83)	10.36 (8.3 - 12.58)	ns	< 0.05	< 0.05
LYVE-1 percentage	0.37 (0.15 - 0.79)	0.17 (0.10 - 1.02)	0.22 (0.07 - 0.28)	ns	ns	ns
CD11b percentage	0.44 (0.28 - 1.03)	1.60 (1.23 - 2.97)	1.43 (0.27 - 3.64)	< 0.05	ns	ns
Collagen percentage	18.45 (10.84 - 19.87)	14.58 (8.36 - 16.57)	13.81 (8.88 - 19.45)	ns	ns	ns
Liposomal uptake						
Liposomes (<i>in vivo</i>)	4.00 (2.92 - 5.01)	2.25 (1.74 - 3.77)	2.04 (1.48 - 2.25)	ns	< 0.01	ns
Liposomes (<i>ex vivo</i>)	4.24 (2.58 - 7.06)	2.70 (2.12 - 3.79)	1.97 (1.54 - 2.48)	ns	< 0.01	ns

Abbreviations: IQR = inter quartile range, ns = not significant; Statistical test used: one-way ANOVA test, two-tailed Kruskal-Wallis test; a = fast growing versus intermediate; b = fast versus slow; c = intermediate versus slow growing

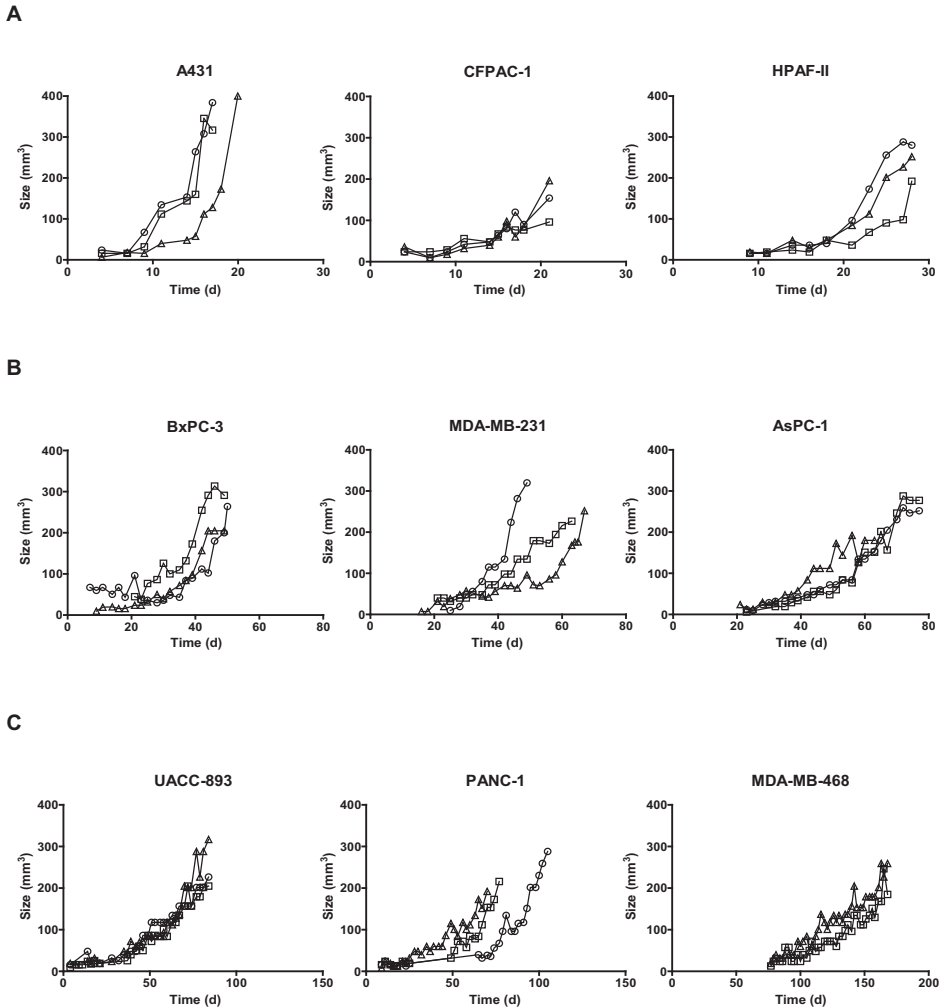


Figure 2. Human tumor cells ($3-5 \times 10^6$) were inoculated s.c. in the right flank of NMRI *nu/nu* mice. Tumor growth was followed over time and measured three times a week. Individual mice are depicted with the following symbols: mouse 1 = \circ , mouse 2 = \square , mouse 3 = \triangle . The tumor xenografts were ordered according to their growth *in vivo*: fast growing (A); intermediate growing (B); slow growing (C). Vertical axis shows tumor size (mm^3); horizontal axis days after inoculation.

the tumors showed a predictable and reproducible growth pattern. This subdivision was used to compare various parameters thought to be involved in the EPR effect and uptake of liposomes. Table 1 shows an increased liposomal uptake *in vivo* and *ex vivo*, in fast growing xenografts compared to slow growing xenografts ($p < 0.01$). However, no other parameter could be clearly identified as being involved in liposomal uptake with this subdivision of xenografts.

***In vivo* stability assay**

Biodistribution experiments (Figure 3) showed that liposomes are cleared from the blood over time, whereas they are retained in liver and spleen, which are known to be involved in the clearance of liposomes. This data shows that most other organs show liposome-specific activity due to perfusion at 24 h, which is cleared after several days.

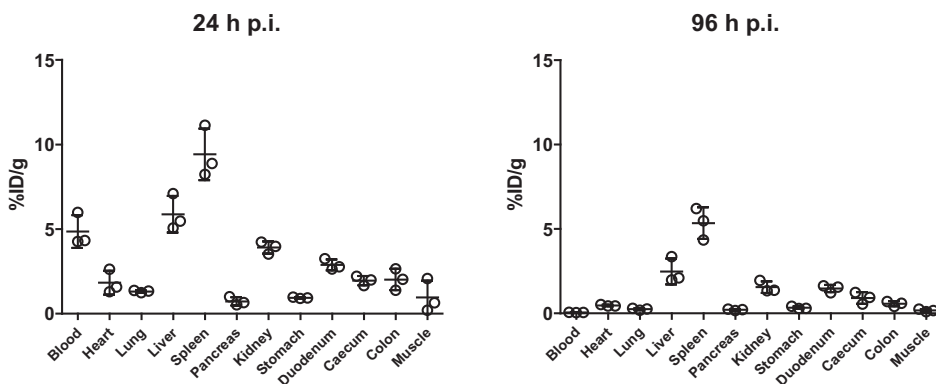


Figure 3. Percentage of injected dose per gram (%ID/g) depicted per mouse after biodistribution at 24 and 96 h post injection (p.i.).

***In vivo* localization of indium-111 labeled liposomes in human tumor xenografts**

All mice were injected intravenously with 1 μmol of liposomes labeled with indium-111 for SPECT imaging. A volume of interest was drawn to quantify liposomal accumulation in the tumor and heart (blood pool). Figure 4A shows accumulation of liposomes in the tumor over time (0, 4, 8, 12, and 24 h after injection) as a percentage injected dose corrected for tumor volume (%ID/ cm^3). The EPR effect ensured accumulation of liposomes in the tumors over time, whereas the heart showed clearance of liposomes from circulation. In the heart, liposomes still accounted for $6.28 \pm 1.50\%$ injected dose per cm^3 (SD) after 24 h, which was confirmed by $t_{1/2\beta}$ of 16.99 ± 1.81 h (SEM). Figure 4B shows representative mice depicting high liposomal uptake (HPAF-II tumor) and low liposomal uptake (PANC-1 tumor). The SPECT/CT scans show radiolabeled liposomes in circulation, visible in the heart, aortic arch, aorta, and continuing downstream into axillary, hepatic, splenic, renal, and femoral arteries. The liposomes in circulation diminished over time and accumulated in the liver, spleen, and, to varying degrees, the tumor. The liposomes were slowly cleared via the liver and spleen (mononuclear phagocytic system), whereas they were retained in the tumor because of the EPR effect³⁰³. Spleen macrophages and hepatic Kupfer cells can ingest liposomes and are responsible for liposome accumulation in these organs. Liver fenestrations (100 nm) and spleen lumina (up to 5 μm) will further contribute to this accumulation³⁰⁴. Figure 5 shows all

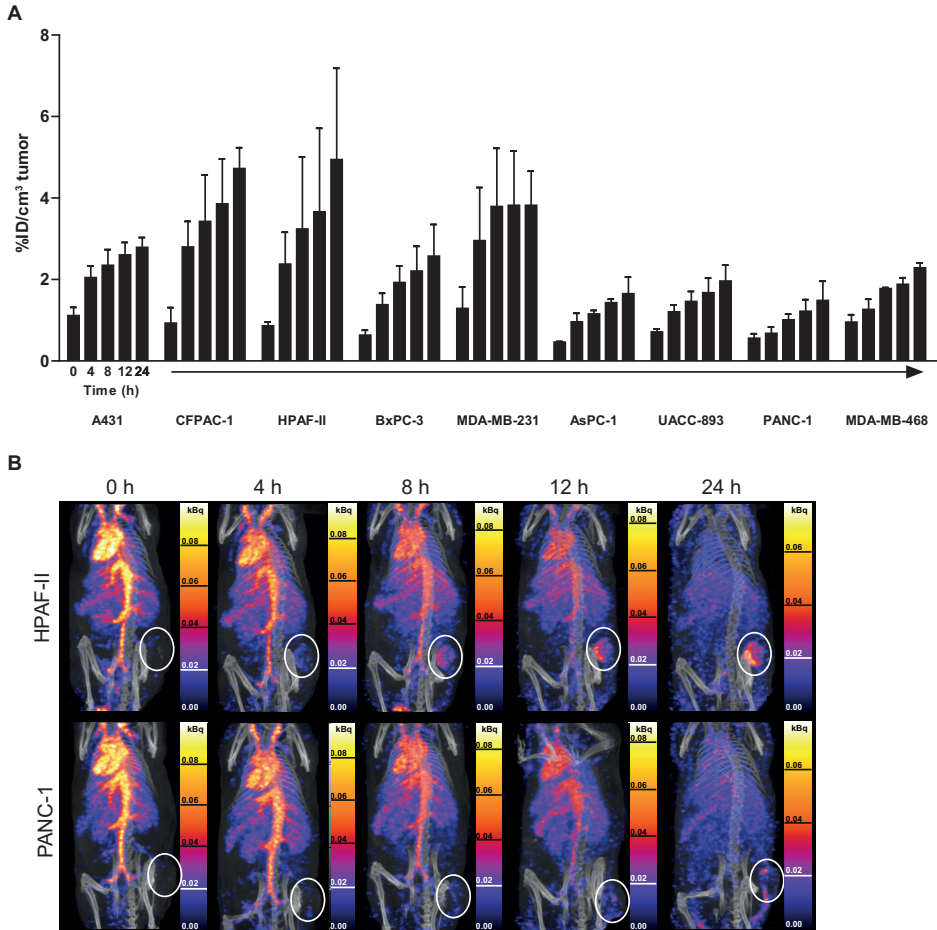


Figure 4. Average tumor uptake in percentage injected dose per cubic centimeter tumor ($\%ID/cm^3$) was calculated and is depicted at $t = 0, 4, 8, 12,$ and 24 h post injection (A). Representative SPECT/CT scans, adjusted for indium-111 half-life, of HPAF-II or PANC-1 tumor (white circle) bearing mice at different time intervals after injection with indium-111 liposomes show uptake of liposomes over time to a higher (HPAF-II) and lesser (PANC-1) degree (B).

studied tumor types 12 h after injection with radiolabeled liposomes. In addition to differences in total uptake, early variations in intratumoral localization were clearly visible and were probably caused by perfusion differences^{305,306}. For example, MDA-MB-231 showed a clear uptake in certain regions of the tumor periphery, whereas other regions remained clear. Other tumors such as CFPAC-1 showed a more homogeneous distribution of liposomes. Importantly, the circulation of liposomes and accumulation in liver and spleen were comparable between different tumor models, as confirmed later by

the biodistribution data. Liposomes are degraded in the liver after 12–24 h, causing a release of free ^{111}In -DTPA, as detected by low levels of radioactivity in the kidney and bladder, because free ^{111}In -DTPA is rapidly cleared from circulation³⁰⁷.

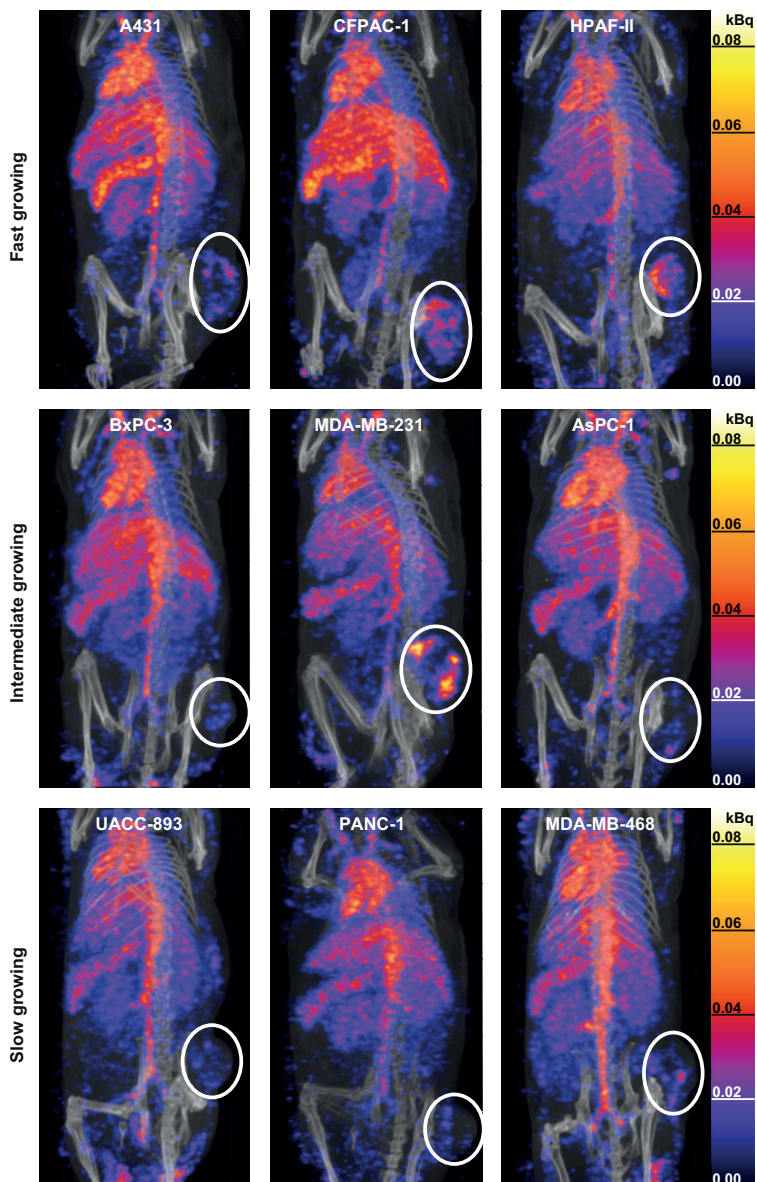


Figure 5. Representative SPECT/CT scans of fast, intermediate, and slow growing tumors 12 h after injection. The scans have been set to the same threshold (in kBq) to compensate for indium-111 half-life. Tumors are circled in white and show uptake of liposomes to various degrees.

Ex vivo organ biodistribution

Radioactivity uptake was measured after resection of the tumors and other relevant tissues and is shown per tumor type in Figure 6 and in more detail for all analyzed organs, including the tumor, in Figure 7. The tumors are again arranged from fast to slow-growing, with levels of uptake ranging from PANC-1 ($1.51 \pm 0.11\%$ injected dose per gram) on the low end to CFPAC-1 ($7.99 \pm 3.59\%$ injected dose per gram) on the high end. A trend was observed between tumor growth and liposomal uptake (Table 2,

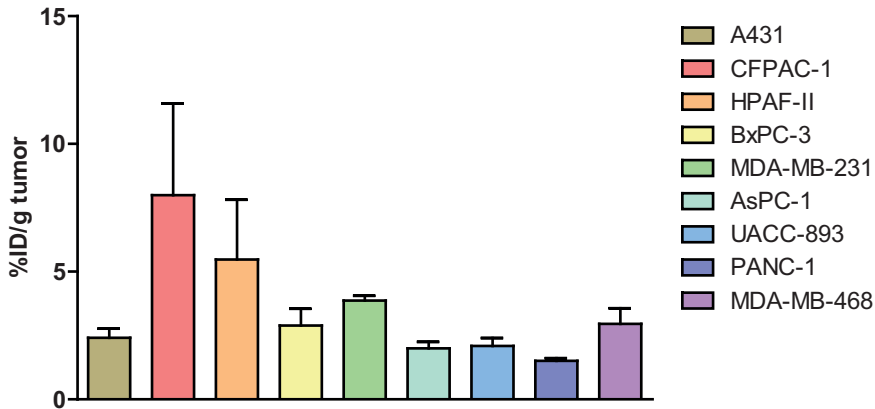


Figure 6. Tumor accumulation of indium-111 in percentage injected dose per gram (%ID/g tumor) at 24 h after i.v. injection ordered from fast to slow growing tumor xenografts showing some association with speed of tumor growth.

Table 2. Correlation between morphological parameters and liposomal tumor uptake

Characteristics (median, IQR)	High uptake (n = 9)	Low uptake (n = 17)	p value
Liposomal uptake			
Liposomes (<i>in vivo</i>)	4.16 (3.67 - 5.01)	2.12 (1.50 - 2.45)	< 0.0001*
Liposomes (<i>ex vivo</i>)	4.24 (3.95 - 7.06)	2.26 (1.76 - 2.62)	< 0.0001*
Time in days	25 (21 - 43)	70 (52 - 79)	0.0104*
Morphological parameters			
PEG percentage	5.64 (4.92 - 11.77)	2.50 (0.97 - 4.07)	0.0018*
CD31 percentage	2.84 (2.08 - 3.98)	2.87 (2.12 - 5.57)	0.5899
Pimonidazole percentage	37.13 (24.12 - 40.72)	33.49 (27.23 - 45.19)	0.6276
Ki67 percentage	7.63 (5.32 - 9.21)	7.79 (5.52 - 11.39)	0.4188
LYVE-1 percentage	0.37 (0.15 - 0.79)	0.21 (0.06 - 0.41)	0.2465
CD11b percentage	1.01 (0.31 - 2.26)	1.40 (0.39 - 2.53)	0.4834
Collagen percentage	18.56 (12.23 - 20.23)	13.72 (8.31 - 16.46)	0.0524

Abbreviation: IQR = inter quartile range; Statistical test used: two-tailed Mann-Whitney *U* test; * significant at $p < 0.05$ level.

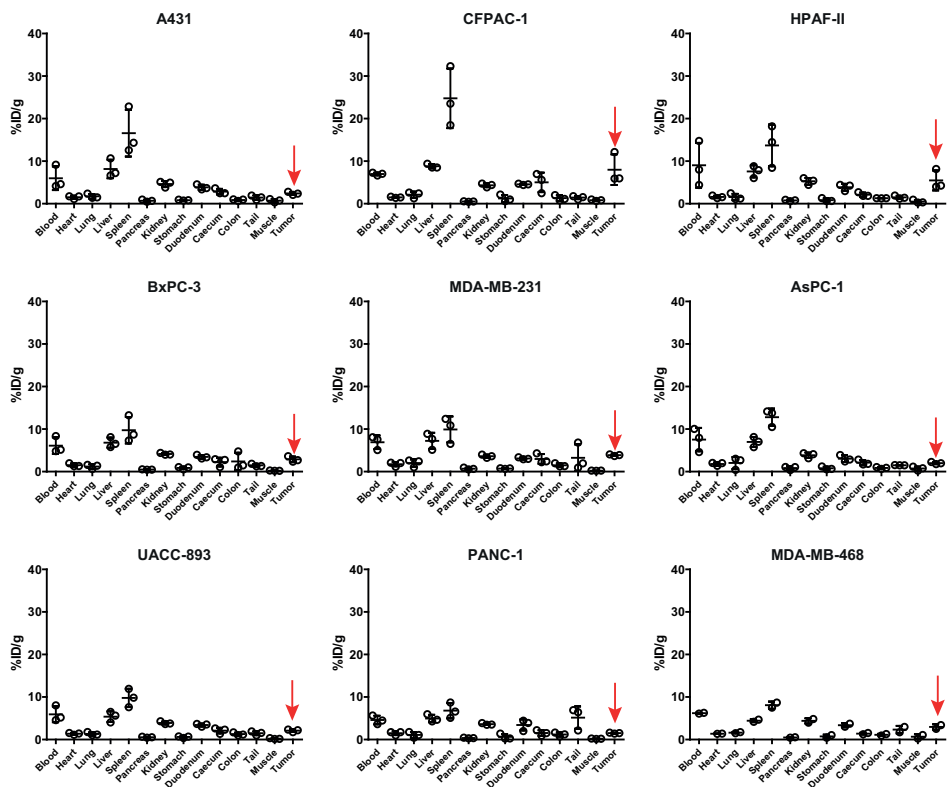


Figure 7. Percentage of injected dose per gram (%ID/g) depicted per mouse and tumor type shows a high uptake in liver, spleen, and other highly perfused tissues. Tumor measurements have been indicated by red arrow.

$p = 0.0104$), although outliers, such as A431, BxPC-3, and MDA-MB-468, indicate that other factors are important and may be influencing liposomal accumulation. The reason for this was investigated in more detail using immunohistochemical stainings, but it is, for example, known that the presence of necrotic or poorly vascularized tumor cores in fast-growing tumors may inhibit liposomal uptake¹⁵⁴. Most of the liposomes accumulate in the liver, spleen, and tumor, after which they are cleared. Biodistribution data up to 96 h after injection are shown in Figure 3, showing clearance of liposomes from most organs. Liposomal uptake *in vivo* was compared with other modalities used to detect liposomal uptake and the morphological parameters thought to influence the EPR effect and nanoparticle accumulation. To this end, the tumors were subdivided into high- and low-uptake groups; the high-uptake group included CFPAC-1, HPAF-II, and MDA-MB-231 xenografts. Table 2 shows that the difference in uptake between these groups can be detected with all tested modalities: *in vivo* SPECT/CT imaging, *ex vivo* biodistribution, and the anti-PEG antibody staining (p value < 0.0001, < 0.0001,

and = 0.0018, respectively). In addition, there was a significant difference in tumor growth, that is, the time required for the tumors to reach 200 mm³ ($p = 0.0104$). We did not observe a statistically significant correlation with any other morphological parameter evaluated.

Immunohistochemistry

To further investigate the underlying mechanisms of the EPR effect and to find possible explanations for the observed variations in liposomal tumor uptake, several morphological parameters were investigated using immunohistochemistry (Table 2). In Figure 8A, the percentage of total tumor areas positive for liposomal content was calculated using an anti-PEG antibody. This shows a significant correlation with the *in vivo* and *ex*

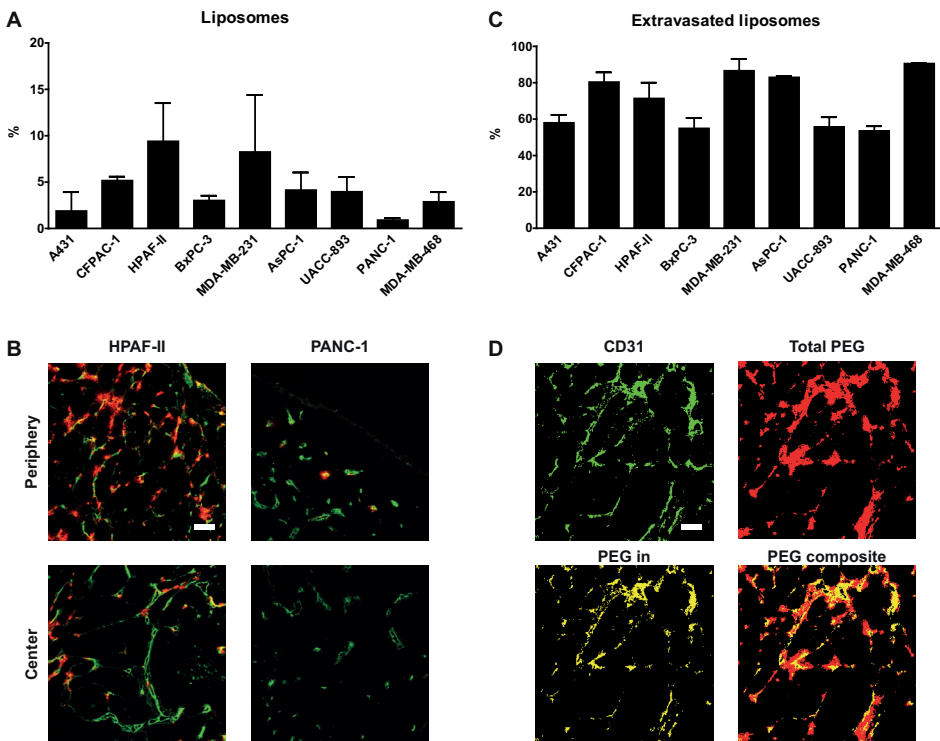


Figure 8. Percentage of liposome uptake calculated from immunohistochemical staining of PEG, which shows a comparable uptake as *in vivo/ex vivo* quantifications (A). Representative images of tumor periphery and center indicate that uptake in the periphery is higher in both high and low uptake tumors (B). Extravasated liposomes calculated for all tumors based on the total PEG (red) minus PEG colocalized (yellow) with blood vessels (CD31, green), leading to a final composite figure showing the colocalized (yellow) and extravasated (red) liposomes (C, D). The degree of extravasation is relatively high in all tumors. All quantifications were performed on whole tile scans of the tumor sections. Scale bars = 100 μ m.

in vivo quantifications (Table 3; $p = 0.007$ and < 0.001 , respectively). Unfortunately, the aforementioned subdivision into slow-, intermediate-, and fastgrowing xenografts did not result in significant correlations (Table 1). Figure 8B shows HPAF-II and PANC-1 frames to demonstrate the difference of liposome localization in tumors with high and low uptake, respectively. Additionally, the intratumoral localization of the liposomes was determined in relation to blood vessels (CD31) showing that most liposomes had indeed extravasated from the vessels (Figure 8C), although the distance traveled from the vessels is minimal. The percentage of extravasated liposomes was calculated by subtracting the amount of CD31-colocalized liposomes from the total amount of liposomes present in the area. This is depicted in Figure 8D, in which an example is given of a CD31 staining (green), total PEG staining (red), and the calculated colocalized liposomes (PEG in; yellow), which shows liposomes within and extravasated from these vessels (shown in PEG composite in yellow and red, respectively). Although nanoparticle distribution and accumulation is undeniably related to the presence of blood vessels³⁰⁸, Figure 9A shows that the number of vessels (depicted in percentage mean vessel density) cannot be used to predict the degree of liposomal uptake. For example, AsPC-1 and UACC-893 have a similar uptake of liposomes, depicted with *in vivo*, *ex vivo*, and immunohistochemical quantifications, but the mean vessel density of UACC-893 is 3 times higher than that of AsPC-1. As mentioned before, the factors influencing the EPR effect and the uptake of liposomes are more complex. The mononuclear phagocytic system also has a major influence on the delivery of liposomes, although detection by the mononuclear phagocytic system may be reduced by pegylation^{309,310}. Monocytes internalize liposomes, after which the drug may be released, resulting in toxic effects to the monocytes. Figure 9B shows that the percentage of macrophages in the tumor tissue is in general relatively low, with the exception of MDA-MB-468 ($5.70\% \pm 2.26\%$). This might explain why a slow growing tumor (5 months) with a poor mean vessel density ($1.79\% \pm 0.42\%$) still has a considerable liposomal uptake ($2.87\% \pm 1.05\%$). Hypoxia is usually correlated with poor vascularization and indicative of poor drug uptake. Because of unrestrained tumor growth, cells move beyond the distance over which oxygen can diffuse (circa $150 \mu\text{m}$), and drugs targeting fast-dividing cells will usually be less effective^{311,312}. All tumors show a comparable degree of hypoxia (Figure 9C), suggesting that this aspect plays a minor role in these tumor models. Representative scans of the aforementioned stainings are shown in Figure 10. The functionality of both blood and lymphatic vessels is thought to be of great importance to the EPR effect and eventual uptake of macromolecules¹⁴². We therefore incorporated a lymphatic marker (LYVE-1) and a collagen IV antibody to measure lymphatic vessel density and collagen IV support of blood vessels. The lymphatic vessels (Figures 11A and 11B) are important for drainage of the tissue, and the result suggests that the high presence of these vessels caused lower accumulation in BxPC-3 tumors. The intermediate-growing

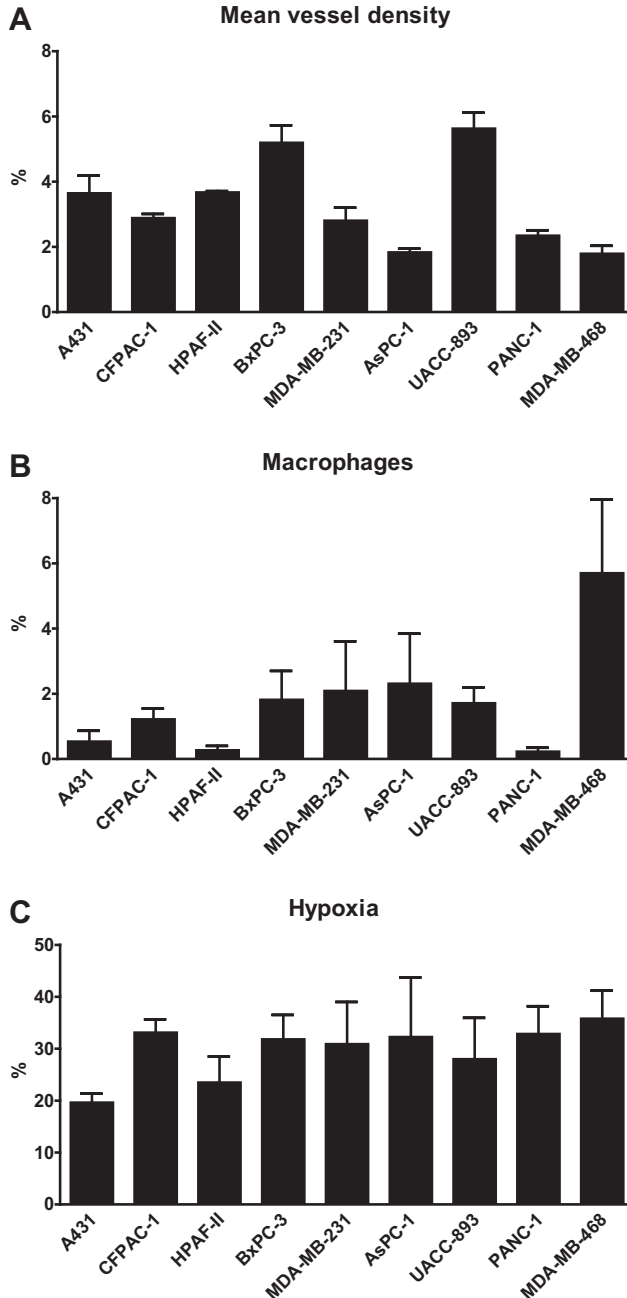


Figure 9. Mean vessel density in tumors based on anti-CD31 staining (A). Macrophages are stained with anti-CD11b antibody (B), and a high percentage is seen in MDA-MB-468 tumors. Hypoxia percentage (C) in different tumors, which was calculated on the basis of presence of pimonidazole after intraperitoneal injection. Degree of hypoxia is comparable for all tumors. All quantifications were performed on whole tile scans of tumor sections.

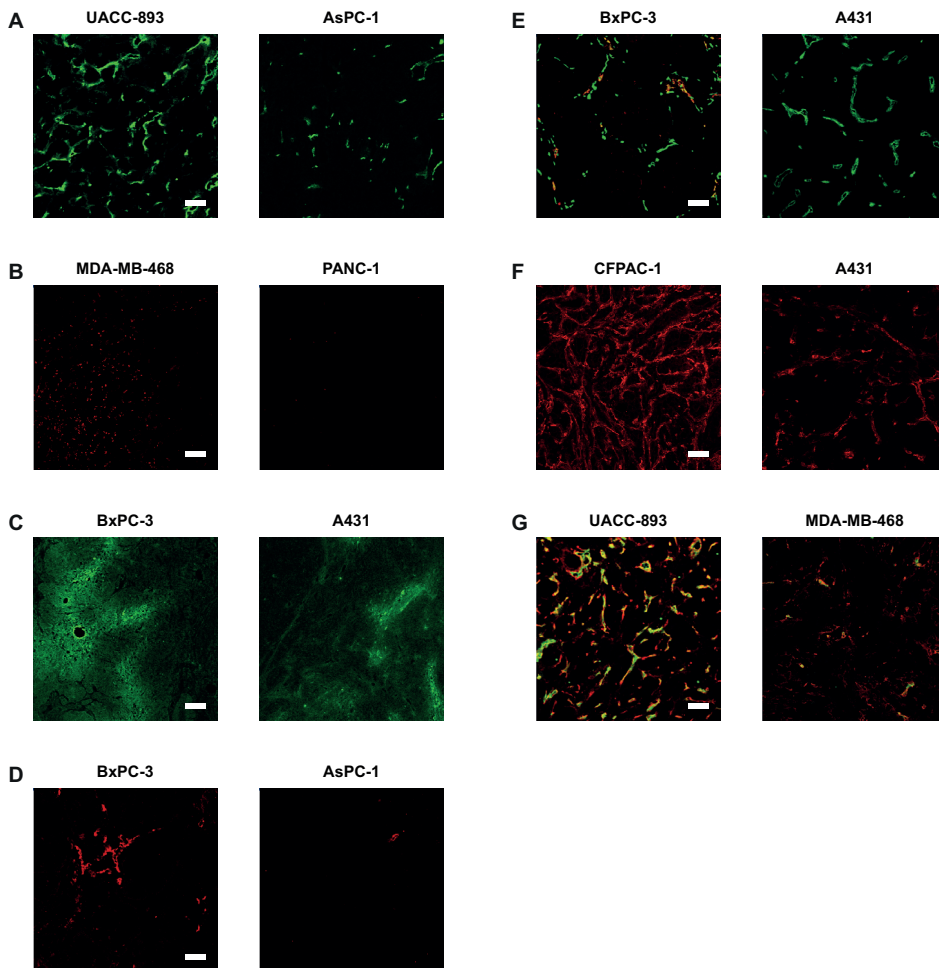


Figure 10. Immunohistochemical stainings showing, mean vessel density (MVD) (A), macrophage density (B), hypoxia based on the presence of pimonidazole (C), LYVE-1 staining for lymphatic vessels (D), lymphatic vessel (LYVE-1, red) to blood vessel (CD31, green) ratio, indicative of the supply and drainage of tumor tissue (E), collagen IV density (F), colocalization of collagen IV and blood vessels (CD31) (G). Scale bars = 100 μ m.

BxPC-3 has a high lymphatic vessel density, $1.52\% \pm 0.86\%$, and a lymphatic-to-blood vessel ratio of 0.35 ± 0.11 , with a well-developed mean vessel density, $5.19\% \pm 0.92\%$, and still showed a relatively poor liposomal accumulation. In addition, BxPC-3 tumor cells grew in tight clusters, which may be an additional factor contributing to the lower uptake, because the tissue is less permeable to liposomes. Most tumors have blood vessels supported with collagen IV matrix, apart from MDA-MB-468 tumors (Figures 11C and 11D). To decipher possible associations between liposomal uptake and the

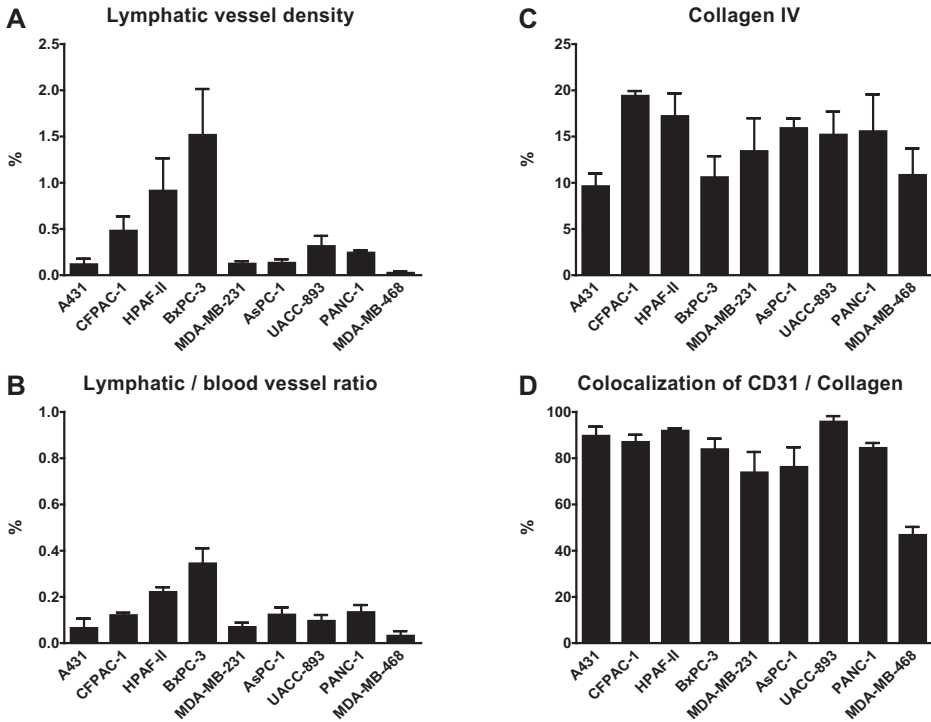


Figure 11. LYVE-1 staining indicates the presence of lymphatic vessels in the different tumors (A), which can be used to interpret possible drainage of the tumor. For example, BxPC-3 has a highly developed lymphatic system, which might explain the relatively low liposomal uptake. Lymphatic vessel (LYVE-1) to blood vessel (CD31) ratio (B), indicative of the supply and drainage of tumor tissue. Collagen IV is important for the support of blood vessels and is used as a marker for mature blood vessels (C). The degree of collagen is comparable between tumors. Colocalization of collagen IV and blood vessels (CD31) (D) supports the observation that most tumor vessels are mature and supported by collagen, with the exception of MDA-MB-468. All quantifications were performed on whole tile scans of the tumor sections.

various morphological parameters tested, we performed a correlation analysis (Table 3). Although there was a significant correlation between the percentage PEG and the liposomal uptake *in vivo*, no further significant correlations related to other tested morphological parameters could be found. A multivariate analysis requiring a much larger dataset may in the future enable elucidation of multiple factors contributing to the EPR effect.

Table 3. Correlation coefficients between various morphological parameters

		PEG %	CD31 %
PEG %	Correlation Coefficient	1.000	0.154
	p value (two-tailed)		0.454
CD31 %	Correlation Coefficient	0.154	1.000
	p value (two-tailed)	0.454	
Pimonidazole %	Correlation Coefficient	0.179	-0.123
	p value (two-tailed)	0.383	0.550
Ki67 %	Correlation Coefficient	-0.128	0.204
	p value (two-tailed)	0.534	0.317
LYVE-1 %	Correlation Coefficient	0.280	0.452
	p value (two-tailed)	0.166	0.020*
CD11b %	Correlation Coefficient	0.185	-0.060
	p value (two-tailed)	0.366	0.772
Collagen %	Correlation Coefficient	0.164	-0.142
	p value (two-tailed)	0.424	0.490
Liposomes (<i>in vivo</i>)	Correlation Coefficient	0.516	0.069
	p value (two-tailed)	0.007*	0.739
Liposomes (<i>ex vivo</i>)	Correlation Coefficient	0.623	0.065
	p value (two-tailed)	< 0.001*	0.754

Statistical test used: two-tailed Spearman's rho test; * significant at $p < 0.05$ level.

DISCUSSION

The EPR effect, first described by Matsumura and Maeda in 1986¹⁴², shows tumor-specific accumulation of large molecules and is dependent on the following parameters: the size of the molecules should be larger than the renal clearance threshold (7 nm) to prevent fast clearance; the molecules should have characteristics that ensure a long circulation time to increase the chance for extravasation; and the nature of the tumor has to be such that it will ensure retention of these molecules, usually ranging from days to weeks, leading to enhanced efficacy. These properties distinguish the EPR effect needed for therapeutic purposes from targeting of low-molecular-weight molecules with a short half-life and fast clearance, which are more suited for imaging purposes³¹³. By utilizing the EPR effect, pegylated liposomes such as Doxil have been successful in the treatment of certain cancers.

This study has consolidated that pegylated liposomes can accumulate in various solid tumors, although considerable differences in uptake were observed. Uptake levels ranged from PANC-1 to CFPAC-1 at the low to high end, respectively. There was a trend between liposome accumulation and the speed of tumor growth. Although tumors,

such as squamous cell carcinoma A431, showed very fast tumor growth but had limited liposomal accumulation in the tumor. This could be explained by the high growth rate and relatively large size of these tumors. Angiogenesis is increased during tumor growth and the tumor will grow exponentially until sufficient vascularization can no longer be sustained³¹⁴. This leads to hypoxic or necrotic tumor cores, which are more difficult to reach with anticancer drugs. Before this point is reached, the chaotic development of tumor vasculature together with the obstruction and collapse of lymphatic vessels at the tumor core will lead to an enhanced EPR effect and possibly an increased accumulation of nanoparticles¹⁴². Lymphatic vessel density evaluation revealed that most tumors had an impaired lymphatic system aiding liposome accumulation. The exception was the intermediate-growing BxPC-3, which had a high lymphatic vessel density and a well-developed mean vessel density, resulting in a relatively poor liposomal accumulation. Although it has been hypothesized that normalization of the vasculature, extracellular matrix, and lymphatic vessels would lead to better delivery of drugs³¹⁵, this may not always hold true for liposomal drugs. Normalization of vessels will lead to a less leaky vasculature, which might impair the EPR effect.

It has also been shown that mean vessel density correlates with the degree of liposome accumulation³⁰⁸, but we did not observe this correlation in our study. The liposomes were still in circulation after 24 h. Various degrees of colocalization of blood vessels and liposomes were observed, but most liposomes had extravasated from tumor vessels. Unfortunately, high levels of extravasation do not always result in high efficacy, due to the poor penetration characteristics of liposomes. The liposomes did not penetrate further than the perivascular space, confirming that smaller particles (12 nm) can penetrate a tumor heterogeneously up to 80 μm , but particles of 60 nm and larger do not leave the perivascular space or even the vessel¹⁵². Several additional barriers such as high interstitial fluid pressure, low oxygenation, and the extracellular matrix need to be overcome²⁹².

Various other variables can influence the uptake of liposomes and the EPR effect in addition to the important role of the vasculature. For example, associated inflammation³¹⁶ and interactions with monocytes³¹⁷ can play a major role to increase the liposomal uptake in the tumor. This may explain why MDA-MB-468 had an intermediate liposomal uptake even though the mean vessel density was low. The monocyte staining to determine the involvement of the immune system showed a high presence of macrophages in MDA-MB-468 as opposed to the other tumors.

This study supports the notion that the EPR effect is a highly complex, multifactorial, heterogeneous phenomenon, which is possibly much larger in animal tumors than in human tumors¹⁵⁰. Because tumors are usually faster-growing in animal models, it is to be expected that they will have a higher degree of vascularization and a lesser developed vascular environment, leading to a high EPR effect. For this reason, we also investi-

gated slowgrowing tumors with a lower vessel density to explore pegylated liposomes in a more clinically relevant setting. Especially the pancreatic tumor models are more representative for the clinical setting, in which human tumors grow over long periods of time³¹⁸. Slow growing tumors, such as prostate and pancreatic tumors, are known to have more normalized vessels and are usually difficult to treat with nanomedicine. Here, we showed that even within the pancreatic tumor models, there is a wide range in liposomal uptake and EPR effect, which accentuates the importance of selecting the appropriate tumor model for preclinical studies. In addition, it is crucial to include an imaging modality in studies investigating the effects of nanoparticle accumulation *in vivo* and to intervene if the therapy is inhibited by poor access to the tumor. Fortunately, an increasing number of methods to enhance the EPR effect in tumors have been developed, both in preclinical and clinical settings, including the use of heat to increase vessel permeability and induce extravasation of nanomedicines³¹⁹⁻³²².

CONCLUSION

The EPR effect can be used to predict liposomal accumulation into tumors or explain limited uptake. In this study, we investigated several parameters and our results suggest that the EPR effect, and thus liposomal uptake, is a complex, multifactorial, and heterogeneous phenomenon. This is caused by tumor (microenvironment) variability, which therefore should be taken into account when considering liposomes as an anticancer therapy.

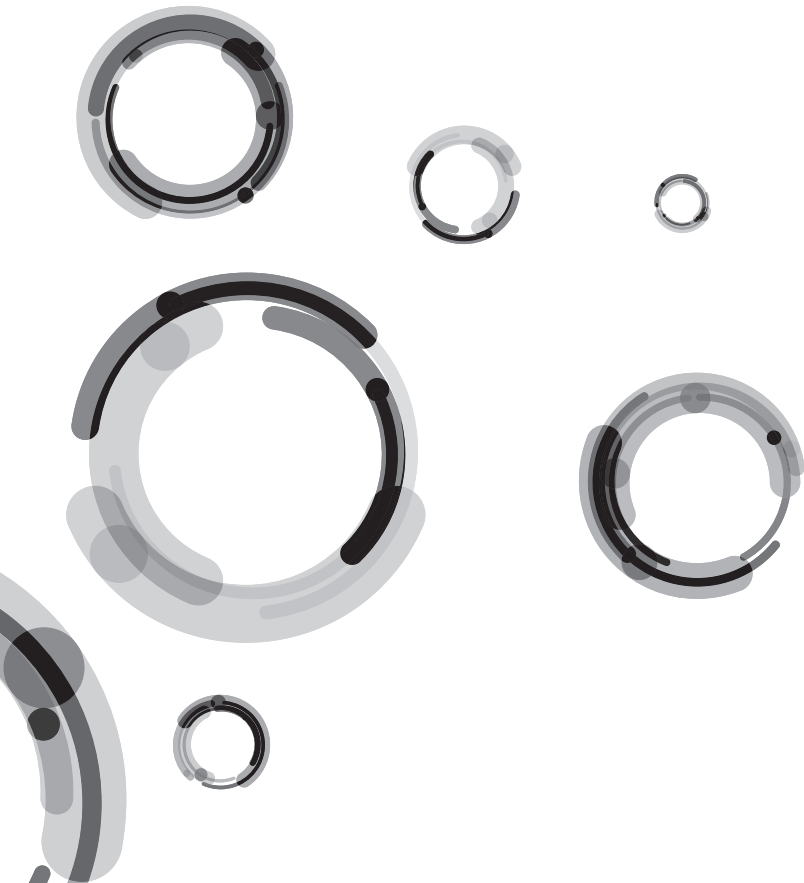


CHAPTER 6

Investigation of Particle Accumulation, Chemosensitivity and Thermosensitivity for Effective Solid Tumor Therapy using Thermosensitive Liposomes and Hyperthermia

Wouter J.M. Lokerse, Michiel Bolkestein, Timo L.M. ten Hagen, Marion de Jong,
Alexander M.M. Eggermont, Holger Gröll, Gerben A. Koning

Adapted from Theranostics, 2016



ABSTRACT

Doxorubicin loaded thermosensitive liposomes (TSLs) have shown promising results for hyperthermia-induced local drug delivery to solid tumors. Typically, the tumor is heated to hyperthermic temperatures (41-42°C), which induced intravascular drug release from TSLs within the tumor tissue leading to high local drug concentrations (1-step delivery protocol). Next to providing a trigger for drug release, hyperthermia (HT) has been shown to be cytotoxic to tumor tissue, to enhance chemosensitivity and to increase particle extravasation from the vasculature into the tumor interstitial space. The latter can be exploited for a 2-step delivery protocol, where HT is applied prior to i.v. TSL injection to enhance tumor uptake, and again after 4 h to induce drug release. In this study, we compare the 1- and 2-step delivery protocols and investigate which factors are of importance for a therapeutic response. In murine B16 melanoma and BFS-1 sarcoma cell lines, HT induced an enhanced doxorubicin uptake in 2D and 3D models, resulting in enhanced chemosensitivity. *In vivo*, therapeutic efficacy studies were performed for both tumor models, showing a therapeutic response for only the 1-step delivery protocol. SPECT/CT imaging allowed quantification of the liposomal accumulation in both tumor models at physiological temperatures and after HT treatment. A simple two compartment model was used to derive respective rates for liposomal uptake, washout and retention, showing that the B16 model has a twofold higher liposomal uptake compared to the BFS-1 tumor. HT increases uptake and retention of liposomes in both tumors models by the same factor of 1.66, maintaining the absolute differences between the two models. Histology showed that HT induced apoptosis, blood vessel integrity and interstitial structures are important factors for TSL accumulation in the investigated tumor types. However, modeling data indicated that the intraliposomal doxorubicin fraction did not reach therapeutic relevant concentrations in the tumor tissue in a 2-step delivery protocol due to the leaking of the drug from its liposomal carrier providing an explanation for the observed lack of efficacy.

INTRODUCTION

Classical chemotherapy for treatment of solid tumors typically employs cytotoxic drugs with low molecular weight that have sizes below 1 nm. The latter allows the drugs to efficiently extravasate upon injection from the vascular compartment into the tumor tissue in order to reach their targets. However, as extravasation is not restricted to the tumor tissue, toxicity imposed on healthy tissues is limiting the therapeutic window. One approach to limit off-target toxicity is the encapsulation of cytotoxic drugs into nanoparticles, such as liposomes with sizes in the range of 50-200 nm, which reduces side effects observed for free drugs. In contrast to healthy tissues, tumors exhibit a poorly organized vascular system^{323,324} with endothelial gaps^{146,325} that allow extravasation and accumulation of nanoparticles up to several hundred nanometers^{323,326}. In addition, as tumors often lack a functional lymphatic system, which impedes efficient clearance of nanoparticles, substantial retention of long circulating nanoparticles is observed^{327,328}. This enhanced permeability and retention (EPR) effect was first described for macromolecules by Matsumura and Maeda and is a prerequisite for liposomal drug targeting¹⁴². Today, several liposomal drug formulations are clinically approved, mostly due to their improved toxicity profile³²⁸. One example is Doxil, a long circulation liposomal formulation of doxorubicin^{37,310}. While liposomal encapsulation reduces off-site toxicity, it unfortunately reduces bioavailability of the parent drug. Drug release from the liposomal carrier is slow as it is based on passive diffusion of the drug across the liposomal lipid bilayer, which strongly reduces peak concentrations³²⁹. An alternative approach is heat-triggered drug delivery using a drug that is encapsulated in the aqueous core of a temperature sensitive liposome (TSL), as first proposed by Yatvin and Weinstein¹⁶⁸. A TSL retains the drug at body temperature, but rapidly release their payload at mild hyperthermic temperatures (40-43°C). Heating the targeted tissue to these temperatures, for example using radiofrequency or high intensity focused ultrasound, leads to rapid intravascular release with subsequent substantial drug deposition in the tumor, which is investigated in numerous preclinical^{179,330-333}, yet also clinical studies^{334,335}.

Next to providing a trigger for drug release, hyperthermia (HT) exposure can induce multiple other changes on cellular as well as tissue level^{336,337}. HT can cause direct cytotoxicity *in vitro* and *in vivo*³³⁸, which depends on the absolute temperature and exposure time, but also on the type of cell or tissue^{339,340}. Secondly, HT can increase chemosensitivity^{341,342} due to a synergistic effect between HT- and drug-induced cytotoxicity or due to an increased drug uptake as HT enhances cell membrane permeability^{343,344}. On tissue level, preclinical studies have shown that HT increased liposomal uptake in tumors^{178,322,345-347}. However, clinical trials using Doxil in combination with HT showed variable therapeutic outcomes, highlighting the clinical need for a liposomal formula-

tions that could more effectively release the drug^{348,349}. The latter inspired the design a 2-step drug delivery scheme, where first HT is applied to enhance the EPR effect followed by injection of TSLs. After accumulation of TSLs in the tumor, drug release is triggered with a second application of HT to ensure bioavailability of the drug.

In a previous study, Li et al. performed a comparative study with doxorubicin loaded TSL using the aforementioned 2-step drug delivery scheme versus a 1-step intravascular HT-drug delivery scheme in a murine BLM melanoma model³⁵⁰. The conclusion of that study was that a 1-step treatment was more efficacious in treating a solid tumor than the 2-step approach. Here we provide a follow-up study, investigating 1-step and 2-step HT TSL based treatments in terms of *in vitro* cytotoxicity, drug uptake by cells, therapeutic efficacy and quantitative TSL uptake by B16 melanoma and BFS-1 sarcoma tumors. Furthermore, extensive *ex vivo* investigation provide data giving more insights into microenvironmental factors that could play a role in TSL accumulation for B16 and BFS-1 tumors and the influence of HT on these factors.

MATERIALS AND METHODS

Materials

1,2-distearoyl-*sn*-glycero-3-phosphocholine (DSPC), 1,2-dipalmitoyl-*sn*-glycero-3-phosphocholine (DPPC) and 1,2-distearoyl-*sn*-glycero-3-phosphoethanolamine-N-(amino(polyethylene glycol)-2000) (DSPE-PEG₂₀₀₀) were purchased from Lipoid (Ludwigshafen, Germany). DSPE-diethylenetriaminepentaacetic acid (DTPA) was obtained from Avanti Polar Lipids Inc. (Alabaster, AL). Doxorubicin-hydrochloride solution (2 mg/ml) was ordered from Accord Healthcare. 4-(2-hydroxyethyl)-1-piperazineethanesulfonic acid (HEPES), (NH₄)₂SO₄, DMEM culture medium, fetal bovine serum (FBS), sulphorhodamine B (SRB), poly(2-hydroxyethylmethacrylate; HEMA), 2-Amino-2-hydroxymethyl-propane-1,3-diol (Tris), NaCl, glycerol, Mayer's hematoxylin, eosin Y, Martius yellow, crystal scarlet and methyl blue were from Sigma Aldrich (St. Louis, MO). Nonyl phenoxy polyethoxyethanol (NP40) was purchased from ICN Biomedicals (Irvine, CA). Penicillin-streptomycin (Pen-Strep) solution was from Lonza (Breda, Netherlands). PD-10 desalting columns were bought from GE Healthcare Life Sciences (Buckinghamshire, UK). Entellan and rabbit-anti mouse Collagen IV antibody were from EMD Millipore (Billerica, MA). CD31 antibody (rat anti-mouse) was bought from Abcam (Cambridge, UK) and AlexaFluor 594 (goat anti-rat) and AlexaFluor 488 (goat anti-rabbit) from Invitrogen (Carlsbad, CA). Matrigel was acquired from BD (San Jose, CA). Cryo compound was from Klinipath (Duiven, Netherlands). Fluoromount-G was provided by Southern Biotech (Birmingham, AL). Cell death detection kit was obtained from Roche (Woerden, Netherlands). Weigert's hematoxylin was purchased from Boom Chemicals (Meppel, Netherlands).

Liposome preparation

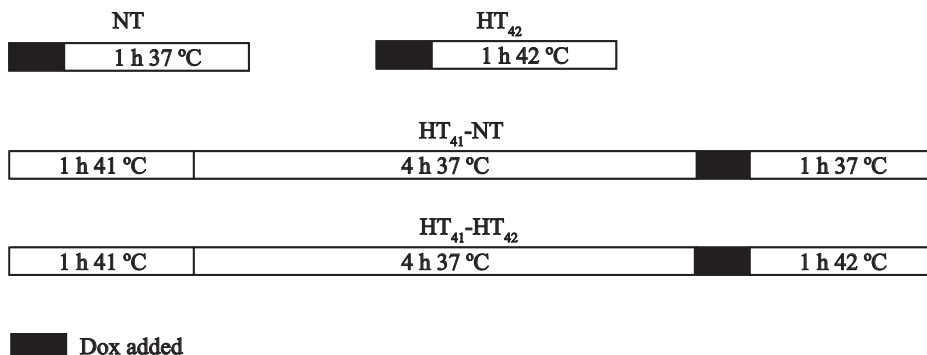
DPPC:DSPC:DSPE-PEG₂₀₀₀ at a molar ratio of 70:25:5 were dissolved in 9:1 (vol:vol) chloroform/methanol. Solvent was evaporated using a rotary evaporator and the resulting lipid film was flushed under a stream of nitrogen. The lipid film was hydrated with a 250 mM solution of (NH₄)₂SO₄ buffer pH 5.5 and extruded five times through 200 nm, 100 nm, 80 nm and 50 nm polycarbonate membrane filters. A pH gradient was established using a PD-10 column and eluting the liposomes with a pH 7.4 HEPES buffered saline (10 mM HEPES, 135 mM NaCl). Phosphate concentration was determined by ammonium molybdate assay³⁵¹. Doxorubicin was loaded into the liposomes by mixing doxorubicin and lipid at a ratio of 0.15:1 (mol:mol) and incubating it for 1 h at 39°C in a thermoshaker. Liposomes were concentrated by ultracentrifugation (193,000 g, 2 h, 4°C) and resuspended in 10 mM HEPES buffered saline pH 7.4 yielding the final formulation of doxorubicin-loaded TSLs (TSL_{Dox}).

Radiolabeled liposome preparation

For radiolabeled TSLs (¹¹¹In-TSL), 0.1 mol% DSPE-DTPA was added to the formulation described above and produced in a similar fashion as the regular TSLs, with the exception that the liposomes were not loaded with doxorubicin. 1 μmol TSLs was incubated with 30 MBq indium-111 for 15 min at room temperature after the pH was set at 5.0 with 2.5 M sodium acetate. After incubation, labeling efficiency was determined by ITLC-SG (Varian Inc.) and the final volume was adjusted to 200 μL with HEPES buffered saline (10 mM HEPES, 135 mM NaCl, pH 7.4).

Cellular toxicity assay

B16 or BFS-1 cells were seeded in 96-well plates and allowed to grow till 50% confluency in DMEM medium enriched with 10% FBS and 1% Pen-Strep. The medium was removed and fresh medium with a desired amount of free doxorubicin or TSL_{Dox} was brought onto the cells and incubated according to Scheme 1. NT: incubation with doxorubicin for 1 h at 37°C; HT₄₂: incubation with doxorubicin for 1 h at 42°C; HT₄₁-NT: Preheating cells 1 h at 41°C, 4 h recovery at 37°C and a 1 h incubation with doxorubicin at 37°C; HT₄₁-HT₄₂: Preheating cells for 1 h at 41°C, 4 h recovery at 37°C and a 1 h incubation doxorubicin at 42°C. For a TSL_{Dox} treatments on cells, 10 μM doxorubicin was used. To apply HT, plates were put into a water bath set at the required temperature. After incubation, the doxorubicin containing medium was removed and cells were given fresh medium for 24 h or 48 h incubation at 37°C. Cells were fixed using 10% (w:v) trichloroacetic acid (TCA). After fixation, the plates were washed with water and 0.5% SRB solution was added to stain the fixed cells for 20 min. When staining was completed, cells were washed with 1% acetic acid and left to dry. In the end, 10 mM Tris was added to resuspend the SRB and absorbance was measured at 590 nm by spectrophotometry (Wallac Victor 2 Counter).



Scheme 1. Overview of different *in vitro* doxorubicin uptake treatments. Cells were exposed to doxorubicin at 37°C (NT) or 42°C (HT₄₂). In two additional groups, cells were pre-heated for 1 h at 41°C (HT₄₁) with a 4 h recovery at 37°C before doxorubicin uptake under NT or HT₄₂ conditions (HT₄₁-NT and HT₄₁-HT₄₂, respectively).

Cellular doxorubicin uptake in 2D and 3D models

B16 or BFS-1 cells were seeded into 75 cm² flasks and grown under similar conditions as mentioned above until 80% confluency was reached. The cells were subjected to 40 μM doxorubicin under four different treatment conditions as stated in Scheme 1. Exposing cells to elevated temperatures was done by submerging the 75 cm² culture flask into a water bath. After incubation, the cells were washed with ice cold PBS, scraped from the flask and centrifuged at 200 *g* at 4°C. The pellets were resuspended in 150 μL lysis buffer (20 mM Tris, 150 mM NaCl, 0.2% NP40, 10% glycerol, pH 7.4), followed by 30 min incubation on ice and centrifugation at 14,000 *g*. The pellets were resuspended and homogenized in 500 μL PBS by brief probe sonication and doxorubicin concentration was measured by fluorometry at 485 nm excitation and 580 nm emission (Wallac Victor 2 Counter). Tumor spheroids were made according to a previously described method³⁵². In short, conical shaped 96-well plates were coated with poly-HEMA and 1 × 10⁵ cells which were centrifuged at 1,000 *g* for 10 min in the presence of 2.5% Matrigel and incubated overnight at 37°C. After incubation, spheroids were handpicked and exposed to identical treatments as in the 2D model in a thermoshaker (no shaking). After incubation, the spheroids were washed in PBS, embedded into Fluoromount-G and imaged by confocal microscopy (Zeiss LSM 510 Meta; Oberkochen, Germany). A 5 μm Z-stack was made over the surface of the spheroid to determine total doxorubicin fluorescence. For each optical slice, the amount of saturated doxorubicin fluorescence pixels were counted. The sum of saturated pixels of all tumor slices was used as an indicator for doxorubicin uptake. For cryosectioning, spheroids were embedded into Cryo Compound and snap frozen in liquid nitrogen. 10 μm slices were made using a Cryostat (Leica CM1850 UV; Wetzlar, Germany), and afterwards embedded into

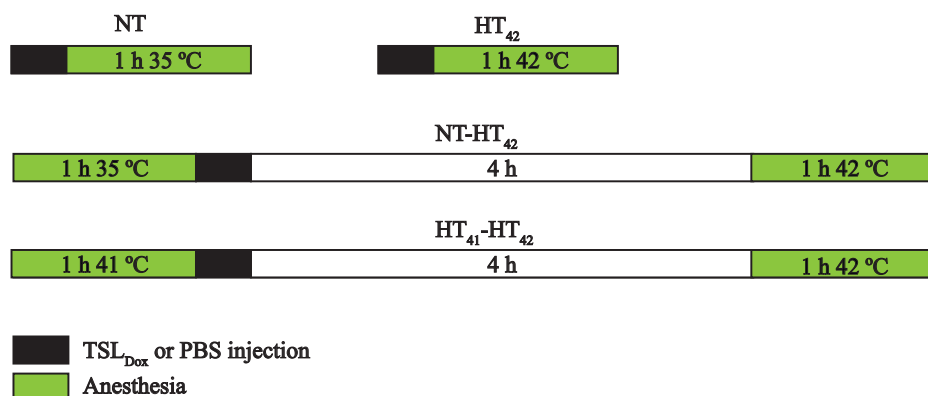
Fluoromount-G and imaged using fluorescence microscopy (Zeiss Axiovert 100M; Hamamatsu Photonics C4742-98 camera controller).

B16 and BFS-1 tumor generation

Murine B16 melanoma or BFS-1 sarcoma cells (1×10^6) were subcutaneously injected into the flank of C57BL6 mice (Harlan) to grow bulk tumors. After reaching volumes of approximately 700 mm^3 , animals were sacrificed and tumor pieces were transplanted to the animals of the therapeutic studies. All animal experiments were approved by the Erasmus MC animal research committee, Rotterdam, the Netherlands.

Therapeutic efficacy studies in a B16 and BFS-1 model

1 mm^3 B16 or BFS-1 tumor pieces were transplanted subcutaneously onto the hind limb of C57BL6 mice and allowed to grow to 200 mm^3 after which treatments were initiated as shown in Scheme 2. NT: 1-step with $100 \mu\text{L}$ i.v. PBS injection and 1 h anesthesia at body temperature; HT₄₂: 1-step with $100 \mu\text{L}$ i.v. PBS injection and 1 h anesthesia with heated tumor at 42°C ; TSL_{Dox} NT: 1-step with $100 \mu\text{L}$ 5 mg/kg TSL_{Dox} i.v. injection and 1 h anesthesia at body temperature; TSL_{Dox} HT₄₂: 1-step with $100 \mu\text{L}$ 5 mg/kg TSL_{Dox} i.v. injection and 1 h anesthesia with heated tumor at 42°C ; HT₄₁-HT₄₂: 2-step with 1 h preheating tumor at 41°C under anesthesia, $100 \mu\text{L}$ i.v. PBS injection, 4 h waiting period and 1 h anesthesia with heated tumor at 42°C ; TSL_{Dox} NT-HT₄₂: 2-step with 1 h anesthesia at body temperature, $100 \mu\text{L}$ 5 mg/kg TSL_{Dox} i.v. injection, 4 h waiting period and 1 h anesthesia with heated tumor at 42°C ; TSL_{Dox} HT₄₁-HT₄₂: 2-step with 1 h preheating tumor at 41°C under anesthesia, $100 \mu\text{L}$ 5 mg/kg TSL_{Dox}



Scheme 2. Overview of 1-step and 2-step treatments *in vivo*. For 1-step, i.v. TSL_{Dox} administration was conducted at body temperature (NT) or when the tumor was brought to 42°C (HT₄₂). Two-step treatments were composed of keeping the mouse under anesthesia at body temperature for 1 h (NT-HT₄₂) or preheating the tumor at 41°C for 1 h (HT_{Dox} injection, 4h rest and a second tumor heating at 42°C).

i.v. injection, 4 h waiting period and 1 h anesthesia with heated tumor at 42°C. In the 1-step treatment protocol, the tumor was submerged into a 42.5°C water bath for heating to 42°C for 10 min, followed by an i.v. injection of TSL (5 mg/kg doxorubicin) and further heating for another hour. The 2-step treatment procedure included heating of the tumor to 41°C for 1 h and an i.v. injection of TSL (5 mg/kg doxorubicin) 10 min after heating. Afterwards, the animal was allowed to rest for 4 h, followed by a second HT treatment for 1 h at 42°C. In control groups normothermic (NT; 35°C) conditions were used, where the animal was put under anesthesia for 1 h and kept at 35°C on a 37°C heating plate while covering the animal with tin foil. During both HT and NT experiments, the tumor bearing limb, with exception of the tumor itself, was coated in vaseline to prevent possible skin burns. Body temperatures of the mice were measured using a rectal probe.

SPECT/CT imaging of TSL accumulation in a B16 and BFS-1 model

1×10^6 cells were subcutaneously injected on the hind limb of C57BL6 mice and tumors were allowed to grow to volumes of 200 mm³. Tumors were either heated for 1 h at 41°C prior to injection or kept at 35°C in a similar fashion as for the therapeutic study. ¹¹¹In-TSL were i.v. injected (200 µL per mouse with an average activity of 33 ± 2 MBq indium-111) and scans were made 4, 8, 24 and 48 h after injection. Scans were acquired using the nanoSPECT/CT (Mediso Medical Imaging Systems) with the following settings for the SPECT scans: 20 projections, 60 s per projection, and a quality factor of 0.8. APT1 apertures were used with 1.4 mm diameter pinholes (FOV 24 + 16 mm). CT scans were acquired with 240 projections, 45 kVp tube voltage and 500 ms exposure. Data analysis was performed using InVivoScope/VivoQuant software (inviCRO, Boston, MA), where three-dimensional regions of interest were drawn over the tumor to calculate uptake of ¹¹¹In-TSL at the selected time points. After the last scan, the animals were sacrificed and tumors and organs were harvested, weighed and radioactivity was determined using a γ counter to calculate percentage injected dose per gram (%ID/g). All data were corrected for radioactive decay.

Pharmacokinetic modelling

The blood kinetics and pharmacokinetic parameters of the TSL_{Dox} formulation were determined in an earlier study³⁵³. Results from that study showed that the blood half-life of liposomal carrier $C_{lip}(t)$ can be described with a mono-exponential function:

$$C_{lip}(t) = C_{lip}(t=0) \cdot \text{Exp}(-\ln 2 / t_{1/2,TSL} \cdot t) \quad \text{Eq. 1}$$

with $C_{lip}(0)=100\%ID$ at time point of injection and $t_{1/2,TSL} = 5.6 \pm 0.4$ h being the circulation half-life of the liposomes. Upon injection, a fraction of doxorubicin is instantaneous

released ($Burst = 8 \pm 3\%$) followed by a slow leakage of doxorubicin from the liposomal carrier with a half-life of $t_{1/2,leak} = 2.7 \pm 0.3$ h. The concentration of intraliposomal dox $C_{Dox,TSL}(t)$ can be described with the following equation:

$$C_{Dox,TSL}(t) = (1 - Burst/100) \cdot Exp(-\ln 2/t_{1/2,leak} \cdot t) \cdot C_{lip}(t) \quad \text{Eq. 2}$$

The concentration of (radiolabeled) liposomes in the tumor, $C_{TSL,tumor}(t)$, can be described with a simple two compartment model:

$$\frac{\partial C_{TSL,tumor}(t)}{dt} = k_{in} \cdot C_{lip}(t) - k_{out} \cdot C_{TSL,tumor}(t) + k_{ret} \quad \text{Eq. 3}$$

where k_{in} , k_{out} and k_{ret} describe the rates of uptake, washout and retention of TSL in the tumor compartment.

Concentration of intraliposomal doxorubicin within the tumor is subsequently numerically calculated assuming the same burst and leakage of doxorubicin from the liposomal carrier as found for TSL_{Dox} in the blood compartment.

Numerical integration of Eq. 3 and fitting of the SPECT data was performed using Mathematica® (version 10.2, Wolfram Research).

Histology

After the SPECT/CT experiments, the excised tumors were snap frozen in liquid nitrogen. Hereafter 5 μm slices were cut and tumors were stained for vessels with an anti-CD31 antibody and AlexaFluor 594 or collagen with anti-collagen IV antibody and AlexaFluor 488. The TUNEL staining was performed with a cell death detection kit. The CD31 and TUNEL stains were quantified using ImageJ (version 1.48) software and by setting a manual threshold. A second set of frozen slices was stained with Maier's hematoxylin and Eosin (H&E) or by Weigert's hematoxylin, Martius yellow, crystal scarlet and methyl blue (MSB), followed by mounting in Entellan. The slices were imaged for fluorescence by confocal microscopy (CD31, collagen IV & TUNEL) or bright field microscopy (Leica DM 4000B) for H&E and MSB stained sections.

Statistics

All statistical tests were carried out using Graphpad Prism 5 software. All figures were subjected to unpaired two tailed t-test or one-way ANOVA Bonferroni test with significant difference at $p < 0.05$.

RESULTS

Preparation of TSL_{Dox}

Loading of TSL with the formulation DPPC:DSPC:DSPE-PEG₂₀₀₀ at a molar ratio of 70:25:5 with doxorubicin was achieved with 100% efficacy. Dynamic light scattering of the resulting TSL_{Dox} indicated an average hydrodynamic diameter of 83 ± 3 nm and a zeta-potential of -7.9 ± 0.9 mV. Stability at 37°C and release kinetics at 42°C were tested in culture medium (10% FBS and 1% Pen-Strep) and were found to be similar to results obtained with 100% FBS as described in our previous work (Figure 1)³⁵³.

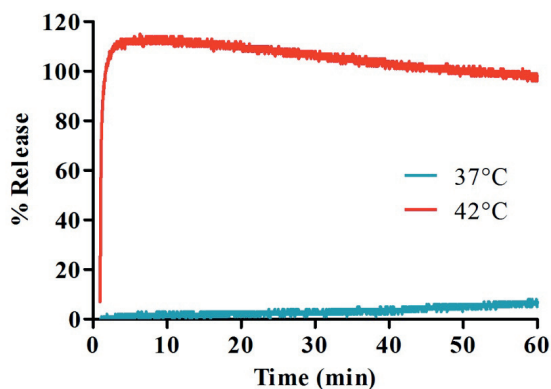


Figure 1. Doxorubicin release from TSL at 37°C and 42°C in DMEM culture medium with 10% FBS and 1% Pen-Strep using fluorescence readout. All experiments have been performed 3 times.

Cytotoxic assays on B16 melanoma and BFS-1 sarcoma cells

In an *in vitro* study, murine B16 melanoma and BFS-1 sarcoma cells were exposed to various doxorubicin concentrations for 1 h under the conditions depicted in Scheme 1. Both cell lines showed an increased sensitivity to doxorubicin when the drug exposure was performed at hyperthermic temperatures (Figure 2). For B16 (Figure 2A, 2B) and BFS-1 (Figure 2C, 2D), the doxorubicin sensitivity increased 8-fold. Additional pre-heating (HT₄₁-HT₄₂) did not result in a further increase in doxorubicin sensitivity for B16. However, the 18-fold increase for BFS-1 was significantly higher than the single HT treatment. In this case direct HT-induced cytotoxicity could have played a predominant role (Figure 3). B16 and BFS-1 cells were furthermore tested for survival after incubation with TSL (empty), 10 μ M TSL_{Dox} or 10 μ M free doxorubicin under normothermic (NT; 37°C) and HT₄₂ conditions for 1 h. After the treatment, the cells were kept in culture medium for 24 h or 48 h. At 37°C, TSL_{Dox} induced little toxicity to the cells, while at 42°C the release of doxorubicin was sufficient to cause high cell death (Figure 4). The TSL by itself had no inhibitory effect on cell growth, while HT did show

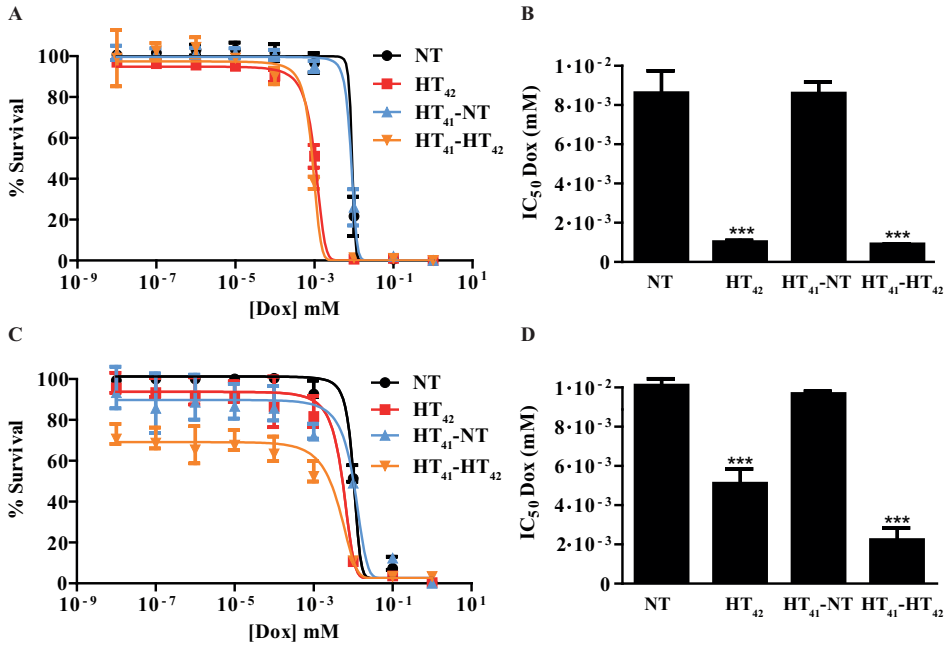


Figure 2. Doxorubicin cytotoxicity assay and IC_{50} values for B16 (A, B) and BFS-1 cells (C, D) 48 h after treatment with different hyperthermia protocols. $N = 3$ for each data set. Curves were fit by non-linear regression and statistical analysis by one-way ANOVA Bonferroni test. The significance scores of all treatments versus NT groups are indicated with asterisks. * = $p < 0.05$, ** = $p < 0.01$, *** = $p < 0.005$.

some direct cytotoxicity, which was only significant for B16 24 h after incubation with $72 \pm 11\%$ viable cells compared to the NT group (Figure 4A). The addition of $10 \mu\text{M}$ TSL_{Dox} to a 1 h incubation with HT_{42} resulted in an immediate cytotoxic effect 24 h after

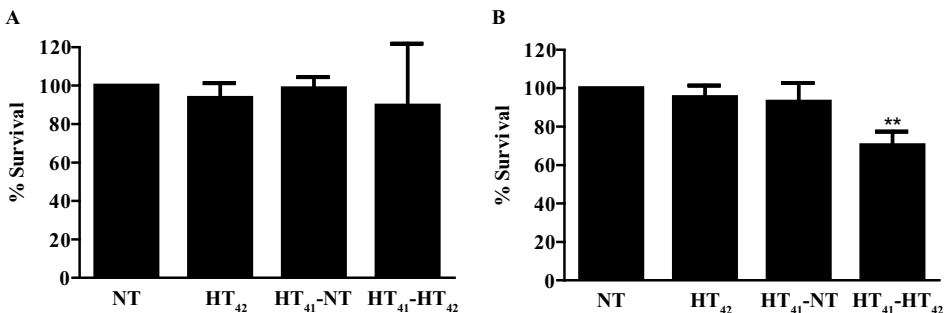


Figure 3. Analysis on HT induced cytotoxicity on B16 (A) and BFS-1 cells (B) in the experimental groups of Figure 1. Survival of experimental groups is normalized to the NT group. $N = 3$ per group and one-way ANOVA Bonferroni test was used for statistical analysis of the data. * = $p < 0.05$, ** = $p < 0.01$, *** = $p < 0.005$.

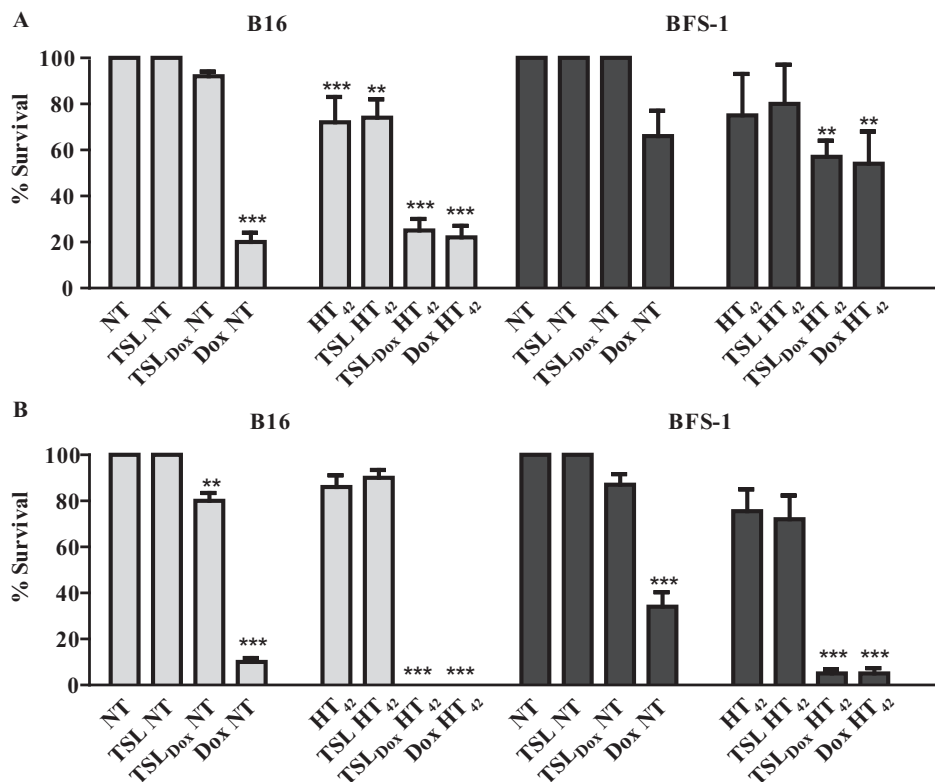


Figure 4. Cytotoxicity assay on B16 and BFS-1 cells 24 h (A) and 48 h (B) after a 1 h incubation with 10 μ M TSL_{Dox} or free doxorubicin under NT (37°C) or HT₄₂ (42°C) conditions. N = 3 for each data set. Statistical analysis was carried out using one way ANOVA Bonferroni test comparing the treatment groups with the NT group separately at 24 h and 48 h. The significance scores of all treatments versus NT groups are indicated with asterisks. * = $p < 0.05$, ** = $p < 0.01$, *** = $p < 0.005$.

the incubation (Figure 4A) with $25 \pm 6\%$ for B16 and $57 \pm 7\%$ cell survival for BFS-1. This cytotoxic effect became even more apparent 48 h after incubation, showing an almost complete cell death for both cell types (Figure 4B). The TSL_{Dox} HT₄₂ group showed similar results as where 10 μ M free doxorubicin was used (Dox HT₄₂), suggesting a total doxorubicin release from TSL_{Dox} in these experimental conditions. A cytotoxicity assay using a 2-step heating protocol was not performed, as the main cytotoxic effect was caused by the increased uptake of free or released doxorubicin during HT₄₂.

***In vitro* doxorubicin uptake in 2D and 3D models**

Next, the effect of HT on doxorubicin uptake was studied in B16 and BFS-1 cells. Both cell lines exhibited a linear uptake of doxorubicin over time at body temperature (Figure 5A, 5B). Incubation of both cell lines with doxorubicin at HT₄₂ significantly increased

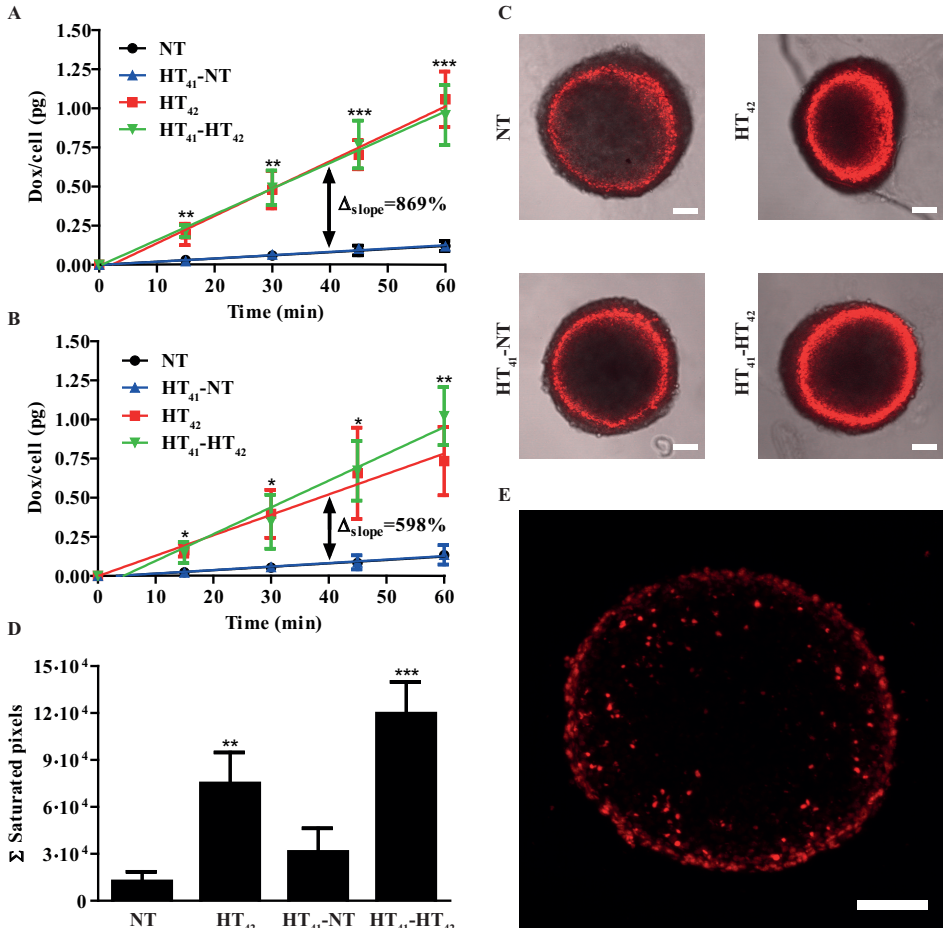


Figure 5. Two-dimensional doxorubicin uptake in B16 (A) and BFS-1 (B) cell cultures and BFS-1 spheroids (C-E). Cells or spheroids were exposed to 40 μM doxorubicin for 1 h at 37°C (NT), 42°C (HT₄₂), or preheated at 41°C followed by 4 h at 37°C before a 1 h exposure to 40 μM doxorubicin. Images of the spheroids made by confocal microscopy (C) were summed up to determine the Σ saturated pixels (red) per spheroid (D). Cryosections of 10 μm (E) of the BFS-1 spheroids show spatial distribution of doxorubicin fluorescence (red). All data sets are composed of an $n = 3$ experiment and compared by one way ANOVA Bonferroni test, * = $p < 0.05$, ** = $p < 0.01$, *** = $p < 0.005$. Asterisks show significance compared to NT groups. Scale bars = 100 μm .

doxorubicin uptake 9-fold for B16 (Figure 5A) and 6-fold for BFS-1 cells (Figure 5B). Groups were added where the cells were preheated at 41°C for 1 h followed by 4 h at 37°C to mimic a 2-step approach therapy. Preheating of the cells before incubation with doxorubicin at NT (HT₄₁-NT) or HT₄₂ (HT₄₁-HT₄₂) conditions did not result in a significant difference compared to doxorubicin uptake without preheating. Next, we

used multicellular spheroids of BFS-1 cells to determine the doxorubicin uptake as well as spatial distribution under the different temperature protocols in a 3D model. After performing similar incubation protocols as described before, the BFS-1 spheroids showed a similar pattern in doxorubicin uptake than BFS-1 cells in the 2D standard culture conditions (Figure 5C). When the doxorubicin fluorescence intensity was quantified (Figure 5D), HT₄₂ and HT₄₁-HT₄₂ presented significantly more doxorubicin positive areas than NT spheroids with a 6-fold and 10-fold increase in the summation of saturated doxorubicin fluorescence pixels, respectively. HT₄₁-NT treatment did not result in a significantly enhanced uptake. Doxorubicin did not penetrate farther than

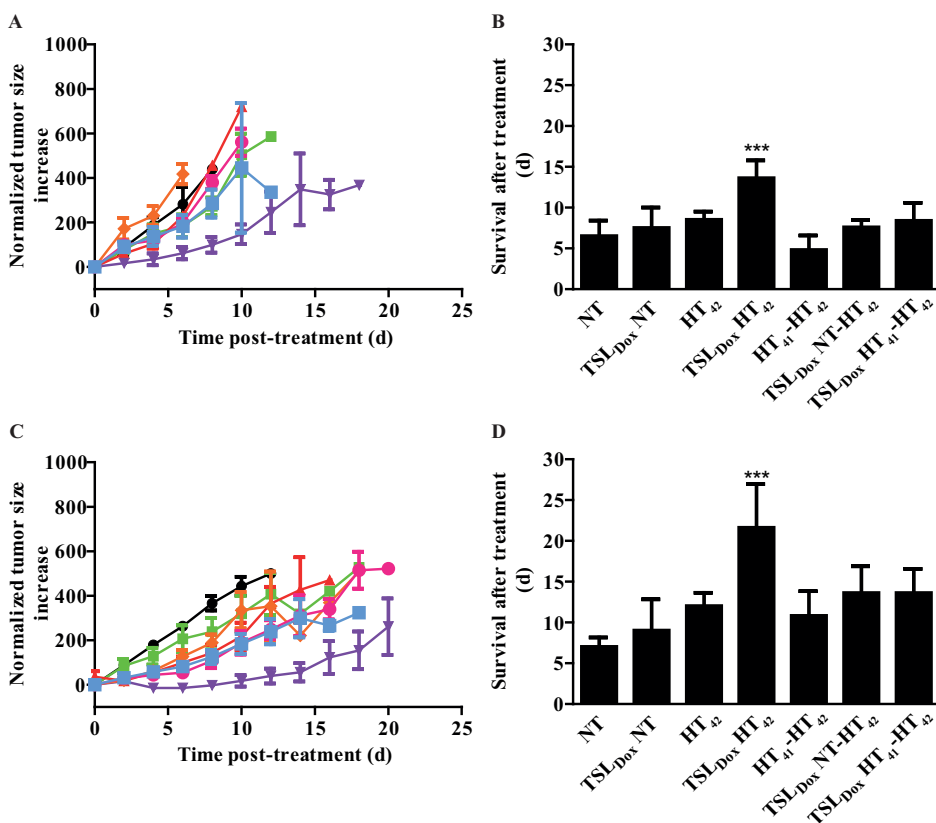


Figure 6. Therapeutic efficacy study in C57BL6 mice with s.c. B16 or BFS-1 tumors. After treatment, results for B16 tumors were plotted for growth (A) and survival (B) with NT (black), HT₄₂ (red), HT₄₁-HT₄₂ (orange), TSL_{Dox}NT (green), TSL_{Dox}HT₄₂ (purple), TSL_{Dox}NT-HT₄₂ (pink) and TSL_{Dox}HT₄₁-HT₄₂ (blue). Survival (B) was based on a size cutoff at 300% tumor size increase. Error bars in growth curve (A) represent SEM and one way ANOVA Bonferroni test was used to determine differences in survival in B (* = $p < 0.05$, ** = $p < 0.01$, *** = $p < 0.005$). Asterisks above bars show significance versus NT. Data for BFS-1 is presented similarly in C and D. N = 4 for NT, TSL₄₂ groups; n = 5 for all other groups.

the first few cell layers into the spheroid, despite the heating protocol used (Figure 5E). B16 cells did not form spheroids and could therefore not be studied in the 3D doxorubicin uptake model.

One-step and two-step therapeutic study

A therapeutic study with B16 (Figure 6A, 6B) and BFS-1 (Figure 6C, 6D) tumors were subjected to 1-step or 2-step therapies (Scheme 2). We chose 41°C as preheating temperature since it has been shown that an intratumoral increase of TSL_{Dox} accumulation can be established³²² without risking significant vascular damage³⁵⁴. In both B16 and BFS-1 tumors, TSL_{Dox} with HT₄₂ significantly outperformed all other treatments with an average improvement of survival of 7.1 ± 1.4 d for B16 and 14.6 ± 2.8 d for BFS-1 when compared to the NT group. The body temperature differed significantly between NT and HT₄₂ treated mice (Figure 7). Nevertheless, it remained at a physiological level with 35.0 ± 0.4 °C and 36.9 ± 1.1 °C, respectively.

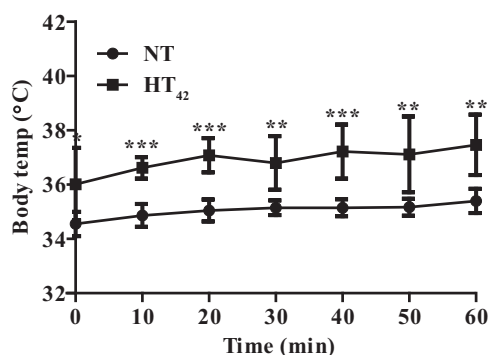


Figure 7. Body temperature readings of mice under anesthesia, on a 37°C heating plate, covered with tin foil (NT), or mice under anesthesia with the tumor bearing limb submerged in a 42.5°C water bath (HT₄₂). *n* = 6 per group. Temperature readings were performed rectally with a probe thermometer every 10 min. For every time point, statistical analysis was performed by unpaired two-tailed t-test. * = *p* < 0.05, ** = *p* < 0.01, *** = *p* < 0.005.

Quantitative SPECT/CT imaging of TSL accumulation in solid tumors

A SPECT/CT study with ¹¹¹In-TSL (labeling efficiency > 99%) was carried out to visualize the particle uptake in B16 and BFS-1 tumor bearing mice, comparing NT conditions versus tumor preheating for 1 h at 41°C prior to injection (HT₄₁). SPECT imaging over time showed that the majority of the injected ¹¹¹In-TSL were cleared by liver and spleen (Figure 8A, 8B) with tumor uptake over time. For all tumors, a maximum uptake was observed approx. 4 h post injection followed by a slight reduction over time leveling off at 48 h post injection. Under NT conditions, plateau values of 3.2 ± 0.5 and $1 \pm 0.3\%$ injected dose per cm³ were reached for B16 and BFS1 tumors respectively. Applying

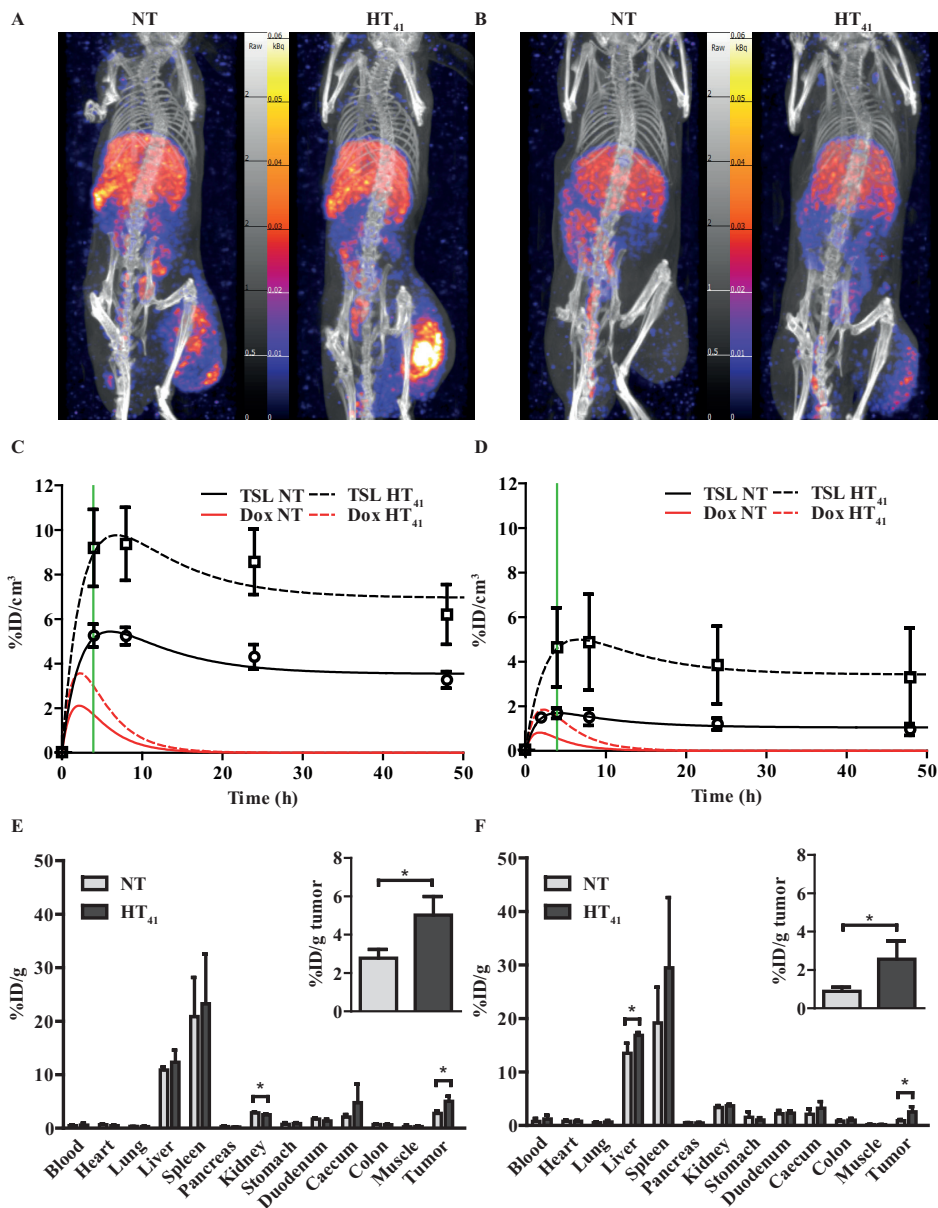


Figure 8. SPECT-CT study on ^{111}In -TSL distribution in B16 (A, C, E) and BFS-1 (B, D, F) tumor bearing mice. After i.v. administration, scans were made at 4 h, 8 h, 24 h and 48 h for all groups. B16 (A, C) and BFS-1 (B, D) tumors showed ^{111}In -TSL accumulation after i.v. administration at NT, which could be significantly enhanced (unpaired two-tailed t-test; $p < 0.05$) by pre-heating the tumor for 1 h at 41°C prior to ^{111}In -TSL administration (HT_{41}). The green line shows the 4 h time point where a second HT treatment would have taken place in case of a 2-step therapy. Biodistribution of excised organs and tumors (E, F) 48 h after injection. Every group consisted of three animals ($n = 3$).

HT₄₁ before injection increased uptake in both tumors, leading to higher maximum as well as plateau concentrations (B16: $6.2 \pm 1.5\%$ injected dose per cm³, BFS1: $3.3 \pm 2.8\%$ injected dose per cm³ at 48 h p.i.) (Figure 8A-D). Biodistribution studies at $t = 48$ h p.i. were consistent with data derived from SPECT showing an uptake of ¹¹¹In-TSL in B16 tumors $2.8 \pm 0.5\%$ injected dose per gram compared to a considerable lower uptake of $0.9 \pm 0.2\%$ injected dose per gram in BFS-1 tumors for NT experiments (Figure 8E, 8F). Applying HT₄₁ before injection resulted in a significantly increased ¹¹¹In-TSL accumulation measured after 48 h in B16 tumors ($5.0 \pm 1.0\%$ injected dose per gram; Figure 8C, 8E) and BFS-1 tumors ($2.6 \pm 1.0\%$ injected dose per gram; Figure 8D, 8F).

SPECT data were used to fit the liposomal tumor uptake according to a simple two compartment model, deriving the rates for uptake, washout and retention, k_{in} , k_{out} , k_{ret} , in the two different tumors under NT and HT₄₁ conditions (Table 1). Taking the earlier determined pharmacokinetic properties of the here used TSL_{Dox} formulation into account, the model also allowed to calculate the concentration of intraliposomal doxorubicin present in the tumors as a function of time (Figure 8C, 8D). Maximum concentrations of intraliposomal doxorubicin were reached approximately 2 h p.i. In contrast to the liposomal concentrations, intraliposomal doxorubicin concentrations decreased to zero 15-20 h p.i. due to the leakage from the liposomal carrier.

The uptake as well as the retention rate of liposomes in B16 tumors was *circa* 2 times higher compared to BFS-1 tumors, while washout was comparable for both tumors. Notably, HT₄₁ induced in both tumors a comparable effect with increasing the k_{in} , and k_{ret} by a factor of 1.66 ± 0.13 leading to a more rapid and higher uptake of liposomes and consequently a high doxorubicin peak concentration.

Table 1. Pharmacokinetic parameters describing the tumor uptake and retention in B16 and BFS-1 tumors

Tumor type	Condition	k_{in} / (1/h)	k_{out} / (1/h)	k_{ret} / (1/h)
B16	NT	0.0157 ± 0.004	0.39 ± 0.16	1.4 ± 0.63
	HT ₄₁	0.0233 ± 0.007	0.36 ± 0.22	2.5 ± 1.64
BFS-1	NT	0.0074 ± 0.003	0.69 ± 0.34	0.7 ± 0.38
	HT ₄₁	0.0127 ± 0.001	0.36 ± 0.07	1.2 ± 0.24

Histology

After the SPECT-CT study, the tumors were used for H&E, MSB, TUNEL, CD31 and collagen IV staining (Figure 9 & 10). H&E staining indicated that B16 tumors have less strong cellular interactions as can be seen by the gaps in the tissue (Figure 9A), whereas BFS-1 has a much more compact morphology. Furthermore, the H&E suggests that the B16 tumors are more apoptotic (Figure 9A, arrows). Yet after HT₄₁, apoptotic

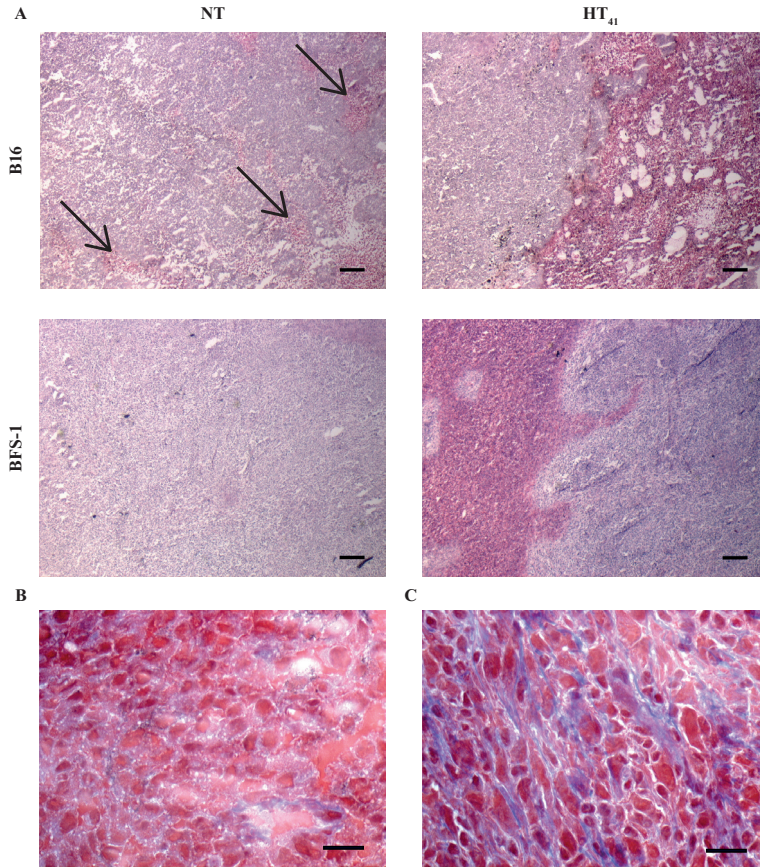


Figure 9. 5 μm H&E stained sections of B16 and BFS-1 tumors 48 h after NT or HT₄₁ (A). Black arrows indicate apoptotic areas. MSB stained B16 (B) and BFS-1 (C) tumors showing collagen in blue. Scale bars = 200 μm in A and 20 μm in B and C.

areas could be seen in both tumor types. MSB staining showed that B16 tumors have a very low presence of extracellular fibers (Figure 9B), whereas BFS-1 showed a more mature extracellular matrix (Figure 9C). Quantitative TUNEL staining (Figure 10A) showed high apoptosis of $14.4 \pm 10.0\%$ for B16 when compared to BFS-1 with $0.4 \pm 0.1\%$. HT₄₁ caused an increase of apoptosis, showing $24.5 \pm 13.2\%$ for B16 and $1.2 \pm 0.4\%$ for BFS-1, which was a significant increase for the latter. The vessel staining using CD31 indicated a comparable mean vessel density for both tumor models (Figure 10B). The quantitative collagen IV staining confirmed the result of the MSB staining with $3.6 \pm 0.3\%$ for B16 and $14.8 \pm 1.2\%$ mean density for BFS-1 (Figure 10C). The B16 vessels were relatively large with collagen almost solely associated with the vessels (Figure 10D), whereas BFS-1 vessels were smaller and the interstitium consisted of more extracellular collagen matrix (Figure 10E).

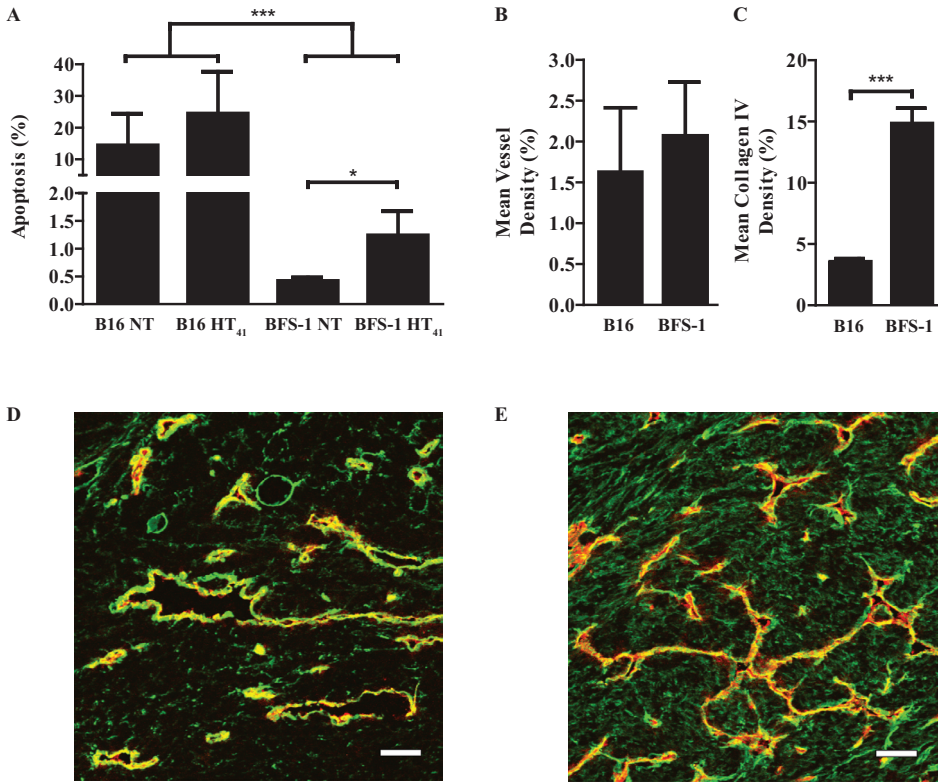


Figure 10. Quantification of cryo-section staining with TUNEL (A), CD31 (B) and collagen IV (C) was analyzed by unpaired two tailed t-test ($* = p < 0.05$). B16 (D) and BFS-1 (E) blood vessels colored red for CD31. Collagen IV stained in green. Scale bars = 50 μ m. N = 3 for all groups.

DISCUSSION

In the field of nanomedicine, substantial research has been performed throughout the last decades on HT-triggered drug release from TSLs for treatment of solid tumors. In this context, mainly 1-step intravascular drug delivery schemes were employed, where tumors are heated to hyperthermic temperatures and drug loaded TSL are injected at the start of the HT treatment. In a previous study conducted by Li et al.³⁵⁰, a 2-step treatment scheme was investigated as a possible alternative in a BLM melanoma xenograft, where first HT₄₁ is applied to enhance vascular permeability, then a TSL_{Dox} formulation was injected that subsequently accumulated in the tumor, followed by a second HT₄₂ step to release the drug from its carrier in order to ensure bioavailability. The aforementioned study showed in contrast to the 1-step therapy, that the 2-step approach was not effective in causing a therapeutic response. In our experimental design we chose for a B16 melanoma and BFS-1 sarcoma cell line because tumors from these

cell lines have been previously reported to show high and low EPR-mediated uptake of TSL, respectively³²². We tested how these tumors respond to a 1-step versus 2-step therapy, expanded the knowledge on how the tumor models responded to single versus multiple HT treatments in combination with local chemotherapy and provide extensive information on what factors can cause the differences in TSL accumulation between these tumors and which of these factors could be influenced by HT to increase TSL accumulation.

B16 and BFS-1 cells showed a significant increase in doxorubicin sensitivity when the drug exposure happened during HT₄₂. The reduced IC₅₀ with HT correlated with the increase doxorubicin uptake by the cells discussed hereafter. Previously published data on this correlation showed that the outcome of these experiments depend on cell type and specific experimental conditions, e.g. exact temperature and duration of HT exposure^{343,355-357}. Testing TSL_{Dox} on these cells showed that at 37°C the cytotoxic effect is minimal, whereas at 42°C, the TSL_{Dox} released all drug and therefore cytotoxicity was comparable to free doxorubicin. The small cytotoxic effect at 37°C could be caused by cellular uptake of TSL_{Dox} or by doxorubicin leaking from the liposomes into culture medium (Figure 1). Next, we investigated the presence of a synergistic effect of doxorubicin and HT for different heating schemes in a 2D and 3D cellular model. In a 2D model, it was shown that HT₄₂ induces a faster cellular uptake of doxorubicin leading to a 6-9 times higher rate of uptake in B16 and BFS-1 cells than at 37°C. Preheating the cells for 1 h with HT₄₁ followed by incubation for 4 h at 37°C before adding doxorubicin did not show any improvement of doxorubicin uptake, indicating that HT-induced effects at 41°C were reversible in nature and could only improve drug uptake during the heating and not thereafter. As the doxorubicin uptake is caused by passive diffusion across the cell membrane, increase of cellular membrane fluidity and permeability during HT is the most likely explanation, since these effects are temporal in nature and fully reversible^{343,344}. Other studies have shown that preheating to slightly higher temperatures of 43-45.5°C lead to a reduced doxorubicin uptake most likely due to a more permanent and irreversible temperature of thermal dose induced damage^{355,358}. However, HT₄₁ used for preheating in this study did not induce this effect and has also been reported by others³⁵⁹. Spheroids mimic a solid tumor in terms of cell physiology, presence of extracellular matrix and an apoptotic core³⁶⁰. For this reason, we employed this model to investigate whether doxorubicin penetration depth into a dense structure of cells is influenced by different heating conditions^{361,362}. BFS-1 spheroids showed a similar response in doxorubicin uptake as the 2D model when different HT protocols were applied. However, it also showed that if cells are closely packed, the drug does not penetrate deep into the structure beyond the first few layers of cells. Neither the spatial distribution nor the penetration depth could be improved by HT in tumor spheroids. A comparative study using B16 cells was not possible since B16 cells did not form spher-

oids. The latter might be caused by the lack of a substantial cell-cell adherence, which was also observed in *ex vivo* examination of B16 tumors described later in this section.

At this stage we have only shown the potential of local chemotherapy and HT *in vitro*. However, the described features are only a small part of the factors that have to be considered for drug delivery to solid tumors. Therefore, we performed a therapeutic study as well as *in vivo* imaging and extensive *ex vivo* investigation on B16 and BFS-1 tumors to better understand the factors that could have played a role in various therapeutic responses. For both tumor types, a 1-step approach where TSL_{Dox} is *i.v.* administered during HT₄₂ gave a significant therapeutic response, whereas a 2-step approach which relied on TSL_{Dox} accumulation in a preheated (HT₄₁) tumor followed by a second HT₄₂ step to induce drug release did not show a therapeutic effect. The SPECT/CT imaging in this case was particularly valuable to follow the TSL accumulation in B16 and BFS-1 tumors. The SPECT data were used for fitting a two compartment model which describes tumor uptake of the liposomal carrier as well as the intraliposomal doxorubicin concentration in the tumor taking the blood kinetic and pharmacokinetic parameters of TSL_{Dox} into account³⁵³. For both tumors and regardless of applying HT₄₁ beforehand, the maximum concentration of liposomes was reached approximately 4 h *p.i.*, when the second HT₄₂ step was applied. The B16 tumors showed a significantly higher liposomal uptake compared to the BFS-1 tumor with *circa* two fold higher k_{in} and k_{ret} parameters reflecting a higher intrinsic EPR effect for the B16 model. Interestingly, 1 h of HT₄₁ induced the same effect in both tumors leading to a 1.66 times increase in k_{in} and k_{ret} and thus maintaining the two fold higher uptake of TSLs in B16 compared to BFS1 tumors.

However, calculations suggested that maximum intraliposomal doxorubicin concentrations were already reached 2 h *p.i.*, and declining to zero within 20 h due to leakage from the TSLs. These data imply that a more favorable time point for the second HT₄₂ step is *circa* 2-3 h post injection³⁵⁰. Based on our calculations, the intraliposomal doxorubicin reached concentrations of 1.7% injected dose per cm³ for B16 and 0.6% injected dose per cm³ doxorubicin for BFS-1 at the moment of the second HT₄₂ step (*i.e.* after 4 h) at normal temperature conditions, and 3.0% injected dose per cm³ and 1.5% injected dose per cm³ doxorubicin with a preceding HT₄₁ treatment. These concentrations are lower compared to typical values found for a 1-step delivery approach³⁶³, which provides an explanation for the lack of a significant therapeutic response in a 2-step drug delivery protocol.

Finally, we performed histological analysis of excised tumors and investigated factors that may cause the differences in TSL uptake and the intrinsically higher EPR effect found in B16 and BFS-1 tumors. B16 tumors grew more aggressively than BFS-1, reaching volumes of 200 mm³ in 7-14 d and 14-21 d after inoculation, respectively. Especially in preclinical models, fast growing tumors show higher structural and func-

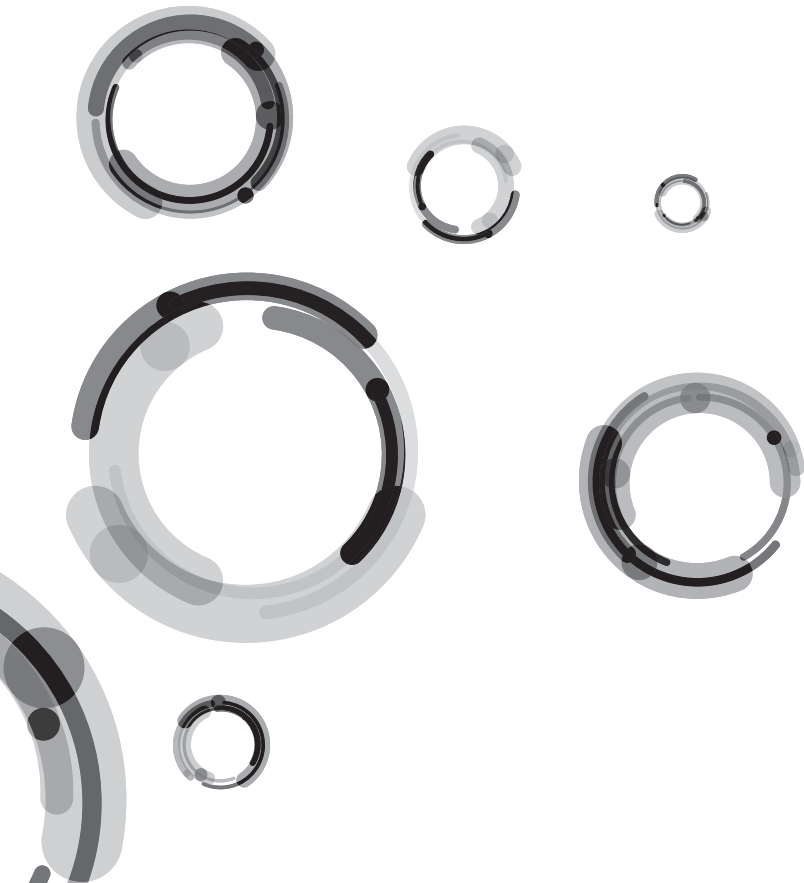
tional abnormalities of the vasculature, thereby increasing the odds for a high EPR effect^{150,288,323}. The mean vessel density was similar for B16 and BFS-1, however the morphology of B16 vessels appeared more tortuous and overall larger in size. Next to the growth rate and vascular properties, we also observed noticeable differences in cell packing and organization, which is important for the penetration depth of extravasated compounds into the tumor interstitium^{291,361,364}. H&E staining showed less dense cellular packing with gaps in the B16 tumor tissue, whereas BFS-1 showed a higher density and no gaps. Therefore, the finding that BFS-1 cells could form spheroids while B16 cells did not, might be indicative for cell packing and organization in an actual tumor. *In vivo*, cell packing density and organization is, among other reasons, depends on the presence of a well-defined extracellular matrix. Analysis on the extracellular matrix by MSB staining and quantitative collagen IV immunostaining showed that B16 tumors have an almost completely absent extracellular matrix, whereas BFS-1 tumors had a more mature extracellular matrix. These findings suggest that the immature interstitium of the B16 tumor could have played a role in facilitating a higher EPR, confirming previously published results¹⁵⁷. Histological analysis and quantitative TUNEL staining also indicated a much higher amount of apoptosis in the B16 tumors than in the BFS-1 tumors, which is typically associated with a more pronounced EPR effect^{365,366}. The HT₄₁ induced increase of apoptosis was significant for the sectioned BFS-1 tumors. While our study is in line with earlier findings showing that HT increases vascular permeability and promotes extravasation of nanoparticles^{322,345,346}, our histology data also suggest that substantial HT₄₁ induced apoptosis can further aid EPR.

In summary, we have shown that HT can aid in drug delivery by making cells more susceptible for doxorubicin uptake, increasing the EPR-mediated uptake of liposomal drugs and by providing a trigger for drug release from TSL_{Dox}. All above factors play a pivotal role in the here employed 2-step delivery scheme. However, the actual amount of doxorubicin delivered in a 2-step approach is determined by liposomal uptake and stability of the formulation and can therefore never exceed the liposomal uptake (in%ID/g). This study has shown that preheated B16 and BFS-1 tumors accumulated a maximum of 9.8% injected dose per cm³ and 5.0% injected dose per cm³ of the injected TSL dose, while the intraliposomal doxorubicin concentration only reached 3 and 1.5% injected dose per cm³ at 4 h p.i. respectively. These doxorubicin concentrations appeared insufficient to induce a noticeable therapeutic response. The 1-step intravascular drug release seems to be advantageous, since the injected TSL_{Dox} provide a high plasma concentration of doxorubicin exposing the tumor to a high area under the curve (AUC) over the time span of HT. Furthermore, the HT induced increase in doxorubicin uptake by tumor cells may lead in both delivery schemes to a higher intracellular concentration.



CHAPTER 7

General Discussion



CURRENT STATUS OF NANOMEDICINE

Anticancer nanomedicine containing chemotherapeutics were developed to cope with drug solubility problems *in vivo* and severe side effects limiting use in patients³⁶⁷. For example, doxorubicin is an important anticancer drug used against various cancers^{368,369}, but unfortunately it is associated with severe cardiotoxicity and potential heart failure³⁷⁰. Liposomal doxorubicin, Doxil, was successfully formulated to increase accumulation in the tumor and reduce cardiotoxicity. Other well known FDA approved nanomedicines are liposomal daunorubicin (DaunoXome), liposomal vincristine (Marqibo), and albumin-bound paclitaxel (Abraxane). These nanomedicines successfully reduce side effects and have shown therapeutic effects in certain tumor types. In addition, nanomedicines with cytarabine, mifamurtide, iron oxide particles, asparaginase, DAB389IL-2, and SMANCS have been clinically approved³⁷¹.

Most chemotherapeutics are encapsulated in lipid (liposomes) or polymer-based vesicles (micelles or polymersomes). Liposomes can encapsulate both hydrophilic and hydrophobic drugs, although the latter associates with the lipid bilayer which has a relatively small volume. Polymeric micelles have a hydrophilic shell and a hydrophobic core, which enables more efficient encapsulation of hydrophobic drugs^{372,373}. Due to their relatively small size and effective tumor penetration³⁷⁴, several formulations are showing improved therapeutic responses and reduced side effects in clinical trials³⁷⁵. The chemotherapeutic drug paclitaxel causes severe adverse effects, in addition to hypersensitivity to its often used solubilizing excipient Kolliphor EL³⁷⁶. Genexol-PM, a Kolliphor EL-free polymeric formulation, is currently in Phase II trials, where it seems highly effective and tolerable in combination with cisplatin³⁷⁷. The FDA approved co-condensate of albumin and paclitaxel, ABI-007, demonstrated increased tumor response rates and delayed tumor progression in patients with metastatic breast cancer³⁷⁸. Irinotecan, a camptothecin derivative, is lipophilic and has an unstable structure on its own, yet it can be encapsulated in polymeric micelles (NK012) and has proven to be tolerated well and showed antitumor activity³⁷⁹. The platinum-based chemotherapeutic, cisplatin³⁸⁰, has also been encapsulated in polymeric micelles (Nanoplatin or NC-6004), and a Phase I study is currently underway where it is being used as first line treatment in combination with 5-FU and cetuximab for metastatic squamous cell carcinoma of the head and neck. This formulation was developed after disappointing results with liposomal cisplatin (SPI-77)^{381,382}, where despite high tumor uptake, a limited effect was observed possibly due to incomplete drug release³⁸³. All the above mentioned formulations rely on passive accumulation in the tumor, which unfortunately is not often effective, and numerous nanomedicine have failed to get into the clinic or mainly received approval due to the reduction in drug related adverse effects.

The variability in therapeutic efficacy can have various reasons, yet in general it comes down to inter- and intratumoral heterogeneity within the patient population³⁸⁴. It has been shown that tumor accumulation can range from 1-10% injected dose per gram in various mouse models depending on the formulation and pharmacokinetics of the nanomedicine³⁸⁵. Furthermore, the formulation of liposomes has a major effect on its biodistribution and interactions with the tumor microenvironment. Clinically used nanomedicines have sizes ranging from dozens to hundreds of nanometers, which results in different pharmacokinetic profiles. It has been implied that the large size of nanoparticles often compromises penetration and homogeneous distribution in tumors³⁸⁶. In 1995, a study with adenocarcinoma transplanted in dorsal skin chambers showed an inverse correlation between microvascular permeability and the size of macromolecules¹⁴⁸. Further research led to the observation that tumor penetration is severely hampered by the composition, structure and distribution of the extracellular matrix³⁸⁷. As a result, nanoparticles primarily concentrate in the perivascular space of the tumor and often do not penetrate the tumor any further^{388,389}. This was supported by a study which showed that increasing molecular weight of dextrans decreased penetration of tumor tissue to only 5 μm from the nearest vessel for the largest dextrans of 2 MDa³⁹⁰. Luckily, the penetration of nanomedicines can be improved by using compounds that remove or weaken barriers present in the tumor, via loosening of the extracellular matrix with MMPs, such as collagenase³⁹¹, hyaluronidase³⁹², and other proteases³⁹³, although some of these molecules play important roles in tumor invasion and metastasis which limits their usability in the clinic³⁹⁴.

A more subtle way of increasing efficacy is by the addition of targeting ligands which can bind specifically to tumor cells, or in their vicinity via targeting of endothelial or stromal cells. Unfortunately, only a small number of targeted formulations are currently in Phase II/III clinical trials out of at least 36 anticancer nanomedicines^{371,395}. In this thesis, we tried to develop diagnostic and therapeutic nanomedicines which use targeting ligands to enhance their specificity to the tumor and augment the beneficial effects of encapsulated drugs.

PERSONALIZED MEDICINE: TARGETING OR NO TARGETING?

Targeting tumor specific antigens is crucial for diagnostics, therapeutics, and evaluation of drugs. Targeting moieties are in constant development to enhance specificity and decrease side effects in patients. As a novel moiety in the search for more targeted anticancer drugs, nanobodies have slowly become established as biotechnological tools and imaging modalities³⁹⁶, although their use as a therapeutic agent is still under development³⁹⁷. After their discovery⁷⁸, their small size, high solubility and affinity, and cost-efficient production have made them the ideal tool for an ever increasing number

of applications¹⁰⁸. Several nanobodies have been developed as targeting ligands against EGFR¹²¹, HER2³⁹⁸, c-MET and HGF^{122,399}, VEGF and VEGFR-2^{124,400}, DR5⁴⁰¹, CXCR4⁴⁰², CXCR7 and CXCL11/12^{123,403}, and the vasculature via PlexinD1¹³². Nanobodies are ideal for imaging, due to their short half-life, although for therapeutic applications various modifications are used to increase their half-life in blood. Hydrophilic PEG chains can be conjugated to the nanobodies via cysteine chemistry, which has no effect on the nanobodies' affinity⁴⁰⁴. The avidity of nanobodies can be enhanced by combining the number of nanobodies in one complex structure, in essence increasing the valency⁴⁰¹. To take it one step further, a nanoparticle can conjugate hundreds of nanobodies on its surface, thereby increasing the specificity of nanomedicine and enhancing therapeutic efficacy. To this end, nanobody functionalized liposomes⁴⁰⁵, micelles⁴⁰⁶, and albumin-based nanomedicine against EGFR were generated⁴⁰⁷, in addition to polymersomes targeted to HER2¹³¹.

In nanomedicine, targeting moieties can increase target cell specificity, reduce aspecific cell binding and potentially be internalized via receptor mediated endocytosis^{151,408,409}. The internalization of HER2-targeted Doxil liposomes has been shown with both monoclonal antibodies and antibody fragments as targeting ligands^{52,68}. After successful extravasation, ligand binding of tumor antigens will prevent diffusion back into circulation, which over time can lead to a higher concentration in the tumor. By using a different route of approach, targeted nanomedicines can circumvent drug resistance⁴¹⁰. In addition, intrinsically active targeting moieties can have synergistic or additive effects in combination with drug loaded nanomedicine¹³⁰. Targeted nanomedicines can use any overexpressed cancer cell surface marker as a potential target, although many such markers are not exclusively expressed by tumor cells²⁷⁶. Targeted nanomedicines have been generated using all types of targeting moieties, such as monoclonal antibodies⁴⁸, antibody fragments, peptides⁴¹¹, aptamers⁴¹², and other small targeting molecules. When using targeting moieties, the nanomedicine first needs to accumulate in the tumor tissue via the EPR effect, before tumor-specific targeting can take place. Ideally, targeting ligands also improve cellular internalization via endocytosis, and commonly used receptors include folate^{65,413}, and transferrin^{414,415}. Receptors overexpressed on angiogenic endothelial cells can be targeted to reduce blood supply and starve the tumor of nutrients. Among the most common targets are integrins, targeted by derivatives of the oligopeptide RGD and NGR⁴¹⁶. In the last year, a number of very interesting pre-clinical studies have been performed which gives an insight into the future of targeted nanomedicine. For example, ICAM-1 targeted immunoliposomes were used to target triple-negative breast cancer and contained siRNA targeting lipocalin 2 (breast cancer progression promoter) to significantly reduce angiogenesis *in vivo*⁴¹⁷. One of the first clinically tested targeted nanomedicine, BIND-014, a docetaxel containing polymer-based nanomedicine targeted against PSMA, recently entered Phase II clinical trials

for the treatment of metastatic castration-resistant prostate cancer^{63,279}. The targeting of this nanomedicine is based on a small hydrophilic molecule, S,S-2-(3-[1-carboxy-5-amino-pentyl]-ureido)-pentanedioic acid, capable of targeting PSMA with high specificity²⁸⁰. Another study showed the use of CD44, identified as a cancer stem cell marker, as a targeting moiety for Doxil⁴¹⁸. In addition to passive targeted doxorubicin formulations, targeted liposomes with single chain variable fragments against HER2 (MM-302) in combination with trastuzumab are currently being tested in a Phase II clinical trial against locally advanced/metastatic breast cancer⁶¹. In one study, glutathione-targeted liposomes were designed to cross the blood brain barrier where encapsulated nanobodies against amyloid beta could have its effect as treatment against neurodegenerative disorders such as Alzheimer's⁴¹⁹. These studies indicate that the optimal combination of nanoparticle formulation and targeting ligand can facilitate improved drug delivery and enhance therapeutic efficacy.

Whether the use of targeting ligands translates into effective therapeutic or diagnostic tools is dependent on several factors. Firstly, the ratio between antigen expression in the target tissue compared to non-target tissues determines the signal-to-background ratio in imaging and the amount of adverse effects in targeted nanomedicines. Secondly, the availability of the receptor at the target site, which depends on receptor density, degree of shedding and the rate of internalization, determines the degree of binding of targeted nanomedicines. Thirdly, the expression of the receptors might not be homogeneous throughout the tumor and may change over time, both naturally or as a reaction to receptor binding drugs. Due to complications with conventional antibodies, smaller antibody fragments are often chosen for either targeting of nanoparticles or imaging. In this thesis, we have generated heavy-chain antibodies against MUC1, which contain a human variable fragment to facilitate clinical translation at a later stage (Chapter 2). MUC1 is overexpressed in breast and ovarian cancer^{198,200}, and is associated with metastatic potential and poor prognosis²⁰². The generated antibodies showed increased avidity to MUC1 expressing cell lines and can be used as a novel targeting moiety for nanomedicine. In addition, we developed a PMSA-specific imaging tracer by conjugating a nanobody with indium-111 (Chapter 3). In this instance, the composition of the nanobody with the radionuclide was determining the biodistribution and modifications had to be made to optimize functionality. The nanobodies used have much shorter circulation times compared to formerly used monoclonal antibodies. The small size of nanobodies does increase the retention in the kidneys, due to glomerular filtration or trapping of metabolites in the lysosomes of renal tubular cells. The aspecific uptake in the kidneys might be problematic for therapeutic and imaging purposes, since it can cause toxicity in the kidney or interfere with visualization of small tumor lesions in the vicinity. The nanobody described in Chapter 3 was targeted against PSMA and produced using a His-tag, which showed high binding to PSMA-expressing PC-310 tumors. Co-injection

with gelofusin and lysine efficiently reduced renal uptake, as described elsewhere²³⁷. The His-tag can also increase renal uptake of radiolabeled nanobodies¹¹⁷, which led to the choice of a SUMO3 expression vector which can be used to produce proteins with minimal additions to its original amino acid sequence. This enabled the production of nanobodies with a C-terminal cysteine to facilitate conjugation to indium-111. The resulting radionuclide-nanobody conjugates showed similar binding to PSMA-expressing tumors compared to His-tag produced nanobodies, and renal uptake was reduced to 3% injected dose per gram tissue at 4 h. These results show that nanobodies can be made that are ideal for imaging purposes, by reducing renal uptake as much as possible, and opening the way to therapeutic applications with these nanobodies.

Further, to make a direct comparison between targeted and non-targeted liposomes, we investigated cancer cell binding, tumor accumulation, and efficacy of both formulations (Chapter 4). PSMA was chosen as a target, which is abundantly present on most prostate cancer cells. After conjugation of the PSMA-specific nanobodies to liposomes, binding was tested using flow cytometry and *in vivo* localization studies using SPECT/CT imaging. The liposomes were highly specific *in vitro*, yet seemed to lose their advantage to non-targeted liposomes *in vivo* when patient-derived xenografts were used. It has been suggested that patient-derived xenografts develop a more organized and less permeable tumor vasculature, comparable to clinical tumors, than cell line xenografts⁴²⁰. PSMA-positive cell line xenografts showed accumulation comparable to the results found *in vitro* with flow cytometry, although PSMA-positive patient-derived xenografts did not show an enhanced accumulation of targeted liposomes. To determine cytotoxicity, liposomes were loaded with doxorubicin and used for *in vitro* cytotoxicity experiments and an *in vivo* efficacy study. *In vitro* cytotoxicity showed that EC50 values were enhanced in PSMA-positive cell lines. The efficacy study showed that tumor inhibition was not significantly different between targeted and non-targeted liposomes in both PSMA-positive and negative xenografts. To find a possible explanation for the lack of efficacy of targeted liposomes, we performed reflectance microscopy on whole tumor xenografts injected with PSMA-targeted liposomes. We observed that while some liposomes did extravasate from tumor vessels, the majority remained confined in and around the tumor vessels. In addition, the coverage of liposomes after diffusion was extremely heterogenous, and several areas showed no liposomal presence. The tumor morphology is clearly a restrictive factor and it is plausible that the vasculature might not have gaps with a size suitable for liposomal extravasation. Additionally, liposomes that extravasated from the tumor vasculature may have been stopped by the first layer of antigen-positive cells, the so-called binding barrier effect^{207,421}. While these experiments show that the use of targeted liposomes clearly enhances specificity and is advantageous over free drug, several issues such as effective biodistribution and bioavailability remain to be addressed and future studies should aim to further clarify these issues.

THE EPR EFFECT, AN ONGOING DEBATE

The EPR effect describes the accumulation of macromolecules in tumors¹⁴², and has been one of the major contributors to the success of nanomedicines in the clinic. Long-circulating molecules have a better chance of using the leaky tumor vasculature described by the EPR effect, hence nanomedicine research initially focused on more stable formulations. Clinical trials with liposomal doxorubicin have shown that the EPR effect is present in patients, although the accumulation of nanomedicine is dependent on the formulation of the nanomedicine and the tumor type being treated⁴²². Nanoparticle extravasation relies on the presence of gaps in the endothelial layer, and tumors have an increased number of leaky cell-to-cell junctions due to an increased expression of angiogenic factors during the transition into the vascular phase of tumor growth^{146,423}. Recently, a dynamic phenomenon has been characterized where vascular bursts take place which eject fluid into the interstitial space of tumors⁴²⁴. Together with the susceptibility of the tumor vasculature to permeability enhancing substances and external stimuli, it shows that blood vessels of the tumor are highly dynamic. Unfortunately, leakage from vessels is slow and nanomedicine can be cleared during circulation, which is one of the reasons that some nanomedicines do not find their way into the clinic²⁸⁴.

Efficacy of anticancer nanomedicines is often constrained by impaired blood flow, restricted extravasation from the blood vessels, and limited intratumoral penetration. These factors are dependent on the type and pathological state of the cancer, and patient-specific factors, including previous antitumor treatment⁴²⁵. The heterogeneous vasculature in the tumors causes nutrient poor and rich regions⁴²⁶, where tumor cells are packed closely around blood vessels, which inhibits drug penetration into the tumor⁴²⁷. Furthermore, the high interstitial fluid pressure created by a poor and heterogeneous perfusion, and the absence of a proper lymphatic drainage system, complicates penetration deeper into the tumor⁴²⁸. Extracellular matrix components, such as collagen⁴²⁹, glycoprotein, proteoglycan, elastin, and hyaluronan, and fast proliferating tumor cells can contribute to a high tumor density, which restricts perfusion and penetration of nanomedicine⁴³⁰. The extracellular matrix is a major contributor to the heterogeneity within the tumor through upregulated secretion of matrix metalloproteinases, collagen fibers, and hyaluronan^{151,431}. In contrast to liposomes, smaller nanoparticles are confronted with a lesser degree of restrictions from the tumor matrix and are given the chance to penetrate deeply within the tumor tissue⁴³², although these smaller particles are more susceptible to clearance. To enable larger nanomedicine to penetrate the tumor, it is possible to alleviate solid stress by targeting stromal cells and thus priming the tumor for drug delivery^{433,434}. The blood flow in tumor vessels can be normalized with vasodilators, such as nitroglycerin, that have reported clinical benefits⁴³⁵. Normalization of the tumor vasculature is predominantly advantageous for smaller nanomedicine,

since normalized vessels tend to decrease the size of fenestrations⁴³⁶. Extravasation from tumor blood vessels can be enhanced with a large number of strategies, including sonoporation⁴³⁷, exogenous VEGF⁴³⁸, TNF⁴³⁹, and hyperthermia¹⁸². Hyperthermia can be applied relatively easily on superficial tumors and it has been shown to increase extravasation of liposomes specifically from tumor vessels¹⁸². Developments with high intensity focused ultrasound (HIFU) to heat the tumor have been effective and can reduce off-target effects by heating the tumor region more specifically⁴⁴⁰. Despite these strategies, the EPR effect remains a heterogeneous and rate-limiting step in the successful application of nanomedicines⁴⁴¹.

Due to the variable success rate of nanomedicines, we wanted to investigate the restrictions of the EPR effect on liposomal accumulation in tumors (Chapter 5). We tried to eliminate variations in liposomal formulation by using stable long-circulating liposomes similar to clinically used Doxil. Tumor size was kept comparable between tumor types, since it is known that small tumors lack the necessary vascular system and large tumors risk the development of hypoxic or necrotic cores. We observed that tumor accumulation can range from < 2% to > 10% injected dose per gram, which in addition to a heterogeneous uptake, can lead to very different clinical outcomes. Further investigations into morphological parameters, such as blood vessel density and hypoxia, did not result in significant correlations, although it was observed that liposomal uptake correlates with tumor growth. Others have shown that mean vessel density strongly correlates with liposomal accumulation³⁰⁸, but our study suggests that the EPR effect is most likely regulated by a combination of morphological parameters, which determine the degree of accumulation and distribution of nanomedicine within the tumor.

The EPR effect has been proven to be a major bottleneck for drug delivery, and therefore the inclusion of imaging modalities remains crucial for determining the true accumulation and distribution of liposomes within the patient and tumor, and to elucidate the presence and degree of EPR. As reviewed recently, radiolabeling nanomedicines to determine drug distribution is relatively easy and can be achieved with a number of radionuclides⁴⁴². With the help of SPECT imaging of indium-111, liposomal distribution has been investigated and shows large differences in tumor uptake, confirming the heterogeneous nature of the EPR effect in different tumors²⁹⁹.

ENHANCING THE EPR EFFECT WITH MILD HYPERTHERMIA

The EPR effect can be very restrictive in a number of tumor types, which often results in rejection of nanomedicine as a viable therapeutic candidate. To this end, a number of approaches have been evaluated to enhance permeability, extravasation or intracellular drug uptake⁴⁴³. To enhance liposomal biodistribution, liposomal formulations with

increased stability were developed, which however impeded content release. To circumvent this issue, liposomes sensitive to pH variations and other environmental factors such as levels of reducing agents or enzymes have been developed, which enable drug release upon uptake by cancer cells^{444,445}. In contrast to environmental stimuli, external triggers can be used to facilitate drug release, such as photoactivation⁴⁴⁶, ultrasound⁴⁴⁷, and hyperthermia^{448,449}. Here we will focus on hyperthermia as a tool to increase tumor vessel permeability and trigger drug release from thermosensitive liposomes. In Chapter 4, hyperthermia was used to increase permeability of the tumor vasculature and enhance liposomal extravasation into the tumor interstitium. This approach proved to be quite successful, increasing the accumulation of targeted liposomes in the tumor more than three-fold compared to their non-treated counterparts.

The main issue with most external stimuli is related to the location of the tumor, and as can be expected, most of these applications have a limited tissue penetration depth. Even when using HIFU, deep seated neoplastic tissues remain difficult to reach. This is also true for metastatic disease, which have small lesions spread around the body for which detection methods remain to be elucidated. Thermosensitive liposomes have shown enhanced tumor accumulation after hyperthermia application in sarcoma-bearing cats³⁴⁷, although it has been suggested that redistribution into the circulation and premature drug release remain issues that need to be solved⁴⁵⁰. The addition of targeting moieties, against endothelial and tumor cells, to thermosensitive nanomedicine can be used to increase accumulation in the tumor^{451,452}.

To circumvent some of the limitations of the EPR effect, such as restricted extravasation from tumor vessels, nanoparticles have been developed with triggered release capabilities. Stability and manufacturing consistency remain issues that impede rapid clinical applications, although more effective nanomedicines for triggered drug delivery are being developed^{453,454}. The application of mild hyperthermia to trigger release of drugs from thermosensitive formulations has shown moderate success and has advanced to clinical trials⁴⁵⁵. Chapter 6 shows the combination of mild hyperthermia and thermosensitive liposomes on two morphologically different murine tumors, B16 melanoma and BFS-1 sarcoma, which show high and low uptake of thermosensitive liposomes, respectively³²². Thermosensitive liposomes released all drug at 42°C and achieved high cytotoxicity compared to liposomes at 37°C, and it was also observed that hyperthermia enabled a faster cellular uptake. An interesting observation was that the hyperthermia induced permeability is transient³⁴³, since preheating followed by 4 h incubation at 37°C did not improve uptake of doxorubicin. It has been reported that it is possible to achieve more permanent permeability changes, although a higher temperature has to be used³⁵⁸. Between the two tumor types used, the B16 tumors showed a higher uptake of liposomes and intratumoral doxorubicin. These tumors have a higher growth rate, a lower cell density and almost no collagen IV matrix. This may

have facilitated an enhanced tumor penetration and hence an increased therapeutic efficacy³⁶⁴. This study shows that despite major advances in liposome formulations and the application of external stimuli, such as hyperthermia, the morphology and heterogeneity of the tumor are still major factors determining accumulation and therapeutic efficacy of liposomes.

CONCLUDING REMARKS

The increased effort in the development of nanomedicines, including antibody conjugates, as potential tools for diagnosis and therapy of cancer, has led to an increased number of clinical trials and FDA approved drugs. The majority of these approaches rely on passive accumulation of the nanomedicine via the EPR effect, although ligand-mediated targeted nanomedicine is increasingly being investigated.

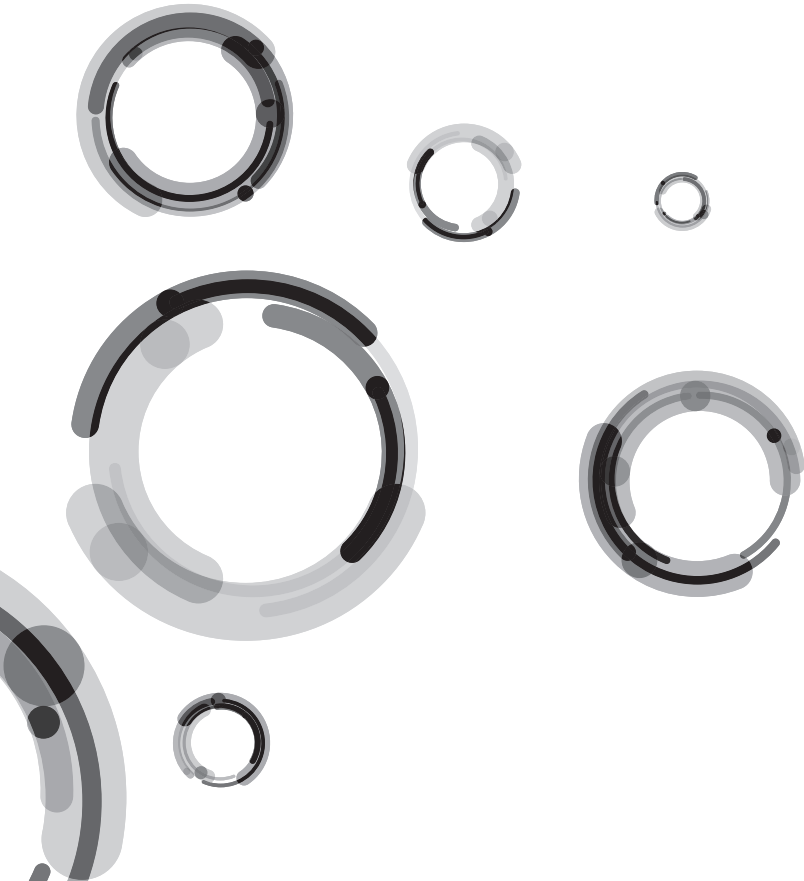
The biological drivers that disqualify the use of nanomedicine in the clinic, due to low efficaciousness or side effects, are multifactorial and often difficult to elucidate. Moreover, these factors are heavily tumor and patient dependent, and correlate to the stage of tumor development, presence of metastasis, and previous treatment received. This disease heterogeneity, in a highly variable patient population, makes it challenging to design effective nanomedicine and build the case towards clinically approved drugs.

As shown in this thesis, drug-free nanoparticles can be used in combination with imaging to predict therapeutic benefit in various models. This can be extrapolated to the clinical setting, wherein patients prior to treatment get a low dose of empty nanoparticles, to determine the biodistribution and observe possible complications due to aspecific targeting to other organs or resistance in the tumor.

With nanomedicine research, insight into biological barriers, pharmacokinetics, (cyto)toxicity, and tumor biology is ever expanding and in combination with sophisticated design strategies, targeting modalities and powerful tools in imaging, enables us to study biodistribution in depth. Eventually, this will lead to the required level of insight to be able to circumvent (patho)physiological barriers and cope with tumor/patient heterogeneity to generate truly personalized treatments.



References



1. Weinberg, R. A. How cancer arises. *Sci Am* 1996, 275, 62-70.
2. Wyld, L.; Audisio, R. A.; Poston, G. J. The evolution of cancer surgery and future perspectives. *Nat Rev Clin Oncol* 2015, 12, 115-24.
3. Bernier, J.; Hall, E. J.; Giaccia, A. Radiation oncology: a century of achievements. *Nat Rev Cancer* 2004, 4, 737-47.
4. Chabner, B. A.; Roberts, T. G., Jr. Timeline: Chemotherapy and the war on cancer. *Nat Rev Cancer* 2005, 5, 65-72.
5. NCI. Doxorubicin Hydrochloride. <http://www.cancer.gov/about-cancer/treatment/drugs/doxorubicinhydrochloride>.
6. Arcamone, F.; Cassinelli, G.; Fantini, G.; Grein, A.; Orezzi, P.; Pol, C.; Spalla, C. Adriamycin, 14-hydroxydaunomycin, a new antitumor antibiotic from *S. peucetius* var. *caesius*. *Biotechnol Bioeng* 1969, 11, 1101-10.
7. Schwartz, J.; Domchek, S. M.; Hwang, W. T.; Fox, K. Evaluation of anemia, neutropenia and skin toxicities in standard or dose-dense doxorubicin/cyclophosphamide (AC)-paclitaxel or docetaxel adjuvant chemotherapy in breast cancer. *Ann Oncol* 2005, 16, 247-52.
8. Minotti, G.; Cairo, G.; Monti, E. Role of iron in anthracycline cardiotoxicity: new tunes for an old song? *FASEB J* 1999, 13, 199-212.
9. Doroshow, J. H. Effect of anthracycline antibiotics on oxygen radical formation in rat heart. *Cancer Res* 1983, 43, 460-72.
10. Singal, P. K.; Segstro, R. J.; Singh, R. P.; Kutryk, M. J. Changes in lysosomal morphology and enzyme activities during the development of adriamycin-induced cardiomyopathy. *Can J Cardiol* 1985, 1, 139-47.
11. Olson, R. D.; MacDonald, J. S.; vanBoxtel, C. J.; Boerth, R. C.; Harbison, R. D.; Slonim, A. E.; Freeman, R. W.; Oates, J. A. Regulatory role of glutathione and soluble sulfhydryl groups in the toxicity of adriamycin. *J Pharmacol Exp Ther* 1980, 215, 450-4.
12. Arena, E.; D'Alessandro, N.; Dusonchet, L.; Geraci, M.; Rausa, L.; Sanguedolce, R. Repair kinetics of DNA, RNA and proteins in the tissues of mice treated with doxorubicin. *Arzneimittelforschung* 1979, 29, 901-2.
13. Takemura, G.; Fujiwara, H. Doxorubicin-induced cardiomyopathy from the cardiotoxic mechanisms to management. *Prog Cardiovasc Dis* 2007, 49, 330-52.
14. Bangham, A. D.; Horne, R. W. Negative Staining of Phospholipids and Their Structural Modification by Surface-Active Agents as Observed in the Electron Microscope. *J Mol Biol* 1964, 8, 660-8.
15. Bangham, A. D.; Standish, M. M.; Watkins, J. C. Diffusion of univalent ions across the lamellae of swollen phospholipids. *J Mol Biol* 1965, 13, 238-52.
16. Papahadjopoulos, D.; Watkins, J. C. Phospholipid model membranes. II. Permeability properties of hydrated liquid crystals. *Biochim Biophys Acta* 1967, 135, 639-52.
17. Lasic, D. D. The mechanism of vesicle formation. *Biochem J* 1988, 256, 1-11.
18. Deamer, D. W. From "banghasomes" to liposomes: a memoir of Alec Bangham, 1921-2010. *FASEB J* 2010, 24, 1308-10.
19. Gregoriadis, G.; Ryman, B. E. Liposomes as carriers of enzymes or drugs: a new approach to the treatment of storage diseases. *Biochem J* 1971, 124, 58P.
20. Gregoriadis, G. Drug entrapment in liposomes. *FEBS Lett* 1973, 36, 292-6.
21. Gulati, M.; Grover, M.; Singh, S.; Singh, M. Lipophilic drug derivatives in liposomes. *Int J Pharm* 1998, 165, 129-168.

22. Hoekstra, D.; Scherphof, G. Effect of fetal calf serum and serum protein fractions on the uptake of liposomal phosphatidylcholine by rat hepatocytes in primary monolayer culture. *Biochim Biophys Acta* 1979, 551, 109-21.
23. Scherphof, G. L.; Dijkstra, J.; Spanjer, H. H.; Derksen, J. T.; Roerdink, F. H. Uptake and intracellular processing of targeted and nontargeted liposomes by rat Kupffer cells in vivo and in vitro. *Ann NY Acad Sci* 1985, 446, 368-84.
24. Drummond, D. C.; Meyer, O.; Hong, K.; Kirpotin, D. B.; Papahadjopoulos, D. Optimizing liposomes for delivery of chemotherapeutic agents to solid tumors. *Pharmacol Rev* 1999, 51, 691-743.
25. Allen, T. M.; Hansen, C.; Martin, F.; Redemann, C.; Yau-Young, A. Liposomes containing synthetic lipid derivatives of poly(ethylene glycol) show prolonged circulation half-lives in vivo. *Biochim Biophys Acta* 1991, 1066, 29-36.
26. Allen, T. M.; Cleland, L. G. Serum-induced leakage of liposome contents. *Biochim Biophys Acta* 1980, 597, 418-26.
27. Damen, J.; Regts, J.; Scherphof, G. Transfer and exchange of phospholipid between small unilamellar liposomes and rat plasma high density lipoproteins. Dependence on cholesterol content and phospholipid composition. *Biochim Biophys Acta* 1981, 665, 538-45.
28. Cullis, P. R. Lateral diffusion rates of phosphatidylcholine in vesicle membranes: effects of cholesterol and hydrocarbon phase transitions. *FEBS Lett* 1976, 70, 223-8.
29. McIntosh, T. J. The effect of cholesterol on the structure of phosphatidylcholine bilayers. *Biochim Biophys Acta* 1978, 513, 43-58.
30. Senior, J.; Gregoriadis, G. Stability of small unilamellar liposomes in serum and clearance from the circulation: the effect of the phospholipid and cholesterol components. *Life Sci* 1982, 30, 2123-36.
31. Bartoli, M. H.; Boitard, M.; Fessi, H.; Beriel, H.; Devissaguet, J. P.; Picot, F.; Puisieux, F. In vitro and in vivo antitumoral activity of free, and encapsulated taxol. *J Microencapsul* 1990, 7, 191-7.
32. Cabanes, A.; Briggs, K. E.; Gokhale, P. C.; Treat, J. A.; Rahman, A. Comparative in vivo studies with paclitaxel and liposome-encapsulated paclitaxel. *Int J Oncol* 1998, 12, 1035-40.
33. Bolotin, E. M.; Cohen, R.; Bar, L. K.; Emanuel, N.; Ninio, S.; Barenholz, Y.; Lasic, D. D. Ammonium Sulfate Gradients for Efficient and Stable Remote Loading of Amphiphathic Weak Bases into Liposomes and Ligandoliposomes. *J Liposome Res* 1994, 4, 455-479.
34. Mayer, L. D.; Tai, L. C.; Bally, M. B.; Mitilenes, G. N.; Ginsberg, R. S.; Cullis, P. R. Characterization of liposomal systems containing doxorubicin entrapped in response to pH gradients. *Biochim Biophys Acta* 1990, 1025, 143-51.
35. Abraham, S. A.; Waterhouse, D. N.; Mayer, L. D.; Cullis, P. R.; Madden, T. D.; Bally, M. B. The liposomal formulation of doxorubicin. *Methods Enzymol* 2005, 391, 71-97.
36. Gabizon, A.; Peretz, T.; Sulkes, A.; Amselem, S.; Ben-Yosef, R.; Ben-Baruch, N.; Catane, R.; Biran, S.; Barenholz, Y. Systemic administration of doxorubicin-containing liposomes in cancer patients: a phase I study. *Eur J Cancer Clin Oncol* 1989, 25, 1795-803.
37. Gabizon, A.; Catane, R.; Uziely, B.; Kaufman, B.; Safra, T.; Cohen, R.; Martin, F.; Huang, A.; Barenholz, Y. Prolonged circulation time and enhanced accumulation in malignant exudates of doxorubicin encapsulated in polyethylene-glycol coated liposomes. *Cancer Res* 1994, 54, 987-92.
38. NCI. FDA Approval for Doxorubicin Hydrochloride Liposome. <http://www.cancer.gov/about-cancer/treatment/drugs/fda-doxorubicin-HCL-liposome>.
39. An, B.; Lin, Y. S.; Brodsky, B. Collagen interactions: Drug design and delivery. *Adv Drug Deliv Rev* 2016, 97, 69-84.

40. Murphy, E. A.; Majeti, B. K.; Barnes, L. A.; Makale, M.; Weis, S. M.; Lutu-Fuga, K.; Wrasidlo, W.; Cheresch, D. A. Nanoparticle-mediated drug delivery to tumor vasculature suppresses metastasis. *Proc Natl Acad Sci U.S.A* 2008, 105, 9343-8.
41. Yoncheva, K.; Momekov, G. Antiangiogenic anticancer strategy based on nanoparticulate systems. *Expert Opin Drug Deliv* 2011, 8, 1041-56.
42. Accardo, A.; Aloj, L.; Aurilio, M.; Morelli, G.; Tesauro, D. Receptor binding peptides for target-selective delivery of nanoparticles encapsulated drugs. *Int J Nanomedicine* 2014, 9, 1537-57.
43. Hansen, C. B.; Kao, G. Y.; Moase, E. H.; Zalipsky, S.; Allen, T. M. Attachment of antibodies to sterically stabilized liposomes: evaluation, comparison and optimization of coupling procedures. *Biochim Biophys Acta* 1995, 1239, 133-44.
44. Blume, G.; Cevc, G.; Crommelin, M. D.; Bakker-Woudenberg, I. A.; Klufft, C.; Storm, G. Specific targeting with poly(ethylene glycol)-modified liposomes: coupling of homing devices to the ends of the polymeric chains combines effective target binding with long circulation times. *Biochim Biophys Acta* 1993, 1149, 180-4.
45. Iden, D. L.; Allen, T. M. In vitro and in vivo comparison of immunoliposomes made by conventional coupling techniques with those made by a new post-insertion approach. *Biochim Biophys Acta* 2001, 1513, 207-16.
46. Li, W. M.; Mayer, L. D.; Bally, M. B. Prevention of antibody-mediated elimination of ligand-targeted liposomes by using poly(ethylene glycol)-modified lipids. *J Pharmacol Exp Ther* 2002, 300, 976-83.
47. Heath, T. D.; Fraley, R. T.; Papahadjopoulos, D. Antibody targeting of liposomes: cell specificity obtained by conjugation of F(ab')₂ to vesicle surface. *Science* 1980, 210, 539-41.
48. Heath, T. D.; Montgomery, J. A.; Piper, J. R.; Papahadjopoulos, D. Antibody-targeted liposomes: increase in specific toxicity of methotrexate-gamma-aspartate. *Proc Natl Acad Sci U.S.A* 1983, 80, 1377-81.
49. Hosokawa, S.; Tagawa, T.; Niki, H.; Hirakawa, Y.; Nohga, K.; Nagaike, K. Efficacy of immunoliposomes on cancer models in a cell-surface-antigen-density-dependent manner. *Br J Cancer* 2003, 89, 1545-51.
50. Allen, T. M. Ligand-targeted therapeutics in anticancer therapy. *Nat Rev Cancer* 2002, 2, 750-63.
51. Drummond, D. C.; Hong, K.; Park, J. W.; Benz, C. C.; Kirpotin, D. B. Liposome targeting to tumors using vitamin and growth factor receptors. *Vitam Horm* 2000, 60, 285-332.
52. Kirpotin, D. B.; Drummond, D. C.; Shao, Y.; Shalaby, M. R.; Hong, K.; Nielsen, U. B.; Marks, J. D.; Benz, C. C.; Park, J. W. Antibody targeting of long-circulating lipidic nanoparticles does not increase tumor localization but does increase internalization in animal models. *Cancer Res* 2006, 66, 6732-40.
53. Allen, T. M.; Sapro, P.; Moase, E.; Moreira, J.; Iden, D. Adventures in targeting. *J Liposome Res* 2002, 12, 5-12.
54. Kontermann, R. E. Immunoliposomes for cancer therapy. *Curr Opin Mol Ther* 2006, 8, 39-45.
55. Nielsen, U. B.; Kirpotin, D. B.; Pickering, E. M.; Hong, K.; Park, J. W.; Refaat Shalaby, M.; Shao, Y.; Benz, C. C.; Marks, J. D. Therapeutic efficacy of anti-ErbB2 immunoliposomes targeted by a phage antibody selected for cellular endocytosis. *Biochim Biophys Acta* 2002, 1591, 109-118.
56. Sapro, P.; Allen, T. M. Internalizing antibodies are necessary for improved therapeutic efficacy of antibody-targeted liposomal drugs. *Cancer Res* 2002, 62, 7190-4.
57. Anselmo, A. C.; Mitragotri, S. Nanoparticles in the clinic. *Bioeng Transl Med* 2016, 1, 10-29.

58. Silverman, J. A.; Deitcher, S. R. Marqibo(R) (vincristine sulfate liposome injection) improves the pharmacokinetics and pharmacodynamics of vincristine. *Cancer Chemother Pharmacol* 2013, 71, 555-64.
59. Carnevale, J.; Ko, A. H. MM-398 (nanoliposomal irinotecan): emergence of a novel therapy for the treatment of advanced pancreatic cancer. *Future Oncol* 2016, 12, 453-64.
60. Feldman, E. J.; Lancet, J. E.; Koltitz, J. E.; Ritchie, E. K.; Roboz, G. J.; List, A. F.; Allen, S. L.; Asatiani, E.; Mayer, L. D.; Swenson, C.; Louie, A. C. First-in-man study of CPX-351: a liposomal carrier containing cytarabine and daunorubicin in a fixed 5:1 molar ratio for the treatment of relapsed and refractory acute myeloid leukemia. *J Clin Oncol* 2011, 29, 979-85.
61. Miller, K.; Cortes, J.; Hurvitz, S. A.; Krop, I. E.; Tripathy, D.; Verma, S.; Riahi, K.; Reynolds, J. G.; Wickham, T. J.; Molnar, I.; Yardley, D. A. HERMIONE: a randomized Phase 2 trial of MM-302 plus trastuzumab versus chemotherapy of physician's choice plus trastuzumab in patients with previously treated, anthracycline-naïve, HER2-positive, locally advanced/metastatic breast cancer. *BMC Cancer* 2016, 16, 352.
62. Senzer, N.; Nemunaitis, J.; Nemunaitis, D.; Bedell, C.; Edelman, G.; Barve, M.; Nunan, R.; Pirollo, K. F.; Rait, A.; Chang, E. H. Phase I study of a systemically delivered p53 nanoparticle in advanced solid tumors. *Mol Ther* 2013, 21, 1096-103.
63. Hrkach, J.; Von Hoff, D.; Mukkaram Ali, M.; Andrianova, E.; Auer, J.; Campbell, T.; De Witt, D.; Figa, M.; Figueiredo, M.; Horhota, A.; Low, S.; McDonnell, K.; Peeke, E.; Retnarajan, B.; Sabnis, A.; Schnipper, E.; Song, J. J.; Song, Y. H.; Summa, J.; Tompsett, D.; Troiano, G.; Van Geen Hoven, T.; Wright, J.; LoRusso, P.; Kantoff, P. W.; Bander, N. H.; Sweeney, C.; Farokhzad, O. C.; Langer, R.; Zale, S. Preclinical development and clinical translation of a PSMA-targeted docetaxel nanoparticle with a differentiated pharmacological profile. *Sci Transl Med* 2012, 4.
64. Von Hoff, D. D.; Mita, M. M.; Ramanathan, R. K.; Weiss, G. J.; Mita, A. C.; LoRusso, P. M.; Burris, H. A., 3rd; Hart, L. L.; Low, S. C.; Parsons, D. M.; Zale, S. E.; Summa, J. M.; Youssoufian, H.; Sachdev, J. C. Phase I Study of PSMA-Targeted Docetaxel-Containing Nanoparticle BIND-014 in Patients with Advanced Solid Tumors. *Clin Cancer Res* 2016, 22, 3157-63.
65. van Dam, G. M.; Themelis, G.; Crane, L. M.; Harlaar, N. J.; Pleijhuis, R. G.; Kelder, W.; Sarantopoulos, A.; de Jong, J. S.; Arts, H. J.; van der Zee, A. G.; Bart, J.; Low, P. S.; Ntziachristos, V. Intraoperative tumor-specific fluorescence imaging in ovarian cancer by folate receptor-alpha targeting: first in-human results. *Nature Med* 2011, 17, 1315-9.
66. Singh, S. R.; Grossniklaus, H. E.; Kang, S. J.; Edelhauser, H. F.; Ambati, B. K.; Kompella, U. B. Intravenous transferrin, RGD peptide and dual-targeted nanoparticles enhance anti-VEGF intra-receptor gene delivery to laser-induced CNV. *Gene Ther* 2009, 16, 645-59.
67. Lopes de Menezes, D. E.; Pilarski, L. M.; Allen, T. M. In vitro and in vivo targeting of immunoliposomal doxorubicin to human B-cell lymphoma. *Cancer Res* 1998, 58, 3320-30.
68. Park, J. W.; Hong, K.; Kirpotin, D. B.; Colbern, G.; Shalaby, R.; Baselga, J.; Shao, Y.; Nielsen, U. B.; Marks, J. D.; Moore, D.; Papahadjopoulos, D.; Benz, C. C. Anti-HER2 immunoliposomes: enhanced efficacy attributable to targeted delivery. *Clin Cancer Res* 2002, 8, 1172-81.
69. Vingerhoeds, M. H.; Steerenberg, P. A.; Hendriks, J. J.; Dekker, L. C.; Van Hoesel, Q. G.; Crommelin, D. J.; Storm, G. Immunoliposome-mediated targeting of doxorubicin to human ovarian carcinoma in vitro and in vivo. *Br J Cancer* 1996, 74, 1023-9.
70. Goren, D.; Horowitz, A. T.; Zalipsky, S.; Woodle, M. C.; Yarden, Y.; Gabizon, A. Targeting of stealth liposomes to erbB-2 (Her/2) receptor: in vitro and in vivo studies. *Br J Cancer* 1996, 74, 1749-56.
71. Padlan, E. A. Anatomy of the antibody molecule. *Mol Immunol* 1994, 31, 169-217.

72. Cai, H. H. Therapeutic Monoclonal Antibodies Approved by FDA in 2015. *MOJ Immunol.* 2016, 3(2), 00087.
73. Sarma, V. R.; Silvertown, E. W.; Davies, D. R.; Terry, W. D. The three-dimensional structure at 6 Å resolution of a human gamma G1 immunoglobulin molecule. *J Biol Chem* 1971, 246, 3753-9.
74. Lipman, N. S.; Jackson, L. R.; Trudel, L. J.; Weis-Garcia, F. Monoclonal versus polyclonal antibodies: distinguishing characteristics, applications, and information resources. *ILAR J* 2005, 46, 258-68.
75. Kohler, G.; Milstein, C. Continuous cultures of fused cells secreting antibody of predefined specificity. *Nature* 1975, 256, 495-7.
76. Dillman, R. O.; Shawler, D. L.; McCallister, T. J.; Halpern, S. E. Human anti-mouse antibody response in cancer patients following single low-dose injections of radiolabeled murine monoclonal antibodies. *Cancer Biother* 1994, 9, 17-28.
77. Nelson, A. L. Antibody fragments: hope and hype. *MAbs* 2010, 2, 77-83.
78. Hamers-Casterman, C.; Atarhouch, T.; Muyldermans, S.; Robinson, G.; Hamers, C.; Songa, E. B.; Bendahman, N.; Hamers, R. Naturally occurring antibodies devoid of light chains. *Nature* 1993, 363, 446-8.
79. Wahner-Roedler, D. L.; Kyle, R. A. Heavy chain diseases. *Best Pract Res Clin Haematol* 2005, 18, 729-46.
80. Alexander, A.; Steinmetz, M.; Barritault, D.; Frangione, B.; Franklin, E. C.; Hood, L.; Buxbaum, J. N. gamma Heavy chain disease in man: cDNA sequence supports partial gene deletion model. *Proc Natl Acad Sci U.S.A* 1982, 79, 3260-4.
81. Cogne, M.; Preud'homme, J. L.; Guglielmi, P. Immunoglobulin gene alterations in human heavy chain diseases. *Res Immunol* 1989, 140, 487-502.
82. Flajnik, M. F.; Kasahara, M. Origin and evolution of the adaptive immune system: genetic events and selective pressures. *Nat Rev Genet* 2010, 11, 47-59.
83. Blanc, M. R.; Anouassi, A.; Ahmed Abed, M.; Tsikis, G.; Canepa, S.; Labas, V.; Belghazi, M.; Bruneau, G. A one-step exclusion-binding procedure for the purification of functional heavy-chain and mammalian-type gamma-globulins from camelid sera. *Biotechnol Appl Biochem* 2009, 54, 207-12.
84. De Genst, E.; Silence, K.; Ghahroudi, M. A.; Decanniere, K.; Loris, R.; Kinne, J.; Wyns, L.; Muyldermans, S. Strong in vivo maturation compensates for structurally restricted H3 loops in antibody repertoires. *J Biol Chem* 2005, 280, 14114-21.
85. Nguyen, V. K.; Hamers, R.; Wyns, L.; Muyldermans, S. Camel heavy-chain antibodies: diverse germline V(H)H and specific mechanisms enlarge the antigen-binding repertoire. *EMBO J* 2000, 19, 921-30.
86. De Genst, E.; Saerens, D.; Muyldermans, S.; Conrath, K. Antibody repertoire development in camelids. *Dev Comp Immunol* 2006, 30, 187-98.
87. Achour, I.; Cavalier, P.; Tichit, M.; Bouchier, C.; Lafaye, P.; Rougeon, F. Tetrameric and homodimeric camelid IgGs originate from the same IgH locus. *J Immunol* 2008, 181, 2001-9.
88. Nguyen, V. K.; Hamers, R.; Wyns, L.; Muyldermans, S. Loss of splice consensus signal is responsible for the removal of the entire C(H)1 domain of the functional camel IGG2A heavy-chain antibodies. *Mol Immunol* 1999, 36, 515-24.
89. Janssens, R.; Dekker, S.; Hendriks, R. W.; Panayotou, G.; van Remoortere, A.; San, J. K.; Grosveld, F.; Drabek, D. Generation of heavy-chain-only antibodies in mice. *Proc Natl Acad Sci U.S.A* 2006, 103, 15130-5.

90. Nguyen, V. K.; Desmyter, A.; Muyldermans, S. Functional heavy-chain antibodies in Camelidae. *Adv Immunol* 2001, 79, 261-96.
91. Holliger, P.; Hudson, P. J. Engineered antibody fragments and the rise of single domains. *Nat Biotechnol* 2005, 23, 1126-36.
92. Hoogenboom, H. R. Selecting and screening recombinant antibody libraries. *Nat Biotechnol* 2005, 23, 1105-16.
93. Muyldermans, S.; Baral, T. N.; Retamozzo, V. C.; De Baetselier, P.; De Genst, E.; Kinne, J.; Leonhardt, H.; Magez, S.; Nguyen, V. K.; Revets, H.; Rothbauer, U.; Stijlemans, B.; Tillib, S.; Wernery, U.; Wyns, L.; Hassanzadeh-Ghassabeh, G.; Saerens, D. Camelid immunoglobulins and nanobody technology. *Vet Immunol Immunopathol* 2009, 128, 178-83.
94. Sundberg, E. J.; Mariuzza, R. A. Molecular recognition in antibody-antigen complexes. *Adv Protein Chem* 2002, 61, 119-60.
95. Chothia, C.; Novotny, J.; Brucoleri, R.; Karplus, M. Domain association in immunoglobulin molecules. The packing of variable domains. *J Mol Biol* 1985, 186, 651-63.
96. Vu, K. B.; Ghahroudi, M. A.; Wyns, L.; Muyldermans, S. Comparison of llama VH sequences from conventional and heavy chain antibodies. *Mol Immunol* 1997, 34, 1121-31.
97. Govaert, J.; Pellis, M.; Deschacht, N.; Vincke, C.; Conrath, K.; Muyldermans, S.; Saerens, D. Dual beneficial effect of interloop disulfide bond for single domain antibody fragments. *J Biol Chem* 2012, 287, 1970-9.
98. Muyldermans, S.; Atarhouch, T.; Saldanha, J.; Barbosa, J. A.; Hamers, R. Sequence and structure of VH domain from naturally occurring camel heavy chain immunoglobulins lacking light chains. *Protein Eng* 1994, 7, 1129-35.
99. Conrath, K. E.; Wernery, U.; Muyldermans, S.; Nguyen, V. K. Emergence and evolution of functional heavy-chain antibodies in Camelidae. *Dev Comp Immunol* 2003, 27, 87-103.
100. Desmyter, A.; Transue, T. R.; Ghahroudi, M. A.; Thi, M. H.; Poortmans, F.; Hamers, R.; Muyldermans, S.; Wyns, L. Crystal structure of a camel single-domain VH antibody fragment in complex with lysozyme. *Nat Struct Biol* 1996, 3, 803-11.
101. Transue, T. R.; De Genst, E.; Ghahroudi, M. A.; Wyns, L.; Muyldermans, S. Camel single-domain antibody inhibits enzyme by mimicking carbohydrate substrate. *Proteins* 1998, 32, 515-22.
102. De Genst, E.; Silence, K.; Decanniere, K.; Conrath, K.; Loris, R.; Kinne, J.; Muyldermans, S.; Wyns, L. Molecular basis for the preferential cleft recognition by dromedary heavy-chain antibodies. *Proc Natl Acad Sci U.S.A* 2006, 103, 4586-91.
103. Cortez-Retamozo, V.; Backmann, N.; Senter, P. D.; Wernery, U.; De Baetselier, P.; Muyldermans, S.; Revets, H. Efficient cancer therapy with a nanobody-based conjugate. *Cancer Res* 2004, 64, 2853-7.
104. Baral, T. N.; Magez, S.; Stijlemans, B.; Conrath, K.; Vanhollebeke, B.; Pays, E.; Muyldermans, S.; De Baetselier, P. Experimental therapy of African trypanosomiasis with a nanobody-conjugated human trypanolytic factor. *Nature Med* 2006, 12, 580-4.
105. Coppieters, K.; Dreier, T.; Silence, K.; de Haard, H.; Lauwereys, M.; Casteels, P.; Beirnaert, E.; Jonckheere, H.; Van de Wiele, C.; Staelens, L.; Hostens, J.; Revets, H.; Remaut, E.; Elewaut, D.; Rottiers, P. Formatted anti-tumor necrosis factor alpha VHH proteins derived from camelids show superior potency and targeting to inflamed joints in a murine model of collagen-induced arthritis. *Arthritis Rheum* 2006, 54, 1856-66.
106. Keyaerts, M.; Xavier, C.; Heemskerk, J.; Devoogdt, N.; Everaert, H.; Ackaert, C.; Vanhoeij, M.; Duhoux, F. P.; Gevaert, T.; Simon, P.; Schallier, D.; Fontaine, C.; Vaneycken, I.; Vanhove, C.; De

- Greve, J.; Lamote, J.; Caveliers, V.; Lahoutte, T. Phase I Study of ⁶⁸Ga-HER2-Nanobody for PET/CT Assessment of HER2 Expression in Breast Carcinoma. *J Nucl Med* 2016, 57, 27-33.
107. Bartunek, J.; Barbato, E.; Heyndrickx, G.; Vanderheyden, M.; Wijns, W.; Holz, J. B. Novel antiplatelet agents: ALX-0081, a Nanobody directed towards von Willebrand factor. *J Cardiovasc Transl Res* 2013, 6, 355-63.
108. Muyldermans, S. Nanobodies: natural single-domain antibodies. *Annu Rev Biochem* 2013, 82, 775-97.
109. Klarenbeek, A.; El Mazouari, K.; Desmyter, A.; Blanchetot, C.; Hultberg, A.; de Jonge, N.; Roovers, R. C.; Cambillau, C.; Spinelli, S.; Del-Favero, J.; Verrips, T.; de Haard, H. J.; Achour, I. Camelid Ig V genes reveal significant human homology not seen in therapeutic target genes, providing for a powerful therapeutic antibody platform. *MABs* 2015, 7, 693-706.
110. Holland, M. C.; Wurthner, J. U.; Morley, P. J.; Birchler, M. A.; Lambert, J.; Albayaty, M.; Serone, A. P.; Wilson, R.; Chen, Y.; Forrest, R. M.; Cordy, J. C.; Lipson, D. A.; Bayliffe, A. I. Autoantibodies to variable heavy (VH) chain Ig sequences in humans impact the safety and clinical pharmacology of a VH domain antibody antagonist of TNF-alpha receptor 1. *J Clin Immunol* 2013, 33, 1192-203.
111. Papadopoulos, K. P.; Isaacs, R.; Bilic, S.; Kentsch, K.; Huet, H. A.; Hofmann, M.; Rasco, D.; Kundamal, N.; Tang, Z.; Cooksey, J.; Mahipal, A. Unexpected hepatotoxicity in a phase I study of TAS266, a novel tetravalent agonistic Nanobody(R) targeting the DR5 receptor. *Cancer Chemother Pharmacol* 2015, 75, 887-95.
112. Cordy, J. C.; Morley, P. J.; Wright, T. J.; Birchler, M. A.; Lewis, A. P.; Emmins, R.; Chen, Y. Z.; Powley, W. M.; Bareille, P. J.; Wilson, R.; Tonkyn, J.; Bayliffe, A. I.; Lazaar, A. L. Specificity of human anti-variable heavy (VH) chain autoantibodies and impact on the design and clinical testing of a VH domain antibody antagonist of tumour necrosis factor-alpha receptor 1. *Clin Exp Immunol* 2015, 182, 139-48.
113. Vincke, C.; Loris, R.; Saerens, D.; Martinez-Rodriguez, S.; Muyldermans, S.; Conrath, K. General strategy to humanize a camelid single-domain antibody and identification of a universal humanized nanobody scaffold. *J Biol Chem* 2009, 284, 3273-84.
114. Van Bockstaele, F.; Holz, J. B.; Revets, H. The development of nanobodies for therapeutic applications. *Curr Opin Investig Drugs* 2009, 10, 1212-24.
115. Vaneycken, I.; D'Huyvetter, M.; Hernot, S.; De Vos, J.; Xavier, C.; Devoogdt, N.; Caveliers, V.; Lahoutte, T. Immuno-imaging using nanobodies. *Curr Opin Biotechnol* 2011, 22, 877-81.
116. Rashidian, M.; Keliher, E. J.; Bilate, A. M.; Duarte, J. N.; Wojtkiewicz, G. R.; Jacobsen, J. T.; Cragolini, J.; Swee, L. K.; Victora, G. D.; Weissleder, R.; Ploegh, H. L. Noninvasive imaging of immune responses. *Proc Natl Acad Sci U.S.A* 2015, 112, 6146-51.
117. D'Huyvetter, M.; Vincke, C.; Xavier, C.; Aerts, A.; Impens, N.; Baatout, S.; De Raeve, H.; Muyldermans, S.; Caveliers, V.; Devoogdt, N.; Lahoutte, T. Targeted radionuclide therapy with A 177Lu-labeled anti-HER2 nanobody. *Theranostics* 2014, 4, 708-20.
118. Chatalic, K. L.; Veldhoven-Zweistra, J.; Bolkestein, M.; Hoeben, S.; Koning, G. A.; Boerman, O. C.; de Jong, M.; van Weerden, W. M. A Novel (1)(1)(1)In-Labeled Anti-Prostate-Specific Membrane Antigen Nanobody for Targeted SPECT/CT Imaging of Prostate Cancer. *J Nucl Med* 2015, 56, 1094-9.
119. Oliveira, S.; van Dongen, G. A.; Stigter-van Walsum, M.; Roovers, R. C.; Stam, J. C.; Mali, W.; van Diest, P. J.; van Bergen en Henegouwen, P. M. Rapid visualization of human tumor xenografts through optical imaging with a near-infrared fluorescent anti-epidermal growth factor receptor nanobody. *Mol Imaging* 2012, 11, 33-46.

120. Kijanka, M.; Warnders, F. J.; El Khattabi, M.; Lub-de Hooge, M.; van Dam, G. M.; Ntziachristos, V.; de Vries, L.; Oliveira, S.; van Bergen En Henegouwen, P. M. Rapid optical imaging of human breast tumour xenografts using anti-HER2 VHHs site-directly conjugated to IRDye 800CW for image-guided surgery. *Eur J Nucl Med Mol Imaging* 2013, 40, 1718-29.
121. Roovers, R. C.; Laeremans, T.; Huang, L.; De Taeye, S.; Verkleij, A. J.; Revets, H.; de Haard, H. J.; van Bergen en Henegouwen, P. M. Efficient inhibition of EGFR signaling and of tumour growth by antagonistic anti-EFGR Nanobodies. *Cancer Immunol Immunother* 2007, 56, 303-317.
122. Vosjan, M. J.; Vercammen, J.; Kolkman, J. A.; Stigter-van Walsum, M.; Revets, H.; van Dongen, G. A. Nanobodies targeting the hepatocyte growth factor: potential new drugs for molecular cancer therapy. *Mol Cancer Ther* 2012, 11, 1017-25.
123. Maussang, D.; Mujic-Delic, A.; Descamps, F. J.; Stortelers, C.; Vanlandschoot, P.; Stigter-van Walsum, M.; Vischer, H. F.; van Roy, M.; Vosjan, M.; Gonzalez-Pajuelo, M.; van Dongen, G. A.; Merchiers, P.; van Rompaey, P.; Smit, M. J. Llama-derived single variable domains (nanobodies) directed against chemokine receptor CXCR7 reduce head and neck cancer cell growth in vivo. *J Biol Chem* 2013, 288, 29562-72.
124. Farajpour, Z.; Rahbarizadeh, F.; Kazemi, B.; Ahmadvand, D. A nanobody directed to a functional epitope on VEGF, as a novel strategy for cancer treatment. *Biochem Biophys Res Commun* 2014, 446, 132-6.
125. Ebrahimizadeh, W.; Mousavi Gargari, S. L.; Javidan, Z.; Rajabibazl, M. Production of Novel VHH Nanobody Inhibiting Angiogenesis by Targeting Binding Site of VEGF. *Appl Biochem Biotechnol* 2015, 176, 1985-95.
126. Oliveira, S.; Heukers, R.; Sornkom, J.; Kok, R. J.; van Bergen En Henegouwen, P. M. Targeting tumors with nanobodies for cancer imaging and therapy. *J Control Release* 2013, 172, 607-17.
127. Bolkestein, M.; de Blois, E.; Koelewijn, S. J.; Eggermont, A. M.; Grosveld, F.; de Jong, M.; Koning, G. A. Investigation of Factors Determining the Enhanced Permeability and Retention Effect in Subcutaneous Xenografts. *J Nucl Med* 2016, 57, 601-7.
128. Longmire, M.; Choyke, P. L.; Kobayashi, H. Clearance properties of nano-sized particles and molecules as imaging agents: considerations and caveats. *Nanomedicine (Lond)* 2008, 3, 703-17.
129. van der Meel, R.; Oliveira, S.; Altintas, I.; Haselberg, R.; van der Veeken, J.; Roovers, R. C.; van Bergen en Henegouwen, P. M.; Storm, G.; Hennink, W. E.; Schiffelers, R. M.; Kok, R. J. Tumor-targeted Nanobullets: Anti-EGFR nanobody-liposomes loaded with anti-IGF-1R kinase inhibitor for cancer treatment. *J Control Release* 2012, 159, 281-9.
130. Talelli, M.; Oliveira, S.; Rijcken, C. J.; Pieters, E. H.; Etrych, T.; Ulbrich, K.; van Nostrum, R. C.; Storm, G.; Hennink, W. E.; Lammers, T. Intrinsically active nanobody-modified polymeric micelles for tumor-targeted combination therapy. *Biomaterials* 2013, 34, 1255-60.
131. Zou, T.; Dembele, F.; Beugnet, A.; Sengmanivong, L.; Trepout, S.; Marco, S.; de Marco, A.; Li, M. H. Nanobody-functionalized PEG-b-PCL polymersomes and their targeting study. *J Biotechnol* 2015, 214, 147-55.
132. Debets, M. F.; Leenders, W. P.; Verrijp, K.; Zonjee, M.; Meeuwissen, S. A.; Otte-Holler, I.; van Hest, J. C. Nanobody-functionalized polymersomes for tumor-vessel targeting. *Macromol Biosci* 2013, 13, 938-45.
133. Steeland, S.; Vandenbroucke, R. E.; Libert, C. Nanobodies as therapeutics: big opportunities for small antibodies. *Drug Discov Today* 2016, 21, 1076-113.
134. Wark, K. L.; Hudson, P. J. Latest technologies for the enhancement of antibody affinity. *Adv Drug Deliv Rev* 2006, 58, 657-70.

135. Hoseinpoor, R.; Mousavi Gargari, S. L.; Rasooli, I.; Rajabibazl, M.; Shahi, B. Functional mutations in and characterization of VHH against *Helicobacter pylori* urease. *Appl Biochem Biotechnol* 2014, 172, 3079-91.
136. Orcutt, K. D.; Rhoden, J. J.; Ruiz-Yi, B.; Frangioni, J. V.; Wittrup, K. D. Effect of small-molecule-binding affinity on tumor uptake in vivo: a systematic study using a pretargeted bispecific antibody. *Mol Cancer Ther* 2012, 11, 1365-72.
137. Juweid, M.; Neumann, R.; Paik, C.; Perez-Bacete, M. J.; Sato, J.; van Osdol, W.; Weinstein, J. N. Micropharmacology of monoclonal antibodies in solid tumors: direct experimental evidence for a binding site barrier. *Cancer Res* 1992, 52, 5144-53.
138. Banerjee, R. K.; van Osdol, W. W.; Bungay, P. M.; Sung, C.; Dedrick, R. L. Finite element model of antibody penetration in a prevascular tumor nodule embedded in normal tissue. *J Control Release* 2001, 74, 193-202.
139. Adams, G. P.; Schier, R.; McCall, A. M.; Simmons, H. H.; Horak, E. M.; Alpaugh, R. K.; Marks, J. D.; Weiner, L. M. High affinity restricts the localization and tumor penetration of single-chain fv antibody molecules. *Cancer Res* 2001, 61, 4750-5.
140. Zou, X.; Smith, J. A.; Nguyen, V. K.; Ren, L.; Luyten, K.; Muyldermans, S.; Bruggemann, M. Expression of a dromedary heavy chain-only antibody and B cell development in the mouse. *J Immunol* 2005, 175, 3769-79.
141. Bruggemann, M.; Smith, J. A.; Osborn, M. J.; Corcos, D.; Zou, X.; Nguyen, V. K.; Muyldermans, S. Heavy-chain-only antibody expression and B-cell development in the mouse. *Crit Rev Immunol* 2006, 26, 377-90.
142. Matsumura, Y.; Maeda, H. A new concept for macromolecular therapeutics in cancer chemotherapy: mechanism of tumoritropic accumulation of proteins and the antitumor agent smancs. *Cancer Res* 1986, 46, 6387-92.
143. Skinner, S. A.; Tutton, P. J.; O'Brien, P. E. Microvascular architecture of experimental colon tumors in the rat. *Cancer Res* 1990, 50, 2411-7.
144. Suzuki, M.; Takahashi, T.; Sato, T. Medial regression and its functional significance in tumor-supplying host arteries. A morphometric study of hepatic arteries in human livers with hepatocellular carcinoma. *Cancer* 1987, 59, 444-50.
145. Konno, T.; Maeda, H.; Iwai, K.; Maki, S.; Tashiro, S.; Uchida, M.; Miyauchi, Y. Selective targeting of anti-cancer drug and simultaneous image enhancement in solid tumors by arterially administered lipid contrast medium. *Cancer* 1984, 54, 2367-74.
146. Hashizume, H.; Baluk, P.; Morikawa, S.; McLean, J. W.; Thurston, G.; Roberge, S.; Jain, R. K.; McDonald, D. M. Openings between defective endothelial cells explain tumor vessel leakiness. *Am J Pathol* 2000, 156, 1363-80.
147. Ruoslahti, E. Specialization of tumour vasculature. *Nature reviews. Cancer* 2002, 2, 83-90.
148. Yuan, F.; Dellian, M.; Fukumura, D.; Leunig, M.; Berk, D. A.; Torchilin, V. P.; Jain, R. K. Vascular permeability in a human tumor xenograft: molecular size dependence and cutoff size. *Cancer Res* 1995, 55, 3752-6.
149. Stohrer, M.; Boucher, Y.; Stangassinger, M.; Jain, R. K. Oncotic pressure in solid tumors is elevated. *Cancer Res* 2000, 60, 4251-5.
150. Lammers, T.; Kiessling, F.; Hennink, W. E.; Storm, G. Drug targeting to tumors: principles, pitfalls and (pre-) clinical progress. *J Control Release* 2012, 161, 175-87.
151. Jain, R. K.; Stylianopoulos, T. Delivering nanomedicine to solid tumors. *Nat Rev Clin Oncol* 2010, 7, 653-64.

152. Popovic, Z.; Liu, W.; Chauhan, V. P.; Lee, J.; Wong, C.; Greytak, A. B.; Insin, N.; Nocera, D. G.; Fukumura, D.; Jain, R. K.; Bawendi, M. G. A nanoparticle size series for in vivo fluorescence imaging. *Angew Chem Int Ed Engl* 2010, 49, 8649-52.
153. Toy, R.; Hayden, E.; Shoup, C.; Baskaran, H.; Karathanasis, E. The effects of particle size, density and shape on margination of nanoparticles in microcirculation. *Nanotechnology* 2011, 22, 115101.
154. Harrington, K. J.; Rowlinson-Busza, G.; Syrigos, K. N.; Abra, R. M.; Uster, P. S.; Peters, A. M.; Stewart, J. S. Influence of tumour size on uptake of(111)In-DTPA-labelled pegylated liposomes in a human tumour xenograft model. *British journal of cancer* 2000, 83, 684-8.
155. Folkman, J. Tumor angiogenesis: therapeutic implications. *N Engl J Med* 1971, 285, 1182-6.
156. Jain, R. K. Transport of molecules in the tumor interstitium: a review. *Cancer Res* 1987, 47, 3039-51.
157. Netti, P. A.; Berk, D. A.; Swartz, M. A.; Grodzinsky, A. J.; Jain, R. K. Role of extracellular matrix assembly in interstitial transport in solid tumors. *Cancer Res* 2000, 60, 2497-503.
158. Park, K. Questions on the role of the EPR effect in tumor targeting. *J Control Release* 2013, 172, 391.
159. Rosenecker, J.; Zhang, W.; Hong, K.; Lausier, J.; Geppetti, P.; Yoshihara, S.; Papahadjopoulos, D.; Nadel, J. A. Increased liposome extravasation in selected tissues: effect of substance P. *Proc Natl Acad Sci U.S.A* 1996, 93, 7236-41.
160. Kong, G.; Anyarambhatla, G.; Petros, W. P.; Braun, R. D.; Colvin, O. M.; Needham, D.; Dewhirst, M. W. Efficacy of liposomes and hyperthermia in a human tumor xenograft model: importance of triggered drug release. *Cancer Res* 2000, 60, 6950-7.
161. Al-Ahmady, Z.; Kostarelos, K. Chemical Components for the Design of Temperature-Responsive Vesicles as Cancer Therapeutics. *Chem Rev* 2016, 116, 3883-918.
162. Oude Blenke, E.; Mastrobattista, E.; Schiffelers, R. M. Strategies for triggered drug release from tumor targeted liposomes. *Expert Opin Drug Deliv* 2013, 10, 1399-410.
163. Bibi, S.; Lattmann, E.; Mohammed, A. R.; Perrie, Y. Trigger release liposome systems: local and remote controlled delivery? *J Microencapsul* 2012, 29, 262-76.
164. Kanamala, M.; Wilson, W. R.; Yang, M.; Palmer, B. D.; Wu, Z. Mechanisms and biomaterials in pH-responsive tumour targeted drug delivery: A review. *Biomaterials* 2016, 85, 152-67.
165. Sirsi, S. R.; Borden, M. A. State-of-the-art materials for ultrasound-triggered drug delivery. *Adv Drug Deliv Rev* 2014, 72, 3-14.
166. Hussein, G. A.; Pitt, W. G.; Martins, A. M. Ultrasonically triggered drug delivery: breaking the barrier. *Colloids Surf B Biointerfaces* 2014, 123, 364-86.
167. Li, L.; ten Hagen, T. L.; Bolkestein, M.; Gasselhuber, A.; Yatvin, J.; van Rhoon, G. C.; Eggermont, A. M.; Haemmerich, D.; Koning, G. A. Improved intratumoral nanoparticle extravasation and penetration by mild hyperthermia. *J Control Release* 2013, 167, 130-7.
168. Yatvin, M. B.; Weinstein, J. N.; Dennis, W. H.; Blumenthal, R. Design of liposomes for enhanced local release of drugs by hyperthermia. *Science* 1978, 202, 1290-3.
169. Weinstein, J. N.; Magin, R. L.; Yatvin, M. B.; Zaharko, D. S. Liposomes and local hyperthermia: selective delivery of methotrexate to heated tumors. *Science* 1979, 204, 188-91.
170. Evans, E.; Needham, D. Physical properties of surfactant bilayer membranes: thermal transitions, elasticity, rigidity, cohesion and colloidal interactions. *J Phys Chem* 1987, 91, 4219-4228.
171. Mills, J. K.; Needham, D. Lysolipid incorporation in dipalmitoylphosphatidylcholine bilayer membranes enhances the ion permeability and drug release rates at the membrane phase transition. *Biochim Biophys Acta* 2005, 1716, 77-96.

172. Grull, H.; Langereis, S. Hyperthermia-triggered drug delivery from temperature-sensitive liposomes using MRI-guided high intensity focused ultrasound. *J Control Release* 2012, 161, 317-27.
173. Mouritsen, O. G.; Zuckermann, M. J. Softening of lipid bilayers. *Eur Biophys J* 1985, 12, 75-86.
174. Kaasgaard, T.; Leidy, C.; Crowe, J. H.; Mouritsen, O. G.; Jorgensen, K. Temperature-controlled structure and kinetics of ripple phases in one- and two-component supported lipid bilayers. *Biophys J* 2003, 85, 350-60.
175. Winter, N. D.; Schatz, G. C. Coarse-grained molecular dynamics study of permeability enhancement in DPPC bilayers by incorporation of lysolipid. *J Phys Chem B* 2010, 114, 5053-60.
176. Ickenstein, L. M.; Arfvidsson, M. C.; Needham, D.; Mayer, L. D.; Edwards, K. Disc formation in cholesterol-free liposomes during phase transition. *Biochim Biophys Acta* 2003, 1614, 135-8.
177. Gaber, M. H.; Hong, K.; Huang, S. K.; Papahadjopoulos, D. Thermosensitive sterically stabilized liposomes: formulation and in vitro studies on mechanism of doxorubicin release by bovine serum and human plasma. *Pharm Res* 1995, 12, 1407-16.
178. de Smet, M.; Langereis, S.; van den Bosch, S.; Bitter, K.; Hijnen, N. M.; Heijman, E.; Grull, H. SPECT/CT imaging of temperature-sensitive liposomes for MR-image guided drug delivery with high intensity focused ultrasound. *J Control Release* 2013, 169, 82-90.
179. Needham, D.; Anyarambhatla, G.; Kong, G.; Dewhirst, M. W. A new temperature-sensitive liposome for use with mild hyperthermia: characterization and testing in a human tumor xenograft model. *Cancer Res* 2000, 60, 1197-201.
180. Lencioni, R.; Cioni, D. RFA plus lyso-thermosensitive liposomal doxorubicin: in search of the optimal approach to cure intermediate-size hepatocellular carcinoma. *Hepat Oncol* 2016, 3, 193-200.
181. Manzoor, A. A.; Lindner, L. H.; Landon, C. D.; Park, J. Y.; Simnick, A. J.; Dreher, M. R.; Das, S.; Hanna, G.; Park, W.; Chilkoti, A.; Koning, G. A.; ten Hagen, T. L.; Needham, D.; Dewhirst, M. W. Overcoming limitations in nanoparticle drug delivery: triggered, intravascular release to improve drug penetration into tumors. *Cancer Res* 2012, 72, 5566-75.
182. Kong, G.; Braun, R. D.; Dewhirst, M. W. Hyperthermia enables tumor-specific nanoparticle delivery: effect of particle size. *Cancer Res* 2000, 60, 4440-5.
183. Lokerse, W. J.; Kneepkens, E. C.; ten Hagen, T. L.; Eggermont, A. M.; Grull, H.; Koning, G. A. In depth study on thermosensitive liposomes: Optimizing formulations for tumor specific therapy and in vitro to in vivo relations. *Biomaterials* 2016, 82, 138-50.
184. Haeri, A.; Zalba, S.; Ten Hagen, T. L.; Dadashzadeh, S.; Koning, G. A. EGFR targeted thermosensitive liposomes: A novel multifunctional platform for simultaneous tumor targeted and stimulus responsive drug delivery. *Colloids Surf B Biointerfaces* 2016, 146, 657-669.
185. Kullberg, M.; Owens, J. L.; Mann, K. Listeriolysin O enhances cytoplasmic delivery by Her-2 targeting liposomes. *J Drug Target* 2010, 18, 313-20.
186. Negussie, A. H.; Miller, J. L.; Reddy, G.; Drake, S. K.; Wood, B. J.; Dreher, M. R. Synthesis and in vitro evaluation of cyclic NGR peptide targeted thermally sensitive liposome. *J Control Release* 2010, 143, 265-73.
187. Gaber, M. H. Modulation of doxorubicin resistance in multidrug-resistance cells by targeted liposomes combined with hyperthermia. *J Biochem Mol Biol Biophys* 2002, 6, 309-14.
188. Muyldermans, S.; Lauwereys, M. Unique single-domain antigen binding fragments derived from naturally occurring camel heavy-chain antibodies. *J Mol Recognit* 1999, 12, 131-40.
189. Kitamura, D.; Roes, J.; Kuhn, R.; Rajewsky, K. A B cell-deficient mouse by targeted disruption of the membrane exon of the immunoglobulin mu chain gene. *Nature* 1991, 350, 423-6.

190. Benner, R.; Hijmans, W.; Haaijman, J. J. The bone marrow: the major source of serum immunoglobulins, but still a neglected site of antibody formation. *Clin Exp Immunol* 1981, 46, 1-8.
191. Manz, R. A.; Thiel, A.; Radbruch, A. Lifetime of plasma cells in the bone marrow. *Nature* 1997, 388, 133-4.
192. Radbruch, A.; Muehlinghaus, G.; Luger, E. O.; Inamine, A.; Smith, K. G.; Dorner, T.; Hiepe, F. Competence and competition: the challenge of becoming a long-lived plasma cell. *Nat Rev Immunol* 2006, 6, 741-50.
193. Brayman, M.; Thathiah, A.; Carson, D. D. MUC1: a multifunctional cell surface component of reproductive tissue epithelia. *Reprod Biol Endocrinol* 2004, 2, 4.
194. Hilken, J.; Ligtenberg, M. J.; Vos, H. L.; Litvinov, S. V. Cell membrane-associated mucins and their adhesion-modulating property. *Trends Biochem Sci* 1992, 17, 359-63.
195. Lloyd, K. O.; Burchell, J.; Kudryashov, V.; Yin, B. W.; Taylor-Papadimitriou, J. Comparison of O-linked carbohydrate chains in MUC-1 mucin from normal breast epithelial cell lines and breast carcinoma cell lines. Demonstration of simpler and fewer glycan chains in tumor cells. *J Biol Chem* 1996, 271, 33325-34.
196. Kim, Y. S.; Gum, J., Jr.; Brockhausen, I. Mucin glycoproteins in neoplasia. *Glycoconj J* 1996, 13, 693-707.
197. Wesseling, J.; van der Valk, S. W.; Vos, H. L.; Sonnenberg, A.; Hilken, J. Episialin (MUC1) overexpression inhibits integrin-mediated cell adhesion to extracellular matrix components. *J Cell Biol* 1995, 129, 255-65.
198. Price, C. E.; Rona, R. J.; Chinn, S. Height of primary school children and parents' perceptions of food intolerance. *Br Med J (Clin Res Ed)* 1988, 296, 1696-9.
199. Reddish, M. A.; MacLean, G. D.; Poppema, S.; Berg, A.; Longenecker, B. M. Pre-immunotherapy serum CA27.29 (MUC-1) mucin level and CD69+ lymphocytes correlate with effects of Theratope sialyl-Tn-KLH cancer vaccine in active specific immunotherapy. *Cancer Immunol Immunother* 1996, 42, 303-9.
200. Kobayashi, H.; Terao, T.; Kawashima, Y. Serum sialyl Tn as an independent predictor of poor prognosis in patients with epithelial ovarian cancer. *J Clin Oncol* 1992, 10, 95-101.
201. Bresalier, R. S.; Niv, Y.; Byrd, J. C.; Duh, Q. Y.; Toribara, N. W.; Rockwell, R. W.; Dahiya, R.; Kim, Y. S. Mucin production by human colonic carcinoma cells correlates with their metastatic potential in animal models of colon cancer metastasis. *J Clin Invest* 1991, 87, 1037-45.
202. Nakamori, S.; Ota, D. M.; Cleary, K. R.; Shirotani, K.; Irimura, T. MUC1 mucin expression as a marker of progression and metastasis of human colorectal carcinoma. *Gastroenterology* 1994, 106, 353-61.
203. Mehla, K.; Singh, P. K. MUC1: a novel metabolic master regulator. *Biochim Biophys Acta* 2014, 1845, 126-35.
204. Litvinov, S. V.; Hilken, J. The epithelial sialomucin, episialin, is sialylated during recycling. *J Biol Chem* 1993, 268, 21364-71.
205. Nielsen, U. B.; Adams, G. P.; Weiner, L. M.; Marks, J. D. Targeting of bivalent anti-ErbB2 diabody antibody fragments to tumor cells is independent of the intrinsic antibody affinity. *Cancer Res* 2000, 60, 6434-40.
206. Fujimori, K.; Fisher, D. R.; Weinstein, J. N. Integrated microscopic-macroscopic pharmacology of monoclonal antibody radioconjugates: the radiation dose distribution. *Cancer Res* 1991, 51, 4821-7.
207. Fujimori, K.; Covell, D. G.; Fletcher, J. E.; Weinstein, J. N. A modeling analysis of monoclonal antibody percolation through tumors: a binding-site barrier. *J Nucl Med* 1990, 31, 1191-8.

208. Ward, E. S.; Gussow, D.; Griffiths, A. D.; Jones, P. T.; Winter, G. Binding activities of a repertoire of single immunoglobulin variable domains secreted from *Escherichia coli*. *Nature* 1989, 341, 544-6.
209. Alexis, F.; Pridgen, E.; Molnar, L. K.; Farokhzad, O. C. Factors affecting the clearance and biodistribution of polymeric nanoparticles. *Mol Pharm* 2008, 5, 505-15.
210. Stylianopoulos, T.; Jain, R. K. Design considerations for nanotherapeutics in oncology. *Nano-medicine* 2015, 11, 1893-907.
211. Olafsen, T.; Cheung, C. W.; Yazaki, P. J.; Li, L.; Sundaresan, G.; Gambhir, S. S.; Sherman, M. A.; Williams, L. E.; Shively, J. E.; Raubitschek, A. A.; Wu, A. M. Covalent disulfide-linked anti-CEA diabody allows site-specific conjugation and radiolabeling for tumor targeting applications. *Protein Eng Des Sel* 2004, 17, 21-7.
212. Kenanova, V.; Olafsen, T.; Crow, D. M.; Sundaresan, G.; Subbarayan, M.; Carter, N. H.; Ikke, D. N.; Yazaki, P. J.; Chatziioannou, A. F.; Gambhir, S. S.; Williams, L. E.; Shively, J. E.; Colcher, D.; Raubitschek, A. A.; Wu, A. M. Tailoring the pharmacokinetics and positron emission tomography imaging properties of anti-carcinoembryonic antigen single-chain Fv-Fc antibody fragments. *Cancer Res* 2005, 65, 622-31.
213. Siegel, R.; Naishadham, D.; Jemal, A. Cancer statistics, 2012. *CA Cancer J Clin* 2012, 62, 10-29.
214. Bostwick, D. G.; Pacelli, A.; Blute, M.; Roche, P.; Murphy, G. P. Prostate specific membrane antigen expression in prostatic intraepithelial neoplasia and adenocarcinoma: a study of 184 cases. *Cancer* 1998, 82, 2256-61.
215. Silver, D. A.; Pellicer, I.; Fair, W. R.; Heston, W. D.; Cordon-Cardo, C. Prostate-specific membrane antigen expression in normal and malignant human tissues. *Clin Cancer Res* 1997, 3, 81-5.
216. Wright, G. L., Jr.; Haley, C.; Beckett, M. L.; Schellhammer, P. F. Expression of prostate-specific membrane antigen in normal, benign, and malignant prostate tissues. *Urol Oncol* 1995, 1, 18-28.
217. Wright, G. L., Jr.; Grob, B. M.; Haley, C.; Grossman, K.; Newhall, K.; Petrylak, D.; Troyer, J.; Konchuba, A.; Schellhammer, P. F.; Moriarty, R. Upregulation of prostate-specific membrane antigen after androgen-deprivation therapy. *Urology* 1996, 48, 326-34.
218. Sokoloff, R. L.; Norton, K. C.; Gasior, C. L.; Marker, K. M.; Grauer, L. S. A dual-monoclonal sandwich assay for prostate-specific membrane antigen: levels in tissues, seminal fluid and urine. *Prostate* 2000, 43, 150-7.
219. Ellis, R. J.; Kaminsky, D. A.; Zhou, E. H.; Fu, P.; Chen, W. D.; Brelvi, A.; Faulhaber, P. F.; Bodner, D. Ten-year outcomes: the clinical utility of single photon emission computed tomography/computed tomography capromab pendetide (Prostascint) in a cohort diagnosed with localized prostate cancer. *Int J Radiat Oncol Biol Phys* 2011, 81, 29-34.
220. Apolo, A. B.; Pandit-Taskar, N.; Morris, M. J. Novel tracers and their development for the imaging of metastatic prostate cancer. *J Nucl Med* 2008, 49, 2031-41.
221. Bander, N. H.; Nanus, D. M.; Milowsky, M. I.; Kostakoglu, L.; Vallabhajosula, S.; Goldsmith, S. J. Targeted systemic therapy of prostate cancer with a monoclonal antibody to prostate-specific membrane antigen. *Semin Oncol* 2003, 30, 667-76.
222. Milowsky, M. I.; Nanus, D. M.; Kostakoglu, L.; Vallabhajosula, S.; Goldsmith, S. J.; Bander, N. H. Phase I trial of yttrium-90-labeled anti-prostate-specific membrane antigen monoclonal antibody J591 for androgen-independent prostate cancer. *J Clin Oncol* 2004, 22, 2522-31.
223. Tagawa, S. T.; Beltran, H.; Vallabhajosula, S.; Goldsmith, S. J.; Osborne, J.; Matulich, D.; Petrillo, K.; Parmar, S.; Nanus, D. M.; Bander, N. H. Anti-prostate-specific membrane antigen-based radioimmunotherapy for prostate cancer. *Cancer* 2010, 116, 1075-83.

224. Mease, R. C.; Foss, C. A.; Pomper, M. G. PET imaging in prostate cancer: focus on prostate-specific membrane antigen. *Curr Top Med Chem* 2013, 13, 951-62.
225. Barrett, J. A.; Coleman, R. E.; Goldsmith, S. J.; Vallabhajosula, S.; Petry, N. A.; Cho, S.; Armor, T.; Stubbs, J. B.; Maresca, K. P.; Stabin, M. G.; Joyal, J. L.; Eckelman, W. C.; Babich, J. W. First-in-man evaluation of 2 high-affinity PSMA-avid small molecules for imaging prostate cancer. *J Nucl Med* 2013, 54, 380-7.
226. Cho, S. Y.; Gage, K. L.; Mease, R. C.; Senthamizhchelvan, S.; Holt, D. P.; Jeffrey-Kwanisai, A.; Endres, C. J.; Dannals, R. F.; Sgouros, G.; Lodge, M.; Eisenberger, M. A.; Rodriguez, R.; Carducci, M. A.; Rojas, C.; Slusher, B. S.; Kozikowski, A. P.; Pomper, M. G. Biodistribution, tumor detection, and radiation dosimetry of 18F-DCFBC, a low-molecular-weight inhibitor of prostate-specific membrane antigen, in patients with metastatic prostate cancer. *J Nucl Med* 2012, 53, 1883-91.
227. Afshar-Oromieh, A.; Hetzheim, H.; Kratochwil, C.; Benesova, M.; Eder, M.; Neels, O. C.; Eisenhut, M.; Kubler, W.; Holland-Letz, T.; Giesel, F. L.; Mier, W.; Kopka, K.; Haberkorn, U. The Theranostic PSMA Ligand PSMA-617 in the Diagnosis of Prostate Cancer by PET/CT: Biodistribution in Humans, Radiation Dosimetry, and First Evaluation of Tumor Lesions. *J Nucl Med* 2015, 56, 1697-705.
228. Beheshti, M.; Kunit, T.; Haim, S.; Zakavi, R.; Schiller, C.; Stephens, A.; Dinkelborg, L.; Langsteger, W.; Loidl, W. BAY 1075553 PET-CT for Staging and Restaging Prostate Cancer Patients: Comparison with [18F] Fluorocholine PET-CT (Phase I Study). *Mol Imaging Biol* 2015, 17, 424-33.
229. Cortez-Retamozo, V.; Lauwereys, M.; Hassanzadeh Gh, G.; Gobert, M.; Conrath, K.; Muyldermans, S.; De Baetselier, P.; Revets, H. Efficient tumor targeting by single-domain antibody fragments of camels. *Int J Cancer* 2002, 98, 456-62.
230. Behar, G.; Siberil, S.; Groulet, A.; Chames, P.; Pugniere, M.; Boix, C.; Sautes-Fridman, C.; Teillaud, J. L.; Baty, D. Isolation and characterization of anti-FcγRIII (CD16) llama single-domain antibodies that activate natural killer cells. *Protein Eng Des Sel* 2008, 21, 1-10.
231. Mikolajczyk, J.; Drag, M.; Bekes, M.; Cao, J. T.; Ronai, Z.; Salvesen, G. S. Small ubiquitin-related modifier (SUMO)-specific proteases: profiling the specificities and activities of human SENPs. *J Biol Chem* 2007, 282, 26217-24.
232. Chatalic, K. L.; Franssen, G. M.; van Weerden, W. M.; McBride, W. J.; Laverman, P.; de Blois, E.; Hajjaj, B.; Brunel, L.; Goldenberg, D. M.; Fehrentz, J. A.; Martinez, J.; Boerman, O. C.; de Jong, M. Preclinical comparison of Al18F- and 68Ga-labeled gastrin-releasing peptide receptor antagonists for PET imaging of prostate cancer. *J Nucl Med* 2014, 55, 2050-6.
233. Lutje, S.; van Rij, C. M.; Franssen, G. M.; Fracasso, G.; Helfrich, W.; Eek, A.; Oyen, W. J.; Colombatti, M.; Boerman, O. C. Targeting human prostate cancer with 111In-labeled D2B IgG, F(ab')₂ and Fab fragments in nude mice with PSMA-expressing xenografts. *Contrast Media Mol Imaging* 2015, 10, 28-36.
234. Viola-Villegas, N. T.; Sevak, K. K.; Carlin, S. D.; Doran, M. G.; Evans, H. W.; Bartlett, D. W.; Wu, A. M.; Lewis, J. S. Noninvasive Imaging of PSMA in prostate tumors with (89)Zr-Labeled huJ591 engineered antibody fragments: the faster alternatives. *Mol Pharm* 2014, 11, 3965-73.
235. Kampmeier, F.; Williams, J. D.; Maher, J.; Mullen, G. E.; Blower, P. J. Design and preclinical evaluation of a 99mTc-labelled diabody of mAb J591 for SPECT imaging of prostate-specific membrane antigen (PSMA). *EJNMMI Res* 2014, 4, 13.
236. Evazalipour, M.; D'Huyvetter, M.; Tehrani, B. S.; Abolhassani, M.; Omidfar, K.; Abdoli, S.; Arezumand, R.; Morovvati, H.; Lahoutte, T.; Muyldermans, S.; Devoogdt, N. Generation and characterization of nanobodies targeting PSMA for molecular imaging of prostate cancer. *Contrast Media Mol Imaging* 2014, 9, 211-20.

237. Gainkam, L. O.; Caveliers, V.; Devoogdt, N.; Vanhove, C.; Xavier, C.; Boerman, O.; Muylderms, S.; Bossuyt, A.; Lahoutte, T. Localization, mechanism and reduction of renal retention of technetium-99m labeled epidermal growth factor receptor-specific nanobody in mice. *Contrast Media Mol Imaging* 2011, 6, 85-92.
238. Eder, M.; Schafer, M.; Bauder-Wust, U.; Hull, W. E.; Wangler, C.; Mier, W.; Haberkorn, U.; Eisenhut, M. 68Ga-complex lipophilicity and the targeting property of a urea-based PSMA inhibitor for PET imaging. *Bioconjug Chem* 2012, 23, 688-97.
239. Hillier, S. M.; Maresca, K. P.; Femia, F. J.; Marquis, J. C.; Foss, C. A.; Nguyen, N.; Zimmerman, C. N.; Barrett, J. A.; Eckelman, W. C.; Pomper, M. G.; Joyal, J. L.; Babich, J. W. Preclinical evaluation of novel glutamate-urea-lysine analogues that target prostate-specific membrane antigen as molecular imaging pharmaceuticals for prostate cancer. *Cancer Res* 2009, 69, 6932-40.
240. Siegel, R. L.; Miller, K. D.; Jemal, A. Cancer statistics, 2016. *CA Cancer J Clin* 2016, 66, 7-30.
241. Harris, W. P.; Mostaghel, E. A.; Nelson, P. S.; Montgomery, B. Androgen deprivation therapy: progress in understanding mechanisms of resistance and optimizing androgen depletion. *Nat Clin Pract Urol* 2009, 6, 76-85.
242. Eisenberger, M. A.; Walsh, P. C. Early androgen deprivation for prostate cancer? *N Engl J Med* 1999, 341, 1837-8.
243. Miller, R. E.; Sweeney, C. J. Chemotherapy for metastatic castrate-sensitive prostate cancer. *Prostate Cancer Prostatic Dis* 2016, 19, 139-44.
244. Tannock, I. F.; de Wit, R.; Berry, W. R.; Horti, J.; Pluzanska, A.; Chi, K. N.; Oudard, S.; Theodore, C.; James, N. D.; Turesson, I.; Rosenthal, M. A.; Eisenberger, M. A.; Investigators, T. A. X. Docetaxel plus prednisone or mitoxantrone plus prednisone for advanced prostate cancer. *N Engl J Med* 2004, 351, 1502-12.
245. Petrylak, D. P.; Tangen, C. M.; Hussain, M. H.; Lara, P. N., Jr.; Jones, J. A.; Taplin, M. E.; Burch, P. A.; Berry, D.; Moinpour, C.; Kohli, M.; Benson, M. C.; Small, E. J.; Raghavan, D.; Crawford, E. D. Docetaxel and estramustine compared with mitoxantrone and prednisone for advanced refractory prostate cancer. *N Engl J Med* 2004, 351, 1513-20.
246. Beer, T. M.; Armstrong, A. J.; Rathkopf, D. E.; Lortot, Y.; Sternberg, C. N.; Higano, C. S.; Iversen, P.; Bhattacharya, S.; Carles, J.; Chowdhury, S.; Davis, I. D.; de Bono, J. S.; Evans, C. P.; Fizazi, K.; Joshua, A. M.; Kim, C. S.; Kimura, G.; Mainwaring, P.; Mansbach, H.; Miller, K.; Noonberg, S. B.; Perabo, F.; Phung, D.; Saad, F.; Scher, H. I.; Taplin, M. E.; Venner, P. M.; Tombal, B.; Investigators, P. Enzalutamide in metastatic prostate cancer before chemotherapy. *N Engl J Med* 2014, 371, 424-33.
247. Ryan, C. J.; Smith, M. R.; Fizazi, K.; Saad, F.; Mulders, P. F.; Sternberg, C. N.; Miller, K.; Logothetis, C. J.; Shore, N. D.; Small, E. J.; Carles, J.; Flaig, T. W.; Taplin, M. E.; Higano, C. S.; de Souza, P.; de Bono, J. S.; Griffin, T. W.; De Porre, P.; Yu, M. K.; Park, Y. C.; Li, J.; Kheoh, T.; Naini, V.; Molina, A.; Rathkopf, D. E.; Investigators, C.-A.-. Abiraterone acetate plus prednisone versus placebo plus prednisone in chemotherapy-naive men with metastatic castration-resistant prostate cancer (COU-AA-302): final overall survival analysis of a randomised, double-blind, placebo-controlled phase 3 study. *Lancet Oncol* 2015, 16, 152-60.
248. van Soest, R. J.; de Wit, R. Irrefutable evidence for the use of docetaxel in newly diagnosed metastatic prostate cancer: results from the STAMPEDE and CHARTED trials. *BMC Med* 2015, 13.
249. McKeage, K. Docetaxel: a review of its use for the first-line treatment of advanced castration-resistant prostate cancer. *Drugs* 2012, 72, 1559-77.
250. van Soest, R. J.; van Royen, M. E.; de Morree, E. S.; Moll, J. M.; Teubel, W.; Wiemer, E. A.; Mathijssen, R. H.; de Wit, R.; van Weerden, W. M. Cross-resistance between taxanes and new hormonal

- agents abiraterone and enzalutamide may affect drug sequence choices in metastatic castration-resistant prostate cancer. *Eur J Cancer* 2013, 49, 3821-30.
251. de Morree, E. S.; Bottcher, R.; van Soest, R. J.; Aghai, A.; de Ridder, C. M.; Gibson, A. A.; Mathijssen, R. H.; Burger, H.; Wiemer, E. A.; Sparreboom, A.; de Wit, R.; van Weerden, W. M. Loss of SLCO1B3 drives taxane resistance in prostate cancer. *Br J Cancer* 2016, 115, 674-81.
252. O'Neill, A. J.; Prencipe, M.; Dowling, C.; Fan, Y.; Mulrane, L.; Gallagher, W. M.; O'Connor, D.; O'Connor, R.; Devery, A.; Corcoran, C.; Rani, S.; O'Driscoll, L.; Fitzpatrick, J. M.; Watson, R. W. Characterisation and manipulation of docetaxel resistant prostate cancer cell lines. *Mol Cancer* 2011, 10, 126.
253. de Morree, E.; van Soest, R.; Aghai, A.; de Ridder, C.; de Bruijn, P.; Ghobadi Moghaddam-Helmantel, I.; Burger, H.; Mathijssen, R.; Wiemer, E.; de Wit, R.; van Weerden, W. Understanding taxanes in prostate cancer; importance of intratumoral drug accumulation. *Prostate* 2016, 76, 927-36.
254. Ganju, A.; Yallapu, M. M.; Khan, S.; Behrman, S. W.; Chauhan, S. C.; Jaggi, M. Nanoways to overcome docetaxel resistance in prostate cancer. *Drug Resist Updat* 2014, 17, 13-23.
255. Barenholz, Y. Doxil(R)--the first FDA-approved nano-drug: lessons learned. *J Control Release* 2012, 160, 117-34.
256. Gill, P. S.; Espina, B. M.; Muggia, F.; Cabriales, S.; Tulpule, A.; Esplin, J. A.; Liebman, H. A.; Forsen, E.; Ross, M. E.; Levine, A. M. Phase I/II clinical and pharmacokinetic evaluation of liposomal daunorubicin. *J Clin Oncol* 1995, 13, 996-1003.
257. Uziely, B.; Jeffers, S.; Isacson, R.; Kutsch, K.; Wei-Tsao, D.; Yehoshua, Z.; Libson, E.; Muggia, F. M.; Gabizon, A. Liposomal doxorubicin: antitumor activity and unique toxicities during two complementary phase I studies. *J Clin Oncol* 1995, 13, 1777-85.
258. Northfelt, D. W.; Martin, F. J.; Working, P.; Volberding, P. A.; Russell, J.; Newman, M.; Amantea, M. A.; Kaplan, L. D. Doxorubicin encapsulated in liposomes containing surface-bound polyethylene glycol: pharmacokinetics, tumor localization, and safety in patients with AIDS-related Kaposi's sarcoma. *J Clin Pharmacol* 1996, 36, 55-63.
259. Zhang, H.; Li, R. Y.; Lu, X.; Mou, Z. Z.; Lin, G. M. Docetaxel-loaded liposomes: preparation, pH sensitivity, pharmacokinetics, and tissue distribution. *J Zhejiang Univ Sci B* 2012, 13, 981-9.
260. van der Meel, R.; Vehmeijer, L. J.; Kok, R. J.; Storm, G.; van Gaal, E. V. Ligand-targeted particulate nanomedicines undergoing clinical evaluation: current status. *Adv Drug Deliv Rev* 2013, 65, 1284-98.
261. Li, X.; Tian, X.; Zhang, J.; Zhao, X.; Chen, X.; Jiang, Y.; Wang, D.; Pan, W. In vitro and in vivo evaluation of folate receptor-targeting amphiphilic copolymer-modified liposomes loaded with docetaxel. *Int J Nanomedicine* 2011, 6, 1167-84.
262. Yuan, Z.; Chen, D.; Zhang, S.; Zheng, Z. Preparation, characterization and evaluation of docetaxel-loaded, folate-conjugated PEG-liposomes. *Yakugaku Zasshi* 2010, 130, 1353-9.
263. Yamamoto, Y.; Yoshida, M.; Sato, M.; Sato, K.; Kikuchi, S.; Sugishita, H.; Kuwabara, J.; Matsuno, Y.; Kojima, Y.; Morimoto, M.; Horiuchi, A.; Watanabe, Y. Feasibility of tailored, selective and effective anticancer chemotherapy by direct injection of docetaxel-loaded immunoliposomes into Her2/neu positive gastric tumor xenografts. *Int J Oncol* 2011, 38, 33-9.
264. Perner, S.; Hofer, M. D.; Kim, R.; Shah, R. B.; Li, H.; Moller, P.; Hautmann, R. E.; Gschwend, J. E.; Kuefer, R.; Rubin, M. A. Prostate-specific membrane antigen expression as a predictor of prostate cancer progression. *Hum Pathol* 2007, 38, 696-701.
265. Kawakami, M.; Nakayama, J. Enhanced expression of prostate-specific membrane antigen gene in prostate cancer as revealed by in situ hybridization. *Cancer Res* 1997, 57, 2321-4.

266. Haberkorn, U.; Eder, M.; Kopka, K.; Babich, J. W.; Eisenhut, M. New Strategies in Prostate Cancer: Prostate-Specific Membrane Antigen (PSMA) Ligands for Diagnosis and Therapy. *Clin Cancer Res* 2016, 22, 9-15.
267. Akhtar, N. H.; Pail, O.; Saran, A.; Tyrell, L.; Tagawa, S. T. Prostate-specific membrane antigen-based therapeutics. *Adv Urol* 2012, 2012, 973820.
268. Lutje, S.; Heskamp, S.; Cornelissen, A. S.; Poeppel, T. D.; van den Broek, S. A.; Rosenbaum-Krumme, S.; Bockisch, A.; Gotthardt, M.; Rijpkema, M.; Boerman, O. C. PSMA Ligands for Radionuclide Imaging and Therapy of Prostate Cancer: Clinical Status. *Theranostics* 2015, 5, 1388-401.
269. Chatalic, K. L.; Heskamp, S.; Konijnenberg, M.; Molkenboer-Kueneen, J. D.; Franssen, G. M.; Clahsen-van Groningen, M. C.; Schottelius, M.; Wester, H. J.; van Weerden, W. M.; Boerman, O. C.; de Jong, M. Towards Personalized Treatment of Prostate Cancer: PSMA I&T, a Promising Prostate-Specific Membrane Antigen-Targeted Theranostic Agent. *Theranostics* 2016, 6, 849-61.
270. Arbabi-Ghahroudi, M.; To, R.; Gaudette, N.; Hiram, T.; Ding, W.; MacKenzie, R.; Tanha, J. Aggregation-resistant VHs selected by in vitro evolution tend to have disulfide-bonded loops and acidic isoelectric points. *Protein Eng Des Sel* 2009, 22, 59-66.
271. Lasic, D. D. Liposomes from physics to applications. 1993, 63-107.
272. Rouser, G.; Fkeischer, S.; Yamamoto, A. Two dimensional thin layer chromatographic separation of polar lipids and determination of phospholipids by phosphorus analysis of spots. *Lipids* 1970, 5, 494-6.
273. Kuroda, K.; Liu, H.; Kim, S.; Guo, M.; Navarro, V.; Bander, N. H. Docetaxel down-regulates the expression of androgen receptor and prostate-specific antigen but not prostate-specific membrane antigen in prostate cancer cell lines: implications for PSA surrogacy. *Prostate* 2009, 69, 1579-85.
274. Laidler, P.; Dulinska, J.; Lekka, M.; Lekki, J. Expression of prostate specific membrane antigen in androgen-independent prostate cancer cell line PC-3. *Arch Biochem Biophys* 2005, 435, 1-14.
275. van Weerden, W. M.; de Ridder, C. M.; Verdaasdonk, C. L.; Romijn, J. C.; van der Kwast, T. H.; Schroder, F. H.; van Steenbrugge, G. J. Development of seven new human prostate tumor xenograft models and their histopathological characterization. *Am J Pathol* 1996, 149, 1055-62.
276. Sawant, R. R.; Torchilin, V. P. Challenges in development of targeted liposomal therapeutics. *AAPS J* 2012, 14, 303-15.
277. Scomparin, A.; Salmaso, S.; Eldar-Boock, A.; Ben-Shushan, D.; Ferber, S.; Tiram, G.; Shmeeda, H.; Landa-Rouben, N.; Leor, J.; Caliceti, P.; Gabizon, A.; Satchi-Fainaro, R. A comparative study of folate receptor-targeted doxorubicin delivery systems: dosing regimens and therapeutic index. *J Control Release* 2015, 208, 106-20.
278. Ernsting, M. J.; Tang, W. L.; MacCallum, N. W.; Li, S. D. Preclinical pharmacokinetic, biodistribution, and anti-cancer efficacy studies of a docetaxel-carboxymethylcellulose nanoparticle in mouse models. *Biomaterials* 2012, 33, 1445-54.
279. Von Hoff, D. D.; Mita, M. M.; Ramanathan, R. K.; Weiss, G. J.; Mita, A. C.; LoRusso, P. M.; Burris, H. A., 3rd; Hart, L. L.; Low, S. C.; Parsons, D. M.; Zale, S. E.; Summa, J. M.; Youssoufian, H.; Sachdev, J. C. Phase I Study of PSMA-Targeted Docetaxel-Containing Nanoparticle BIND-014 in Patients with Advanced Solid Tumors. *Clin Cancer Res* 2016.
280. Maresca, K. P.; Hillier, S. M.; Femia, F. J.; Keith, D.; Barone, C.; Joyal, J. L.; Zimmerman, C. N.; Kozikowski, A. P.; Barrett, J. A.; Eckelman, W. C.; Babich, J. W. A series of halogenated heterodimeric inhibitors of prostate specific membrane antigen (PSMA) as radiolabeled probes for targeting prostate cancer. *J Med Chem* 2009, 52, 347-57.

281. van Osdol, W.; Fujimori, K.; Weinstein, J. N. An analysis of monoclonal antibody distribution in microscopic tumor nodules: consequences of a "binding site barrier". *Cancer Res* 1991, 51, 4776-84.
282. Yokota, T.; Milenic, D. E.; Whitlow, M.; Schlom, J. Rapid tumor penetration of a single-chain Fv and comparison with other immunoglobulin forms. *Cancer Res* 1992, 52, 3402-8.
283. Yuan, F.; Leunig, M.; Huang, S. K.; Berk, D. A.; Papahadjopoulos, D.; Jain, R. K. Microvascular permeability and interstitial penetration of sterically stabilized (stealth) liposomes in a human tumor xenograft. *Cancer Res* 1994, 54, 3352-6.
284. Prabhakar, U.; Maeda, H.; Jain, R. K.; Sevick-Muraca, E. M.; Zamboni, W.; Farokhzad, O. C.; Barry, S. T.; Gabizon, A.; Grodzinski, P.; Blakey, D. C. Challenges and key considerations of the enhanced permeability and retention effect for nanomedicine drug delivery in oncology. *Cancer Res* 2013, 73, 2412-7.
285. Jain, R. K. Transport of molecules across tumor vasculature. *Cancer Metastasis Rev* 1987, 6, 559-93.
286. Konerding, M. A.; Miodonski, A. J.; Lametschwandtner, A. Microvascular corrosion casting in the study of tumor vascularity: a review. *Scanning Microsc* 1995, 9, 1233-43; discussion 1243-4.
287. Fang, J.; Nakamura, H.; Maeda, H. The EPR effect: Unique features of tumor blood vessels for drug delivery, factors involved, and limitations and augmentation of the effect. *Adv Drug Deliv Rev* 2011, 63, 136-51.
288. Dvorak, H. F.; Nagy, J. A.; Dvorak, J. T.; Dvorak, A. M. Identification and characterization of the blood vessels of solid tumors that are leaky to circulating macromolecules. *Am J Pathol* 1988, 133, 95-109.
289. Zhou, Y.; Kopecek, J. Biological rationale for the design of polymeric anti-cancer nanomedicines. *Int J Drug Target* 2013, 21, 1-26.
290. Fukumura, D.; Jain, R. K. Tumor microvasculature and microenvironment: targets for anti-angiogenesis and normalization. *Microvasc Res* 2007, 74, 72-84.
291. Minchinton, A. I.; Tannock, I. F. Drug penetration in solid tumours. *Nat Rev Cancer* 2006, 6, 583-92.
292. Sriraman, S. K.; Aryasomayajula, B.; Torchilin, V. P. Barriers to drug delivery in solid tumors. *Tissue barriers* 2014, 2, e29528.
293. Muggia, F. M.; Hainsworth, J. D.; Jeffers, S.; Miller, P.; Groshen, S.; Tan, M.; Roman, L.; Uziely, B.; Muderspach, L.; Garcia, A.; Burnett, A.; Greco, F. A.; Morrow, C. P.; Paradiso, L. J.; Liang, L. J. Phase II study of liposomal doxorubicin in refractory ovarian cancer: antitumor activity and toxicity modification by liposomal encapsulation. *J Clin Oncol* 1997, 15, 987-93.
294. Northfelt, D. W.; Dezube, B. J.; Thommes, J. A.; Miller, B. J.; Fischl, M. A.; Friedman-Kien, A.; Kaplan, L. D.; Du Mond, C.; Mamelok, R. D.; Henry, D. H. Pegylated-liposomal doxorubicin versus doxorubicin, bleomycin, and vincristine in the treatment of AIDS-related Kaposi's sarcoma: results of a randomized phase III clinical trial. *J Clin Oncol* 1998, 16, 2445-51.
295. Ranson, M. R.; Carmichael, J.; O'Byrne, K.; Stewart, S.; Smith, D.; Howell, A. Treatment of advanced breast cancer with sterically stabilized liposomal doxorubicin: results of a multicenter phase II trial. *J Clin Oncol* 1997, 15, 3185-91.
296. Stewart, S.; Jablonowski, H.; Goebel, F. D.; Arasteh, K.; Spittle, M.; Rios, A.; Aboulafia, D.; Galleshaw, J.; Dezube, B. J. Randomized comparative trial of pegylated liposomal doxorubicin versus bleomycin and vincristine in the treatment of AIDS-related Kaposi's sarcoma. International Pegylated Liposomal Doxorubicin Study Group. *J Clin Oncol* 1998, 16, 683-91.

297. Gordon, A. N.; Fleagle, J. T.; Guthrie, D.; Parkin, D. E.; Gore, M. E.; Lacave, A. J. Recurrent epithelial ovarian carcinoma: a randomized phase III study of pegylated liposomal doxorubicin versus topotecan. *J Clin Oncol* 2001, 19, 3312-22.
298. O'Brien, M. E.; Wigler, N.; Inbar, M.; Rosso, R.; Grischke, E.; Santoro, A.; Catane, R.; Kieback, D. G.; Tomczak, P.; Ackland, S. P.; Orlandi, F.; Mellars, L.; Alland, L.; Tandler, C.; Group, C. B. C. S. Reduced cardiotoxicity and comparable efficacy in a phase III trial of pegylated liposomal doxorubicin HCl (CAELYX/Doxil) versus conventional doxorubicin for first-line treatment of metastatic breast cancer. *Ann Oncol* 2004, 15, 440-9.
299. Harrington, K. J.; Mohammadtaghi, S.; Uster, P. S.; Glass, D.; Peters, A. M.; Vile, R. G.; Stewart, J. S. Effective targeting of solid tumors in patients with locally advanced cancers by radiolabeled pegylated liposomes. *Clin Cancer Res* 2001, 7, 243-54.
300. Lasic, D. D. *Liposomes from physics to applications*. Elsevier: 1993; p 63-107.
301. Bakker, W. H.; Albert, R.; Bruns, C.; Breeman, W. A.; Hofland, L. J.; Marbach, P.; Pless, J.; Pralet, D.; Stolz, B.; Koper, J. W.; et al. [¹¹¹In-DTPA-D-Phe1]-octreotide, a potential radiopharmaceutical for imaging of somatostatin receptor-positive tumors: synthesis, radiolabeling and in vitro validation. *Life Sci* 1991, 49, 1583-91.
302. Gabizon, A. A. Liposomal anthracyclines. *Hematol Oncol Clin North Am* 1994, 8, 431-50.
303. Ishida, T.; Harashima, H.; Kiwada, H. Liposome clearance. *Biosci Rep* 2002, 22, 197-224.
304. Sarin, H. Physiologic upper limits of pore size of different blood capillary types and another perspective on the dual pore theory of microvascular permeability. *J Angiogenesis Res* 2010, 2, 14.
305. Bol, K.; Haeck, J. C.; Groen, H. C.; Niessen, W. J.; Bernsen, M. R.; de Jong, M.; Veenland, J. F. Can DCE-MRI explain the heterogeneity in radiopeptide uptake imaged by SPECT in a pancreatic neuroendocrine tumor model? *PLoS one* 2013, 8, e77076.
306. Toy, R.; Hayden, E.; Camann, A.; Berman, Z.; Vicente, P.; Tran, E.; Meyers, J.; Pansky, J.; Peiris, P. M.; Wu, H.; Exner, A.; Wilson, D.; Ghaghada, K. B.; Karathanasis, E. Multimodal in vivo imaging exposes the voyage of nanoparticles in tumor microcirculation. *ACS nano* 2013, 7, 3118-29.
307. Harrington, K. J.; Rowlinson-Busza, G.; Syrigos, K. N.; Uster, P. S.; Abra, R. M.; Stewart, J. S. Biodistribution and pharmacokinetics of ¹¹¹In-DTPA-labelled pegylated liposomes in a human tumour xenograft model: implications for novel targeting strategies. *Br J Cancer* 2000, 83, 232-8.
308. Koukourakis, M. I.; Koukouraki, S.; Giatromanolaki, A.; Archimandritis, S. C.; Skarlatos, J.; Beroukas, K.; Bizakis, J. G.; Retalis, G.; Karkavitsas, N.; Helidonis, E. S. Liposomal doxorubicin and conventionally fractionated radiotherapy in the treatment of locally advanced non-small-cell lung cancer and head and neck cancer. *J Clin Oncol* 1999, 17, 3512-21.
309. Papahadjopoulos, D.; Allen, T. M.; Gabizon, A.; Mayhew, E.; Matthay, K.; Huang, S. K.; Lee, K. D.; Woodle, M. C.; Lasic, D. D.; Redemann, C.; et al. Sterically stabilized liposomes: improvements in pharmacokinetics and antitumor therapeutic efficacy. *Proc Natl Acad Sci U.S.A* 1991, 88, 11460-4.
310. Gabizon, A.; Shmeeda, H.; Barenholz, Y. Pharmacokinetics of pegylated liposomal doxorubicin - Review of animal and human studies. *Clin Pharmacokinet* 2003, 42, 419-436.
311. Brown, J. M.; Giaccia, A. J. The unique physiology of solid tumors: opportunities (and problems) for cancer therapy. *Cancer Res* 1998, 58, 1408-16.
312. Durand, R. E. The influence of microenvironmental factors during cancer therapy. *In Vivo* 1994, 8, 691-702.
313. Maeda, H. Vascular permeability in cancer and infection as related to macromolecular drug delivery, with emphasis on the EPR effect for tumor-selective drug targeting. *Proc Jpn Acad* 2012, 88, 53-71.

314. Folkman, J. Angiogenesis in cancer, vascular, rheumatoid and other disease. *Nature medicine* 1995, 1, 27-31.
315. Jain, R. K. Normalizing tumor microenvironment to treat cancer: bench to bedside to biomarkers. *J Clin Oncol* 2013, 31, 2205-18.
316. Boerman, O. C.; Storm, G.; Oyen, W. J.; van Bloois, L.; van der Meer, J. W.; Claessens, R. A.; Crommelin, D. J.; Corstens, F. H. Sterically stabilized liposomes labeled with indium-111 to image focal infection. *J Nucl Med* 1995, 36, 1639-44.
317. Caron, W. P.; Song, G.; Kumar, P.; Rawal, S.; Zamboni, W. C. Interpatient pharmacokinetic and pharmacodynamic variability of carrier-mediated anticancer agents. *Clin Pharmacol Ther* 2012, 91, 802-12.
318. Furukawa, H.; Iwata, R.; Moriyama, N. Growth rate of pancreatic adenocarcinoma: initial clinical experience. *Pancreas* 2001, 22, 366-9.
319. Maeda, H.; Nakamura, H.; Fang, J. The EPR effect for macromolecular drug delivery to solid tumors: Improvement of tumor uptake, lowering of systemic toxicity, and distinct tumor imaging in vivo. *Adv Drug Deliv Rev* 2013, 65, 71-9.
320. Wong, P. P.; Demircioglu, F.; Ghazaly, E.; Alrawashdeh, W.; Stratford, M. R.; Scudamore, C. L.; Cereser, B.; Crnogorac-Jurcovic, T.; McDonald, S.; Elia, G.; Hagemann, T.; Kocher, H. M.; Hodivala-Dilke, K. M. Dual-action combination therapy enhances angiogenesis while reducing tumor growth and spread. *Cancer Cell* 2015, 27, 123-37.
321. Bridges, E.; Harris, A. L. Vascular-promoting therapy reduced tumor growth and progression by improving chemotherapy efficacy. *Cancer Cell* 2015, 27, 7-9.
322. Li, L.; ten Hagen, T. L. M.; Bolkestein, M.; Gasselhuber, A.; Yatvin, J.; van Rhooon, G. C.; Eggermont, A. M. M.; Haemmerich, D.; Koning, G. A. Improved intratumoral nanoparticle extravasation and penetration by mild hyperthermia. *J Control Release* 2013, 167, 130-137.
323. Jain, R. K. Normalization of Tumor Vasculature: An Emerging Concept in Antiangiogenic Therapy. *Science* 2005, 307, 58-62.
324. Nagy, J. A.; Chang, S. H.; Dvorak, A. M.; Dvorak, H. F. Why are tumour blood vessels abnormal and why is it important to know? *Br J Cancer* 2009, 100, 865-9.
325. Hobbs, S. K.; Monsky, W. L.; Yuan, F.; Roberts, W. G.; Griffith, L.; Torchilin, V. P.; Jain, R. K. Regulation of transport pathways in tumor vessels: role of tumor type and microenvironment. *Proc Natl Acad Sci U.S.A* 1998, 95, 4607-12.
326. Kobayashi, H.; Watanabe, R.; Choyke, P. L. Improving conventional enhanced permeability and retention (EPR) effects; what is the appropriate target? *Theranostics* 2013, 4, 81-9.
327. Allen, T. M.; Cullis, P. R. Drug delivery systems: entering the mainstream. *Science* 2004, 303, 1818-22.
328. Allen, T. M.; Cullis, P. R. Liposomal drug delivery systems: from concept to clinical applications. *Adv Drug Deliv Rev* 2013, 65, 36-48.
329. Laginha, K. M.; Verwoert, S.; Charrois, G. J. R.; Allen, T. M. Determination of doxorubicin levels in whole tumor and tumor nuclei in murine breast cancer tumors. *Clin Cancer Res* 2005, 11, 6944-6949.
330. Li, L.; ten Hagen, T. L.; Hossann, M.; Suss, R.; van Rhooon, G. C.; Eggermont, A. M.; Haemmerich, D.; Koning, G. A. Mild hyperthermia triggered doxorubicin release from optimized stealth thermosensitive liposomes improves intratumoral drug delivery and efficacy. *J Control Release* 2013, 168, 142-50.
331. de Smet, M.; Langereis, S.; van den Bosch, S.; Grull, H. Temperature-sensitive liposomes for doxorubicin delivery under MRI guidance. *J Control Release* 2010, 143, 120-7.

332. Lindner, L. H.; Eichhorn, M. E.; Eibl, H.; Teichert, N.; Schmitt-Sody, M.; Issels, R. D.; Dellian, M. Novel temperature-sensitive liposomes with prolonged circulation time. *Clin Cancer Res* 2004, 10, 2168-78.
333. de Smet, M.; Heijman, E.; Langereis, S.; Hijnen, N. M.; Grull, H. Magnetic resonance imaging of high intensity focused ultrasound mediated drug delivery from temperature-sensitive liposomes: an in vivo proof-of-concept study. *J Control Release* 2011, 150, 102-10.
334. Celsion. Phase 3 Study of ThermoDox With Radiofrequency Ablation (RFA) in Treatment of Hepatocellular Carcinoma (HCC). 2008.
335. Celsion. Study of ThermoDox With Standardized Radiofrequency Ablation (RFA) for treatment of Hepatocellular Carcinoma (HCC) (OPTIMA). 2014.
336. Overgaard, J. Effect of hyperthermia on malignant cells in vivo: A review and a hypothesis. *Cancer* 1977, 39, 2637-46.
337. Song, C. W. Effect of Local Hyperthermia on Blood-Flow and Microenvironment - a Review. *Cancer Res* 1984, 44, 4721-30.
338. Calabro, A.; Singletary, S. E.; Tucker, S.; Boddie, A.; Spitzer, G.; Cavaliere, R. In vitro thermochemosensitivity screening of spontaneous human tumors: significant potentiation for cisplatin but not adriamycin. *Int J Cancer* 1989, 43, 385-90.
339. Sakaguchi, Y.; Stephens, L. C.; Makino, M.; Kaneko, T.; Strebel, F. R.; Danhauser, L. L.; Jenkins, G. N.; Bull, J. M. Apoptosis in tumors and normal tissues induced by whole body hyperthermia in rats. *Cancer Res* 1995, 55, 5459-64.
340. Yarmolenko, P. S.; Moon, E. J.; Landon, C.; Manzoor, A.; Hochman, D. W.; Viglianti, B. L.; Dewhirst, M. W. Thresholds for thermal damage to normal tissues: an update. *Int J Hyperthermia* 2011, 27, 320-43.
341. Hildebrandt, B.; Wust, P.; Ahlers, O.; Dieing, A.; Sreenivasa, G.; Kerner, T.; Felix, R.; Riess, H. The cellular and molecular basis of hyperthermia. *Crit Rev Oncol Hematol* 2002, 43, 33-56.
342. Issels, R. D.; Lindner, L. H.; Verweij, J.; Wust, P.; Reichardt, P.; Schem, B. C.; Abdel-Rahman, S.; Daugaard, S.; Salat, C.; Wendtner, C. M.; Vujaskovic, Z.; Wessalowski, R.; Jauch, K. W.; Durr, H. R.; Ploner, F.; Baur-Melnyk, A.; Mansmann, U.; Hiddemann, W.; Blay, J. Y.; Hohenberger, P.; European Organisation for, R.; Treatment of Cancer Soft, T.; Bone Sarcoma, G.; European Society for Hyperthermic, O. Neo-adjuvant chemotherapy alone or with regional hyperthermia for localised high-risk soft-tissue sarcoma: a randomised phase 3 multicentre study. *Lancet Oncol* 2010, 11, 561-70.
343. Bates, D. A.; Mackillop, W. J. Hyperthermia, adriamycin transport, and cytotoxicity in drug-sensitive and -resistant Chinese hamster ovary cells. *Cancer Res* 1986, 46, 5477-81.
344. Kawai, H.; Minamiya, Y.; Kitamura, M.; Matsuzaki, I.; Hashimoto, M.; Suzuki, H.; Abo, S. Direct measurement of doxorubicin concentration in the intact, living single cancer cell during hyperthermia. *Cancer* 1997, 79, 214-9.
345. Huang, S. K.; Stauffer, P. R.; Hong, K.; Guo, J. W.; Phillips, T. L.; Huang, A.; Papahadjopoulos, D. Liposomes and hyperthermia in mice: increased tumor uptake and therapeutic efficacy of doxorubicin in sterically stabilized liposomes. *Cancer Res* 1994, 54, 2186-91.
346. Kong, G.; Braun, R. D.; Dewhirst, M. W. Characterization of the effect of hyperthermia on nanoparticle extravasation from tumor vasculature. *Cancer Res* 2001, 61, 3027-32.
347. Matteucci, M. L.; Anyarambhatla, G.; Rosner, G.; Azuma, C.; Fisher, P. E.; Dewhirst, M. W.; Needham, D.; Thrall, D. E. Hyperthermia increases accumulation of technetium-99m-labeled liposomes in feline sarcomas. *Clin Cancer Res* 2000, 6, 3748-55.

348. Alvarez Secord, A.; Jones, E. L.; Hahn, C. A.; Petros, W. P.; Yu, D.; Havrilesky, L. J.; Soper, J. T.; Berchuck, A.; Spasojevic, I.; Clarke-Pearson, D. L.; Prosnitz, L. R.; Dewhirst, M. W. Phase I/II trial of intravenous Doxil and whole abdomen hyperthermia in patients with refractory ovarian cancer. *Int J Hyperthermia* 2005, 21, 333-47.
349. Vujaskovic, Z.; Kim, D. W.; Jones, E.; Lan, L.; McCall, L.; Dewhirst, M. W.; Craciunescu, O.; Stauffer, P.; Liotcheva, V.; Betof, A.; Blackwell, K. A phase I/II study of neoadjuvant liposomal doxorubicin, paclitaxel, and hyperthermia in locally advanced breast cancer. *Int J Hyperthermia* 2010, 26, 514-21.
350. Li, L.; ten Hagen, T. L.; Haeri, A.; Soullie, T.; Scholten, C.; Seynhaeve, A. L.; Eggermont, A. M.; Koning, G. A. A novel two-step mild hyperthermia for advanced liposomal chemotherapy. *J Control Release* 2014, 174, 202-8.
351. Bartlett, G. R. Phosphorus Assay in Column Chromatography. *J Biol Chem* 1959, 234, 466-468.
352. Nagelkerke, A.; Bussink, J.; Sweep, F. C.; Span, P. N. Generation of multicellular tumor spheroids of breast cancer cells: how to go three-dimensional. *Anal Biochem* 2013, 437, 17-9.
353. Lokerse, W. J. M.; Kneepkens, E. C. M.; ten Hagen, T. L. M.; Eggermont, A. M. M.; Grüll, H.; Koning, G. A. In depth study on thermosensitive liposomes: Optimizing formulations for tumor specific therapy and in vitro to in vivo relations. *Biomaterials* 2016, <http://dx.doi.org/10.1016/j.biomaterials.2015.12.023>.
354. Eddy, H. A. Alterations in tumor microvasculature during hyperthermia. *Radiology* 1980, 137, 515-521.
355. Hahn, G. M.; Strande, D. P. Cytotoxic effects of hyperthermia and adriamycin on Chinese hamster cells. *J Natl Cancer Inst* 1976, 57, 1063-7.
356. Herman, T. S. Temperature dependence of adriamycin, cis-diamminedichloroplatinum, bleomycin, and 1,3-bis(2-chloroethyl)-1-nitrosourea cytotoxicity in vitro. *Cancer Res* 1983, 43, 517-20.
357. Nagaoka, S.; Kawasaki, S.; Sasaki, K.; Nakanishi, T. Intracellular uptake, retention and cytotoxic effect of adriamycin combined with hyperthermia in vitro. *Jpn J Cancer Res* 1986, 77, 205-11.
358. Rice, G. C.; Hahn, G. M. Modulation of adriamycin transport by hyperthermia as measured by fluorescence-activated cell sorting. *Cancer Chemother Pharmacol* 1987, 20, 183-7.
359. Moriyama-Gonda, N.; Igawa, M.; Shiina, H.; Wada, Y. Heat-induced membrane damage combined with adriamycin on prostate carcinoma PC-3 cells: correlation of cytotoxicity, permeability and P-glycoprotein or metallothionein expression. *Br J Urol* 1998, 82, 552-9.
360. Hirschhaeuser, F.; Menne, H.; Dittfeld, C.; West, J.; Mueller-Klieser, W.; Kunz-Schughart, L. A. Multicellular tumor spheroids: an underestimated tool is catching up again. *J Biotechnol* 2010, 148, 3-15.
361. Mikhail, A. S.; Etezeadi, S.; Ekdawi, S. N.; Stewart, J.; Allen, C. Image-based analysis of the size- and time-dependent penetration of polymeric micelles in multicellular tumor spheroids and tumor xenografts. *Int J Pharm* 2014, 464, 168-77.
362. Kim, T. H.; Mount, C. W.; Gombotz, W. R.; Pun, S. H. The delivery of doxorubicin to 3-D multicellular spheroids and tumors in a murine xenograft model using tumor-penetrating triblock polymeric micelles. *Biomaterials* 2010, 31, 7386-97.
363. Hijnen, N.; Langereis, S.; Grull, H. Magnetic resonance guided high-intensity focused ultrasound for image-guided temperature-induced drug delivery. *Adv Drug Deliv Rev* 2014, 72, 65-81.
364. McGuire, S.; Yuan, F. Improving interstitial transport of macromolecules through reduction in cell volume fraction in tumor tissues. *Nanomedicine* 2012, 8, 1088-95.

365. Jang, S. H.; Wientjes, M. G.; Au, J. L. Enhancement of paclitaxel delivery to solid tumors by apoptosis-inducing pretreatment: effect of treatment schedule. *J Pharmacol Exp Ther* 2001, 296, 1035-42.
366. Heneweer, C.; Holland, J. P.; Divilov, V.; Carlin, S.; Lewis, J. S. Magnitude of Enhanced Permeability and Retention Effect in Tumors with Different Phenotypes: Zr-89-Albumin as a Model System. *J Nucl Med* 2011, 52, 625-633.
367. Sengupta, S.; Kulkarni, A. Design principles for clinical efficacy of cancer nanomedicine: a look into the basics. *ACS nano* 2013, 7, 2878-82.
368. Young, R. C.; Ozols, R. F.; Myers, C. E. The anthracycline antineoplastic drugs. *N Engl J Med* 1981, 305, 139-53.
369. Tacar, O.; Sriamornsak, P.; Dass, C. R. Doxorubicin: an update on anticancer molecular action, toxicity and novel drug delivery systems. *J Pharm Pharmacol* 2013, 65, 157-70.
370. Volkova, M.; Russell, R., 3rd. Anthracycline cardiotoxicity: prevalence, pathogenesis and treatment. *Curr Cardiol Rev* 2011, 7, 214-20.
371. von Roemeling, C.; Jiang, W.; Chan, C. K.; Weissman, I. L.; Kim, B. Y. Breaking Down the Barriers to Precision Cancer Nanomedicine. *Trends Biotechnol* 2016.
372. Kataoka, K.; Harada, A.; Nagasaki, Y. Block copolymer micelles for drug delivery: design, characterization and biological significance. *Adv Drug Deliv Rev* 2001, 47, 113-31.
373. Nishiyama, N.; Kataoka, K. Current state, achievements, and future prospects of polymeric micelles as nanocarriers for drug and gene delivery. *Pharmacol Ther* 2006, 112, 630-48.
374. Cabral, H.; Matsumoto, Y.; Mizuno, K.; Chen, Q.; Murakami, M.; Kimura, M.; Terada, Y.; Kano, M. R.; Miyazono, K.; Uesaka, M.; Nishiyama, N.; Kataoka, K. Accumulation of sub-100 nm polymeric micelles in poorly permeable tumours depends on size. *Nat Nanotechnol* 2011, 6, 815-23.
375. Cabral, H.; Kataoka, K. Progress of drug-loaded polymeric micelles into clinical studies. *J Control Release* 2014, 190, 465-76.
376. Rowinsky, E. K.; Donehower, R. C. Paclitaxel (taxol). *N Engl J Med* 1995, 332, 1004-14.
377. Kim, H. S.; Lee, J. Y.; Lim, S. H.; Sun, J. M.; Lee, S. H.; Ahn, J. S.; Park, K.; Moon, S. H.; Ahn, M. J. A Prospective Phase II Study of Cisplatin and Cremophor EL-Free Paclitaxel (Genexol-PM) in Patients with Unresectable Thymic Epithelial Tumors. *J Thorac Oncol* 2015, 10, 1800-6.
378. Gradishar, W. J.; Tjulandin, S.; Davidson, N.; Shaw, H.; Desai, N.; Bhar, P.; Hawkins, M.; O'Shaughnessy, J. Phase III trial of nanoparticle albumin-bound paclitaxel compared with polyethylated castor oil-based paclitaxel in women with breast cancer. *J Clin Oncol* 2005, 23, 7794-803.
379. Hamaguchi, T.; Doi, T.; Eguchi-Nakajima, T.; Kato, K.; Yamada, Y.; Shimada, Y.; Fuse, N.; Ohtsu, A.; Matsumoto, S.; Takanashi, M.; Matsumura, Y. Phase I study of NK012, a novel SN-38-incorporating micellar nanoparticle, in adult patients with solid tumors. *Clin Cancer Res* 2010, 16, 5058-66.
380. Wang, X.; Guo, Z. Targeting and delivery of platinum-based anticancer drugs. *Chem Soc Rev* 2013, 42, 202-24.
381. Seetharamu, N.; Kim, E.; Hochster, H.; Martin, F.; Muggia, F. Phase II study of liposomal cisplatin (SPI-77) in platinum-sensitive recurrences of ovarian cancer. *Anticancer Res* 2010, 30, 541-5.
382. White, S. C.; Lorigan, P.; Margison, G. P.; Margison, J. M.; Martin, F.; Thatcher, N.; Anderson, H.; Ranson, M. Phase II study of SPI-77 (sterically stabilised liposomal cisplatin) in advanced non-small-cell lung cancer. *Br J Cancer* 2006, 95, 822-8.
383. Zamboni, W. C.; Gervais, A. C.; Egorin, M. J.; Schellens, J. H.; Zuhowski, E. G.; Pluim, D.; Joseph, E.; Hamburger, D. R.; Working, P. K.; Colbern, G.; Tonda, M. E.; Potter, D. M.; Eiseman,

- J. L. Systemic and tumor disposition of platinum after administration of cisplatin or STEALTH liposomal-cisplatin formulations (SPI-077 and SPI-077 B103) in a preclinical tumor model of melanoma. *Cancer Chemother Pharmacol* 2004, 53, 329-36.
384. Welch, D. R. Tumor Heterogeneity--A 'Contemporary Concept' Founded on Historical Insights and Predictions. *Cancer Res* 2016, 76, 4-6.
385. Dawidczyk, C. M.; Kim, C.; Park, J. H.; Russell, L. M.; Lee, K. H.; Pomper, M. G.; Searson, P. C. State-of-the-art in design rules for drug delivery platforms: lessons learned from FDA-approved nanomedicines. *J Control Release* 2014, 187, 133-44.
386. Waite, C. L.; Roth, C. M. Nanoscale drug delivery systems for enhanced drug penetration into solid tumors: current progress and opportunities. *Crit Rev Biomed Eng* 2012, 40, 21-41.
387. Pluen, A.; Boucher, Y.; Ramanujan, S.; McKee, T. D.; Gohongi, T.; di Tomaso, E.; Brown, E. B.; Izumi, Y.; Campbell, R. B.; Berk, D. A.; Jain, R. K. Role of tumor-host interactions in interstitial diffusion of macromolecules: cranial vs. subcutaneous tumors. *Proc Natl Acad Sci U.S.A* 2001, 98, 4628-33.
388. Grill, J.; Lamfers, M. L.; van Beusechem, V. W.; Dirven, C. M.; Pherai, D. S.; Kater, M.; Van der Valk, P.; Vogels, R.; Vandertop, W. P.; Pinedo, H. M.; Curiel, D. T.; Gerritsen, W. R. The organotypic multicellular spheroid is a relevant three-dimensional model to study adenovirus replication and penetration in human tumors in vitro. *Mol Ther* 2002, 6, 609-14.
389. Kostarelos, K.; Emfietzoglou, D.; Papakostas, A.; Yang, W. H.; Ballangrud, A.; Sgouros, G. Binding and interstitial penetration of liposomes within avascular tumor spheroids. *Int J Cancer* 2004, 112, 713-21.
390. Dreher, M. R.; Liu, W.; Michelich, C. R.; Dewhirst, M. W.; Yuan, F.; Chilkoti, A. Tumor vascular permeability, accumulation, and penetration of macromolecular drug carriers. *J Natl Cancer Inst* 2006, 98, 335-44.
391. Goodman, T. T.; Olive, P. L.; Pun, S. H. Increased nanoparticle penetration in collagenase-treated multicellular spheroids. *Int J Nanomedicine* 2007, 2, 265-74.
392. Eikenes, L.; Tufto, I.; Schnell, E. A.; Bjorkoy, A.; De Lange Davies, C. Effect of collagenase and hyaluronidase on free and anomalous diffusion in multicellular spheroids and xenografts. *Anti-cancer Res* 2010, 30, 359-68.
393. Choi, I. K.; Strauss, R.; Richter, M.; Yun, C. O.; Lieber, A. Strategies to increase drug penetration in solid tumors. *Front Oncol* 2013, 3, 193.
394. Coussens, L. M.; Werb, Z. Matrix metalloproteinases and the development of cancer. *Chem Biol* 1996, 3, 895-904.
395. Wicki, A.; Witzigmann, D.; Balasubramanian, V.; Huwyler, J. Nanomedicine in cancer therapy: challenges, opportunities, and clinical applications. *J Control Release* 2015, 200, 138-57.
396. Wang, Y.; Fan, Z.; Shao, L.; Kong, X.; Hou, X.; Tian, D.; Sun, Y.; Xiao, Y.; Yu, L. Nanobody-derived nanobiotechnology tool kits for diverse biomedical and biotechnology applications. *Int J Nanomedicine* 2016, 11, 3287-303.
397. Van Audenhove, I.; Gettemans, J. Nanobodies as Versatile Tools to Understand, Diagnose, Visualize and Treat Cancer. *EBioMedicine* 2016, 8, 40-8.
398. Jamnani, F. R.; Rahbarizadeh, F.; Shokrgozar, M. A.; Ahmadvand, D.; Mahboudi, F.; Sharifzadeh, Z. Targeting high affinity and epitope-distinct oligoclonal nanobodies to HER2 over-expressing tumor cells. *Exp Cell Res* 2012, 318, 1112-24.
399. Stordahl, T. S.; Denayer, T.; Moen, S. H.; Standal, T.; Borset, M.; Ververken, C.; Ro, T. B. Anti-c-MET Nanobody - a new potential drug in multiple myeloma treatment. *Eur J Haematol* 2013, 91, 399-410.

400. Behdani, M.; Zeinali, S.; Khanahmad, H.; Karimipour, M.; Asadzadeh, N.; Azadmanesh, K.; Khabiri, A.; Schoonoghe, S.; Habibi Anbouhi, M.; Hassanzadeh-Ghassabeh, G.; Muyldermans, S. Generation and characterization of a functional Nanobody against the vascular endothelial growth factor receptor-2; angiogenesis cell receptor. *Mol Immunol* 2012, 50, 35-41.
401. Huet, H. A.; Growney, J. D.; Johnson, J. A.; Li, J.; Bilic, S.; Ostrom, L.; Zafari, M.; Kowal, C.; Yang, G.; Royo, A.; Jensen, M.; Dombrecht, B.; Meerschaert, K. R.; Kolkman, J. A.; Cromie, K. D.; Mosher, R.; Gao, H.; Schuller, A.; Isaacs, R.; Sellers, W. R.; Ettenberg, S. A. Multivalent nanobodies targeting death receptor 5 elicit superior tumor cell killing through efficient caspase induction. *MAbs* 2014, 6, 1560-70.
402. Jahnichen, S.; Blanchetot, C.; Maussang, D.; Gonzalez-Pajuelo, M.; Chow, K. Y.; Bosch, L.; De Vrieze, S.; Serruys, B.; Ulrichts, H.; Vandeveldel, W.; Saunders, M.; De Haard, H. J.; Schols, D.; Leurs, R.; Vanlandschoot, P.; Verrips, T.; Smit, M. J. CXCR4 nanobodies (VHH-based single variable domains) potently inhibit chemotaxis and HIV-1 replication and mobilize stem cells. *Proc Natl Acad Sci U.S.A* 2010, 107, 20565-70.
403. Blanchetot, C.; Verzijl, D.; Mujic-Delic, A.; Bosch, L.; Rem, L.; Leurs, R.; Verrips, C. T.; Saunders, M.; de Haard, H.; Smit, M. J. Neutralizing nanobodies targeting diverse chemokines effectively inhibit chemokine function. *J Biol Chem* 2013, 288, 25173-82.
404. Massa, S.; Xavier, C.; De Vos, J.; Caveliers, V.; Lahoutte, T.; Muyldermans, S.; Devoogdt, N. Site-specific labeling of cysteine-tagged camelid single-domain antibody-fragments for use in molecular imaging. *Bioconjug Chem* 2014, 25, 979-88.
405. Oliveira, S.; Schiffelers, R. M.; van der Veecken, J.; van der Meel, R.; Vongpromek, R.; van Bergen En Henegouwen, P. M.; Storm, G.; Roovers, R. C. Downregulation of EGFR by a novel multivalent nanobody-liposome platform. *J Control Release* 2010, 145, 165-75.
406. Talelli, M.; Rijcken, C. J.; Oliveira, S.; van der Meel, R.; van Bergen En Henegouwen, P. M.; Lammers, T.; van Nostrum, C. F.; Storm, G.; Hennink, W. E. Nanobody-shell functionalized thermosensitive core-crosslinked polymeric micelles for active drug targeting. *J Control Release* 2011, 151, 183-92.
407. Altintas, I.; Heukers, R.; van der Meel, R.; Lacombe, M.; Amidi, M.; van Bergen En Henegouwen, P. M.; Hennink, W. E.; Schiffelers, R. M.; Kok, R. J. Nanobody-albumin nanoparticles (NANAPs) for the delivery of a multikinase inhibitor 17864 to EGFR overexpressing tumor cells. *J Control Release* 2013, 165, 110-8.
408. Davis, M. E.; Chen, Z. G.; Shin, D. M. Nanoparticle therapeutics: an emerging treatment modality for cancer. *Nat Rev Drug Discov* 2008, 7, 771-82.
409. Peer, D.; Karp, J. M.; Hong, S.; Farokhzad, O. C.; Margalit, R.; Langer, R. Nanocarriers as an emerging platform for cancer therapy. *Nat Nanotechnol* 2007, 2, 751-60.
410. Gao, Z.; Zhang, L.; Sun, Y. Nanotechnology applied to overcome tumor drug resistance. *J Control Release* 2012, 162, 45-55.
411. Ruoslahti, E. Peptides as targeting elements and tissue penetration devices for nanoparticles. *Adv Mater* 2012, 24, 3747-56.
412. Janas, T.; Janas, T. The selection of aptamers specific for membrane molecular targets. *Cell Mol Biol Lett* 2011, 16, 25-39.
413. Parker, N.; Turk, M. J.; Westrick, E.; Lewis, J. D.; Low, P. S.; Leamon, C. P. Folate receptor expression in carcinomas and normal tissues determined by a quantitative radioligand binding assay. *Anal Biochem* 2005, 338, 284-93.
414. Qian, Z. M.; Li, H.; Sun, H.; Ho, K. Targeted drug delivery via the transferrin receptor-mediated endocytosis pathway. *Pharmacol Rev* 2002, 54, 561-87.

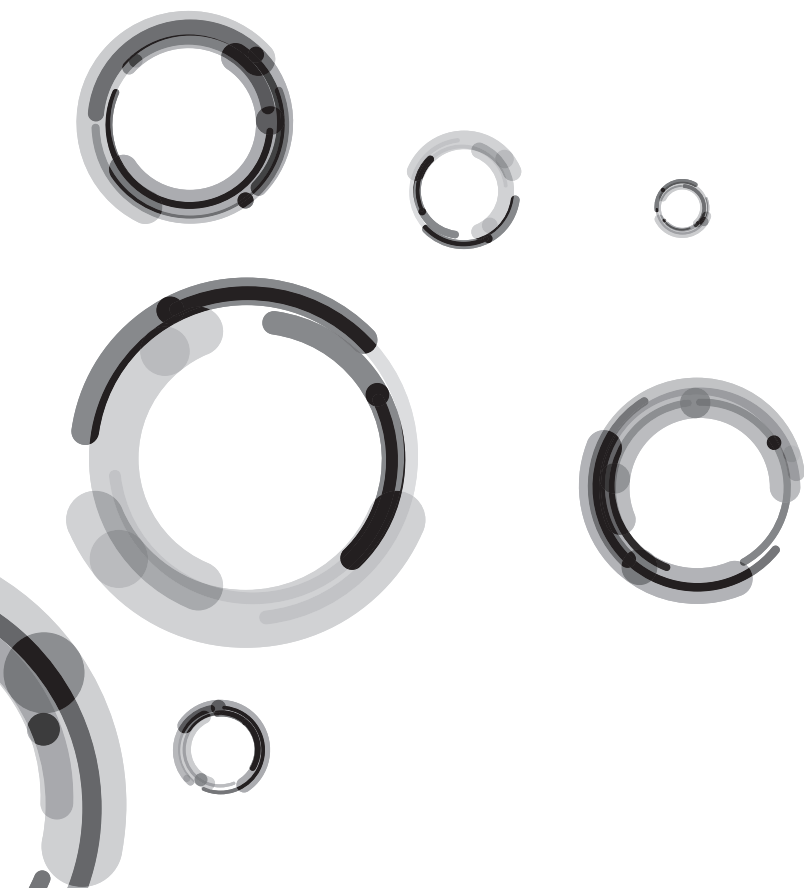
415. Daniels, T. R.; Bernabeu, E.; Rodriguez, J. A.; Patel, S.; Kozman, M.; Chiappetta, D. A.; Holler, E.; Ljubimova, J. Y.; Helguera, G.; Penichet, M. L. The transferrin receptor and the targeted delivery of therapeutic agents against cancer. *Biochim Biophys Acta* 2012, 1820, 291-317.
416. Temming, K.; Schiffelers, R. M.; Molema, G.; Kok, R. J. RGD-based strategies for selective delivery of therapeutics and imaging agents to the tumour vasculature. *Drug Resist Updat* 2005, 8, 381-402.
417. Guo, P.; Yang, J.; Jia, D.; Moses, M. A.; Auguste, D. T. ICAM-1-Targeted, Lcn2 siRNA-Encapsulating Liposomes are Potent Anti-angiogenic Agents for Triple Negative Breast Cancer. *Theranostics* 2016, 6, 1-13.
418. Arabi, L.; Badiie, A.; Mosaffa, F.; Jaafari, M. R. Targeting CD44 expressing cancer cells with anti-CD44 monoclonal antibody improves cellular uptake and antitumor efficacy of liposomal doxorubicin. *J Control Release* 2015, 220, 275-86.
419. Rotman, M.; Welling, M. M.; Bunschoten, A.; de Backer, M. E.; Rip, J.; Nabuurs, R. J.; Gaillard, P. J.; van Buchem, M. A.; van der Maarel, S. M.; van der Weerd, L. Enhanced glutathione PEGylated liposomal brain delivery of an anti-amyloid single domain antibody fragment in a mouse model for Alzheimer's disease. *J Control Release* 2015, 203, 40-50.
420. Lum, D. H.; Matsen, C.; Welm, A. L.; Welm, B. E. Overview of human primary tumorgraft models: comparisons with traditional oncology preclinical models and the clinical relevance and utility of primary tumorgrafts in basic and translational oncology research. *Curr Protoc Pharmacol* 2012, Chapter 14, Unit 14 22.
421. Schmidt, M. M.; Wittrup, K. D. A modeling analysis of the effects of molecular size and binding affinity on tumor targeting. *Mol Cancer Ther* 2009, 8, 2861-71.
422. Tahover, E.; Patil, Y. P.; Gabizon, A. A. Emerging delivery systems to reduce doxorubicin cardiotoxicity and improve therapeutic index: focus on liposomes. *Anticancer Drugs* 2015, 26, 241-58.
423. McDonald, D. M.; Thurston, G.; Baluk, P. Endothelial gaps as sites for plasma leakage in inflammation. *Microcirculation* 1999, 6, 7-22.
424. Matsumoto, Y.; Nichols, J. W.; Toh, K.; Nomoto, T.; Cabral, H.; Miura, Y.; Christie, R. J.; Yamada, N.; Ogura, T.; Kano, M. R.; Matsumura, Y.; Nishiyama, N.; Yamasoba, T.; Bae, Y. H.; Kataoka, K. Vascular bursts enhance permeability of tumour blood vessels and improve nanoparticle delivery. *Nat Nanotechnol* 2016, 11, 533-8.
425. Sykes, E. A.; Dai, Q.; Sarsons, C. D.; Chen, J.; Rocheleau, J. V.; Hwang, D. M.; Zheng, G.; Cramb, D. T.; Rinker, K. D.; Chan, W. C. Tailoring nanoparticle designs to target cancer based on tumor pathophysiology. *Proc Natl Acad Sci U.S.A* 2016, 113, E1142-51.
426. Kizaka-Kondoh, S.; Inoue, M.; Harada, H.; Hiraoka, M. Tumor hypoxia: a target for selective cancer therapy. *Cancer Sci* 2003, 94, 1021-8.
427. Grantab, R.; Sivananthan, S.; Tannock, I. F. The penetration of anticancer drugs through tumor tissue as a function of cellular adhesion and packing density of tumor cells. *Cancer Res* 2006, 66, 1033-9.
428. Baxter, L. T.; Jain, R. K. Transport of fluid and macromolecules in tumors. I. Role of interstitial pressure and convection. *Microvasc Res* 1989, 37, 77-104.
429. Brown, E.; McKee, T.; diTomaso, E.; Pluen, A.; Seed, B.; Boucher, Y.; Jain, R. K. Dynamic imaging of collagen and its modulation in tumors in vivo using second-harmonic generation. *Nature Med* 2003, 9, 796-800.
430. Padera, T. P.; Stoll, B. R.; Tooredman, J. B.; Capen, D.; di Tomaso, E.; Jain, R. K. Pathology: cancer cells compress intratumour vessels. *Nature* 2004, 427, 695.

431. Jacobetz, M. A.; Chan, D. S.; Nesses, A.; Bapiro, T. E.; Cook, N.; Frese, K. K.; Feig, C.; Nakagawa, T.; Caldwell, M. E.; Zecchini, H. I.; Lolkema, M. P.; Jiang, P.; Kultti, A.; Thompson, C. B.; Maneval, D. C.; Jodrell, D. I.; Frost, G. I.; Shepard, H. M.; Skepper, J. N.; Tuveson, D. A. Hyaluronan impairs vascular function and drug delivery in a mouse model of pancreatic cancer. *Gut* 2013, 62, 112-20.
432. Jiang, W.; Huang, Y.; An, Y.; Kim, B. Y. Remodeling Tumor Vasculature to Enhance Delivery of Intermediate-Sized Nanoparticles. *ACS nano* 2015, 9, 8689-96.
433. Lu, D.; Wientjes, M. G.; Lu, Z.; Au, J. L. Tumor priming enhances delivery and efficacy of nano-medicines. *J Pharmacol Exp Ther* 2007, 322, 80-8.
434. Khawar, I. A.; Kim, J. H.; Kuh, H. J. Improving drug delivery to solid tumors: priming the tumor microenvironment. *J Control Release* 2015, 201, 78-89.
435. Yasuda, H.; Yamaya, M.; Nakayama, K.; Sasaki, T.; Ebihara, S.; Kanda, A.; Asada, M.; Inoue, D.; Suzuki, T.; Okazaki, T.; Takahashi, H.; Yoshida, M.; Kaneta, T.; Ishizawa, K.; Yamanda, S.; Tomita, N.; Yamasaki, M.; Kikuchi, A.; Kubo, H.; Sasaki, H. Randomized phase II trial comparing nitroglycerin plus vinorelbine and cisplatin with vinorelbine and cisplatin alone in previously untreated stage IIIB/IV non-small-cell lung cancer. *J Clin Oncol* 2006, 24, 688-94.
436. Chauhan, V. P.; Stylianopoulos, T.; Martin, J. D.; Popovic, Z.; Chen, O.; Kamoun, W. S.; Bawendi, M. G.; Fukumura, D.; Jain, R. K. Normalization of tumour blood vessels improves the delivery of nanomedicines in a size-dependent manner. *Nat Nanotechnol* 2012, 7, 383-8.
437. Theek, B.; Baues, M.; Ojha, T.; Mockel, D.; Veettil, S. K.; Steitz, J.; van Bloois, L.; Storm, G.; Kiessling, F.; Lammers, T. Sonoporation enhances liposome accumulation and penetration in tumors with low EPR. *J Control Release* 2016, 231, 77-85.
438. Monsky, W. L.; Fukumura, D.; Gohongi, T.; Ancukiewicz, M.; Weich, H. A.; Torchilin, V. P.; Yuan, F.; Jain, R. K. Augmentation of transvascular transport of macromolecules and nanoparticles in tumors using vascular endothelial growth factor. *Cancer Res* 1999, 59, 4129-35.
439. Eggermont, A. M.; Schraffordt Koops, H.; Lienard, D.; Kroon, B. B.; van Geel, A. N.; Hoekstra, H. J.; Lejeune, F. J. Isolated limb perfusion with high-dose tumor necrosis factor-alpha in combination with interferon-gamma and melphalan for nonresectable extremity soft tissue sarcomas: a multicenter trial. *J Clin Oncol* 1996, 14, 2653-65.
440. Dromi, S.; Frenkel, V.; Luk, A.; Traugher, B.; Angstadt, M.; Bur, M.; Poff, J.; Xie, J.; Libutti, S. K.; Li, K. C.; Wood, B. J. Pulsed-high intensity focused ultrasound and low temperature-sensitive liposomes for enhanced targeted drug delivery and antitumor effect. *Clin Cancer Res* 2007, 13, 2722-7.
441. Maeda, H. Toward a full understanding of the EPR effect in primary and metastatic tumors as well as issues related to its heterogeneity. *Adv Drug Deliv Rev* 2015, 91, 3-6.
442. van der Geest, T.; Laverman, P.; Metselaar, J. M.; Storm, G.; Boerman, O. C. Radionuclide imaging of liposomal drug delivery. *Expert Opin Drug Deliv* 2016, 13, 1231-42.
443. Goins, B.; Phillips, W. T.; Bao, A. Strategies for improving the intratumoral distribution of liposomal drugs in cancer therapy. *Expert Opin Drug Deliv* 2016, 13, 873-89.
444. Junior, A. D.; Mota, L. G.; Nunan, E. A.; Wainstein, A. J.; Wainstein, A. P.; Leal, A. S.; Cardoso, V. N.; De Oliveira, M. C. Tissue distribution evaluation of stealth pH-sensitive liposomal cisplatin versus free cisplatin in Ehrlich tumor-bearing mice. *Life Sci* 2007, 80, 659-64.
445. Andresen, T. L.; Jensen, S. S.; Jorgensen, K. Advanced strategies in liposomal cancer therapy: problems and prospects of active and tumor specific drug release. *Prog Lipid Res* 2005, 44, 68-97.
446. Shum, P.; Kim, J. M.; Thompson, D. H. Phototriggering of liposomal drug delivery systems. *Adv Drug Deliv Rev* 2001, 53, 273-84.

447. Schroeder, A.; Kost, J.; Barenholz, Y. Ultrasound, liposomes, and drug delivery: principles for using ultrasound to control the release of drugs from liposomes. *Chem Phys Lipids* 2009, 162, 1-16.
448. May, J. P.; Li, S. D. Hyperthermia-induced drug targeting. *Expert Opin Drug Deliv* 2013, 10, 511-27.
449. Ponce, A. M.; Vujaskovic, Z.; Yuan, F.; Needham, D.; Dewhirst, M. W. Hyperthermia mediated liposomal drug delivery. *Int J Hyperthermia* 2006, 22, 205-13.
450. Al-Ahmady, Z. S.; Scudamore, C. L.; Kostarelos, K. Triggered doxorubicin release in solid tumors from thermosensitive liposome-peptide hybrids: Critical parameters and therapeutic efficacy. *Int J Cancer* 2015, 137, 731-43.
451. Al-Ahmady, Z. S.; Chaloin, O.; Kostarelos, K. Monoclonal antibody-targeted, temperature-sensitive liposomes: in vivo tumor chemotherapeutics in combination with mild hyperthermia. *J Control Release* 2014, 196, 332-43.
452. Kim, M. S.; Lee, D. W.; Park, K.; Park, S. J.; Choi, E. J.; Park, E. S.; Kim, H. R. Temperature-triggered tumor-specific delivery of anticancer agents by cRGD-conjugated thermosensitive liposomes. *Colloids Surf B Biointerfaces* 2014, 116, 17-25.
453. Oerlemans, C.; Bult, W.; Bos, M.; Storm, G.; Nijssen, J. F.; Hennink, W. E. Polymeric micelles in anticancer therapy: targeting, imaging and triggered release. *Pharm Res* 2010, 27, 2569-89.
454. Deckers, R.; Moonen, C. T. Ultrasound triggered, image guided, local drug delivery. *J Control Release* 2010, 148, 25-33.
455. Swenson, C. E.; Haemmerich, D.; Maul, D. H.; Knox, B.; Ehrhart, N.; Reed, R. A. Increased Duration of Heating Boosts Local Drug Deposition during Radiofrequency Ablation in Combination with Thermally Sensitive Liposomes (ThermoDox) in a Porcine Model. *PLoS One* 2015, 10, e0139752.



Summary, Future Perspectives Samenvatting, Toekomstperspectief



SUMMARY

Advances in molecular biology have changed the field of cancer therapy dramatically over the past few decades by providing tools for the discovery and understanding of molecular features that determine and dictate therapeutic responses. Conventional chemotherapeutic regimens are associated with a small therapeutic window, limitations in optimal dosing, the development of drug resistance and high-grade toxicities, which often lead to the withdrawal of patients from treatment.

To address these problems, several adapted and novel drugs have been developed. Firstly, an ever increasing number of therapies are focused on specifically targeted drugs, using peptides or antibodies to deliver the drug to the desired target. Secondly, with the help of lipid or other nanoparticles the drug can be encapsulated, thereby favoring an enhanced biodistribution and preventing interaction with the immune system or healthy tissues. This approach has been shown to decrease adverse effects related to anticancer drugs. Finally, the combination of targeting and nanoparticles may have the added benefit of an enhanced internalization of the drug and/or drug-carrying nanoparticle, leading to an increase in therapeutic efficacy.

Despite successes in (targeted) nanomedicine, several issues remain to be solved. Biodistribution of nanomedicine is highly dependent on tumor morphology and the ability of nanoparticles to extravasate from blood vessels and accumulate in the tumor tissue. It has been stated that the structurally chaotic vasculature in solid tumors shows an enhanced permeability where nanoparticles can extravasate and remain in the tumor tissue due to a diminished clearing. This principle is called the enhanced permeability and retention effect and has been observed in many solid tumors, although the degree of tumor accumulation varies. Understandably, this has a major effect on all nanomedicines, including targeted nanoparticles. Moreover, the targeting modalities alone can often lead to complications. It is known that large structures, like liposomes or antibodies can elicit immune reactions leading to adverse effects. To minimize such effects, stealth-liposomes and nanobodies have been developed which are known to escape detection in the body and thus do not trigger an immune response. These liposomes are stable and long circulating, although the increased stability has led to an impaired drug release. To this end, thermosensitive formulations have been created which remain stable in circulation yet can be heat-activated to release their chemotherapeutic content at the target site.

Anticancer therapies require continuous development of nanomedicines to counteract the challenges provided by the tumor and its microenvironment. Challenges such as impaired biodistribution, adverse drug-related effects and drug resistance remain, yet the benefit of using multifunctional nanomedicine facilitates the rapid adjustment to any challenge that may arise.

This thesis describes research into the development of antibodies, nanomedicine and solutions to complications of *in vivo* application. A general introduction to these topics is presented in **Chapter 1**.

In **Chapter 2** we describe the development of novel heavy chain antibodies against MUC1, a tumor antigen present on various cancers. After immunization of a transgenic mouse able to express antibodies containing human variable domains, a number of antibodies were successfully produced. These heavy chain antibodies showed specificity to MUC1-positive cancer cells, making this the first step towards novel targeted nanomedicines.

In **Chapter 3** we produced novel PSMA-specific nanobodies for imaging of prostate cancer. Purified camelid-derived nanobodies were produced with the addition of only one single cysteine, to ensure stable conjugation to the radionuclide indium-111. This antibody-radionuclide conjugate enabled imaging of PSMA positive tumors *in vivo* with high specificity.

In **Chapter 4** we continued with the nanobodies described in Chapter 3 and conjugated these to liposomes containing the drug doxorubicin. We observed an increased binding *in vitro* with PSMA positive cells and an enhanced uptake in PSMA positive tumors *in vivo*. Determination of the efficacy of targeted versus non-targeted doxorubicin liposomes did not result in significant differences. To explore this issue, we investigated the distribution of the liposomes within the tumor and observed that the liposomes remained in and around the vasculature. Penetration of the tissue was limited, although the use of mild hyperthermia significantly increased extravasation and accumulation of liposomes in the tumor.

In **Chapter 5** we further investigated the issue of limited extravasation and accumulation of liposomes in solid tumors. We followed the biodistribution of radiolabeled non-targeted liposomes to evaluate the influence of the enhanced permeability and retention effect in various human tumor xenografts. Numerous morphological variables were investigated, such as blood vessel density, tumor growth, intratumoral hypoxia, infiltrating macrophages and lymphatic vessel density. In the end, no clear biological determinants could be found, although there was a significant correlation of liposomal accumulation with tumor growth. We concluded that the EPR effect varies profoundly between tumor types and that it can be highly constrictive in the application of nanomedicine.

In **Chapter 6** we tried to increase nanoparticle accumulation and anti-tumor efficacy by using hyperthermia in combination with thermosensitive liposomes. The application of mild hyperthermia (41-42°C) increased liposomal accumulation in the tumor and thermosensitive liposomes were able to release the drug specifically at the tumor site.

Taken together, this thesis shows drug development from antibody production and characterization, to conjugation with liposomes and eventually, the application of drug-loaded liposomes *in vivo* with or without hyperthermia to increase efficacy. **Chapter 7** discusses the implication of these results and reviews the advantages and drawbacks of targeted nanomedicine.

FUTURE PERSPECTIVES

The field of nanomedicine progressed rapidly since the discovery of liposomes in the sixties. Since then, numerous lipid, polymer-based, inorganic and viral nanoparticles, and drug-conjugates have been developed and known formulations have been improved upon. Any kind of anticancer drug can be loaded into a nanoparticle for increased target specificity and efficacy, and decreased drug-related adverse effects and drug resistance.

As indicated in this thesis, despite all developments in and outside of nanomedicine, cancer remains one of the most challenging diseases of our time. Several issues such as tumor heterogeneity, tumor cell plasticity and treatment of metastases remain to be solved. Collectively, the results in this thesis address challenges in current nanomedicine and propose solutions to combat these problems. That nanomedicine continues to remain one of the focal points of anticancer therapy indicates that much progress will still be made.

SAMENVATTING

Het onderzoek naar kanker therapie heeft de afgelopen jaren veel veranderingen doorgemaakt met de realisatie dat moleculaire eigenschappen van de tumorcellen de therapeutische respons bepalen. Conventionele chemotherapeutica worden geassocieerd met een beperkt therapeutisch venster, beperkingen aan een optimale dosering, de ontwikkeling van medicijnresistentie en hoge toxiciteit. Dit alles leidt vaak tot het stoppen van de behandeling door deze groep patiënten. Om deze problemen aan te pakken, worden veel nieuwe medicijnen ontwikkeld en deze worden continu geoptimaliseerd. Allereerst is er een steeds groter wordend aantal therapieën die gericht zijn tegen specifieke doelen, waar met behulp van peptides of antilichamen de medicijnen worden afgeleverd. Ten tweede, kunnen medicijnen worden ingesloten in nanodeeltjes, zoals liposomen, zodat deze een verbeterde biodistributie krijgen en interactie met het immuunsysteem en gezond weefsel wordt tegengegaan. Deze methode is zeer succesvol in het beperken van nadelige effecten gerelateerd aan antikanker medicijnen. Uiteindelijk kan de combinatie van een gerichte therapie met liposomen een positief effect hebben op de opname van het medicijn in kankercellen, wat een verhoogde effectiviteit tot gevolg kan hebben.

Ondanks recente successen in (gerichte) nanomedicijnen zijn er verscheidene problemen die nog opgelost moeten worden. Zo is de biodistributie van nanomedicijnen zeer afhankelijk van de morfologie van de tumor en de mate van extravasatie uit de bloedvaten en opname in het tumorweefsel. Onderzoek heeft uitgewezen dat de bloedvaten in solide tumoren een zeer chaotische architectuur hebben, waardoor ze zeer permeabel voor nanodeeltjes zijn. Deze kunnen dan uit de bloedvaten treden, waarna ze door beperkte (lymfatische) afvoer achterblijven in de tumor. Dit principe heet het 'enhanced permeability and retention' effect en is in veel solide tumoren vastgesteld, hoewel de mate van deze zeer kan variëren. Het is dan ook begrijpelijk dat dit een groot effect heeft op alle nanomedicijnen, dus ook op gerichte nanodeeltjes. Daarnaast kan het gebruik van gerichte liganden ook tot problemen leiden. Grote structuren, zoals liposomen en antilichamen, kunnen een immuunrespons oproepen wat uiteindelijk tot nadelige effecten kan leiden. Om dit zoveel mogelijk te beperken, zijn zogenaamde 'stealth'-liposomen en 'nanobodies' ontwikkeld die detectie in het lichaam ontlopen en zo geen immuunrespons opwekken. Deze liposomen zijn zeer stabiel en hebben een lange circulatietijd, maar helaas beperkt dit het vrijkomen van het ingesloten medicijn. Om dit probleem op te lossen zijn er thermosensitieve liposomen ontwikkeld die stabiel zijn tijdens circulatie, maar op commando bij een bepaalde temperatuur de medicijnen in de tumor kunnen vrijgeven.

Het vergt een continue ontwikkeling van nanomedicijnen om alle aspecten van de tumor en zijn omgeving tegen te gaan. Uitdagingen blijven bestaan in de beperkte

biodistributie van de medicijnen, nadelige bijwerkingen en de ontwikkeling van medicijnresistentie, maar gelukkig zijn nanomedicijnen zeer flexibel inzetbaar en kunnen ze aangepast worden op het specifieke doel.

In dit proefschrift wordt onderzoek beschreven aan de ontwikkeling van antilichamen, nanomedicijnen en de complicaties van *in vivo* gebruik van deze. Een globale introductie die deze onderwerpen behandelt is weergegeven in **Hoofdstuk 1**.

In **Hoofdstuk 2** is de ontwikkeling van nieuwe 'heavy chain' antilichamen tegen MUC1, een tumor antigeen, beschreven. Na immunisatie van een transgene muis hebben we verscheidene antilichamen geproduceerd die humane variabele domeinen bevatten. Deze heavy chain antilichamen zijn succesvol geconjugeerd aan liposomen, wat dit de eerste stap richting een nieuw antikanker medicijn maakt.

In **Hoofdstuk 3** hebben we nieuwe PMSA-specifieke antilichamen gebruikt voor visualisatie van prostaatkanker. Nanobodies waren afgeleid na immunisatie van een lama en deze zijn geproduceerd met een enkele cysteine voor conjugatie aan radionuclide indium-111. Het antilichaam-radionuclide conjugaat zorgt voor zeer specifieke visualisatie van PSMA positieve tumoren.

Hoofdstuk 4 gaat verder met de nanobodies, zoals beschreven in hoofdstuk 3, die hier geconjugeerd werden met liposomen die geladen zijn met het chemotherapeuticum doxorubicine. Dit leidde tot een verhoogde binding met PSMA positieve cellen *in vitro* en een verhoogde opname in PSMA positieve tumoren *in vivo*. Echter de werkzaamheid van gerichte en ongerichte liposomen verschilde niet van elkaar, wat mogelijk te verklaren valt door een ophoping van beide liposomen in en om de bloedvaten. Om de opname in de tumor te verhogen hebben we uiteindelijk milde hyperthermie toegepast, die zowel extravasatie als ophoping verhoogde in de PSMA positieve tumoren.

In **Hoofdstuk 5** zijn we dieper ingegaan op het beperkte binnendringen en ophopen van liposomen in solide tumoren. Hiervoor volgden we de biodistributie van radionuclide-gelabelde liposomen om de invloed van het enhanced permeability and retention effect op verschillende tumoren te bepalen. Variabelen, zoals bloedvatdichtheid, tumorgroei, intratumorale hypoxie, infiltrerende macrofagen en lymfevatdichtheid, zijn vergeleken tussen de verschillende tumoren. Uiteindelijk is er geen eenduidige biologische determinant gevonden, hoewel er een duidelijk verband was tussen de snelheid van tumorgroei en opname van liposomen. We concludeerden dat het enhanced permeability and retention effect zeer variabel is tussen de verschillende tumortypes en dat het zeer beperkend kan werken op het gebruik van nanomedicijnen.

Hoofdstuk 6 beschrijft het gebruik van thermosensitieve liposomen voor een verhoogde ophoping en groter antitumor effect. Door een verhoogde temperatuur van 41-42°C in de tumor kunnen de liposomen de ingesloten medicijnen gelokaliseerd vrijgeven.

Dit proefschrift laat de ontwikkeling van een kankermedicijn zien, beginnend bij de ontwikkeling en validatie van antilichamen tot aan de conjugatie met liposomen en uiteindelijk de toepassing van doxorubicine-geladen liposomen *in vivo* met of zonder hyperthermie. Dit alles met het uiteindelijk doel voor een verbeterd antitumor effect. **Hoofdstuk 7** bespreekt de gevolgen van deze resultaten en beschrijft de voor- en nadelen van doelgerichte nanomedicijnen en de huidige ontwikkelingen in antikanker medicijnen.

TOEKOMSTPERSPECTIEF

De ontwikkeling van nanomedicijnen heeft niet stilgestaan sinds de ontdekking van liposomen in de jaren zestig. Sindsdien heeft menig lipide, polymeer, inorganisch en viraal nanodeeltje of medicijnconjugaat zijn opwachting gemaakt en er worden continu nieuwe deeltjes ontwikkeld. Voor ieder soort antikankermedicijn kan een passend nanodeeltje gemaakt worden met als voordelen, een verhoogde specificiteit en werkzaamheid en verminderde nadelige effecten en medicijnresistentie.

Zoals in dit proefschrift is beschreven, blijft kanker een van de meest uitdagende ziekten van onze tijd. Tumorheterogeniteit, tumorcel plasticiteit en de behandeling van metastase blijven uitdagingen in het kankeronderzoek. De medicijnontwikkelingen binnen de nanotechnologie geven hoop en de verwachting is dat er nog veel vooruitgang zal worden geboekt.

LIST OF PUBLICATIONS

Nanobody-targeted prostate cancer therapy with anti-PSMA doxorubicin-loaded liposomes

Michiel Bolkestein, Gabriela N. Doeswijk, Erik de Blois, Joost A.P. Rens, Wiggert A. van Cappellen, Marion de Jong, Alexander M.M. Eggermont, Frank Grosveld, Gerben A. Koning, Wytske van Weerden

Submitted

The dynamics of fast- and slow-cycling stem cells in liver homeostasis and injury

Wanlu Cao, **Michiel Bolkestein**, Kan Chen, Yuebang Yin, Nesrin Tuysuz, Luc J. W. van der Laan, Derk ten Berge, Dave Sprengers, Herold J. Metselaar, Jaap Kwekkeboom, Ron Smits, Maikel P. Peppelenbosch, Qiuwei Pan

Submitted

TIMP3 expression decreases during melanoma progression and inhibits melanoma cell migration

Asha M. Das, **Michiel Bolkestein**, Thom van der Klok, Charlotte M.C. Oude Ophuis, Cindy E. Vermeulen, Joost A.P. Rens, Winand N. Dinjens, Peggy N. Atmodimedjo, Cornelis Verhoef, Senada Koljenovic, Ron Smits, Timo L.M. ten Hagen, Alexander M.M. Eggermont

European Journal of Cancer, 2016

Investigation of particle accumulation, chemosensitivity and thermosensitivity for effective solid tumor therapy using thermosensitive liposomes and hyperthermia

Wouter J.M. Lokerse, **Michiel Bolkestein**, Timo L.M. ten Hagen, Marion de Jong, Alexander M.M. Eggermont, Holger Gröll, Gerben A. Koning

Theranostics, 2016

Investigation of factors determining the enhanced permeability and retention effect in subcutaneous xenografts

Michiel Bolkestein, Erik de Blois, Stuart J. Koelewijn, Alexander M.M. Eggermont, Frank Grosveld, Marion de Jong, Gerben A. Koning

Journal of Nuclear Medicine, 2016

A novel ¹¹¹In-labeled anti-prostate-specific membrane antigen nanobody for targeted SPECT/CT Imaging of prostate cancer

Kristell L. Chatalic, Joke Veldhoven-Zweistra, **Michiel Bolkestein**, Sander Hoeben, Gerben A. Koning, Otto C. Boerman, Marion de Jong, Wytske M. van Weerden

Journal of Nuclear Medicine, 2015

Improved intratumoral nanoparticle extravasation and penetration by mild hyperthermia

Li Li, Timo L.M. ten Hagen, **Michiel Bolkestein**, Astrid Gasselhuber, Jeremy Yatvin, Gerard C. van Rhooen, Alexander M.M. Eggermont, Dieter Haemmerich, Gerben A. Koning

Journal of Controlled Release, 2013

Generation of novel heavy-chain antibodies against MUC1

Michiel Bolkestein, Dubravka Drabek, Rien van Haperen, Alexander M.M. Eggermont, Frank Grosveld, Gerben A. Koning

In preparation

Exploring the potency of thermosensitive liposomal Doxorubicin delivery in an orthotopic breast cancer model

Wouter J.M. Lokerse, **Michiel Bolkestein**, Simone Dalm, Timo L.M. ten Hagen, Alexander M.M. Eggermont, Marion de Jong, Gerben A. Koning

In preparation

Biological profiling of the migratory phenotype of melanoma identifies WNT5A as a metastasis determinant

Asha M. Das, **Michiel Bolkestein**, Mario Pescatori, Joost A.P. Rens, Cindy E. Vermeulen, Gerben A. Koning, Alexander M.M. Eggermont, Ron Smits, Timo L.M. ten Hagen

In preparation

Liver proliferative stem cells participate in the progression of liver tumors

Wanlu Cao, **Michiel Bolkestein**, Luc J. W. van der Laan, Dave Sprengers, Herold J. Metselaar, Jaap Kwekkeboom, Ron Smits, Maikel P. Peppelenbosch, Qiuwei Pan

In preparation

Loss of Cebpd is a driver in hepatocellular carcinoma and associated with disease progression

Pengyu Liu, Michiel Bolkestein, Luc J. W. van der Laan, Derk ten Berge, Dave Sprengers, Herold J. Metselaar, Jaap Kwekkeboom, Ron Smits, Maikel P. Peppelenbosch, Qiuwei Pan

In preparation

PhD PORTFOLIO OF MICHIEL BOLKESTEIN

Department of Surgery

Research School of Molecular Medicine

PhD period: 2011 - 2016

Promotors: Prof. dr. A.M.M. Eggermont & Prof. dr. F.G. Grosveld

Supervisor: Dr. G.A. Koning

General Courses	Year	ECTS
Laboratory Animal Science Art 9 (Rijksuniversiteit Groningen)	2010	3.0
Practical Radiation Protection Level 5b (Rijksuniversiteit Groningen)	2010	1.0
<i>In vivo</i> Imaging: from Molecule to Organism (Erasmus MC, Rotterdam)	2011	1.8
Course on Advanced Drug Delivery & Drug Targeting (Universiteit Leiden)	2011	1.8
Course on Animal Management System (Erasmus MC, Rotterdam)	2012	0.1
Course Molecular Immunology (Erasmus MC, Rotterdam)	2012	3.0
Course on Molecular Medicine (Erasmus MC, Rotterdam)	2012	0.7
Course Basic and Translational Oncology (Erasmus MC, Rotterdam)	2012	1.8
Course Scientific Integrity (Erasmus MC, Rotterdam)	2014	0.3
Seminars and workshops		
PhD-day (Erasmus MC, Rotterdam)	2011	0.3
Mini-symposium: 25 years of Radiopeptide Research (Erasmus MC, Rotterdam)	2011	0.3
ENCITE final public workshop (Leiden University Medical Center)	2012	0.3
Daniël den Hoed Day (Erasmus MC, Rotterdam)	2012 - 2013	0.3
1st Transatlantic Conference on Personalized Medicine (Erasmus MC, Rotterdam)	2015	0.3
Presentations / posters at conferences		
Journal club at the Department of Surgery (Erasmus MC, Rotterdam) (every fortnight)	2011 - 2015	2.0
Research meeting at the Department of Surgery (Erasmus MC, Rotterdam) (every week)	2011 - 2015	2.0
Research meeting at the Department of Cell Biology (Erasmus MC, Rotterdam) (2 orals)	2013 - 2015	0.3
Molecular Medicine Day (Congress Center Engels, Rotterdam) (3 posters)	2011 - 2014	1.0
5th ILS Liposome Advances Conference (School of Pharmacy, University of London, United Kingdom) (1 poster)	2011	2.0
COST Action TD1004 Annual Meeting (London, United Kingdom; Torino, Italy; Istanbul, Turkey) (2 posters, 2 orals)	2012 - 2014	2.0
22nd Liposome Workshop (Ameland, the Netherlands) (1 oral)	2012	1.8

European Molecular Imaging Meeting (Torino, Italy; Antwerpen, Belgium; Tübingen, Germany) (1 oral, 3 posters)	2012 - 2015	4.5
Wetenschapsdag Heelkunde (Department of Surgery, Erasmus MC, Rotterdam) (1 oral)	2012 - 2015	1.0
European Cancer Congress (Amsterdam, the Netherlands) (1 poster)	2013	0.3
13th European Symposium on Controlled Drug Delivery (Egmond aan Zee, the Netherlands) (1 poster)	2014	2.0
Controlled Release Society Annual Meeting (Chicago, United States; Edinburgh, United Kingdom) (2 posters)	2014 - 2015	3.0

Supervision of students

Priscilla van Haperen (HLO-student)	2011 - 2012	6.4
Angelique G.A. Kooij (HLO-student)	2013 - 2014	3.2

ACKNOWLEDGEMENTS

Mijn eerste dankwoord is voor mijn copromotor en directe begeleider **Gerben**. We hadden vanaf het begin een goede band en ik kan oprecht zeggen dat ik door zijn begeleiding een betere onderzoeker ben geworden. Daarnaast was het sociale aspect ook altijd belangrijk voor hem en we hebben dan ook meerdere malen wijntjes en biertjes genuttigd. In Turiijn gingen zelfs de voetjes van de vloer. Hij heeft me zo ook al vroeg geleerd hoe belangrijk het is om verder dan je eigen lab te kijken en hieraan heb ik veel contacten en samenwerkingen te danken binnen en buiten het Erasmus MC. De goede tijden mochten helaas niet eeuwig duren en we kregen te horen dat het niet goed met hem ging. Desondanks heeft hij me zolang dat nog ging, altijd bijgestaan om mijn promotie tot een goed einde te brengen en hij heeft me geleerd dat het werk niet altijd de prioriteit kan hebben. Ik ben dan ook blij dat hij de laatste jaren van zijn leven met zijn familie heeft kunnen doorbrengen en ik heb in december 2015 met verdriet afscheid van hem genomen. Naast zijn stopwoorden “goed zo!” en “prima!” zal me zijn onderzoeksgeest, vriendelijkheid en optimisme altijd bijblijven.

Daarnaast wil ik mijn promotor **Lex** bedanken. Ondanks je drukke bestaan als algemeen directeur van het Instituut Gustave Roussy in Parijs, ben je in Gerben's afwezigheid naar voren gestapt om mij tijdens mijn promotie extra te ondersteunen. Wat in het begin van mijn promotie een jaarlijks overleg betrof, werd later een maandelijks telefoontje vanuit het buitenland om publicaties en dergelijke te regelen. Ik dank je dan ook voor de steun die ik tot het einde van mijn promotie van je heb mogen ontvangen.

Ook mijn promotor **Frank** wil ik bedanken voor zijn steun. Wat begon met een simpele samenwerking tussen de heerkunde en celbiologie werd voor mij al snel een tweede thuis. Ik prijs mezelf gelukkig om jou als promotor te hebben. Je was altijd bereid om mijn onderzoek te bespreken, of het nu om liposomen, antilichamen of muizenexperimenten ging, en ik maakte altijd dankbaar gebruik van jouw bijna oneindige wijsheid.

Beste **Joek**, hierbij wil ik jou als hoofd van de afdeling heerkunde bedanken dat jij destijds mede de verantwoordelijk voor mijn promotie op je hebt genomen.

Een onmisbare samenwerking was met de nucleaire geneeskunde en **Marion**. Zoals in dit proefschrift is te zien, heb ik dankbaar gebruik gemaakt van jouw vakkennis. Ook kon ik tijdens mijn promotie altijd langslopen voor advies, bedankt voor alles.

Daarnaast wil ik ook **Wytske** in het bijzonder bedanken voor jouw steun vanuit de afdeling urologie en voor jouw begeleiding en hulp met het PSMA manuscript.

Ik wil graag **Paul en zijn groep** bedanken van de afdeling moleculaire oncologie in Utrecht, waarmee ik met Gerben een laatste samenwerking heb opgezet. Jullie nanobodies werkten fantastisch na koppeling aan de liposomen, helaas heb ik geen tijd om hier nog een publicatie van te maken.

Je zou bijna vergeten dat alles op de 1e verdieping van het faculteitsgebouw is begonnen. We zaten dan wel in de kelder, maar dat was des te meer reden om het gebouw af en toe te verlaten. Allereerst wil ik **Wouter** bedanken. We startten in hetzelfde jaar en hebben sindsdien een lange reeks cursussen en conferenties afgelopen. Ondanks het feit dat je jezelf tot een van de weinige Nederlanders kan rekenen die niet van kaas houdt (zelfs niet Parmezaanse kaas) hebben we ons zeker goed vermaakt, zoals met Billy en Gerben in Turijn. Ik dank je voor de gezelligheid en wens je het allerbeste in München.

I would also like to thank the old and new members of the lab. **Lilia** and **Billy**, I remember how glad you were that finally some guys joined the lab, although you may have wished otherwise during our trips to London and Torino. I have fond memories of the drinks and (homemade) dinners we used to have, although we ended up at the Westerpaviljoen too often. I also had the pleasure to meet several exchange students joining from Iran and Spain, **Azadeh**, **Reza** and **Sara**, I will remember our trip to Amsterdam and the Sinterklaas party we held, in true Dutch style, including gifts and poems. I wish you all well in life and your further careers.

Joost en **Cindy**, onze analisten, ik wil jullie bedanken voor de prettige atmosfeer en de samenwerking die ik aan het einde van mijn promotie met jullie heb gehad. Cindy werkte hard en was altijd recht voor zijn raap. Joost, we hebben in ons laatste jaar (of maanden) toch nog succesvol samen kunnen werken. Je bent altijd enthousiast en ik wens je veel geluk met je nieuwe carrière.

Ik wil iedereen van het Harbour antibodies lab danken: **Alex**, **Dubi**, **Ernie**, **Rick**, **Rien** en later ook **Michael**. Jullie hebben me wegwijs gemaakt binnen de celbiologie en ik zat ook altijd graag op 7e (nu 10e) verdieping. Velen van jullie kwam ik ook 's avonds en in het weekend op het lab tegen, wat voor mij handig was voor de zoveelste vraag van mijn kant. Ik voelde me bij jullie altijd welkom, wat misschien deels lag aan het feit dat we daar in de zon konden zitten, die we op de 1e verdieping helaas nooit zagen. Ook de rest van de voormalige 7e verdieping wil ik bedanken, met in het bijzonder **Ralph** en **Ruud** voor de helaas niet gepubliceerde samenwerking betreffende de Anchor-Away methode.

Gert en **Gert-Jan**, jullie zijn altijd bereid geweest om raad en assistentie te verlenen als het ging om welke vorm van microscopie dan ook, mijn dank hiervoor.

Jeroen, **Sasha** en **Yanto**, ik wil jullie graag bedanken voor de steun met de IVIS en microCT. Helaas ben ik al vroeg verleid door de hogere resolutie van de SPECT, maar ik zal mijn eerste jaren met de IVIS en FMT niet vergeten.

Ik wil **Joyce** en **Sari** bedanken voor advies met de (micro)FPLC en eiwitproductie in het algemeen en Joyce in het bijzonder voor het opzetten van de Biacore bepaling voor mijn nieuwe antilichamen.

Deze promotie was ook niet mogelijk geweest zonder de pragmatische houding van **Wout** en **Erik** (en daarvoor **Harald**). Toen mijn project klaar was voor radiogelabelde

liposomen, hebben we binnen een week een protocol opgesteld en geoptimaliseerd. Daarnaast was het altijd gezellig bij de radiolabeling en daarvoor wil ik ook **Ho-Sze** en **Rory** bedanken.

Hierop volgt automatisch de steun die ik kreeg vanuit de afdelingen nucleaire geneeskunde en radiologie voor de injecties en af en toe een scan of biodistributie. Hiervoor wil ik allereerst **Stuart** bedanken; jij bezat het zelfde pragmatisme, zodat altijd alles mogelijk was. Jij (en later Gaby) hebt me destijds altijd goed ondersteund. **Gaby**, jij bent ook onmisbaar geweest voor de vele scans en de efficacy studie van de PSMA-liposomen. Hier mag ik ook **Jan, Joost** (Haeck) en **Sandra** niet vergeten, jullie stonden altijd voor me klaar als de apparatuur of Stuart/Gaby het af lieten weten.

Costanza and **Kristell**, thank you for the many discussions regarding targeting *in vivo* and the EPR effect. It was always nice to see a familiar face at conferences.

I would also like to thank **Abdullah and his team** from the department of gastroenterology and hepatology. A special shout-out to **Wanlu** and **Yuebang** for the productive collaborations and I think it is fair to say that everybody benefited from our meetings. I admire the limitless optimism shown by all of you.

Dank gaat ook uit naar **Angelique, Ashraf, Corrina, Joke, Martijn** en **Mirella** en de rest van de afdeling urologie voor de assistentie met celkweek, eiwitproductie en natuurlijk het produceren van de PSMA nanobodies in hun nieuwe format.

Beste **Aart** en **Anton**, als de begeleiders van mijn master stages wil ik jullie bedanken om mij het vertrouwen te geven een promotietraject te starten.

Dear **Asha** and **Roel**, my paranymphs. I would like to thank you for all your support and the numerous distractions during my PhD project. Both of you really know what it means to get your PhD. That, together with the fact that you are two of the smartest people I know, makes me feel very confident defending my PhD thesis with both of you by my side.

Mijn goede vrienden, **Arnie, Arjan, Daan, Joost** en **Tim**, we zijn aan het begin van onze studie in Groningen bij elkaar gekomen en ik waardeer alles wat we sindsdien met elkaar hebben meegemaakt. Al moest ik dan wel elke keer weer opnieuw uitleggen wat ik ook alweer deed, maar uiteindelijk hebben jullie geholpen om mijn gedachten af en toe te verzetten.

Beste **Frank** en **Martijn**, ook wij kennen elkaar sinds Groningen en ik wil jullie bedanken voor de vele avonden afleiding die we samen met Tim hebben gedeeld. Ik hoop dat er nog vele mogen volgen.

Diewerke, Jan-Willem, Johanneke en **Stijn**, jullie zijn met Roel altijd de reden geweest om naar het noorden af te reizen. De grote afstanden hebben nooit in de weg gestaan om elkaar toch nog regelmatig blijven zien en ik kijk uit naar onze volgende ontmoeting.

I would like to thank my new friends; **Maron** and **little Caleb**, **Martín**, **Priyanka**, **Shweta**, **Sreeleena** and **Unni** for the times spent in Amsterdam, Münster and the petting zoo. We've had a lot of fun and we'll meet again soon. Thanks for all the good times.

Theo en **Reinier**, het is eindelijk zover. In het begin vroegen jullie altijd netjes hoe het ging met de studie/promotie, maar naar het einde toe werd het stiller en stiller. Maar nu is dan zo ver, jullie wachten wordt beloond en binnenkort is de familie weer een doctor rijker.

Lieve **Pa** en **Ma** en mijn broers **Daniël** en **Tobias**, misschien dat het naar het einde toe allemaal iets te lang ging duren maar uiteindelijk is het dan toch afgerond. Ik weet nog goed dat ik in Rotterdam begon en op mijn eerste werkdag was gaan borrelen met het lab. Daarmee heb ik gelijk de schijn de das omgedaan dat de wetenschap een serieus beroep is. En ik heb daarna ook nog vaak moeten aanhoren of dat 'harde werken' in die weekenden wel echt werken was. Dank voor alle steun tijdens mijn promotie en daarvoor, en weet dat ik het zonder jullie steun niet had kunnen doen.

Hier eindigt mijn dankwoord en voor velen ook het lezen van mijn proefschrift. Al mijn collega's, vrienden en familie, mijn dank is groot.

Ik zal beloven mijn promotie niet langer als excuus te gebruiken.

Echter als men vraagt wat ik ook alweer deed verwijst ik vanaf nu naar dit proefschrift.

CURRICULUM VITAE

Michiel Bolkestein was born on the 3rd of February 1984 in the city of Tiel, the Netherlands. In 2002, he completed his secondary education at the RSG Lingecollege in Tiel, before moving to the University of Groningen, the Netherlands, to obtain his Bachelor's degree in Medical Biology. He went on to obtain his Master of Science in Medical and Pharmaceutical Biology with internships at the departments of Pharmaceutical Biology and Medical Oncology at the University Medical Center of Groningen. From 2011 till 2016 he performed his PhD research at the department of Surgery in close collaboration with the department of Cell Biology at the Erasmus Medical Center, Rotterdam, the Netherlands. His doctoral thesis focused on critical aspects of drug development, targeting and theranostics. In his research he has used various tools in optical and nuclear imaging modalities, antibody functionality assessment and liposomal development. These skills have led to productive collaborations with the departments of Gastroenterology and Hepatology, Nuclear Medicine, Radiology and Urology.